UNDERSTANDING WHEAT STRIPE RUST THROUGH STUDIES ON HOST AND PATHOGEN METABOLISM

Veronica Roman-Reyna

August, 2017

A thesis submitted for the degree of Doctor of Philosophy of The Australian National University

DECLARATION

I declare that the content of this thesis is my original work unless otherwise stated.

Veronica Roman-Reyna

ACKNOWLEDGEMENTS

During my PhD and the writing of this thesis, I met several people who improve my personal and academic life and make my PhD an enlightening experience.

First, I would like to thank my parents who have been a buffer since the beginning of my scientific career and have push me through years to learn from the situations and move on.

Many thanks to Dr. John Rathjen for giving me the opportunity to be in his lab and for teaching me different aspects of science. I learn from him to always be critical about science, use proper aesthetics and write proper English.

In John's lab, I was lucky to be in two different groups of lab mates. Both enrich my life with different insights in science. I would like to thank the old team: Dr. Diana Garnica ("D1"), Dr. Isabel Saur, Dr. Brendon Conlan and Rebeca Drown. Also the new team: Dr. Diana Ramirez ("Dee"), Dr. Ben Schwessinger, Yiheng Hu and Alex Sloan. Special thanks to "D1", "Dee" and Ben for their guidance and friendship. Thanks to "Dee" and Ben for make me addicted to ocean swimming.

I would also like to thank Dr. Spencer Whitney and Dr. Peter Solomon, my PhD advisors, for their suggestions that improved my research.

Thanks to Dr. Florian Bush, Dr. John Evans, Dr. Josette Masle, Dr. Brita Foster and Dr. Bob Furbank. They were always willing to answer my questions and giving me feedback when I decided to use plant physiology in my research.

Thanks to Dr. Evans Lagudah for providing resistant wheat lines and for sharing his thoughts about Adult Plant Resistance.

Thanks to Dr. Megan McDonald and Dr. Susan Breen for their help during my PhD and for showing me "weird sports" that I end up enjoying.

Last but not least, thanks to Paola Reynales, Dr. Jaime Simbaqueba, Dr. Maria Ermakova, Dr. Mary Gray, Sabrina Chin, Oliver Mead, Annamaria De Rosa, Jacinta Watkins, Dr. Elena Martin, Sara Chick and Meenu Trapat. They helped me to have a life outside the Lab.

ABSTRACT

Wheat stripe rust, caused by the biotrophic Basidiomycete fungus *Puccinia striiformis* f. sp. *tritici* (*Pst*), is one of the most important crop diseases worldwide. *Pst* has a complex lifecycle with an asexual cycle and a sexual cycle, consisting of five possible spore types. The asexual cycle, which is the economically damaging phase on wheat, occurs repeatedly throughout the growing season through the germination of urediniospores, vegetative growth of the fungus and ultimate sporulation. During colonization, urediniospores germinate on the upper leaf surface and penetrate it via stomata. Vegetative growth starts when infectious hyphae branch off from a substomatal vesicle and ramify throughout the intercellular spaces. When the tip of a growing hypha touches a mesophyll cell, the fungus can develop an invasive structure called the haustorium. This specialized structure penetrates the cell wall but not the plasma membrane, expresses nutrient transporters and is the main site for secretion of virulence effector proteins. At this point the biotrophic growth starts. This stage If sufficient nutrients are available the fungus is able to complete the asexual cycle by developing spore-forming pustules that erupt from the leaf epidermis releasing millions of urediniospores (sporulation). Here I used physiological, molecular biology, metabolomics, and transcriptomics approaches to provide a broad view of metabolic processes during the infection. I measured the chitin content of infected wheat tissue as a proxy for fungal biomass, as chitin content is the major component of the fungal wall. Using this technique, I found that the *Pst* asexual lifecycle can be divided into two main phases. In the early part of *Pst* cycle from two to eight days after infection, it has limited requirements for nutrients, whereas the second phase from 9 to 15 dai leading to sporulation has high nutrient requirements. As all fungal nutrients are derived from the host, I measured aspects of carbon and nitrogen metabolic pathways. In the first phase, most photosynthesis parameters were unaffected. During the second phase, the high nutrient demand caused by the infection shifted the metabolic status of the infected tissue from source to strong sink. This conclusion was derived from the fact that all photosynthesis parameters related to carbon fixation and chlorophyll content decreased by at least half compared to healthy leaves. Moreover, genes related to asparagine and sucrose metabolism were up regulated in non-inoculated leaves while head weights were reduced. These data are consistent with a model in which the *Pst* infection induces nutrients reallocation from healthy to infected tissue in the second phase of infection to meet the sporulation phase demands. The second aspect that I studied was the relationship between plant development and *Pst* growth. One approach was to investigate the phenomenon of Adult Plant Resistance (APR), in this case conferred by the hexose transporter gene, *Yr46*. The *Yr46* resistance is manifested as reduced production of *Pst* spores on the infected flag leaves of adult plants. I found that *Yr46* seems to prevent the flag leaf from acting as sink tissue, possibly by accumulating sugars in the apoplast. This mechanism may reduce the cytoplasmic nutrients available for uptake by the haustoria. I suggest that immunity and plant development should be studied together, and observe that systemic responses provide additional information to understand the infection. I propose that in addition to the recognition of pathogen molecules, plant immunity may also concern the detection of pathogen manipulation of host metabolic pathways.

ABBREVIATIONS

6-SFT	Sucrose:fructan 6-fructosyltransferase
6PG	Glucose to 6-phosphogluconate
AA2	Aminotransferase 2
AAT	Amino acid transporters
ABA	Abscisic acid
ABC	ATP-binding cassette
AGP	ADP-glucose pyrophosphorylase
APR	Adult plant resistance
ASN	Asparagine synthetase 3
ATP	Adenosine triphosphate
BFF	Beta-fructofuranosidase
BLAST	Basic local alignment search tool
BSA	Bovine Serum Albumin
BWA	Burrows-Wheeler Alignment tool
C-INV	Cytoplasmic invertase
CAT	Catalase 2
CC	Coiled-coil
CW-INV	Cell-wall invertase
CYP	Cytochrome P450
DTT	Dithiothreitol
EDTA	Ethylenediaminetetraacetic acid
EHM	Extra-haustorial membrane
EHMx	Extra-haustorial matrix
F6H	Fructan 6-exohydrolase
FAR	Fatty acyl-coenzyme A reductase 1
Fd	Ferrodoxin
FDR	False discovery rate
FK1	Fructokinase-1
FLC	Flowering locus
Fv/Fm	Potential efficiency of PSII
G6PDH	Glucose-6-phosphate dehydrogenase
GAD	Glutamate decarboxylase
GCMS	Gas chromatography–mass spectrometry analysis
GFPT	Glutamine--fructose-6-phosphate aminotransferase
GHs	Glycosyl hydrolases
GLUT	Glucose transporter
GO	Gene ontology
GPM	Glucose phosphomutase, putative
GPR	Gamma-glutamyl phosphate reductase
HMC	Haustorial mother cells
HXK	Hexokinase
HXT1	Glucose transporter

INV	Invertase
IT	Infected tissue
JA	Jasmonic acid
MC1	Metacaspase 1
MDH	Enzyme malate dehydrogenase
MFS	Major facilitator superfamily
MSTFA	N-trimethylsilyl-N-methyl trifluoroacetamide
N-INV	Neutral invertase
NADP	Adenine dinucleotide phosphate
NASE	Nitrilase
NB-LRR	Nucleotide binding and leucine-rich repeats domains
NPQ	Non-photochemical quenching
OAA	Oxaloacetic acid
OPP	Oxidative pentose phosphate
OPT	The oligopeptide transporter family
PAHBAH	4-Hydroxybenzhydrazide acid hydrazide
PAL	Phenylalanine Ammonia-Lyase 2
Pc	Plastocyanin
PCMBS	Para-chloro-mercuribenzene sulphonic acid
PCR	Polymerase chain reaction
PDR	Pleiotropic drug resistance protein
PEPCK	Phosphoenolpyruvate carboxykinase
PFKB	ATP-dependent 6-phosphofructokinase isozyme 2
PGI	Phosphoglucose isomerase
PGSB	Plant Genome and Systems Biology
PIG	Planta-induced genes
POT	Proton-dependent oligopeptide transporter
Pq	Plastoquinone
PR	Pathogen-related
PSBP	Photosystem II 23 kDa protein
PSI	Photosystem I
PSII	Photosystem II
***PST*-79**	*Puccinia striiformis* f. sp. *tritici* from 1979
qRT-PCR	Quantitative Reverse transcriptase-PCR
Rd	Respiration rates during the day
ROS	Reactive Oxygen species
S	Urediniospore
SA	Salicilic acid
SAG	Senescence-associated genes
SPP	Sucrose-phosphatase
SPS	Sucrose-phosphate synthase
SPX	SPX domain-containing membrane protein
SSV	Sub-stomatal vesicle
ST	Stoma
START	Star-related lipid-transfer domain

STP13	Sugar transporter 13
SuCoA	Succinyl-coenzyme a
SUT	Sucrose uptake transporters
SV	Sub-stomatal vesicle
SWEET	Sugars Will Eventually be Exported by Transporters
T3SS	Type 3 secretion system
TAL	Transcription activator-like
TCA	Tricarboxylic acid cycle
TGA	Triacylglycerol
TIR	Toll/interleukin-1 receptor/resistance
TMS	Trimethylsilyl
TPP	Trehalose-6-phosphate phosphatase
TPS	Trehalose-6-phosphate synthase
TPT	Triose-phosphate/phosphate translocator
TPU	Triose phosphate use
TRIS	Trisaminomethane
UDP	Uracil-diphosphate
Vc	Carboxylation activity
WGA	Wheat germ agglutinin
WKS1	Wheat kinase start1
WPK4	Wheat protein kinase 4
YSL7	Yellow stripe like 7
ZIFL1	Zinc-induced facilitator-like 1
ϕPSII	Actual efficiency of PSII

BOX 1: LIST OF PATHOGENS REFERENCED

Disease	Pathogen	Phylum	Host
Stripe rust	*Puccinia striiformis* f. sp. *tritici (Pst)*	*Basidiomycota*	*Triticum aestivum*
Asian soybean rust	*Phakopsora pachyrhizi*	*Basidiomycota*	*Glycine max*
Barley powdery mildew	*Blumeria graminis* f. sp. *hordei*	*Ascomycota*	*Hordeum vulgare*
Bean rust	*Uromyces appendiculatus*	*Basidiomycota*	*Phaseolus vulgaris*
Rice blast	*Magnaporthe oryzae*	*Ascomycota*	*Oryza sativa*
Broad bean rust	*Uromyces fabae*	*Basidiomycota*	*Vicia faba*
Brown rust	*Puccinia hordei*	*Basidiomycota*	*Hordeum vulgare*
Corn smut	*Ustilago maydis*	*Basidiomycota*	*Zea may*
Crown rust	*Puccinia coronata* var. *avenae*	*Basidiomycota*	*Avena sativa*
Flax rust	*Melampsora lini*	*Basidiomycota*	*Linum marginale*
Leaf rust	*Puccinia triticina (Pt)*	*Basidiomycota*	*Triticum aestivum*
Millet leaf rust	*Puccinia substriata*	*Basidiomycota*	*Pennisetum glaucum*
Pea powdery mildew	*Erysiphe pisi*	*Ascomycota*	*Pisum sativum*
Poplar rust	*Melampsora larici-populina*	*Basidiomycota*	*Populus sp.*
Grapevine powdery mildew	*Erysiphe necator*	*Ascomycota*	*Vitis vinifera*
Grape mold	*Botrytis cinerea*	*Ascomycota*	*Vitis vinifera*
Stem rust	*Puccinia gramnis* f. sp. *tritici (Pgt)*	*Basidiomycota*	*Triticum aestivum*
Wheat powdery mildew	*Blumeria graminis* f.sp. *tritici*	*Ascomycota*	*Triticum aestivum*
Tobacco powdery mildew	*Erysiphe cichoracerum*	*Ascomycota*	*Nicotiana*

TABLE OF CONTENTS

CHAPTER 1
Introduction to wheat and fungal rust pathogens

Plant domestication emerged from the desire to select and combine beneficial traits to increase food nutrition. One such plant is wheat. Selection of wheats commenced in the Fertile Crescent about 10,000 years ago (Marcussen et al., 2014). With the Green Revolution, beginning in the 1930s but with the greatest impact in the late 1960s, wheat productivity and the area under cultivation increased dramatically. This revolution alongside deployment of other technologies has made a major contribution to reduction of global starvation. Today wheat production is split evenly between developing and developed countries, providing approximately 20% of total calories and protein for human consumption (Shiferaw et al., 2013). Plant domestication helps to provide elite crop varieties over large areas of production. However, it narrows the range of species under cultivation and their genetic diversity, and together with the limited number of resistance genes available makes modern agricultural systems vulnerable to attack by diverse pathogens and pests.

The major foliar pathogens of wheat are fungi, particularly *Fusarium graminearum*, *Mycosphaerell*a *graminicola*, *Stagonospora nodorum, Zymoseptoria tritici, Blumeria graminis, Cochliobolus sativus* and the rusts (*Puccinia spp.)* (Shiferaw et al., 2013), while an emerging concern is wheat blast (*Magnaporthe oryzae*) reported recently in Bangladesh (Islam et al., 2016). Rusts are one of the major challenges to food security; an estimated $USD 1 billion is lost annually in wheat production due to stripe rust (Beddow et al., 2015). Part of what makes rusts such successful pathogens is the capacity to produce millions of urediniospores in a single infection by repeated cycles of asexual reproduction. The massive production of urediniospores

increases the number of mutations in the progeny, allowing the fungus to overcome resistant crops rapidly (Ali et al., 2014; Wellings, 2007). Another characteristic of urediniospores is their capacity to travel long distances; for example, a particular wheat stripe rust isolate migrated 2400 km in North America within a six month period (Chen et al., 2014). The current strategies available for controlling wheat fungal diseases include the intense use of fungicides, deployment of host resistance genes, and to a lesser extent agricultural practices such as adjusting the sowing dates; however these are not fully effective and losses to infection remain significant (Ali et al., 2014; Beddow et al., 2015).

Rust fungi are biotrophic and hence survive exclusively on live host plants. There are three types of wheat rust; stem rust (*Pgt*, *P. graminis* forma specialis (f. sp.) *tritici*), leaf rust (*Pt*, *P. triticina*) and stripe or yellow rust (*Pst*, *P. striiformis* f. sp. *tritici)* (see Box 1 for fungal disease, common and proper names). Stem rust occurs primarily on stems but can also be found on leaves, sheaths, glumes, awns and seeds. The spore-producing pustules are reddish-brown due to the colour of the spores. Leaf rust produces light brown spores and is found mainly on leaves, but also on glumes, seeds and awns (Kolmer et al., 2001). Finally, stripe rust is a foliar disease but is also reported on heads. *Pst* produces pustules arranged in parallel lines on the leaves of adult plants, hence the name. The transverse growth of the fungus is restricted by the leaves' vascular bundles, however in seedlings this limitation does not exist and the fungus grows as non-polarized spots (Figure 1.1).

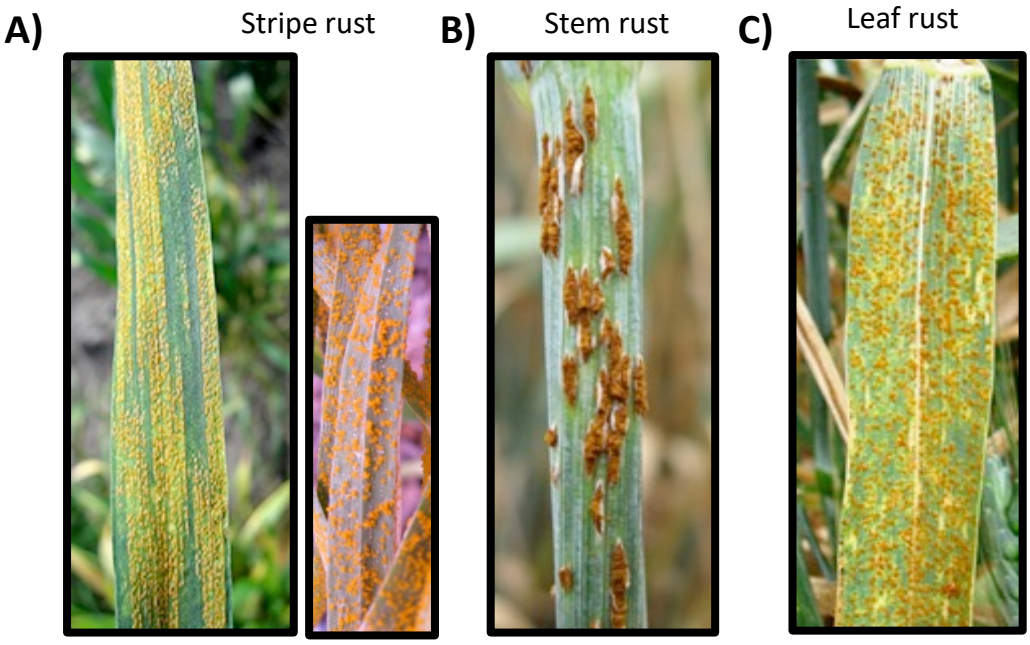

Figure 1.1. The three wheat rusts. A) *Pst* pustules on a wheat flag leaf (left) and seedlings (right), only on adult plants are the pustules organized as stripes. B) Pgt pustules on a wheat stem. C) Pt pustules on a flag leaf. Image sourced from http://agriculture.vic.gov.au/

1.1 The life cycles of wheat rust fungi

Wheat rusts (*Puccinia* spp.) have complex life cycles that require two hosts (heteroecious) and five different spore types (macrocyclic). The life cycle can be divided into two stages, asexual and sexual, which correspond to the primary and alternative hosts respectively. *Pst* reproduces asexually on wheat, with the potential to produce two different types of spores (Figure 1.2). One of these, urediniospores, can re-infect wheat during the growing season, enabling repeated asexual reproduction over the growing season. This stage causes significant economic damage on wheat crops. At the end of the northern hemisphere growing season *Puccinia* spp. produce dikaryotic teliospores. These spores represent the commencement of the sexual phase of the cycle. The sexual stage is best characterized for *Pgt*, here karyogamy (fusion of nuclei) and meiosis occur in teliospores, ultimately producing recombinant monokaryotic basidiospores. These spores infect the alternate host *Barberry* spp. to produce two types of haploid hyphae, the pycniospores and the receptive hyphae. A pycniospore can fertilise a receptive hypha of the opposite mating type, producing a dikaryotic mycelium which in turn produces aeciospores. These can infect wheat leading to urediniospore formation, and the cycle can start again. The complete cycle can occur only once in a year, while the asexual cycle is iterative throughout the wheat growing season. The host for the *Pgt* sexual phase is the shrub barberry (*Berberis* spp.), whereas for *Pt* it is the herbaceous flowering plant *Thalictrum* spp. (Zhao et al., 2016). For *Pst,* Oregon grape (*Mahonia aquifolium*) and barberry can function as alternative hosts in controlled conditions (Chen et al., 2014; Jin et al., 2010), however the natural infection of barberry has only been observed in China (Wang et al., 2015; Zhao et al., 2013). *Pst* maintains sexual populations in the Pakistani Himalayan region on barberry, but elsewhere in the world it has proven extremely difficult to demonstrate sexual recombination on this species (Ali et al., 2014; Chen et al., 2014; Liang et al., 2015; Rodriguez-Algaba et al., 2014). The current understanding based on genetic marker data is that the centre of *Pst* genetic diversity is the Pakistani Himalayan region.

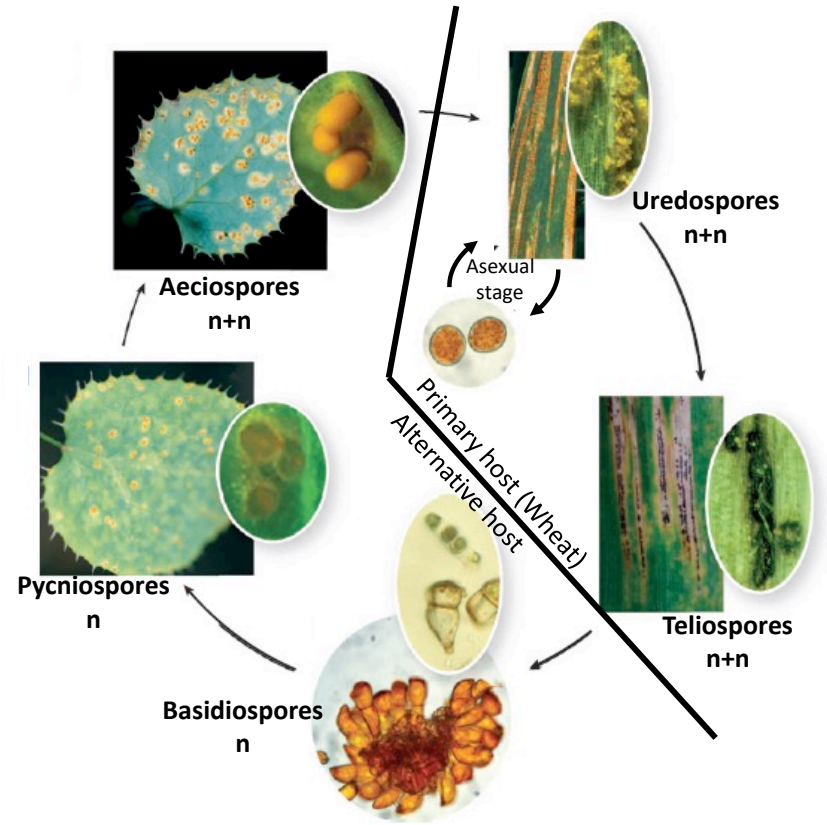

Figure 1.2. The complete life cycle of *Puccinia* spp. The asexual stage for Pt, Pgt and *Pst* is the cyclic infection of wheat by dikaryotic urediniospores. At the end of the wheat growing season the mycelia form telia which produce black dikaryotic teliospores. These fuse their haploid nuclei and ultimately produce haploid monokaryotic basidiospores by meiosis, which can then infect the alternate host. After basidiospore germination, the resulting mycelia produce pycnia which fuse and ultimately produce dikaryotic aeciospores that will infect wheat and restart the cycle (Hovmøller et al., 2011).

1.1.1 Rust epidemics

Stem rust has long been considered the most devastating wheat disease. The ancient Romans (384-322 B.C.) sacrificed animals to protect wheat crops from the rust god Robigus (Schumann and Leonard, 2000). All wheat-growing continents experienced stem rust epidemics in the 20th century (Hodson, 2011). After the elucidation of its complete life cycle, the *Pgt* alternate host barberry (*Berberis* spp.) was eradicated in North America to help control the disease. A further improvement in genetic control was a key aspect of the Green Revolution. Norman Borlaug incorporated the gene *Sr31* which confers resistance to stem rust and helped to control the disease for more than 30 years. However, in 1999 a new race of *Pgt* called Ug99 was reported in Uganda (Pretorius et al., 2000). This race overcame *Sr31* resistance and 90% of wheat varieties were susceptible. Ug99 is considered a major threat to food security (Singh et al., 2011). This stimulated a range of new investment and breeding activities to create more genetic options to

control the disease. In Australia some wheat varieties still carry *Sr31* as it is effective against local *Pgt* races (Cuddy et al., 2016).

Recently, wheat stripe rust has received greater attention due to severe and widespread epidemics. *Pst* is present on all continents where wheat is grown and quickly overcomes resistant wheat lines (Figure 1.3). The increase in severity is due to the emergence of rust variants that can sporulate two to three days earlier than older strains, are adapted to warmer temperatures and have overcome resistance genes (Milus et al., 2009). These more aggressive strains explain the increases in crop losses due to stripe rust since 2000, after which the disease was reported in most growing seasons and in new countries where it had not been previously recorded (Beddow et al., 2015). The evolution of new *Pst* strains is hypothesised to be driven by increases in global temperature, generation of sexual recombinants at the centre of origin, increases in human-mediated spore dispersion between countries and non-optimal distribution of resistant wheat lines (Walter et al., 2016).

Three major migrations have been reported for *Pst* (Figure 1.3). The first was in the 1979s from Europe to Australia and later in the 1900s to America (Ali et al., 2014). The second migration was in 2000 from East Africa to North America, Australia and Northern Africa. In 2011, a more heterogeneous incursion from the Himalayan region was reported in Europe (Hovmøller et al., 2016). The 2000 migration was more aggressive and is divided into strains *PstS1* and *PstS2*. The *PstS1* strain comprises North American, Australian. The *PstS*2 strain corresponds to more recent isolates from East Africa and all the isolates from Europe and Middle East (Ali et al., 2014; Schwessinger, 2017; Walter et al., 2016). In Australia, *Pst* has made two major incursions; first in Victoria in 1979 which likely originated from the United Kingdom, followed by an independent incursion (*PstS1/S2*) in Western Australia in 2002 (Figure 1.3). A pathotype is a pathogenic variant with a specific virulence profile, i.e. the ability to grow on particular host containing a set of specific resistance genes. The 1979 and 2002 incursion isolates are quite different from each other and designated as pathotypes 104 E137 and 134 E16 A+ respectively (Wellings, 2007). In 1981, the pathotype 104 E137 overcome the seedling resistance gene YrA (107 E137 A+) and became endemic in southern and central New South Wales, subsequently mutating to overcome many other resistance genes (Wellings, 2007). The incursion of a new isolate in Western Australia in 2002 resulted in displacement of the 1979 lineage throughout the country. The pathotype 134 E16 A+ is derived from *PstS1/S2* , grows faster in warmer conditions (12 to 28°C), and produces more spores (Milus et al., 2009; Walter et al., 2016; Wellings et al., 2003).

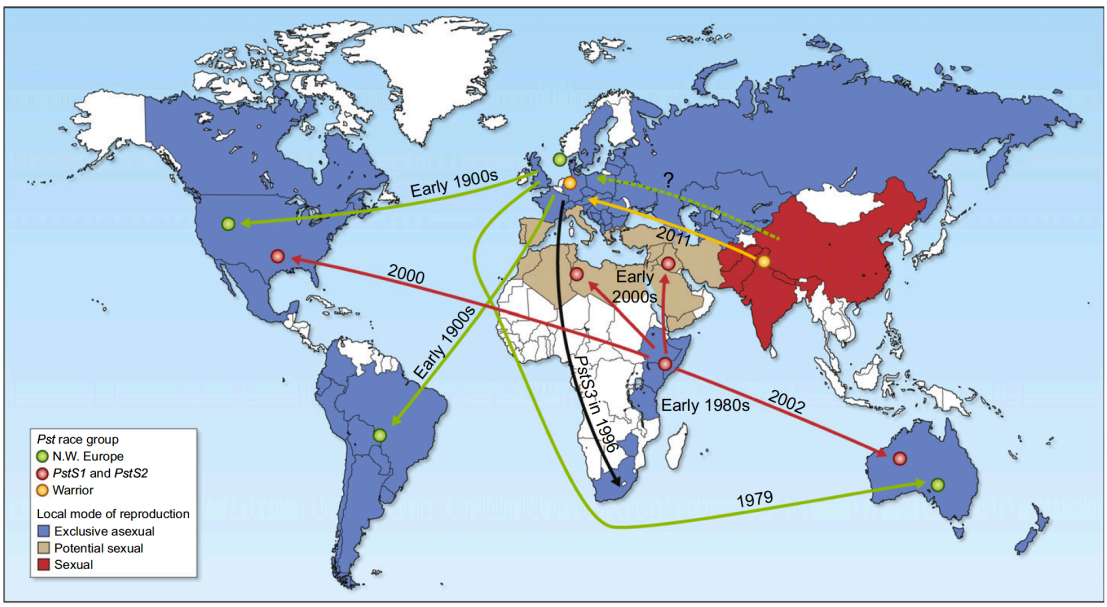

Figure 1.3. Global *Pst* migration. There are three *Pst* race groups. The race group from Europe (represented in green) had the incursion in the early 1900s. The first incursion into Australia (1979) is part of that group. This group is proposed to reproduce asexually. The second race group (represented in red) is divided in the aggressive strains *Pst*S1 and *Pst*S2. This group was thought to be originally produced through sexual reproduction. The third and most recent race group is Warrior (represented in yellow) with origin in the Himalaya region and mainly spread to Europe. There is evidence that this *Pst* race group reproduce sexually in the Himalaya region. Figure taken from (Schwessinger, 2017).

1.1.2 The *Pst* asexual cycle

The asexual cycle represents the agriculturally most damaging form of the pathogen and can be divided into three main phases; colonization, intercellular growth and sporulation (Figure 1.4) (Garnica et al., 2014). Progression of the disease from urediniospore germination to sporulation lasts about 14 days, but sporulation can continue for several weeks. The absence of symptoms during the first 7-8 days of infection makes the disease difficult to control with fungicides, as early detection is necessary for effective treatment. At about 8 days after infection (dai) the infected tissue displays chlorotic spots, and two to six days later spore-bearing pustules erupt through the upper leaf epidermis and can restart the infection.

After urediniospores germinate on the wheat leaf surface, they penetrate stomata to invade the leaf (colonization). Inside the host, they grow as both infectious hyphae and haustoria (Figure 1.4). Towards the end of the cycle, the fungus forms sporogenic structures from the mycelial mass called uredia that produce urediniospores (sporulation). These spore-bearing pustules erupt through the upper leaf epidermis releasing millions of urediniospores, which in turn re-infect the same, proximal host plants, or host plants in long distance. This contrasts with the sexual phase, which for the better-described *Pgt* occurs only once a year if the alternate host is

available. In the following sections the three phases of infection are described in more detail, with particular emphasis on nutrient acquisition.

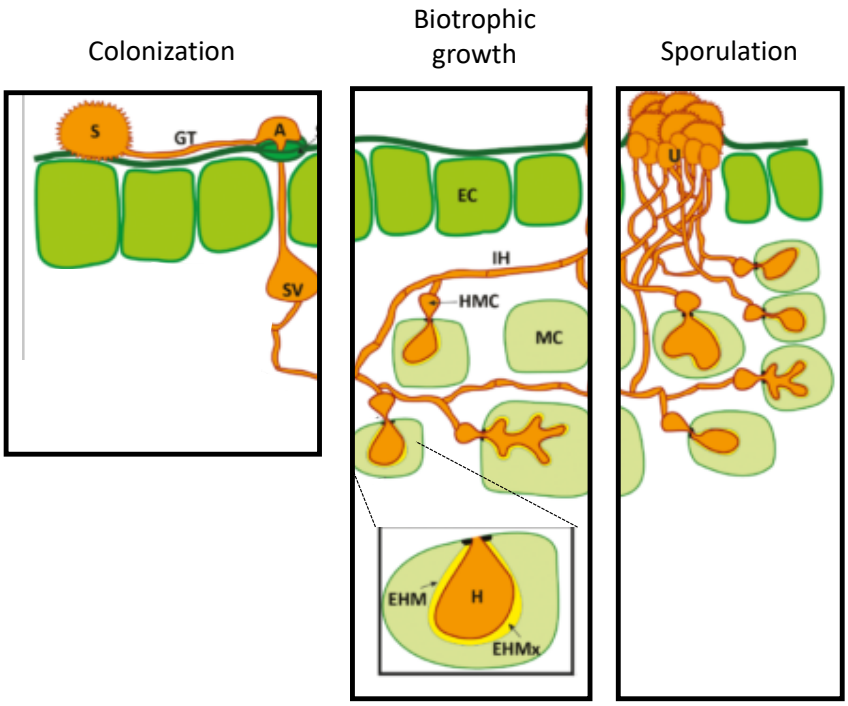

Figure 1.4. The *Pst* asexual infection cycle. The germinating urediniospore (S) produces a germination tube (GT) that grows until it founds a stoma (ST) to penetrate. Once inside the leaf the invading fungus forms a sub-stomatal vesicle (SV) from which infectious hyphae (IH) branch off and explore the apoplast. When hyphae reach a mesophyll cell (MC), they form haustorial mother cells (HMC) and then a complex cellular structure known as the haustorium (H). The fungus extracts nutrients via the haustorium by active transport. Each haustorium is surrounded by an extra-haustorial matrix (EHMx) that lies external to the fungal plasma membrane, and an extra-haustorial membrane (EHM) that is derived but differentiated from the host plasma membrane. The infection cycle is completed within 10–14 days after ramified hyphae form a mycelium and ultimately the spore-forming bodies called uredia (U). Upon maturity, millions of urediniospores erupt through the leaf epidermis forming the yellow-orange pustules characteristic of the disease. Cartoon modified from (Garnica et al., 2014).

1.1.3 Leaf colonization by *Pst*

Pst urediniospores are single-celled dikaryons dihaploid (N + N') with one haploid per nucleus. They are spherical to oval structures, 17 to 20 µm long, and protected by a cell wall composed mainly of chitin. The surface of the spores has ridges and spines which may assist in adhesion to host surfaces (K. Mendgen et al., 1996). Urediniospores can survive for several months in dry conditions and can travel more than 2000 km by wind (Chen et al., 2014). *Pst* urediniospore germination depends on certain environmental and metabolic conditions. Environmental conditions that favour germination include high humidity and relatively low temperatures (0-18°C) (Milus et al., 2009) . Low humidity can block germination. In nature, moisture is provided by rain or dew. The optimum temperature range for germination is between 8-12°C and

germination is halted above 20°C (Vallavieille-Pope et al., 1995). A high density of spores on the leaf surface also inhibits germination, which is attributed to the presence of germination inhibitors within the spores. This is typical for spores and has been demonstrated for rusts, saprophytic fungi and some oomycetes (Allen, 1965). Even under appropriate environmental conditions, urediniospore germination can be affected by an internal condition referred to as the resting state or dormancy; this can be broken in different fungal spores by a heat shock treatment (Allen, 1965). All of these conditions comprise check points for appropriate germination.

Under favourable conditions, urediniospores produce an elongated outgrowth called the germ tube that extends across the leaf until it reaches an open stoma which it uses to gain access to the leaf interior (Figure 1.5),(Bushnell W, 1984). *Pst* urediniospores entry host tissue only via stomata. This process depends on thigmotropism signals, recognition of leaf alcohols by *Pst*, the presence of external plant metabolites that can inhibit spore germination (Daly et al., 1967; Mendgen and Hahn, 2002). Leaf penetration by rust fungi is host specific and likely has co-evolved to the point that monocot pathogens do not efficiently recognise dicot plants as potential hosts. For example, only 12% of *Pt* urediniospore germ tubes located a stomatal aperture on the non-host species *Arabidopsis thaliana* (Shafiei et al., 2007). Conversely, 55% of *Pgt* and 42% of *P. hordei* urediniospore germ tubes were able to locate and penetrate stomata on leaves of the non-host plant rice (*Oryza sativa*) (Ayliffe et al., 2011). These results suggest that rust fungi have specialized to particular hosts.

For germ tubes to successfully locate and penetrate plant stomata, they require sufficient energy from stores within the urediniospore. Urediniospores store high energy molecules including lipids, glycogen and polyols; for example 18-25% of spore weight is due to lipids. These storage products are used by *Pgt* as substrates for catabolism and respiration to release energy. During the first hour of germination, *Pgt* urediniospores lost 6.5% of total initial spore carbon as carbon dioxide production (i.e. as the final product of respiration) (Daly et al., 1967). After seven hours of germination, 80% of the total polyols present in urediniospores were depleted. The sources of urediniospore energy and their mechanisms of release have not been deeply investigated for *Pst* but are likely to be similar to *Pgt* (Garnica et al., 2013). This is based on their up-regulation of genes related to lipids, glycerol and glycogen breakdown which are carbon sources to produce sugars for glycolysis (Daly et al., 1967) This has also been observed in other fungi including *Blumeria graminins* f. sp. *hordei* and *M. oryzae* (Both et al., 2005; Ehrlich and Ehrlich, 1969; Soanes et al., 2012). Spore metabolism during germination must shape the fungal nutrient demand from the host during sporogenesis.

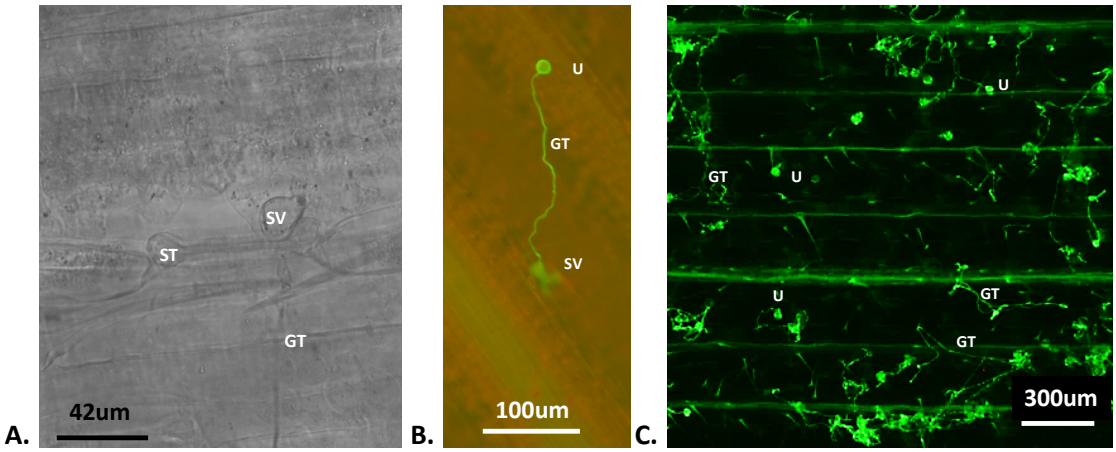

Figure 1.5. Colonization of a wheat leaf by *Pst*. A) A germination tube (GT) locates a stoma (ST) and penetrates the leaf, forming a sub-stomatal vesicle (SV). B) Germination of a urediniospore (U) showing the germ tube (GT) passing through a stoma and formation of a sub-stomatal vesicle (SV) (top view). Fungal structures were stained with fluorescent wheat germ agglutinin (WGA-FITC) to visualise chitin. C) Germinated urediniospores (U) showing long germ tubes (GT) throughout the wheat leaf surface. The vascular tissue of the leaf is visible. Fungal structures were stained with WGA-FITC and viewed by fluorescence microscopy. Images taken by Veronica Roman-Reyna, ANU.

1.1.4 Intercellular growth and sporulation

Once inside the leaf, the cytoplasmic contents of the germ tube migrate to a new vesicle beneath the stoma called the sub-stomatal vesicle (SV) (Figure 1.4 and Figure 1.5). In *Uromyces viciae* the SV develops six hours after infection and can secrete pectinases, possibly as an anti-defence plant response. Mature SVs produce primary infection hyphae. Leaf rust SVs have up to eight nuclei, not all of which migrate to the growing hyphae (Bushnell W, 1984). Secondary infection hyphae ramify from primary hyphae and spread through the leaf intercellular spaces (intercellular hyphae, Figure 1.6A).

Usually, when a hypha contacts a mesophyll cell it forms a vesicle called the haustorial mother cell (Moldenhauer et al., 2006) (Figure 1.6 B). The HMC area that contacts the host cell wall is resistant to proteases, which suggests that it requires a fixed interface to begin penetration (Bushnell W, 1984). A septum forms to protect the HMC cell contents from leakage and a penetration peg develops. The plant cell wall dissolves (by the fungus) at the site of penetration, and the penetration peg pushes on the host cell membrane without piercing it (Figure 1.4). The fungal mitochondria and nuclei move to the tip of the peg, expanding what will become the haustorium. Not all rust fungi have the same number of nuclei in the haustorium, for example *P. coronata* and *P. poarum* have only a single nucleus (Harder and Chong, 1984). The new structure is not truly intracellular because it is not within the host cytoplasm but is separated by the extra-haustorial membrane (see below). The haustorium has a body and a neck region that

connects to the HMC. As the haustorium expands, the HMC vacuole expands and pushes all cellular contents into the haustorium. Immature and mature haustoria vary in their protein, carbohydrate and lipid compositions. For example, only the bodies of mature haustoria possess chitin, whereas immature haustoria body contain other carbohydrates (Bushnell W, 1984).

The haustorium is the key structure underlying biotrophy. It is a complex structure with both fungal and plant origins, highly efficient in nutrient uptake, and its presence seems to modify host metabolism (Voegele et al., 2006). The haustorium is separated from the host cytoplasm by its own plasma membrane, the extra-haustorial matrix (EHMx) and the extra-haustorial membrane (EHM) (Figure 1.4). The EHMx lies between the EHM and the fungal cell wall. EHMx material has not been isolated therefore characterisation of its composition are limited to microscopic and *in situ* cytochemistry studies. The EHMx of *P. coronata* and *Pgt* contain lipids, polysaccharides and proteins of both fungal and host origin. The *Pgt* EHMx does not contain chitin but possesses other fungal polysaccharides that bind to the lectin concavalin A (Bushnell W, 1984). Cellulose can also be found in the EHMx, possibly as a host response to fortify its cell wall. The *Pgt* EHMx has variable electron densities though microscopy that suggests that it changes in composition with haustorial age. Based on the presence of small molecule transporters in the HPM and the diverse material within the EHMx, this matrix seems to facilitate the nutrient uptake by haustoria (Harder and Chong, 1984, 1991; Harder and Mendgen, 1982; Knauf et al., 1989).

The EHM is the host-pathogen interface. Despite the continuity with the host plasma membrane, the EHM is cytological and biochemically distinguishable from the plant membrane from the point where it connects to the haustorial neck. The EHM seems to lack some lipids, proteins and intermembrane particles with respect to the host PM. For example, the EHM lacks phytosterols, aquaporins and the H+/ATPase activity common in membranes (Harder and Chong, 1991; Harder and Mendgen, 1982; Knauf et al., 1989; O'Connell and Panstruga, 2006). Like the EHMx, the EHM composition changes with age; for example, mature *Pgt* EHM contains various glycoproteins not detected in young or immature haustoria (Harder and Chong, 1984). The lack of phytosterols in the EHM is proposed to decrease its flexibility and therefore facilitate the exchange of nutrients and proteins between the host and parasite (O'Connell and Panstruga, 2006).

Other eukaryotic pathogens such as oomycetes and parasitic plants also form haustoria. Two models have been proposed to explain EHM formation. Both propose expansion of the normal cell membrane by addition of membrane material via plant vesicles (Koh et al., 2005). One

suggests that the normal plant membrane is expanded by recycling membrane lipids by endocytosis, while the second hypothesis proposes *de novo* synthesis of plant vesicles to form a new type of membrane (O'Connell and Panstruga, 2006). These hypotheses might help to understand EHM development since their genesis and compositions are not well understood. Also, these ideas could help explain the relocation of plant endoplasmic reticulum, nucleus, mitochondria and Golgi proximal to haustoria (Coffey et al., 1972).

Rust fungi develop intercellular hyphae and haustoria within their hosts (Harder and Chong, 1991). In barley leaves infected with *P. hordei*, haustoria occupy only 19% of the total infected area. For the same pathogen, haustoria seem to be more efficient in hexose uptake than intercellular hyphae. These calculations are based on fungal mannitol turnover and the volume occupied by hyphae and haustoria in the leaves (Kneale and Farrar, 1985). These results suggest that both structures have the capacity to take up nutrients from the host. Clark and Spencer-Phillips, (1993) found that the intercellular hyphae of *Erysiphe pisi* can take up host nutrients. They studied haustorial and hyphal sugar transport using the inhibitor para-chloro-mercuribenzene sulphonic acid (PCMBS), which blocks sucrose uptake by plant cells from the apoplast. Consequently, haustoria will have reduced access to sugars because infected host cells cannot import them. They tracked labelled sucrose by autoradiography and detected it in hyphal fragments with and without PCMBS. A possible role for sucrose uptake by intercellular hyphae might be to provide more energy for spore production. However, there are too few studies on intercellular hyphae to allow a complete understand of their roles in nutrient uptake during infection, and recent studies have focussed on the role of haustoria in nutrient uptake and evasion of plant recognition.

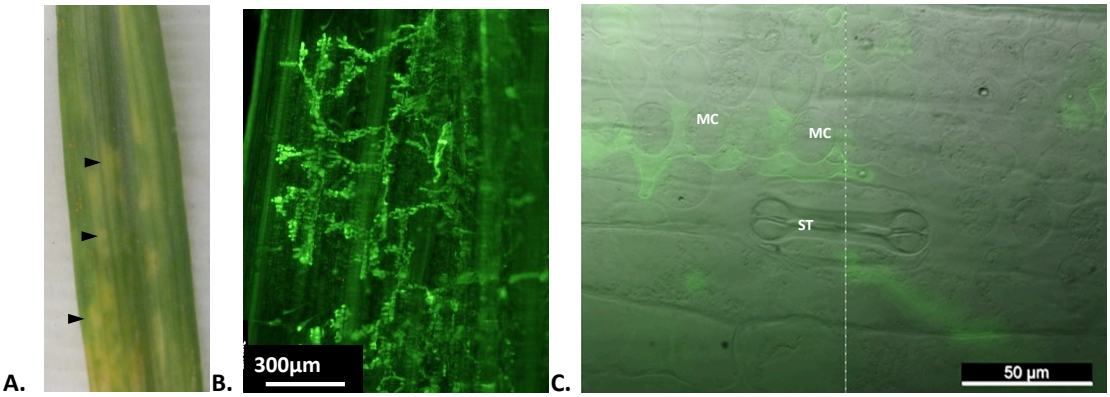

Figure 1.6. The biotrophic growth phase of *Pst*. A) Wheat seedlings 9 dai showing typical chlorotic spots (black arrows) due to *Pst* infection. B) Growth of *Pst* throughout the mesophyll of a wheat leaf viewed from above (light microscopy, chitin stained with WGA-FITC. Bar = 300 µm). C) Infectious hyphae of *Pst* in the wheat leaf mesophyll, top view. The hyphae surround mesophyll cells (MC). In the same view, it is possible to see a closed stoma (ST). Bar = 50 µm. Images taken by Veronica Roman-Reyna, ANU.

The haustoria of biotrophic fungi are believed to be that major sites of nutrient acquisition (Garnica et al., 2014). For rusts, the haustoria of *Uromyces fabae* have been studied extensively. Transcriptomic studies, immunolocalization of nutrient-associated proteins, and accumulation of mitochondria and multi-vesicular bodies in the haustoria support the conclusions that haustoria are metabolically active and that their main function is nutrient uptake (O'Connell and Panstruga, 2006). Early transcriptomic studies from *U. fabae* haustoria revealed a set of *in planta-induced genes* (*PIGs*) expressed only in haustoria and associated predominantly with primary metabolism (Hahn and Mendgen, 1997). For example, the proteins encoded by the *PIGs AAT1*, *AAT2* and *AAT3* (*Amino Acid Transporters*) and a high affinity glucose transporter, *HXT1*, were detected in the haustorial plasma membrane (Mendgen et al., 2000; Voegele et al., 2001). The presence of these transporters in the membrane supports the hypothesis that haustoria actively transport nutrients present in the EHMx. HXT1 from *U. fabae* was biochemically characterized as a glucose and fructose transporter in heterologous systems (Voegele et al., 2001). HXT may act on substrates provided by the fungal invertase INV1 that belongs to a class of enzymes involved in converting sucrose, the main form of sugar present in plants, into glucose and fructose (β-D-fructofuranoside fructohydrolase, EC 3.2.1.26). *INV1* gene expression was detected in intercellular hyphae, and haustoria (Voegele et al., 2006), and the protein was detected in the EHMx. In addition to the presence of many transporter proteins, the *U. fabae* haustorial plasma membrane has higher H^+-ATPase activity than urediniospore membranes (Struck et al., 1996). The H^+-ATPase pumps protons across the fungal plasma membrane to create a gradient that is required for some transporters to function. This suggests that the haustorial plasma membrane is a site of active nutrient transport.

The *U. fabae PIG8* gene encodes mannitol dehydrogenase 1 (MAD1, EC 1.1.1.138), which synthesizes the polyol mannitol by oxidation of fructose (Voegele et al., 2005). This enzyme is present in haustoria and urediniospores. Mannitol has three roles in fungi; for carbon storage, and as a protectant against both osmotic and oxidative stresses (Patel and Williamson, 2016). Mannitol is present at high concentrations in *Pgt* and *U. fabae* urediniospores compared to infectious hyphae (Maclean and Scott, 1976; Voegele et al., 2005). The presence of this enzyme in both vegetative tissues and spores supports the hypothesis that mannitol is a key storage component for rust urediniospores, and is synthesised during intercellular growth (Voegele et al., 2005). Mannitol is an osmotic agent; its presence in the hyphae could promote cell expansion or maintain a hypertonic solution that would induce the movement of water and possibly solutes from the plant to the fungus. Once the fungus extracts glucose from the plant it converts it to mannitol, keeping glucose at lower concentrations in the hyphae and hence a favourable glucose concentration gradient towards the fungus (Patel and Williamson, 2016). MAD1 catalyses both

the forward and reverse reactions. In the forward reaction, the enzyme uses fructose as a substrate to produce mannitol, whereas at high mannitol concentrations as in spores, MAD1 increases fructose abundance to provide energy for germination (Voegele et al., 2005).

The role of haustoria during biotrophic interactions proposed for *U. fabae* was complemented by analysis of *Pst* transcriptomic data (Garnica et al., 2013). Comparing transcriptional profiles of isolated haustoria and germinated spores using next-generation sequencing technology, close homologs of *UfAAT* and *UfHXT* transporters were highly expressed in *Pst* haustoria but very low in germinated spores (Garnica et al., 2013). In the same dataset, all genes encoding enzymes of the pentose phosphate shunt (PPS) were expressed in germinated spores and haustoria. Some intermediates of the PPS are used in nucleotide synthesis (oxidative branch) or energy production through glycolysis (non-oxidative). Garnica et al., (2013) found higher expression of an enzyme, transaldolase, from the non-oxidative branch of PPS in the haustoria transcriptome. They suggested that the enzyme could be part of ribose-5-phosphate synthesis pathway, instead of going to glycolysis. Altogether, these data support the conclusion that haustoria are structures devoted to extraction of nutrients, biosynthesis of macromolecules and antioxidant responses to stress conditions. This type of metabolism was also found in the transcriptomes of the rust fungi *Melampsora larici-populina*, *Phakopsora pachyrhizi*, *Pgt* and *Pst* strains (Dobon et al., 2016; Duplessis et al., 2011; Link et al., 2014). The data suggest that the fungi actively extracts nutrients from the host by up-regulating genes coding for transmembrane transporters and catabolic pathways.

The asexual cycle is complete when the host nutrients extracted in the biotrophic phase are used to produce spores (Figure 1.7). Around 10 days after infection, *Pst* spores erupt from the leaf epidermis, reinfecting the same host or being dispersed to infect other hosts. The nutrients provide enough energy to allow spore germination and infection before they develop new structures for nutrient uptake.

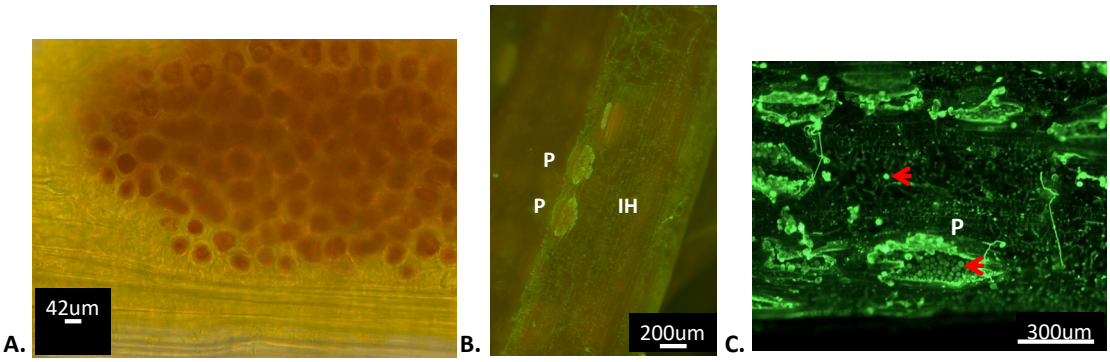

Figure 1.7. Sporulation of *Pst* 14 days post inoculation. A) A single pustule under light microscopy showing orange urediniospores. B, C) Infected leaves stained for chitin with WGA-FITC under light microscopy showing infectious hyphae (IH) and spores erupting from pustules (P). Red arrows indicate spores. Pictures taken by Veronica Roman-Reyna, ANU.

1.2 Physiology and metabolism of wheat

In the previous section, the structures and strategies of *Pst* required to source nutrients from the plant host were described. It is notable that infected leaves are still alive after several cycles of *Pst* sporulation, even when the mesophyll is occupied by the fungus and the epidermis is ruptured. This suggests that infected plants are not nutrient-starved and may continue to produce sugars. To explore the mechanisms through which *Pst* avoids tissue damage, it is first necessary to understand how the plant's physiology changes during development and in response to infection. While rust fungi actively take up nutrients from the plant, few modern transcriptomic or physiological studies have focussed on how the plant responds to this parasitism. Open questions include; does the plant increase the rate of photosynthesis to compensate for removed sugars? Does the infected tissue rely on other carbon sources within the plant to compensate for the changes? These questions are addressed in Chapters 3 and 4 of this thesis.

1.2.1 The life cycle of wheat

The wheat growth cycle has been adapted by human selection to optimize grain yield (Figure 1.8). Wheat is classified into spring and winter wheat, based on to the growing season where they perform better. The life cycle of spring wheat last approximately three to four months; while the life cycle of winter wheat last between six to eleven months. Each part of the life cycle, from germination to grain maturity, uses nutrients differently. Seed germination requires moisture and the carbon reserves accumulated in the previous cycle. After germination, a primary root develops and a coleoptile emerges from the seed to form the growing shoot. During vegetative growth, plants obtain energy from sunlight by day, and at night they metabolise

sugars accumulated during the day by a process called respiration to meet energetic demands. Younger and older leaves have different nutrient demands. Younger leaves require nutrients from older leaves while they build the capacity to produce their own nutrients. When older leaves enter senescence, their nutrients are mobilized to other leaves.

After development of the ultimate leaf (called the flag leaf), the shoot stops growing and flowering begins. A plant is mature once it reaches flowering. This phase is stimulated by cold temperatures in winter wheat or by long day length in spring wheat. The heads hold large numbers of flowers that will produce grains. Grain development relies on mobilisation of plant nutrients. The flag leaf provides 45% of all carbohydrates to the head for grain filling; therefore, fungicides are applied to the flag leaf to reduce crop losses due to fungal infections (Figure 1.9). During head growth, a lot of factors including light intensity, ambient [CO2], temperature conditions and nutrient availability affect photosynthesis, which in turn affects development of the grain. Macro and micronutrient deficiencies promote head abortion or reduce grain size. During the final phase of grain filling most plant undergoes senescence and nutrients are transferred to head.

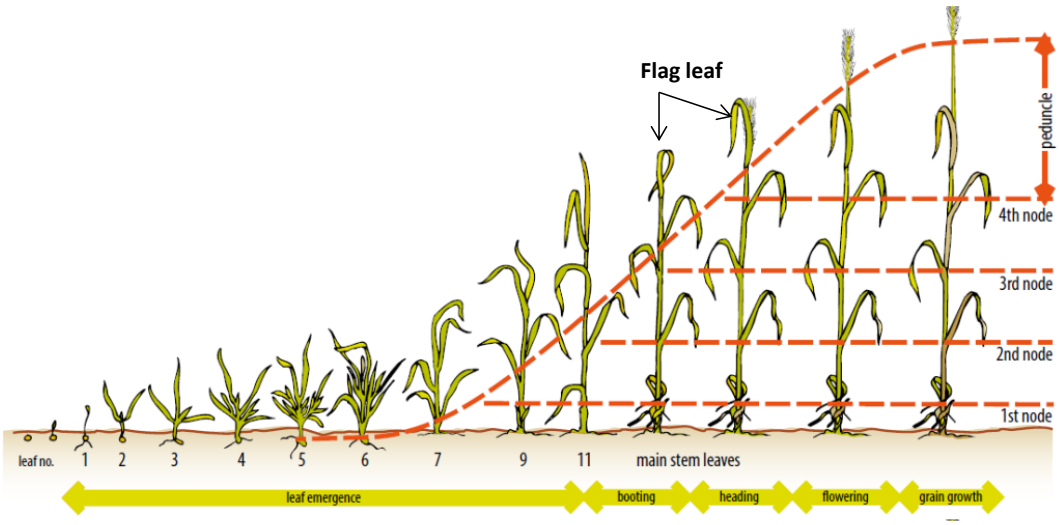

Figure 1.8. The wheat life cycle. In Australia, the first leaf appears in May and the plant grows vegetatively over the next four months. In September the stem stops growing, the flag leaf appears, and the head develops. During October the grain grows and ripens prior to harvesting. Modified from (White and Edwards, 2008).

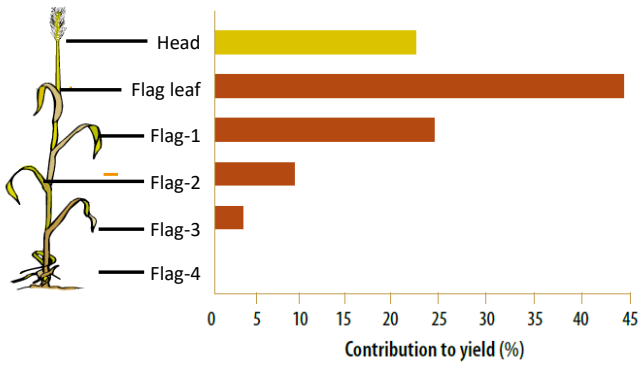

Figure 1.9. The photosynthetic contribution of individual wheat leaves to yield. The flag leaf (the fully-expanded leaf closest to the head) contributes most of the nutrients for head development. The flag leaf makes the largest contribution to grain-filling compared to older leaves (leaves 2-4). In the diagram, flag-3 is the oldest functional leaf and does not contribute to grain filling. The head can also photosynthesise via glumes. Modified from (White and Edwards, 2008).

1.2.2 The light and dark reactions of photosynthesis

Plants capture energy from sunlight to fix carbon into carbohydrates, used ultimately as building blocks for life or as energy intermediates (Tomitani et al., 2006). This process is called photosynthesis. The organelle that mediates this transformation is the chloroplast (Figure 1.10). Chloroplasts are present mainly in the mesophyll and guard cells. Here energy absorption (photon capture) and carbon fixation occurs through interconnected pathways (Taiz and Zeiger, 2010). Thus, three carbon (3C) sugars are produced, which can be stored as macromolecules such as starch or exported to the cytoplasm for carbohydrate metabolism. In the following sections photon capture, carbon fixation, carbon storage and export are described in detail.

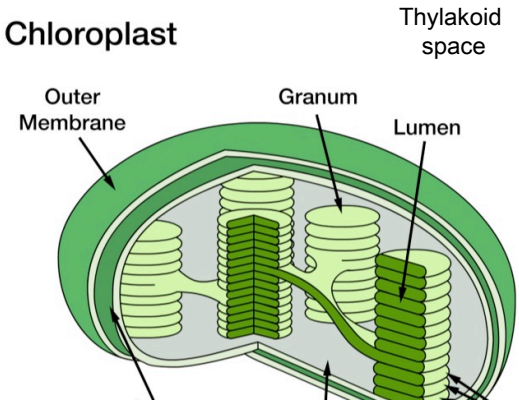

Figure 1.10. Chloroplast structure. The chloroplast is contained by a double membrane. In the lumen (or stroma), there are further membrane-bound compartments called thylakoids which contain membrane proteins for photon capture. The structure of the thylakoid membranes increases the available surface area for photon capture and the light reactions. Several thylakoids together form a granum. There are about 100 chloroplasts per mesophyll cell. Diagram taken from http://www.diagrama.xyz/chloroplast-diagram/

1.2.3 Photon capture by chloroplasts

Photon capture is the most important process in plants; it transforms light into chemical energy to fix carbon (Figure 1.11). The integral membrane protein complexes involved in photon capture are photosystem II (PSII) and photosystem I (PSI), and in the subsequent chemiosmotic process are the cytochrome b6f complex and ATP synthase (Anderson, 1986). These complexes are physically separated in the thylakoid membrane and require the electron carriers plastoquinone (Pq), plastocyanin (Pc) and ferrodoxin (Fd) to move electrons between them. The photosystems are composed of light-harvesting complexes that surround a reaction-centre complex. The light-harvesting complex (or light-gathering antenna) contains various pigments that absorb light energy and transfer it to the reaction-centre. The reaction-centre has a primary electron acceptor called chlorophyll a that absorbs light at 680nm and 700nm respectively. Therefore, chlorophyll a is called P680 in PSII and P700 in PSI.

The first step in photon capture is the absorption of each photon's energy by PSII light-harvesting pigments (Taiz and Zeiger, 2010) (Figure 1.11). This excites the pigment's electrons, transferring its energy to the reaction-centre by resonance energy transfer. Chlorophyll a (P680) absorbs the energy, releasing an electron to start the electron transfer chain. To replace the electron lost by chlorophyll, two water molecules are broken down by photolysis to oxygen (O_2), four hydrogen ions (4 H^+) and four electrons (4 e^-). To continue this electron flow, which is also known as photochemical quenching, Pq receives the P680 electron from the reaction-centre and transfers it to the cytochrome b6f complex. This complex pump four protons into the thylakoid space; two from the chloroplast stroma and two from oxidised plastoquinone. The PSI complex harvests photons via pigments and transfers the energy to P700. P700 becomes excited and releases an electron to $NADP^+$ reductase, carried by Fd. $NADP^+$ reductase uses the electron to reduce nicotinamide adenine dinucleotide phosphate (NADP) to NADPH. The unstable P700 recovers its electron from Pc. The high concentration of protons (H^+) in the lumen, transferred by the cytochrome complex after water hydrolysis, creates a pH gradient across the thylakoid membrane that is exploited by ATP synthase to synthesise adenosine triphosphate (ATP) from adenosine diphosphate (ADP) and Pi.

The main products of photon capture are ATP and NADPH. These molecules are transported to the stroma for carbon fixation. Photon capture is also called the light-dependent reactions, distinct from those required to fix CO_2. Carbon fixation does not require light, and is referred to as the light-independent or dark reactions. Photon capture is affected by environmental and internal conditions, the latter including the integrity of the thylakoid membranes, the pH in the

thylakoid lumen, and the functionality of the thylakoid membrane proteins and electron carriers. If thylakoid membranes are damaged (for example, by freezing or desiccation) the integral proteins will not transfer electrons and protons will not accumulate in the lumen. A basic pH (low availability of protons) of the thylakoid lumen reduces the proton motive force that is necessary for ATP synthase and NADP reductase. On the other hand, energy that accumulates due to the lack of electron transfer is instead released as heat, also called non-photochemical quenching which will be explained in detail in Chapter 3 (Govindjee, 2002). Finally, photosystem proteins and pigments are necessary for electron transport. Some proteins of PSII and chlorophyll are replaced continuously because they are oxidized during electron transfer. If they are damaged and not replaced, this will stop electron transfer which ultimately will affect carbon fixation.

Photon capture is very sensitive to environmental conditions. Light intensity can damage the photosystems because they do not have the capacity to transfer excess electrons. When plants experience high light conditions the excess of electrons oxidizes other PSII pigments to dissipate the energy and protect the photosystem. This is observed as the accumulation of purple pigments in the leaves. Under conditions of light deprivation, plants do not need chlorophyll and its synthesis stops. Therefore, leaves become yellow and their photosynthetic capacity is reduced.

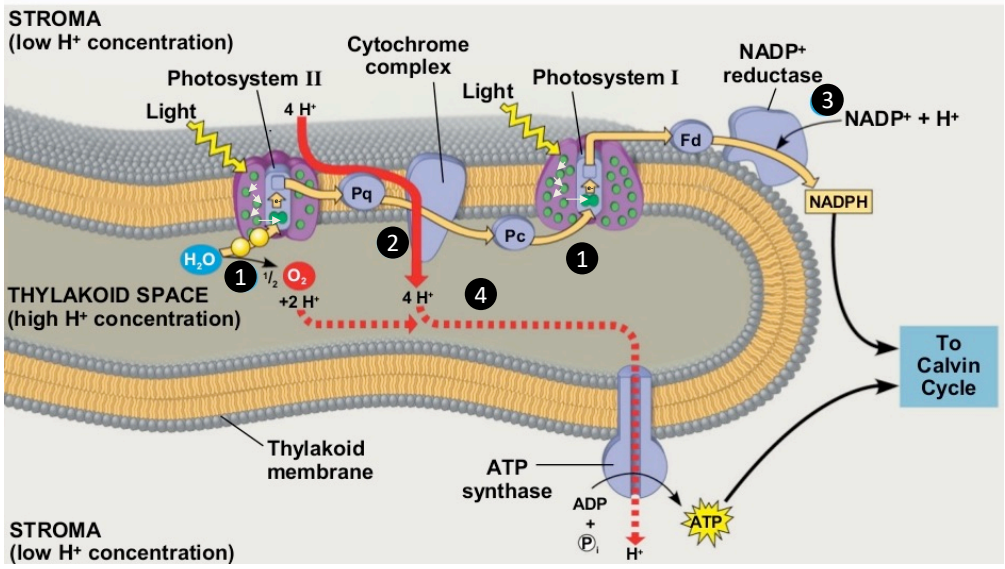

Figure 1.11. **The light-dependent reactions on chloroplast thylakoid membranes**. 1) Photons are absorbed by photosystems II and I. Each complex releases an electron from the reaction centre. The electron lost from photosystem II is replaced by electrons released during water oxidation. The electron from PSI is replaced with the electron from PSII. 2) The electron released from PSII is transferred to the cytochrome complex by plastoquinone (Pq). Here protons from the stroma are transported to the thylakoid space. 3) The electron released from PSI is transferred to $NADP^+$ reductase by ferrodoxin (Fd) for $NADP^+$ reduction. 4) The protons accumulated during the reactions create a concentration gradient that is used by ATP synthase to phosphorylate ADP. ©2011 Pearson Education, Inc.

1.2.4 Carbon fixation in chloroplasts

Carbon fixation occurs in the chloroplast stroma through the Calvin-Benson cycle (Figure 1.12). This cycle uses ATP and NADPH from photon capture to fix CO2 into sugars. The cycle uses five different substrates and as its name implies, they are replaced continuously to maintain CO_2 fixation. The cycle is divided into three phases. Firstly, CO_2 is fixed into an existing five carbon sugar, ribulose 1,5-bisphosphate, by ribulose-1,5-bisphosphate carboxylase-oxygenase (Rubisco). The resulting six-carbon molecule is unstable and it breaks down by hydrolysis into two 3C molecules, 3-phosphoglycerate. In the second phase, the 3C molecules are reduced to triose-phosphate (triose-P) using ATP and NADPH. One triose-P molecule goes to sucrose or starch synthesis, while the other replenishes the cycle. In the third phase, the 5C sugar ribulose-5-phosphate is regenerated from triose-P (Figure 1.12).

The cycle is affected by the conductance of air through stomata, which reflects whether stomata are open or closed. Stomata are the portals for CO_2, water and O_2 exchange for the leaf. High humidity stimulates stomatal opening that increases CO_2-O_2 gas exchange by cells. Rubisco has affinity to both CO_2 and O_2. When CO_2 levels are low, Rubisco has higher affinity for O_2 and the efficiency of Calvin-Benson cycle is reduced. When CO_2 levels are higher, Rubisco activity is limited by the levels of phosphate, ATP and NADPH which are depleted by carbon fixation.

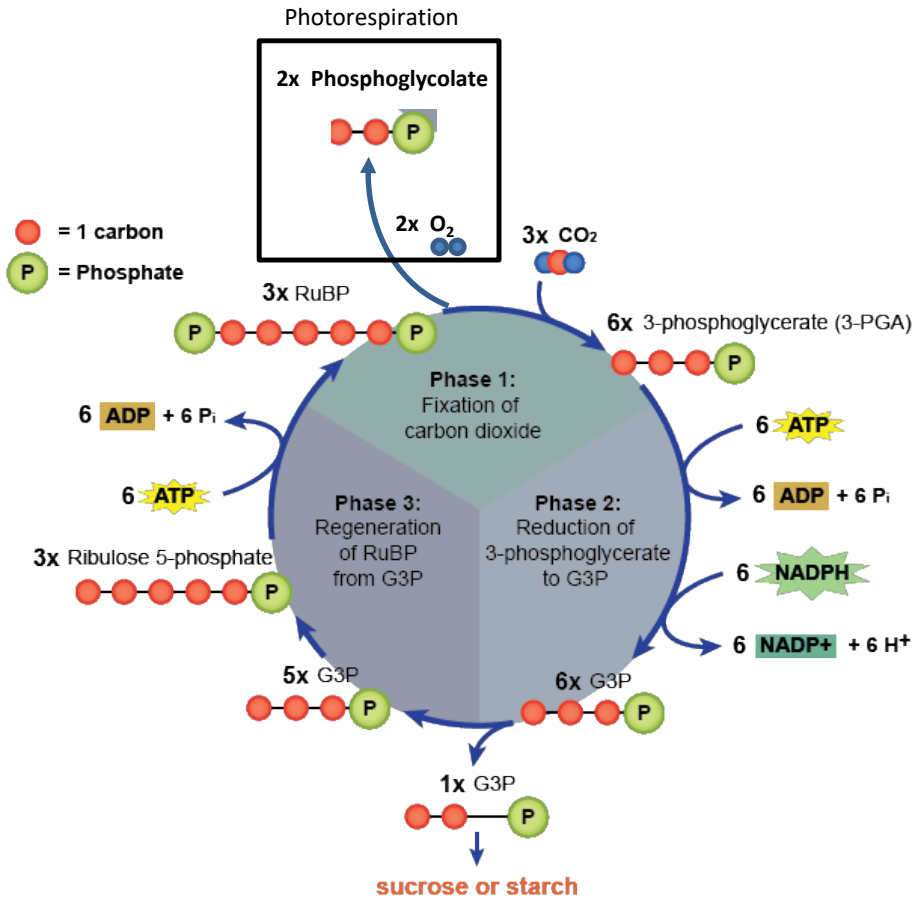

Figure 1.12. The Calvin-Benson cycle. The cycle is divided into three phases. First, CO_2 is fixed into the 5C sugar ribulose 1,5-bisphosphate (RuBP) by the enzyme Rubisco (ribulose-1,5-bisphosphate carboxylase-oxygenase). The new 6C molecule is unstable and splits into two 3C molecules of 3-phosphoglycerate (3PGA). Secondly, 3-PGA is reduced to glyceraldehyde 3-phosphate (G3P) using NADPH and ATP. G3P, also known as triose phosphate, replenishes the cycle and is used in the starch and sucrose synthesis pathways. During the final phase RuBP is regenerated from G3P using ATP. When oxygen levels are high, Rubisco will use RuBP to produce phosphoglycolate which goes into the photorespiration pathway. Taken from **http://www.shmoop.com/photosynthesis/light-independent-reactions.html**

1.2.5 Starch, sucrose and fructans synthesis in plants

The main product of the Calvin-Benson cycle, triose-P, is used in the production of sucrose and starch (Figure 1.13). Starch is a carbon reserve, accumulated during the day when there are more sugars available than needed. Starch is made of long branched chains of glucose and is deposited as granules in the chloroplast. Starch synthesis begins in the thylakoid lumen where two triose phosphate molecules are converted to fructose-1,6-biphosphate by aldolase. One phosphate is then removed to leave fructose 6-phosphate, which is used in turn to produce glucose-6-phosphate. The phosphate on C6 is transferred by isomerase to make glucose-1-phosphate. Glucose-1-phosphate is the substrate for ADP-glucose pyrophosphorylase (AGPase) to produce ADP-glucose (ADP-G) using ATP. AGPase and ADP-G are the main starch synthesis regulators.

Low levels of ADP-G or the oxidized (inactive) form of AGPase reduce starch accumulation. ADP-G is the starting point for elongation of the nascent starch chain by starch synthases which adds further ADP-glucose units. Starch is composed of amylose and amylopectin. Amylose is a linear glucose polymer chains with α(1-4) glycosidic bonds. Amylopectin is a highly branched glucose polymer with α(1-4) and α(1-6) glycosidic bonds. Debranching enzymes including amylases and amylopectinases break starch down into maltose (two glucose units). Maltose is then exported to the cytosol, or broken into glucose within the chloroplast. Starch breakdown usually occurs at night to provide glucose for glycolysis. In cereals, starch represents 90% of the grain dry weight.

Starch metabolism is regulated not only by the enzymes mentioned above but also by inorganic phosphorus (Pi) levels and the concentrations of certain sugars. Chloroplastic triose-P levels and the cytoplasmic Pi concentration regulate starch synthesis. The triose phosphate/phosphate translocator (TPT) located in the chloroplast membrane requires Pi to export triose-P to the cytosol (Figure 1.13). The TPT regulates movement of carbon from the chloroplast to the cytoplasm as a starting point for various metabolic processes. When cytoplasmic Pi decreases, triose-P is not exported and accumulates in the chloroplast. High triose-P levels stimulate starch synthesis. Lower cytoplasmic Pi levels are associated with increased levels of phosphorylated sugars such as fructose and glucose (Smith and Stitt, 2007; Trevanion, 2002).

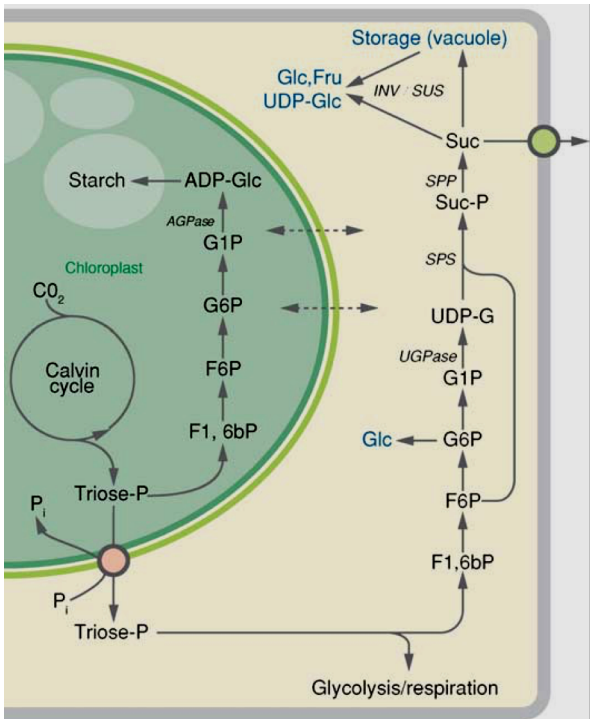

Figure 1.13. Sucrose and starch synthesis. Starch synthesis occurs in the thylakoid space where two molecules of triose-P are converted to fructose-1,6-biphosphate (F1,6bP), then to fructose 6-phosphate (F6P), then to glucose 6-phosphate (G6P), and finally to glucose 1-phosphate (G1P). The enzyme ADP-glucose pyrophosphorylase (AGPase), the control point for starch synthesis, produces ADP-glucose (ADP-Glc), the backbone of starch. Sucrose is synthesized in the cytoplasm where UDP-glucose pyrophosphorylase (UGPase) produces UDP-glucose (UDP-G). UDP-G and F6P are combined by sucrose-phosphate synthase (SPS) to produce sucrose-phosphate (Suc-P). Sucrose-phosphatase (SPP) removes the phosphate from Suc-P. Sucrose (Suc) then is exported to other tissues, stored in the vacuole, or used as a source of hexoses. Picture from (Rolland et al., 2006).

Triose-P is exported to the cytoplasm for sucrose synthesis. Sucrose is a dimer (disaccharide) of fructose and glucose that is stored in the vacuole and transported to distal organs with high demand for catabolic processes. Starch and sucrose have identical pathways for synthesis from triose phosphate to glucose-1-phosphate, but diverge thereafter. The starch pathway uses AGPase for subsequent steps, whereas the sucrose pathway uses UDP-glucose pyrophosphorylase (UGPase) to produce UDP-glucose from G1P. UDP-glucose is the substrate for both sucrose and cell wall synthesis. The enzyme sucrose-phosphate synthase (SPS) uses UGP-glucose and fructose-6-phosphate to produce phosphorylated sucrose. Sucrose (dephosphorylated by sucrose-P phosphatase (SPP)) is metabolically inert and for this reason is the main photosynthesis product that is transported throughout the plant.

Sucrose is the substrate for production of several carbohydrate compounds. Two of these are fructans and raffinose. Fructans are fructose polymers, and raffinose is a trisaccharide composed of galactose, glucose and fructose. Fructans are more abundant than starch in 15% of flowering plants, while raffinose is present in all plants. In wheat and barley, the most common fructan is

6-kestotriose, which is composed of one unit of glucose and two units of fructose. Synthesis of 6-kestriose requires the enzyme sucrose:fructan 6-fructosultransferase (6-SFT) to add fructose to sucrose. Degradation of fructans requires the enzyme fructanexohydrolases (FEHs) which hydrolyses the terminal fructose, thus releasing sucrose. For raffinose, the enzyme raffinose synthase adds galactinol to sucrose. The role of fructans and raffinose is mainly as vacuolar carbohydrate reserves. Fructans are also involved in flowering and stress tolerance responses. In wheat, high levels of fructans accumulate in leaf sheaths and stems. Raffinose is a phloem-mobile molecule, like sucrose, which means that it can be transported to demanding tissues (Valluru and Van den Ende, 2008; Van den Ende, 2013).

Sugars are stored in soluble forms such as sucrose, fructans and raffinose, or insoluble as starch. Sugar storage can be for short or long periods of time. In general, starch accumulates in the stems for short periods (hours or days) as a close and rapid sugar reserve for the entire plant. Long term storage (months or years) occurs in fruits and tubers. Sugar reserves change depending on metabolic demand, during organ development, and under stress conditions. For example, starch is used mainly at night, while soluble reserves are used during days and nights. Soluble sugars increase during cold stress for frost protection, because they can work as osmoprotectants to avoid membrane damage. In wheat, synthesis of starch and fructans precursors increases during flowering to provide nutrients to the head.

1.2.6 Nitrogen metabolism in plants

Nitrogen is a fundamental nutrient in biology. Together with carbon, nitrogen is a core component of enzymes and structural molecules including amino acids and proteins, Rubisco, cell wall components and secondary metabolites. Nitrogen is a limiting nutrient for plant biology and is taken up mainly by roots as nitrate (NO_3^-). Nitrate then is transported to the chloroplast or stored in the vacuole. In the chloroplast, nitrate is used for glutamine and glutamate synthesis, which are the starting points for several amino acid synthesis pathways and play central roles in nitrogen transport (Gaufichon et al., 2010). Importantly, both photon capture and the Calvin-Benson cycle require large amounts of nitrogen. Rubisco and chlorophyll synthesis together use 50% of the nitrogen taken up by the plant. An alternate pathway for amino acid synthesis is through photorespiration. This occurs when Rubisco uses oxygen instead of CO_2 and produces phosphoglycolate instead of 3-PGA (Figure 1.12). This substrate is transported to the peroxisomes, a plant organelle, that uses it to produce glycine and serine.

The mobile forms of nitrogen in the phloem (analogous to sucrose for carbon) are amino acids, mainly asparagine. The metabolism of carbon and nitrogen is interlinked; therefore, many physiological studies report C/N ratios. Increasing the carbon supply induces nitrogen uptake, while nitrogen deficiencies cause leaf yellowing and reduce growth capacity. In wheat crops this balance is important since 60% of total nitrogen is taken up by roots during stem elongation and head emergence.

1.2.7 Source and sink relationships in plant organs

The previous section described chloroplast pathways involved in sugar metabolism in a single cell. However, the role of sugars should be studied in the context of the whole plant. Sugars and certain nitrogenous compounds are signal and energy molecules that respond to environmental and systemic stimuli, connecting the whole organism (Smith and Stitt, 2007) and linking abundance with need. Carbon and nitrogen metabolism is tightly coordinated to provide balance and respond to the metabolic requirements of different plant organs (Stitt and Zeeman, 2012). Sugars and nitrogenous compounds, among other molecules, regulate plant growth, flowering and allocation of nutrients (Stitt and Zeeman, 2012).

Each plant organ has a characteristic metabolism with different requirements not only for sugars but also for amino acids and water, here referred to collectively as “nutrients”. Within a plant organ nutrient requirements also change during development. Plant organs are either sink or source, where photosynthetic source organs provide nutrients to sink (non-photosynthetic) organs (Figure 1.14). Typically, leaves provide carbon to roots and shoots. For wheat, the flag leaf provides around 45% of the total carbon to the developing head for grain filling. Leaves are not the only photosynthetic tissue; any green part is. For example, wheat sheaths and glumes also fix carbon.

The first step for nutrient transport throughout the plant is phloem loading (Figure 1.14). This occurs in source organs, or mesophyll cells, where amino acids and sucrose enter the vascular plant tissue, specifically the phloem (Taiz and Zeiger, 2010). Within the phloem, nutrients are transported through sieve elements, which are elongated cells with perforated walls. Sucrose concentrations increase during phloem loading, inducing water movement from xylem (vascular tissue) to the phloem by osmosis. This flow makes turgor pressure higher in source organs and lower in sink tissue. The pressure causes movement from source to sink. The two mechanisms for phloem loading are symplastic and apoplastic loading. The symplast is the inner side of the plasma membrane while the apoplast is the outside space of the membrane. Symplastic loading

uses plasmodesmata, channels that traverse the cell wall and connect to the cell cytoplasm. Sucrose is translocated by plasmodesmata to sieve elements by diffusion. Another plant strategy is to convert sucrose into raffinose in the companion cells (Van den Ende, 2013). These cells lie between mesophyll cells and sieve elements. This strategy is called polymer trapping because raffinose, which is a bigger molecule than sucrose, will not cross plasmodesmata in the reverse direction. Raffinose will be loaded into sieve elements and will help to maintain the sugar flow.

Compared to the symplastic mechanism, apoplast loading is energetically more demanding because it goes against a concentration gradient (Taiz and Zeiger, 2010). Sucrose is loaded from the cytoplasm into the apoplast and actively taken up by phloem transporters. Two types of transporters are involved in loading sucrose into the phloem. One is the sucrose uptake transporters (SUT) from the major facilitator superfamily (MFS) transporters. The other is Sugars Will Eventually be Exported Transporters (SWEETs) from the MtN3 family (Eom et al., 2015). SUT are symporters that require protons (H+) to move sucrose. They localize in the plasma membrane of companion cells and in the tonoplast membrane. SWEET transporters move sucrose from the phloem parenchyma to the apoplast, where it can be taken up by SUT in the companion cells. Sucrose accumulates in high levels in companion cells, after which it is loaded in to sieve elements to transport to other parts of the plant.

Once nutrients are in the phloem, they move throughout the plant to an area of lesser concentration. The final step in nutrient transport from source to sink cells is phloem unloading. This is the transport from sieve elements and companion cells to sink cells. Sucrose in companion cells is released through plasmodesmata, or is taken up from the apoplast by SWEET and SUT transporters. Sucrose concentrations are low in sink organs to maintain the sucrose flux from source organs.

Sucrose metabolism is controlled mainly by invertases (INVs), hexokinases (HXKs) and hexose transporters. These work together in sink tissue by increasing hexose concentrations, and are partly responsible for the transition from sink to source (Granot et al., 2013; Roitsch and González, 2004). Hexose levels increase with higher levels of INVs. For example, apoplastic INVs help in the unloading process by hydrolysing sucrose into fructose and glucose. This reduces the sucrose concentration in sink cells thus maintaining the flux of apoplastic sucrose to sink organs. Plant INVs with different pH optima are also present in the vacuole and cytoplasm (Table 1.1). Higher levels of hexoses up-regulate genes coding for HXK and fructokinases (FRK); these irreversibly phosphorylate glucose and fructose to glucose 6-phosphate and fructose 6-phosphate respectively. Phosphorylation ensures that hexoses are not exported to other cells

but instead feed metabolic pathways, including glycolysis, respiration and cell wall synthesis (Granot et al., 2013). Hexose levels are also regulated by hexose transporters (HXT). Plant HXTs belong to the MFS family, and like SUT they are proton symporters. They are present in the plasma membrane and membranes of several organelles, moving hexoses and changing their concentrations in different compartments. For example, they move apoplastic hexoses inside the cell after sucrose hydrolysis and move cytoplasmic hexoses to the vacuole and to plastids (Granot et al., 2013).

In summary, plant nutrient transport changes during development to fulfil the demand of sink organs. The flux is regulated by gradients of nutrient concentrations and water potential. Nutrients taken up by sink organs are used for cell growth and development, and for carbon storage. Invertases, hexokinases and hexose transporters regulate sucrose metabolism in sink and source organs. Their activities change the hexoses to sucrose ratios, which define the developmental stage of the organ and the transition from sink to source. Sink organs have higher levels of hexoses stimulating import of sucrose for anabolic metabolism. When sucrose increases over hexoses, sink organs transition to source, increasing their photosynthetic rates and exporting nutrients to more demanding organs (Braun and Slewinski, 2009).

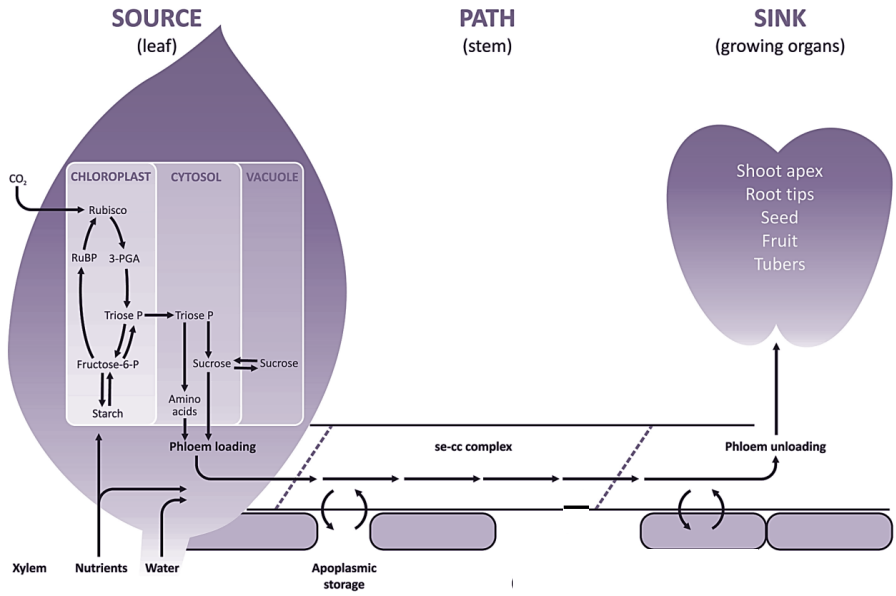

Figure 1.14. Source and sink nutrient dynamics in plants. Source tissues fix carbon through the Calvin-Benson cycle to produce triose phosphate that can be used for starch synthesis in the chloroplast, or exported to the cytoplasm where it is a substrate for sucrose and amino acid synthesis. Sucrose can be stored in the vacuole, or exported along with amino acids to sink tissues via the phloem. Nutrients are loaded from apoplast and symplast to sieve element—companion cell (se—cc) complexes of the phloem. These mechanisms are referred to as phloem loading and unloading. Modified from http://plantsinaction.science.uq.edu.au/book/export/html/23.

Table 1.1. The plant invertases. Adapted from (Roitsch and González, 2004)

Types invertases	Optimum pH	Localization
Vacuolar invertase	5.0–5.5	Vacuole
Cell wall invertase	3.5–5.0	Apoplast
Neutral invertase	6.8 and 8.0	Cytoplasm, mitochondria and plastids

1.3 Plant immunity

The previous sections describe fungal development and plant physiology, wherein the major aim of fungal pathogenicity is to take nutrients from the host, whereas plants need energy to produce seeds. These antagonistic purposes conflict during plant-pathogen interactions. The host can recognize the pathogen and trigger responses to reduce pathogen growth. Pathogens have evolved mechanisms to avoid recognition or manipulate host responses. These dynamics can be explained based on external or internal host immune receptors. This section provides an overview of plant-pathogen interactions; however immunity is not the central topic of this thesis.

Many plant pathogens are perceived at the host plasma membrane. Here plant immune receptors (called pattern recognition receptors, PRRs) recognize conserved molecules known as pathogen-associated molecular patterns (PAMPs). For example, chitin, a conserved molecule in fungal cell walls, is recognized by the receptor lysin motif receptor kinase 5 (AtLYK5) in Arabidopsis and by the receptor CEBiP (chitin-elicitor binding protein) in rice (Cao et al., 2014; Hayafune et al., 2014). In both cases the interaction triggers downstream defence responses to reduce fungal growth (Miya et al., 2007; Shimizu et al., 2010). CERK1 is also involved in the recognition of bacterial peptidoglycans, components of bacterial cell walls, as *cerk1* mutants are more susceptible to bacterial infection (Gimenez-Ibanez et al., 2009). After plant membrane receptors recognize pathogen molecules they activate downstream signaling. Some of these downstream signals include the generation of reactive oxygen species (ROS), induction of mitogen-activated protein kinase (MAPK) pathways, changes in plant hormones, and activation of transcription factors (Dodds and Rathjen, 2010). Recognition also induces accumulation of callose, a plant polysaccharide, to reinforce the plant wall and reduce fungal or bacterial access to the cell. These defence responses create a harsh environment for the pathogen to reduce its growth, or trigger cell death to stop further colonization.

Pathogens have evolved means to evade or suppress plant defence responses. One general strategy is by secreting virulence proteins called effectors. Effectors are pathogen-encoded proteins that are secreted into plant apoplast or cytoplasm, which target plant molecules to facilitate pathogen fitness. For example, the apoplastic effector Pep1 (Protein essential during

penetration-1) from the biotrophic fungus *U. maydis* (see Box 1) inhibits ROS generation to allow fungal establishment in neighbouring cells (Hemetsberger et al., 2012). Effectors that are recognised by plant receptors triggering defence responses are called avirulence (Avr) proteins. Some well characterized apoplastic effectors are from the biotrophic tomato leaf mould fungus *Cladosporium fulvum* that infects tomato. From this pathogen, the apoplastic effector AVR2 inhibits host proteases while AVR4 inhibits host chitinases (De Wit, 2016). These effectors are recognized by the cell surface receptor-like proteins (RLP), Cf-2 (C. *fulvum*-2) and Cf-4 respectively, leading to host resistance (De Wit, 2016).

Plant pathogens not only secrete proteins into the apoplast but also into the host cytoplasm. Some plant pathogens can manipulate host gene expression to increase nutrient availability. The bacterial pathogen *Xanthomonas oryzae* pv. *oryzae* which causes rice blast disease secretes PthXo1, a transcription activator-like (TAL) effector, which targets the promoter of the *OsSWEET11* transporter gene in rice, increasing apoplastic glucose levels for bacterial uptake (Chen et al., 2010). The TAL proteins among other bacterial effectors are delivered to the host cell by the type III secretion system (T3SS) upon the recognition of a secretion signal peptide embedded in the effector. The T3SS forms a needle-like structure to penetrate the host plasma membrane (Cunnac et al., 2009). For haustorial (biotrophic) fungal pathogens, haustoria are believed to be responsible for the delivery of intracellular effectors. This is supported by transcriptomic studies in *M. lini*, *B. graminis* f. sp. *hordei* and *U. fabae*, where some genes are only expressed in infected tissue or in haustoria. This expression pattern suggests that they could have roles in nutrient acquisition or defence suppression (Catanzariti et al., 2006; Kemen et al., 2005; Ridout et al., 2006). Six genes that encode effectors have been identified from rust fungi, including *AvrL567*, *AvrM*, *AvrP123* and *AvrP4* from the flax rust fungus *Melampsora lini*, *Uf-RTP1* from *U. fabae*, and *GTAUSPE-10-1* from *Pgt* (Catanzariti et al., 2006; Dodds et al., 2004; Kemen et al., 2005; Upadhyaya et al., 2013). Flax rust effectors are translocated from haustoria to the host cytoplasm where they are recognized by host receptor proteins. This is based on indirect data from haustorial transcriptomic and defence responses in flax plants (Catanzariti et al., 2006; Dodds et al., 2004). On the other hand, Uf-RTP1 is the only effector directly shown to be translocated to the host cytoplasm (Kemen et al., 2005). The proposed function for RTP1 is to protect the haustorium from host defences by stabilising host cells (Kemen et al., 2013). The *Pgt* effector GTAUSPE-10-1 gives a cell death response only when expressed in a wheat line carrying the resistance gene *Sr22*; this suggests that it is potentially an Avr protein (Upadhyaya et al., 2013). The types of effectors secreted varies depending on the pathogen lifestyle. Fungi that take nutrients from dead cells (such as saprotrophic, necrotrophic and hemibiotophic fungi) secrete plant cell-wall degrading enzymes, whereas the genes encoding these types of enzymes

are reduced in biotrophic and symbiotic fungi due to their need to keep their hosts alive. Interestingly, obligate biotrophs have higher number of predicted effectors compared to fungi with alternate lifestyles (Presti et al., 2015).

Intracellular effectors can be recognized specifically by cytoplasmic resistance (R) proteins that trigger strong defence responses with cell death. Such R proteins canonically possess nucleotide binding and leucine-rich repeats domains (NB-LRR), but other N- and C-terminal domains are known and important for function (Gururani et al., 2012). Two classes of NB-LRR protein are separated by the presence of alternate N-terminal toll/interleukin-1 receptor/resistance (TIR) or coiled-coil (CC) domains, both of which seem to mediate downstream signalling (Bernoux et al., 2011; Cesari et al., 2016). Conformational changes in the NB and LRR domains activate defence responses after recognition of a pathogen's Avr component. Recognition follows a gene-for-gene model because *R* and *Avr* genes tend to be polymorphic in hosts and pathogens respectively (Flor, 1971). Binding (recognition) of an effector can be direct, or indirect mediated by an accessory protein (Elmore et al., 2011). Interestingly, R proteins can also be susceptibility factors for necrotrophic pathogens; in oats, the NB-LRR gene *Pc2* confers resistance to the biotroph *P. coronata* but susceptibility to the necrotrophic fungus *Cochliobolus victoriae*. In the latter interaction, *Pc2* triggers cell death which is a requirement for fungal colonization (Mayama et al., 1995), but also impedes the infection of biotrophs (Cook et al., 2015).

1.3.1 Adult plant resistance to wheat rust fungi

Genetic resistance to wheat rusts may be conferred by race-specific *R* genes or adult plant resistance (*APR*) genes (Griffey, 1993). Race-specific resistance is conferred by single major *R* genes and is active throughout development from the seedling stage. For this reason, it is also referred to as whole plant resistance. *R* genes are widely used in crop breeding programs to protect against pathogens of all classes (Wellings, 2007). However due to the strong selective pressures that they place upon pathogens, a single *R* gene is easily overcome. For example, in Australia more than 20 stripe rust *R* genes were overcome between 1979 and 2006. One strategy to sustain effective resistance is *R* gene pyramiding or stacking, which means combining several resistance genes with the same specificity or spectrum of action within the same variety (Ellis et al., 2014). This strategy has been used for over 10 years in plant breeding and can also have an additive effect on defence responses.

APR is active only in adult plants. The resistance phenotype of such genes is partial or quantitative, and is typically observed as reduced spore production (slow rusting) compared to

susceptible wheat cultivars. In contrast to *R* genes, *APR* seems to be more durable, and so far as is known such genes do not encode NB-LRR proteins (Ellis et al., 2014; Krattinger et al., 2009). The wheat *APR* genes *Yr18* (also named as *Yr18*), *Yr36* and *Yr46* (also named as *Yr46*) have been cloned and code for a putative ATP-binding cassette (ABC) transporter, a wheat kinase start1 (WKS1) and an H^+/hexose symporter, respectively. *Yr18* expression is more abundant in the leaf tip than the leaf base. *Yr18* alleles are expressed in both susceptible and resistant lines, and both the resistant and susceptible forms of the gene have the same promoter. The proposed mechanisms of the *Yr18* resistant form is to trigger senescence signals in the flag leaf tip or to export toxic compounds to the fungus (Krattinger et al., 2009). Recently, it has been suggested that the role of *Yr18* in wheat seedlings might be associated with overexpression of abiotic stress-response genes (Rinaldo et al., 2017). Similar to *Yr18*, *Yr46* alleles are expressed in susceptible and resistant lines and have the same promoter (Moore et al., 2015). The *Yr46* protein belongs to the sugar transport protein 13 (STP13) family, contains 12 predicted transmembrane helices and can transport glucose. Two non-synonymous mutations in the transmembrane domains change the protein to the resistant form, and also decreases the glucose transport rate in the heterologous system yeast (Moore et al., 2015). It is proposed that *Yr46* reduces the levels of apoplastic glucose in infected leaves (Moore et al., 2015). The *Yr18* and *Yr46* genes are associated with a similar leaf tip necrosis phenotype that is best observed in the flag leaf of adult plants under field conditions. *Yr18* and *Yr46* confer partial resistance to *Pst*, *Pgt, Pt* and *Blumeria graminis* f. sp. *tritici*, while *Yr36* confers partial resistance only to *Pst* (Gou et al., 2015; Spielmeyer et al., 2013). The Yr36 protein contains a serine/threonine protein kinase domain and a lipid-binding domain (StAR-related lipid-transfer, START) domain. WKS is a chloroplast protein, encoded in the nucleus, that phosphorylates wheat thylakoid-associated ascorbate peroxidase (tAPX) to keep peroxide levels high during infection. As a consequence, it triggers cell death and reduces rust growth (Gou et al., 2015). The expression of *APR* genes at the adult stage only, their slow-rusting phenotypes, and their broad spectrum of anti-pathogen action, suggest roles for plant development and metabolism in susceptibility. To my knowledge by the time of my research, there are no studies that are explicitly focussed on the relationships between plant development and APR.

1.3.2 Plant defence responses during infection with biotrophic pathogens

Infection by microbes triggers the production of defence-related molecules including hormones, changes in the host transcriptome and metabolism, and chemically-reactive radicals, among other responses not covered in this thesis. These responses may appear early or late during infection to create a toxic environment for pathogens or to trigger expression or repression of

defence-related genes. However, these defence pathways are targeted by pathogen effectors to allow infection, creating a dynamic environment of host and pathogen suppression and induction responses.

Salicylic acid (SA) is a phenolic compound which regulates plant defence against biotrophic pathogens. For example, when cereal millet is pre-treated with SA and then infected with the rust fungi *Puccinia substriata* the number of pustules is reduced compared to untreated controls (Crampton et al., 2009). Similarly, *U. fabae* infections are reduced when SA is applied to broad bean. Moreover, *U. maydis* secretes two SA-degrading effector proteins that are induced during pathogenic growth, showing the importance of this hormone to defence against biotrophs (Rabe et al., 2013; Rauscher et al., 1999).

Jasmonic acid (JA) is another hormone that is involved in host defence responses. In contrast to SA, JA is associated with resistance to necrotophic pathogens and insects. The SA and JA pathways are antagonistic. SA and NPR1 suppress JA synthesis (Antico et al., 2012). JA is derived from fatty acids (α-linolenic acid) present in the chloroplast. Plant stress (amongst other signals) induces JA synthesis, and JA conjugated to isoleucine (JA-Ile) interacts with the cytoplasmic receptor proteins COI and JAZ. Together, these proteins de-repress MYC2, a transcription factor that activates expression of defence-related genes (Chini et al., 2007; Turner et al., 2002). JA does not affect rust infections consistent with its role as a necrotrophic defence response (Crampton et al., 2009).

Reactive oxygen and nitrogen species are generated as part of plant defence responses. The free radicals O_2, H_2O_2 and nitric oxide (NO) work cooperatively with calcium to activate immunity associated genes and cell death (Delledonne et al., 1998). ROS are produced by peroxidases and respiratory burst oxidases (RBOH); while NO is produced by nitrate reductase and nitric oxide synthases (NOS). ROS and NO are produced in the cytosol, chloroplasts and peroxisomes, and can work together to reduce pathogen growth. For example, cereals produce NO and H_2O_2 when infected by biotrophic fungi (Guo et al., 2004; Prats et al., 2005). These radicals reduce penetration and haustoria formation by creating a toxic environment and inducing host death in infected cells (Orczyk et al., 2010; Prats et al., 2005). Similarly, NO reduces *Pst* growth in wheat by inducing the enzyme phenylalanine ammonia-lyase (PAL), which is associated with secondary metabolite production (Guo et al., 2004). Overall hormones and chemically-reactive radicals are defence responses triggered differentially according to the biology of the pathogen and the progression of the infection. Likewise, pathogens suppress specific defence responses via effectors to ameliorate toxic environments and promote their growth via nutrient acquisition.

1.3.3 Plant physiological responses during infection by biotrophic pathogens

Biotrophic interactions affect the photosynthetic pathways that were described above in Section 1.3.2. They can alter photon capture efficiency, the carbon fixation cycle and sink-source distribution of nutrients. *Ustilago maydis* infections shift the metabolism of the infected tissue radically to sink by increasing hexose and amino acid levels, causing nutrient import from healthy leaves and tumors in infected leaves. This changes leaf metabolism by down-regulating light reactions (photon capture), carbon fixation, SA synthesis and nitrogen assimilation pathways (Doehlemann et al., 2008; Horst et al., 2008, 2010a). Wheat, oats and barley have lower levels of chlorophyll when they are infected with *Pst*, *P. coronata* var. *avenae* and brown rust respectively (Calonge, 1967; Chen et al., 2015b). Interestingly the tissue immediately surrounding the infection with crown rust has higher levels of chlorophyll and photosynthesis rates. This pattern is known as a "green island" and suggests that non-infected leaf tissue supplies nutrients to infection sites (Scholes and Rolfe, 1996).

Chlorophyll reduction is also a consequence of damage to the components of the photon capture pathway. The complex that is most affect by such damage is photosystem II (PSII). In stress conditions, PSII produces ROS and can disassemble, changing the concentration and dynamics of chlorophyll photon absorption. This has been reported for broad bean and barley infected with bean rust and powdery mildew, respectively (Peterson and Aylor, 1995; Swarbrick et al., 2006). When photon capture is damaged, less ATP and NADPH are available for carbon fixation; consequently, the cycle cannot fix CO_2 efficiently. Cereal rust infections also reduce stomata opening and CO_2 fixation rates (Carretero et al., 2011; Livne, 1964; Mitchell, 1979; Owera et al., 1981; Scholes and Rolfe, 1996). However the CO_2 fixation rates were higher in a susceptible wheat line 48 h after infection with *Pst* (Chang et al., 2013). Similarly, *Pst* infection induces expression of genes related to PSII, ATP synthase and cytochrome b6f two days post inoculation (Dobon et al., 2016). These results suggest that cereal rust infections are not comparable since the hosts responses are different.

Infections with biotrophic fungi change the metabolism of the entire plant. For example, when lower (older) broad bean leaves are infected with *U. fabae*, the upper non-infected leaves have more Rubisco activity and higher carbon fixation rates (Murray and Walters, 1992). The infected tissue likely draws more nutrients from the plant, becoming a sink organ. *Ustilago maydis* not only changes plant metabolism but also induces plant tumours that change the leaf morphology (Doehlemann et al., 2008). The levels of hexoses and invertases increased in *Pst*-infected wheat tissue, decreasing sucrose levels (Heisterüber et al., 1994; Liu et al., 2015a; Voegele et al., 2001).

The metabolic shifts in the plant due to fungal infection can reduce grain size and root growth as these sinks have to compete with the fungal sink (Bethenod et al., 2005; Doodson et al., 1965; Horst et al., 2010a; Paul and Ayres, 1986). For example *Pst* infected plants have lower nitrogen content in wheat grains and increased susceptibility to the fungus when nitrogen is applied to infected crops (Devadas et al.; Park et al., 1988). Thus, the uptake of carbon and nitrogen components by biotrophic fungi affects plant performance since carbon and nitrogen metabolism are highly coordinated.

The reported levels of hexoses, starch, fructans and sucrose differed in each infection. For example, starch and fructans accumulate in barley and wheat leaves infected with *P. hordei* and *Pgt* respectively (Heisterüber et al., 1994; Owera et al., 1981; Scholes and Farrar, 1987). In addition, hexose and sucrose levels did not change between healthy and *Pst*-infected wheat (Chang et al., 2013), while *P. hordei* reduces barley apoplastic sugars and increases the apoplastic pH by almost one unit, from 6.6 to 7.3. These changes reduce phloem loading so that more hexoses accumulate in the apoplast, which is apparently beneficial for the fungus (Tetlow and Farrar, 1993). This shows again how rust infections are variable and probably that the infection conditions used in each experiment are not comparable. Thus, there is a need for carefully controlled infections under standardized conditions to examine the effects of *Pst* infections on wheat carbon metabolism.

We currently lack a general model of how plant nutrient allocations change in response to *Pst* infection of wheat. Many of the studies are not comparable due to variability in experimental conditions. For example, the experiments use different plant growth conditions, host genetic backgrounds, stripe rust isolates, and plant ages (or developmental stages). In addition, most studies reported in the older literature quantify metabolites without taking into account the plant metabolites as background. A full understanding of the biology of rust infections is limited by a lack of integration with plant developmental stages and responses to environmental conditions. Uptake of plant nutrients by biotrophic fungi must change with respect to plant development and growth conditions. For example, young wheat plants direct carbon to roots and young leaves for vegetative growth, whereas adult plants direct most nutrients to the heads (White and Edwards, 2008). Generation and utilisation of nutrients also changes in response to different environmental conditions; evidence for this is the contrasting plant phenotypes grown in glasshouse or field conditions. Using this knowledge, it is possible to design better experiments for cereal rust studies. For example, sugars accumulate during the day and are consumed at night. If sampling is performed at different times of the day across the infection period, comparisons with healthy plants are going to show inconsistencies. In summary, growth

conditions, developmental stages and time points should be standardised across experiments to ensure comparability.

Studies can further be improved with new mass spectrometry and nucleic acid sequencing technologies that allow the metabolomics and transcriptomics of the infection respectively to be studied in greater depth and with greater accuracy. Moreover, with better quality genome sequences for both the fungus and the host it is possible to complement physiology and metabolomics data with genetics. These tools will help to perform robust studies and will integrate several aspects of the infection to enable a more holistic understanding.

1.4 Project aims

Rust fungi take up nutrients from the plant, thus altering host metabolism. How plants respond to and compensate for these changes during infection is the major question of my thesis. Here I have focussed on the *Pst*-wheat interaction from a physiological perspective, combining techniques from plant physiology and molecular biology.

I studied infected leaves examining three major hypotheses. The first is that *Pst* enhances carbon fixation during infection, because it mainly infects mesophyll cells and photosynthesis can be stimulated when some sugars are at low concentrations. This part of the thesis also involves studying the dynamics in photochemistry as well as genes and proteins involved in the process.

The second hypothesis is that plant primary metabolites are lower at infection sites due to uptake by the fungus. Starch, sucrose and fructans could be source of carbon nutrients for the fungus during infection. The approach that I used was to compare plant primary metabolites in whole tissue or in the plant apoplast in healthy and infected wheat leaves, at different stages of infection. Because sugar concentrations are regulated by invertases, I measured their activity during the infection. I also studied distal non-infected leaves under the hypothesis that infected tissue might trigger systemic metabolic responses. The flux of nutrients should change so that it is directed towards infected leaves; the new nutrient requirements might be met by distal leaves. For this hypothesis I measured gene expression, sugar levels and invertase activities.

The third hypothesis is that *Pst* growth is affected by the developmental age of the leaves. Older leaves provide nutrients (source organs) to younger leaves (the sink) as they build their own photosynthetic machinery to transition to source as they age. This sink-source division is accompanied by metabolite concentrations at each age (or developmental stage). When the

fungus infects, the progression of the infection is not going to be the same in each leaf type, because the leaves differ metabolically. To test this, I shaded older or younger leaves to alter the allocation of nutrients. When leaves are shaded, they should demand more nutrients from other leaves, and this new sink should affect the infection. For these experiments, I measured chitin as a direct indicator of fungal biomass.

CHAPTER 2
Effects of host growth stage and metabolism on the development of *Puccinia striiformis* f. sp *tritici* infections

2.1 Introduction

As biotrophic fungi, rusts infect and keep host tissues alive while extracting nutrients to complete their infection cycles. Rust fungi develop a specialized structure called the haustorium for uptake of cytoplasmic nutrients while suppressing host defence responses (Garnica et al., 2013). The major roles of haustoria have been suggested by interpretation of transcriptomic and proteomic data from isolated haustoria (Garnica et al., 2013; Mendgen et al., 2000; Voegele et al., 2001). Haustorial transcriptomics from wheat stripe rust, broad bean rust, stem rust and soybean rust fungi (see Box 1 in Chapter 1 for common and scientific fungal names) has revealed the up-regulation of genes coding for amino acid transporters, carbohydrate transporters and ATPases, suggesting active transport of nutrients (Garnica et al., 2013; Hahn and Mendgen, 1997; Link et al., 2014). The haustorial proteome of *Puccinia triticina* revealed that 33% of all peptides identified proteins related to energy metabolism, including ATPases, ATP synthases, and glycerol metabolism, among others (Song et al., 2011). Additionally, a fungal invertase involved in hexose uptake was immunolocalised to *Uromyces fabae* haustoria (Voegele et al., 2006). Studies in the non-rust biotrophs barley and pea powdery mildew suggested that their haustoria take up host sugars. In *Blumeria graminis* f. sp. *hordei* haustoria, the electric potential across mitochondrial membranes changed when infected cells were provided with glucose,

suggesting active transport (Mendgen and Nass, 1988). In *Erysiphe pisi,* ^{14}C labelled photosynthates were found in haustoria by electron microscopy (Spencer-Phillips and Gay, 1980). Overall specific roles for haustoria are apparent, but little has been studied directly due to the difficulty in working with these specialised cells.

Sugar alcohols (or polyols) are commonly present during fungal infections. Polyols are storage molecules that are utilised later for germination. Fungi also turn sugars into polyols, reducing their internal sugar concentrations and thus maintaining a favourable concentration gradient toward the fungus (Clancy and Coffey, 1980; Meena et al., 2015; Reisener et al., 1962; Voegele et al., 2005). Polyols accumulate in haustoria and hyphae, and are then probably translocated to the spores for storage (Maclean and Scott, 1976; Voegele et al., 2005). Other metabolites important for germination include abundant lipids which have a high capacity to store energy (Solomon et al., 2003). During germination of *P. striiformis* f. sp. *tritici* and *U. appendiculatus* spores, lipids are broken down by the β-oxidation pathway and the glyoxylate cycle for the ultimate production of sugars and amino acids (Cooper et al., 2007; Zhao et al., 2015). Most of the data available to help understand the metabolic transition from dormancy to germination is derived from early metabolic studies and proteomics. The existing metabolomics data are from *Melampsora lini* and *P. graminis* f. sp. *tritici* (Daly et al., 1967; Jackson and Frear, 1967; Reisener et al., 1962). In both fungi, the lipid composition of urediniospores changed in the first 8 hours of germination, while esterified fatty acids, including triglycerides, decreased in *Pgt* within the first hour of germination with a consequent increased in glycerol due to the lipases activity. However more accurate and modern techniques are now available that might help to improve our knowledge of spore metabolism. Therefore, the first part of this Chapter describes experiments to measure the abundance and changes in metabolites present in *Pst* urediniospores and germinated spores, and compares these observations with the literature.

The nutrient demands of biotrophic fungi changes the metabolism of infected host cells. Several studies have reported the metabolic reprogramming of infected tissue to increase its sink capacity and hence divert photosynthate to the fungus (Bethenod et al., 2005; Carretero et al., 2011; Swarbrick et al., 2006; Voegele, 2006). Sink metabolism can also be induced by plant developmental and environmental conditions, and some studies have shown that these conditions affect how plant respond to fungal infection. For example, soybean leaves grown under reduced light (20% of normal) are more susceptible to *Phakopsora pachyrhizi* during the early stages of infection (Dias et al., 2010), while external application of nitrogen seems to enhance the development of fungal diseases (Devadas et al.; Neumann et al., 2004; Solomon and Oliver, 2001). Some resistance genes expressed only in adult plants (*APR* genes; adult plant

resistance) reduce growth and sporulation by rust fungi and *Blumeria graminis* f. sp. *tritici* (Dakouri et al., 2013; Griffey, 1993; Herrera-Foessel et al., 2014). The underlying resistance mechanism for one of these, *Yr46*, is thought to be the reduction of carbon nutrients to the pathogen (Dodds and Lagudah, 2016).

Overall the available data suggest that the growth of rust fungi is sensitive to plant nutrient status, which can change due to environmental and developmental conditions. However, while older studies focussed on metabolism during rust infections, the aim of most recent studies has been to understand host resistance mechanisms and suppression of defence responses by the fungus (Cantu et al., 2011; de Carvalho et al., 2016; Dobon et al., 2016). Consequently, the interaction between fungal and host biology is still not well understood. To expand the study of the metabolomics of the *Pst*-wheat interaction, I manipulated plant growth conditions to modify photosynthesis and hence nutrient availability, which should impact on fungal growth. This is an indirect way to understand fungal metabolism, since direct manipulation of the fungus is still not possible without affecting the plant. I took different approaches to alter the content of nutrients in *Pst*-susceptible wheat leaves. After standardizing the infection methods, I manipulated the growth of plants expressing two different *APR* genes which code for a sugar transporter and an ATP-binding cassette (ABC) transporter, respectively. The results showed a direct correlation between nutrient availability and fungal growth in susceptible plants, while in resistant plants changes in nutrient distribution increased susceptibility. The results suggest alternative strategies for the control of fungal infection.

2.2 Material and methods

2.2.1 Biological materials

The experiments were performed using two *Puccinia striiformis* f. sp *tritici* (*Pst*)-susceptible wheat (*Triticum aestivum*) cultivars, cvs. Morocco and Thatcher. Two near-isogenic wheat lines carrying the *APR* genes *Yr18* and *Yr46*, RL6068 (T_Yr18) and RL6607 (T_Yr46) respectively (Spielmeyer et al., 2013), were also used in this study. Both have the cv. Thatcher background, and differ mainly in the presence of the *APR* resistance genes. Seeds of *cv*. Thatcher, T_Yr18 and T_Yr46 were a kind gift of Dr. Evans Lagudah, Commonwealth Scientific and Industrial Research Organisation (CSIRO) Agriculture and Food, Crace, ACT. The *Pst* isolate 104 E137 A- (*PST*-79) corresponding to the first Australian incursion of the fungus in 1979 was used in all infections (Wellings et al., 1988). Plants were grown in a mixture of soil, pine bark and sand (3:2:1), in a

controlled chamber at 21°C, 150 µE of light, 65% humidity, 400 ppm CO_2, with a 16 h light/8 h dark cycle. Before infection, plant fertilizer (Thrive® all purposes) was applied fortnightly.

Two different developmental stages were defined for cv. Morocco plants (Figure 2.1). These included plants in which the 7th leaf had emerged but not expanded (Z23) and plants with an expanded flag leaf (Z47) (See Figure 1.8 for wheat developmental stages). For cv. Thatcher, T_Yr18 and T_Yr46, adult stage plants were studied because these genotypes develop *PST*-79 resistance only in the flag leaf.

2.2.2 Infections of wheat plants with *PST*-79

Urediniospores from previous *PST*-79 infections stored at -80°C were heat-shocked at 44°C for 4 min and mixed with talcum powder in a 1:20 ratio (243604, SIGMA-ALDRICH®). Wheat plants were infected using one of two methods; spraying or painting. The spray method was used to infect whole plants. Plants were first sprayed with water using an atomizer to create a mist, and then the spore-talcum mixture was sprayed over the leaves using a manual air pump. This process was repeated twice. To maintain humidity, seedlings were kept in a closed container and larger plants were covered with plastic bags. Plants were maintained for two days at 9^{o}C in the dark. On the third day, they were transferred to a controlled growth chamber at 17°C with 150 µE of light and a 16:8 h light cycle.

The painting method was used to infect defined leaf areas. For this method, leaf areas were painted with a 1:5 ratio of spore-talcum using a paintbrush. The infected area was covered with a piece of aluminium foil sprayed previously with water to maintain humidity (Figure 2.2). Plants were kept for two days in the same conditions described above but without the plastic bags. For most experiments plants were sampled 2, 8, and 14 days after inoculation (dai), as representatives of the three phases of the asexual reproductive cycle of *Pst*: germination, biotrophic growth and sporulation (Section 1.1.2).

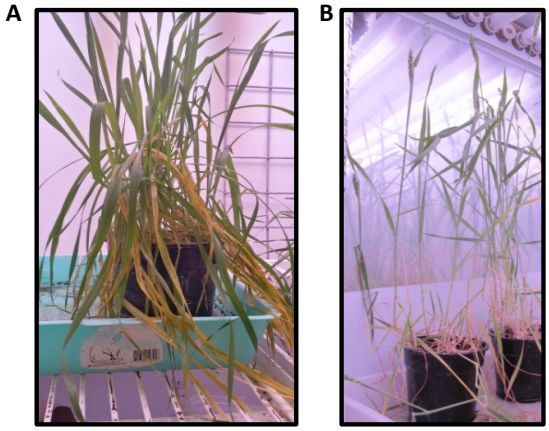

Figure 2.1. Developmental stages of wheat plants used in this study. A) Young stage (four-week-old plants). B) Adult stage (two to three-month-old plants).

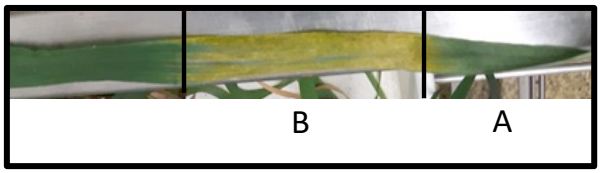

Figure 2.2. Infection of a defined area on wheat flag leaves using the painting method 14 days after inoculation with *PST*-79. A). Non-painted area. B) Painted area.

2.2.3 Extraction of polar components from urediniospores and germinated spores

Fresh urediniospores from three different *PST*-79 infections were collected from plants and germinated on water in Petri dishes at 9°C in darkness for 17 h. Germinated spores formed a film of germ tubes that was collected on a 0.5 µm cloth mesh and blotted dry with absorbent paper. Freshly collected spores and germinated spores were ground in liquid nitrogen with a mortar and pestle for metabolite extraction. Polar components from fresh and germinated spores were extracted in 500 µL of 50% methanol spiked with the amino acid norleucine (0.084 mg/mL), used as an internal standard as this compound is absent from eukaryotes. The samples in methanol were agitated in a small orbital shaker for 45 min at 4°C. They were then mixed by hand with 500 µL chloroform and centrifuged at 2000 *g* for 10 min at room temperature (RT) to remove non-polar components such as chlorophyll. The aqueous supernatant was recovered (around 100-200 µL) and dried in a vacuum concentrator at 30°C for one to two h. The brown pellet was kept at 4°C until analysis.

Metabolite standards including glucose, asparagine, glutamine, serine, ribitol, fructose, arabitol, trehalose, myo-inositol, nor-leucine, sucrose, mannitol and sorbitol were dissolved in methanol spiked with norleucine (0.084 mg/mL) to a final concentration of 0.01 mg/mL.

2.2.4 Gas chromatography–mass spectrometry analysis for polar components

Gas chromatography–mass spectrometry (GC/MS) was used to measure polar components in urediniospores and germinated urediniospores. Chemical derivatization was performed to make components less polar but more volatile for GC/MS. Derivatization was performed using the Gerstel MultiPurpose Sampler (Linthicum, MD, USA) and the dried extracts (dry brown pellet) from plant and fungal material. The pellets were first dissolved in 20 µL methylamine (20 mg/mL in pyridine) and incubated at 37°C for 90 min with shaking (1200 rpm). This caused replacement of carbonyl groups with aliphatic groups (methoximation). Finally, the remaining polar groups were substituted by trimethylsilyl (TMS) groups by trimethylsilyation. For this, 40 µL of N-trimethylsilyl-N-methyl trifluoroacetamide (MSTFA) was added and samples were shaken for 30 min at 37°C (Du Fall and Solomon, 2013). The analysis of samples was performed on an Agilent GC (7890A)/MS (5975) with Gerstel MultiPurpose Sampler (at the Mass spectrometry facility at ANU operated by Dr. Thy Truong) as described below in splitless and split mode (20:1).

The polar components were separated on a VF-5ms FactorFour™ column (Varian, Inc) coupled to an Agilent quadrupole 7990A spectrometer. Components were ionized by electron ionization (70 eV electrons). Metabolite characterization was performed using the software AnalyzerPro (SpectralWorks Ltd, Runcorn, Cheshire, UK) and the data were analysed using the software Excel (Microsoft™). Metabolite peaks were normalized to the internal standard (norleucine), to the sample weights, and to the total area of all peaks in the sample.

2.2.5 Fungal biomass estimations

As it is not possible to measure fungal biomass directly, the lectin wheat germ agglutinin (WGA) which binds specifically to the fungal cell wall component chitin was used to quantify fungal growth (Ayliffe et al., 2013). WGA conjugated to a fluorescent tag (FITC) interacts with fungal cell walls, and the amount of binding measured by fluorescence intensity is directly related to fungal biomass. *Pst* infections are characteristically variable; to obtain reliable results, three 4 mm^2 leaf disks were sampled from each infected leaf using a cork borer in the infected area. At least five different plants were analyzed in each experiment. Samples were collected by area rather than weight because fungal infection may change the leaf density. Collected tissue was frozen immediately in liquid nitrogen to preserve the samples and prevent further fungal growth. Leaf discs were autoclaved in 1 M potassium hydroxide (KOH) to remove chlorophyll and to make the tissue permeable to WGA-FITC. They were then washed twice with 50 mM Tris-HCl pH 7.5 to remove KOH before pulverization in 200 µL 50 mM Tris-HCl pH 7.5 using 3 mm

glass beads in a Tissue-lyser machine (Qiagen). Further 50 mM Tris-HCl pH 7.5 was added to a final volume of 500 µL. Samples were mixed with WGA-FITC solution (initial concentration of 1 mg/mL in phosphate-buffered saline buffer,
Table 2.1) to a final concentration of 18 µg/mL and incubated for 20-40 min with shaking at RT. Unbound WGA-FITC was washed away three times with 500 µL of 50 mM Tris-HCl pH 7.5 and centrifuged each time at 3000 *g* for 5 min at RT. After the last wash, samples were suspended in a final volume of 200 µL 50 mM Tris-HCl pH 7.5, and 150 µL of each sample was transferred to a single well of a black 96-well plate. Fluorescence in each well was measured using a plate reader (Infinite® M1000 PRO, TECAN) using the settings indicated in Table 2.2.

Another method for microscopic observations, besides lectin wheat germ agglutinin, is the staining with Iodine-potassium iodide solution (or Lugol's solution). Iodine in solution with potassium reacts with starch and glycogen producing a brown/purple colour. Before the staining, the chlorophyll was removed with hot ethanol, to observe better contrast of stained leaves. For this, the leaves were place in tubes with 80% (v/v) ethanol solution and incubated in a hot water bath until the green colour (chlorophyll) of the leave decreases. This process can be repeated several times until the leaves are yellow or whitish. The leaves are dry and incubate in iodine solution for 2 min. The excess of staining is removed and the leaves can be observed in the microscope.

Table 2.1 Phosphate-buffered saline (PBS)

Final concentrations (10x)
1.37 M NaCl
27 mM KCl
100 mM Na_2HPO_4
18mM KH_2PO_4
Adjust pH with HCl to 7.4

Table 2.2. Plate reader fluorescence parameters for the WGA-FITC assay.

Mode	Fluorescence Top Reading
Multiple Reads per Well (Circle (filled))	4 x 4
Multiple Reads per Well (Border)	750
Excitation Wavelength	485
Emission Wavelength	535
Excitation Bandwidth	5
Emission Bandwidth	5
Gain	136
Number of Flashes	50
Flash Frequency	400
Integration Time	2000
Lag Time	0
Settle Time	1000
Z-Position (Manual)	20000

2.2.6 Detached leaf experiments

The youngest fully expanded leaf of young stage plants, or the flag leaf of adult stage plants, were painted with *PST*-79 urediniospores in talc as described in Section 2.2.2. After four days of infection, leaves were excised from the plant, cleaned by dipping in 80% (v/v) ethanol and then in 2% (v/v) sodium hypochlorite solution, and finally washed in MilliQ water (Ultrapure water type 1). Washed leaves were placed in 14 mL round bottom Falcon™ tubes with 2 mL of Hoagland's solution supplemented with sugars as follows (Figure 2.3). Hoagland's solution consists of a mixture of Hoagland's modified basal salt mixture (Hoagland and Arnon, 1950)(H353, PhytoTechnology Laboratories, LLC™) supplemented with 18 mM or 1.8 mM sucrose, or one of glucose, fructose or 2-deoxy-D-glucose at 2.2 mM or 22 mM . The tops of the lids were cut off and covered with 3M™ Micropore™ paper tape to allow gas exchange. Tubes were placed in a growth chamber as described above with side lighting.

Figure 2.3 Sugar feeding experiments for detached wheat leaves. Infected leaves were excised from plants 4 days after infection and placed into 15 mL clear Falcon tubes in 2 mL of Hoagland's solution supplemented with sugars.

2.3 Results and discussion

2.3.1 Measurement of polar metabolites of *PST*-79 urediniospores and germinated urediniospores

Polar chemical components were extracted from freshly collected spores and germinated spores from three different infections. Polar components were quantified by GC/MS, and 20 different metabolites were identified (Table 2.3,Figure 2.4 A, B). I only evaluated 11 amino acids as they are key components of amino acids synthesis and respiration. From the 11 amino acids selected, six (leucine, proline, phenylalanine, serine, threonine and glutamine) had similar abundances in spores and germinated spores. Valine, asparagine and aspartic acid levels were higher in spores, while glycine and glutamic acid were higher in germinated spores. These results suggest that spores store nitrogen as aspartic acid and asparagine, which could be converted to glutamic acid when they germinate. Glutamic acid is the starting point of most amino acid synthesis pathways and is part of the synthesis of N-acetylglucosamine, the building block of chitin (Cabib et al., 1996). Therefore, glutamic acid may be higher in germinated spores for germling expansion. This hypothesis is consistent with *PST*-79 transcriptomic data, where genes coding for aspartate aminotransferase and asparaginase are up-regulated in germinated spores compared to haustoria (Garnica et al., 2013).

Table 2.3 List of metabolites selected for GC/MS analysis and some of their roles in fungi.

Metabolite[1]	**Roles**
Proline	Substrate for glutamic acid synthesis
Valine	Substrate for succinyl-CoA synthesis
Leucine	Substrate for acetyl-CoA synthesis
Glycine	Substrates for pyruvate synthesis
Serine	
Threonine	
Phenylalanine	Substrate for secondary metabolites synthesis
Glutamic acid	Main substrates in nitrogen metabolism
Aspartic acid	
Glutamine	
Asparagine	
Trehalose	Reported to accumulate in urediniospores
Arabitol	
Ribitol	
Mannitol	
Sorbitol	
Sucrose	Main substrates in carbohydrate metabolism
Glucose	
Fructose	
Myo-inositol	For phosphatidylinositol synthesis

The 11 amino acids evaluated are substrates for the synthesis of tricarboxylic acid cycle (TCA cycle) metabolites. The TCA cycle releases energy as ATP from stored metabolites and produces NADH; these molecules are used in many biochemical reactions. Valine, which was highly abundant in spores, is degraded to produce succinyl-CoA which is part of the TCA cycle. However this contradicts the *PST*-79 transcriptomic data where genes coding for TCA cycle are up-regulated in haustoria compared to germinated spores (Garnica et al., 2013).

Serine is used for glycine synthesis, and both amino acids are part of the pyruvate metabolic pathway. Despite this, no differences between spores and germinated spores were found for serine, whereas glycine abundance was 6 times higher in germinated spores compared to spores. These amino acids are involved in the folate cycle, which is required for synthesis of vitamin B12 and nucleotide synthesis (Cossins and Chen, 1997; Yang and Vousden, 2016). Nucleotide synthesis is likely to be important in spores as DNA and RNA are required for nuclear division and gene expression. The high levels of glycine in germinated spores suggests that it is important for the folate cycle, glutathione synthesis and TCA cycle during germination.

[1] Metabolites with a differential content between spores and germinated spores are bolded.

Glutathione might be used in germinated spores as an anti-oxidant compound for protection against plant reactive oxygen compounds (Garnica et al., 2013). Thus, both metabolomics and transcriptomic data suggest the importance of glycine as a metabolic hub for germinating spores.

To evaluate carbohydrate accumulation, I measured four sugars (trehalose, sucrose, glucose and fructose) and five different polyols (arabitol, ribitol, mannitol, sorbitol, myo-inositol) in spores and germinated spores. Glucose, fructose and sucrose have been reported to be taken up by the fungus during infections and can enter glycolysis, while trehalose has been reported to accumulate in *Pgt* urediniospores but is not a substrate for the hexose transporter 1 (HXT1) from *Uromyces fabae* (Maclean and Scott, 1976; Voegele et al., 2001). The levels of glucose, fructose and trehalose were similar in spores and germinated spores, while the disaccharide sucrose was present in spores but almost undetectable in germinated spores (Figure 2.4 C). This represents a novel finding as sucrose has not been previously reported in the spores of rust fungi. Only a sucrose transporter has been identify in the biotrophic fungus *Ustilago maydis*. (Horst et al., 2010b). The five polyols evaluated have been found previously in *Pgt* urediniospores and mycelia (Maclean and Scott, 1976). Here, sorbitol and myo-inositol levels were similar between spores and germinated spores while arabitol, ribitol and mannitol abundance were higher in germinated spores than spores (Figure 2.4 D). Arabitol levels were four times higher in germinated spores. Ribitol and mannitol levels were more than 10 times higher in germinated spores. It seems that polyols are required during germination, however my data contradict the results of Voegele et al., (2005) who found that mannitol present in *U. fabae* urediniospores disappeared during germination. Mannitol may be used during germination to increase turgor pressure and facilitate penetration, since polyols are osmolytes (Voegele et al., 2005).

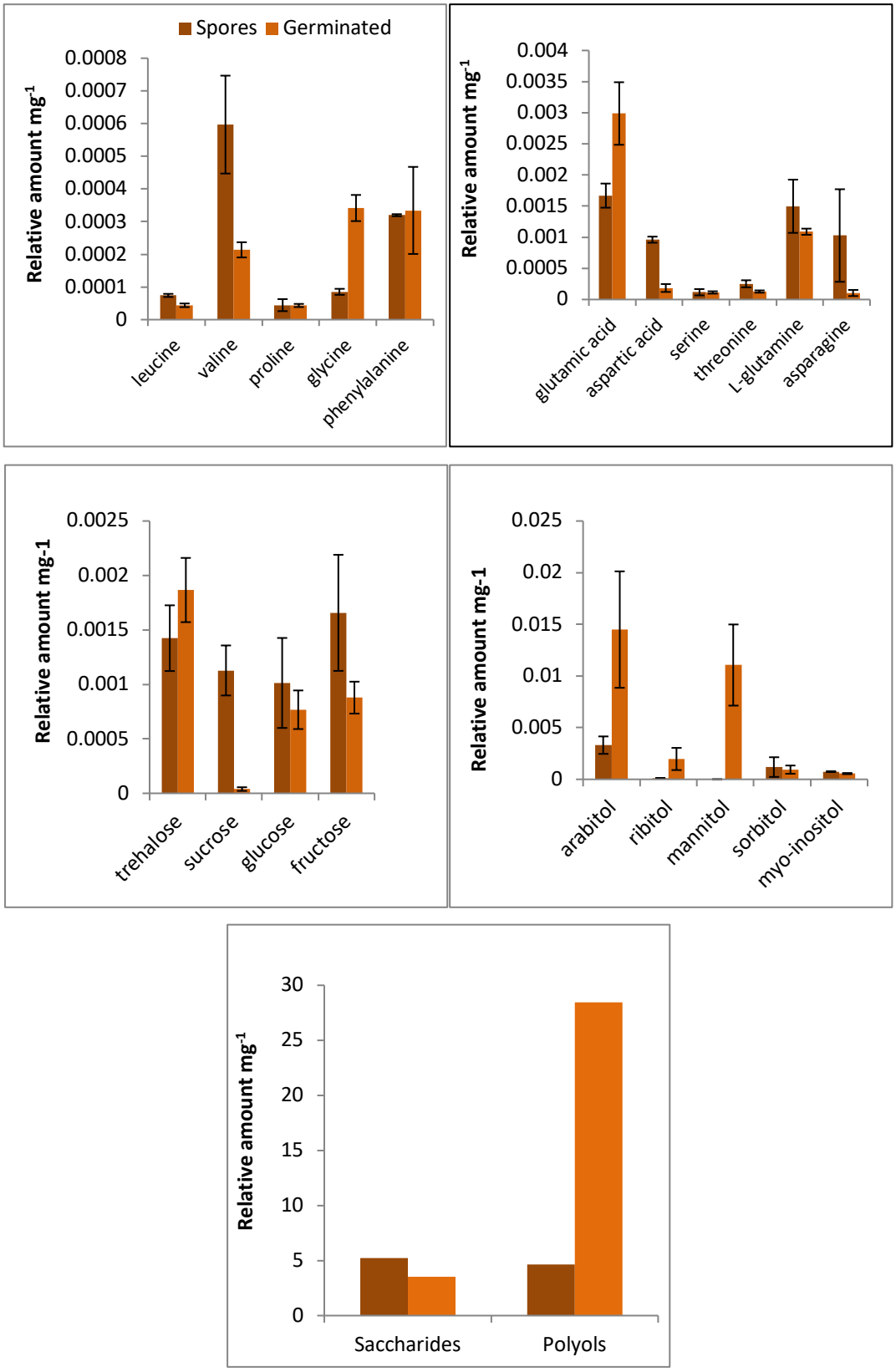

Figure 2.4. Primary metabolites in *PST*-79 urediniospores and germinated urediniospores. Y-axis values or relative amounts represent relative peak areas after normalization to the total metabolite peak areas and leaf weight. A) Non-polar amino acids B) Polar and charged amino acids. C) Disaccharides and monosaccharides. D) Polyols. E) Total amount of saccharides and polyols in spores and germinated spores. Error bars represent standard error, n=3.

In germinated spores, the total amount of polyols was 8 times higher than total saccharides. This implies a conversion of carbon compounds to polyols as spores germinate (Figure 2.4 E). The carbon source for polyols synthesis could be lipids (Rosenberg et al., 1992). This idea is supported by the higher levels of gene transcripts for β-oxidation and glyoxylate cycle enzymes in germinated spores compared to haustoria (Garnica et al. 2013). Another possible carbon source is glycogen, which I detected in spores and hyphae by microscopy after Lugol's staining (section 2.2.5) (Figure 2.5). In Figure 2.5 A, purple-stained pustules are close to leaf vascular bundles and surrounded by brown fungal hyphae. Hyphae are visible across the entire infected leaf. The purple staining of hyphae which is visible close to pustules only might represent glycogen translocation to spores. Figure 2.5 B is a close-up view of brown-stained hyphae surrounding mesophyll cells.

I measured polar compounds in urediniospores and germinated urediniospores, the two fungal forms that occur separate from the host. The comparison between the metabolites in spores and germinated spores might help explain which carbohydrates and amino acids are used preferentially during the host colonization phase. In general, my GC/MS results support the model for germinated spores' metabolism proposed by Garnica et al. (2013). Spore germination is an anabolic process that relies on glutamic acid and on the TCA cycle as an energy source, but also on the synthesis of polyols, most likely for cell-wall expansion or for quenching reactive oxygen species. Metabolite analysis of isolated haustoria would complement the current understanding of fungal metabolism during infection. Haustoria from *Pst* are viable after extraction (Dr. Diana Garnica, Ph.D. thesis, The Australian National University, 2013). To fulfil this aim, high quality data might be obtained by working with isolated haustoria and by using more sensitive detection techniques such as nuclear magnetic resonance spectroscopy (NMR) to measure metabolites.

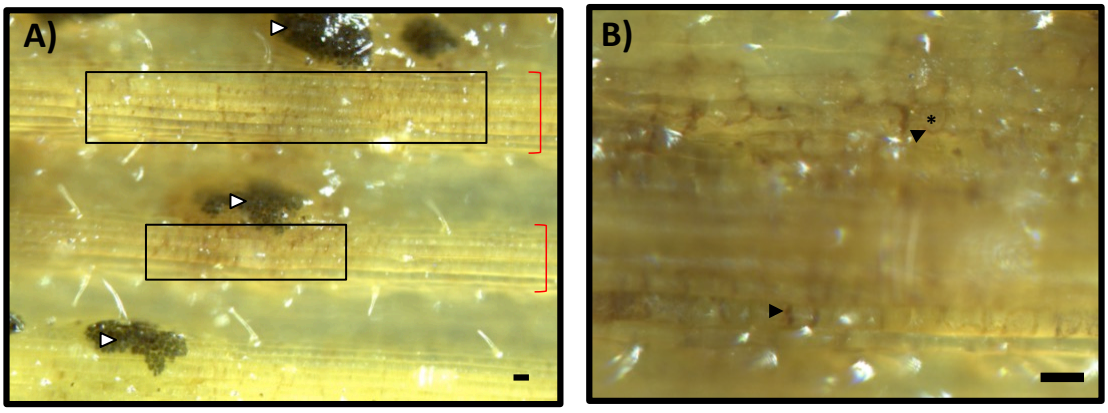

Figure 2.5. Lugol-stained spores and hyphae of *PST*-79 in young stage leaves at 14 dai. A) *Pst* pustules (white arrows) between wheat vascular bundles (red brackets). Intercellular *Pst* hyphae are visible within the black rectangles. B) Zoom-in of A), showing hyphae (black arrows) surrounding mesophyll cells (*). Scale bar = 82 µm. The pictures were taken under a light microscopy.

2.3.2 Effect of wheat developmental stage on *PST*-79 biomass accumulation

To understand how plant nutrient status affects fungal infection, I manipulated the light conditions in the plant growth cabinets and measured fungal chitin accumulation in the leaves. The control (younger stage) plants were grown under a light intensity of 150 µE in a 16 h light/8 h night cycle. To test the effect of zero-light conditions on fungal growth, I covered *PST*-79 whole infected plants with aluminium foil during infection. In the control conditions, *PST*-79 growth increases 1.7 times before 9 dai and then become stable (Figure 2.6). The chitin method does not measure released spores, because the leaves were wiped clean of them before staining, therefore, my method underestimates fungal biomass during infection. Under both regimes, the germinating spores developed a sub-stomatal vesicle after two dai, and infectious hyphae from 6 dai (data not shown). Under zero-light conditions *PST*-79 growth did not increase significantly after the 6 dai time point (Figure 2.6). These data show a strong influence of lighting conditions on fungal growth and are consistent with a model in which *PST*-79 is not nutrient-limited under a normal lighting regime but in a zero-light scenario, the plant and the fungus compete against each other for a limited nutrient pool. My results suggest that the competition was visible in the data from 8 dai.

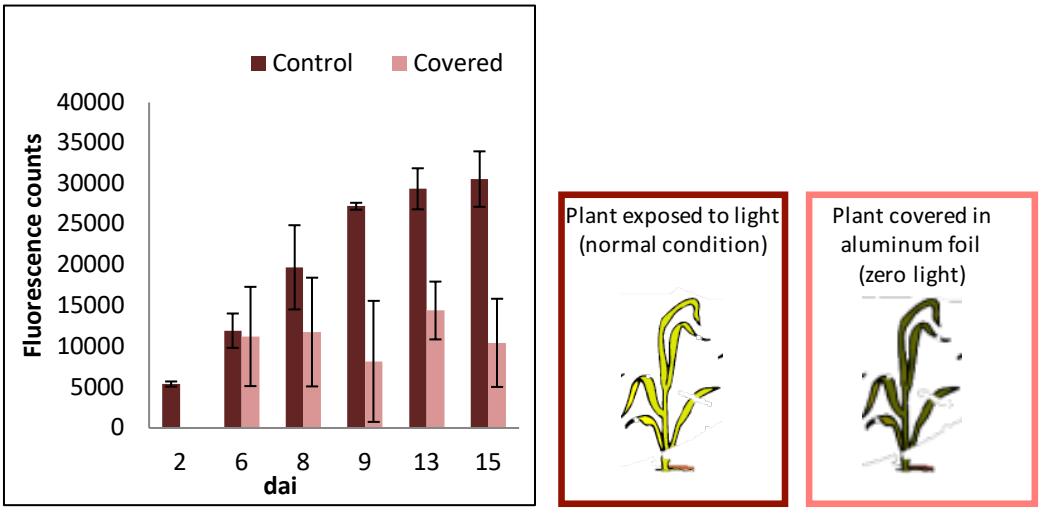

Figure 2.6 Growth of *PST*-79 under normal and zero-light conditions. Chitin was detected by WGA-FITC fluorescence quantification after tissue disruption, and levels are represented as fluorescence counts. Dark brown bars represent normal light (control), where plants were exposed to light (dark frame in the plant cartoon). "Covered" (light brown bars in the graph) represents the zero-light condition. For these plants, all aerial parts were covered with aluminium foil (light frame in the plant cartoon). Asterisks represent significant differences compared to the control using the statistical parameters a t-test and a p-value lower than 0.05.

To test the effect of increased light intensity on *PST*-79 infections, I grew infected plants under high light (600 µE) and compared fungal growth to that under the control condition (150 µE). The leaves grown under high light were the same size as control plants, but were lighter green in colour, suggesting less accumulation of chlorophyll. The plants grown under high light

conditions accumulated purple anthocyanin pigments in the stems (Figure 2.7 A). Anthocyanins quench reactive oxygen species (ROS) that are generated through photosynthesis as a stress response to the excess of photons (Kovinich et al., 2015). Despite the plant stress responses, the chitin content in the high-light condition was similar to the control at 8 dai, and at 14 dai fungal growth was almost three times more than in control plants (Figure 2.7 B).

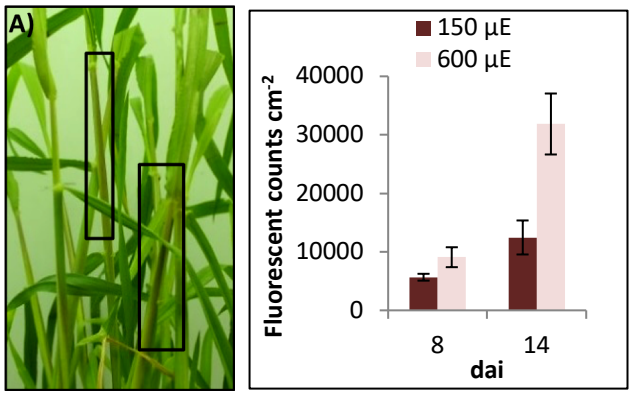

Figure 2.7. Growth of *PST*-79 under high light conditions. A) Young stage wheat plants (cv. Morocco) grown at 600 µE in a growth cabinet. The black rectangles show stems with purple pigments. B) Fungal growth estimated using WGA-FITC, under normal (150 µE) and high light (600 µE) conditions. The experiment was repeated twice with similar results. Error bars represent standard error of 5 replicates. Asterisk represents significant differences compared to low light using a t-test and a p-value lower than 0.05.

These results reveal a correlation between light intensity and fungal growth. One potential explanation for this is the increased accumulation of carbon nutrients due to greater carbon fixation under high light. Infected plants under high light conditions contained more fructose than in normal conditions (data not shown); interestingly, glucose remained the same under both high and normal light conditions. The increase in fungal growth under high light conditions raises the question of whether further application of inorganic fertilizer would enhance plant susceptibility. For example, nitrogen application to crops increases the growth of some fungal pathogens (Devadas et al.; Neumann et al., 2004; Solomon and Oliver, 2001). As nitrogen availability often limits photosynthesis, it follows that application of nitrogenous fertiliser would increase the supply of both N and C nutrients to the fungus.

The high light and zero-light experiments reported here were performed independently; therefore, the fungal growth that I measured in each cannot be compared directly. However, a synthesis of the results, particularly the dramatically increased fungal growth under high light at 14 dai, and the inhibition of growth under zero-light after 6 dai, suggests that prior to about 8 dai the fungus does not require high levels of nutrients. Hence these might be sourced from the locally infected tissue. After 8 dai, fungal growth including spore formation increases

considerably, and hence has a higher requirement for nutrients that can be met by higher levels of photosynthesis.

Light availability affects fungal growth, probably due to correlated changes in the sugars produced by the host (data not shown). Nutrients, including sugars, also change during plant development. For example, younger leaves are a sink, importing nutrients from distal parts of the plant for growth, but when they are fully developed they are sources that produce excess nutrients that can be routed to other parts of the plant (Braun and Slewinski, 2009). In this way, the distribution of nutrients shifts according to demand and is affected during pathogen infections.

I developed a scheme to test the effect of leaf development on fungal growth (Figure 2.8). I first investigated the contribution of leaves of different ages to the growth of the fungus. In this scheme, I infected the youngest fully expanded leaf and the leaf immediately below it (referred to here as the "older leaf") from four-week old plants by painting defined areas with *Pst* urediniospores (Figure 2.8 A). The infected leaves were collected at 8, 9, 11, and 14 dai for chitin measurements. The experiment had four biological replicates, however I repeated it independently three further times because the data were very variable in the initial experiment. Figure 2.9 shows the average and variability of the combined data from the four experiments. Unfortunately, the data were too variable to make conclusions about the effects of leaf age on fungal growth.

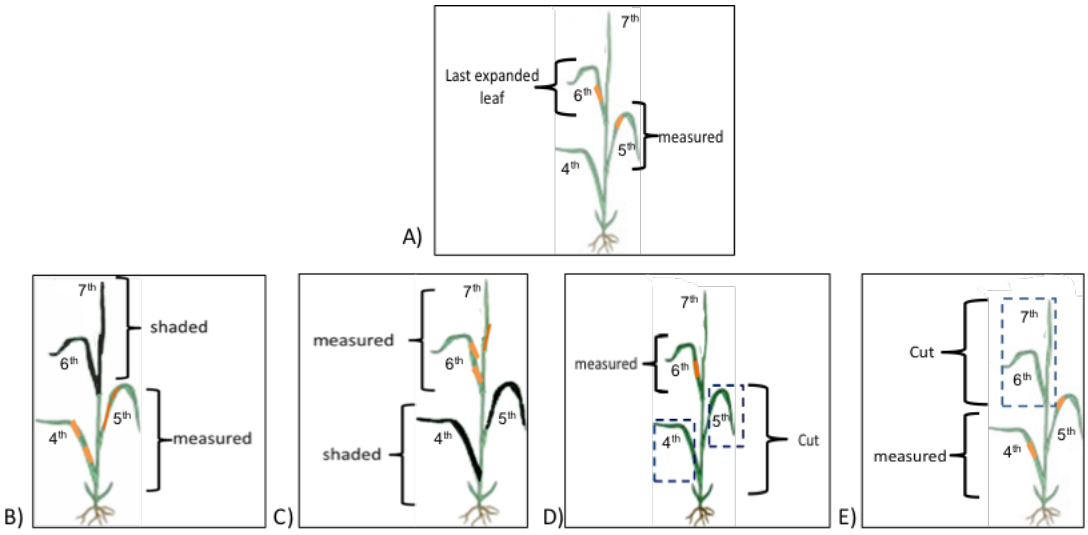

Figure 2.8. Scheme of *Pst* infections on wheat plants based on leaf developmental stage. Young stage cv. Morocco plants were infected after the 7th leaf appeared. The 6th leaf is the youngest fully expanded leaf and the 4th leaf is the oldest leaf. Orange areas represent the sites of inoculation. Black leaves represent leaves that were covered with aluminium foil to block light. A) The 6th and 5th leaves were infected with *Pst* urediniospores. B and C represent the schemes to measure the effect of covering leaves with aluminium foil on fungal growth, while D and E are for evaluating the effect of removing leaves. B) The 5th and 4th leaves were infected and at the same time the 6th and 7th leaves were covered with aluminium foil. C) The 5th and 4th leaves were covered with aluminium foil and the 6th leaf was infected. D) The 5th and 4th leaves were removed with scissors from the stem, and at the same time the 6th leaf was infected. E) The 5th and 4th leaves were infected and the 6th and 7th leaves were removed.

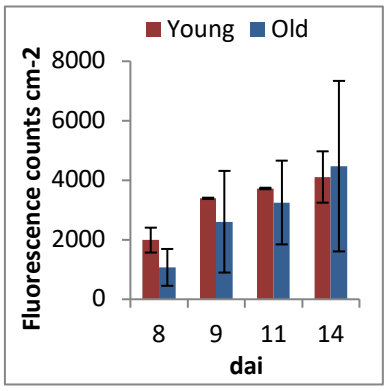

Figure 2.9. Growth of *PST*-79 on younger and older wheat leaves. The 6th and 5th leaves (Figure 2.8 A) were infected after the 7th leaf appeared in young stage cv. Morocco plants. Fungal growth was measured using the WGA-FITC quantification method, normalized to the infected leaf area. The experiment was repeated four times; here all data were combined in a single graph. Error bars represent the standard error of 16 replicates.

To further manipulate nutrient distribution in infected plants, I depleted the contribution of other leaves by shading them or excising them from the plant (Figure 2.8). This should modify transfer of nutrients to the infected leaf and hence fungal growth should be reduced. To test this hypothesis, I performed two experiments. The first tested the effect of blocking leaves from light by covering them with aluminium foil. The control for these experiments was unshaded plants (Figure 2.8 A). In one experiment, I infected the 5th leaf while covering younger leaves with aluminium foil (Figure 2.8 B). I also performed the experiment in reverse, so that younger

leaves were infected while older leaves were covered (Figure 2.8 C). The rationale behind this experiment is that the covered leaf should become a sink, forcing nutrient relocation from uncovered leaves. I measured fungal chitin at 8, 11 and 15 dai. I did not include earlier infection points because I wanted to measure the sink effect in advance fungal growth. I found that fungal growth increased in older leaves from 8 to 11 dai in control conditions, but did not increase from 11 to 15 dai (Figure 2.10). When younger leaves were covered, growth was like the control at 11 dai, but there was a remarkable increase at 15 dai. In younger leaves, fungal growth increased strongly from 8 dai to 11 dai and declined at 15 dai (Figure 2.10 A). A decline in values is possible because the measurement is per unit leaf area, and the leaves are still expanding in these experiments. When the older leaves were covered in these plants, fungal growth was reduced at both 11 and 15 dai. This is by contrast to infection of older leaves while younger leaves were covered, which lead to an increase in leaf chitin content (Figure 2.10). These results are consistent with changes in nutrient distribution forced by leaf covering.

By analogy to the previous results achieved by manipulating light intensity, it seems likely that the changes in fungal growth observed in this set of experiments after leaf shading was due to changes in nutrient availability. Thus, older leaves apparently accumulated more nutrients when younger leaves are covered, because there was more fungal growth compared to unshaded plants. Conversely, younger leaves apparently had fewer nutrients when older leaves are covered, because fungal growth was reduced compared to control conditions (Figure 2.10). These observations could have two root explanations; increased metabolism of infected leaves, or less nutrient transport to infected leaves. Covered young leaves might represent a new sink for the plant, as they cannot fix their own carbon, therefore infected older leaves are forced to increase carbon fixation to fulfil the new demands. An increase in metabolism would mean that more nutrients would be available to the fungus. Older leaves are normally a source of nutrients for younger leaves; therefore, if older leaves are covered, fewer nutrients will be exported to the younger leaves. The reduction in nutrient distribution to infected leaves could explain the reduction of fungal growth. The lack of direct data on nutrient production or consumption by older or younger leaves limits the interpretation of my results. Such information could reveal nutrient competition between the infected and shaded leaves. Overall, covering leaves changes plant metabolism which affects fungal growth, possibly by shifting the nutrient accumulation required for fungal growth.

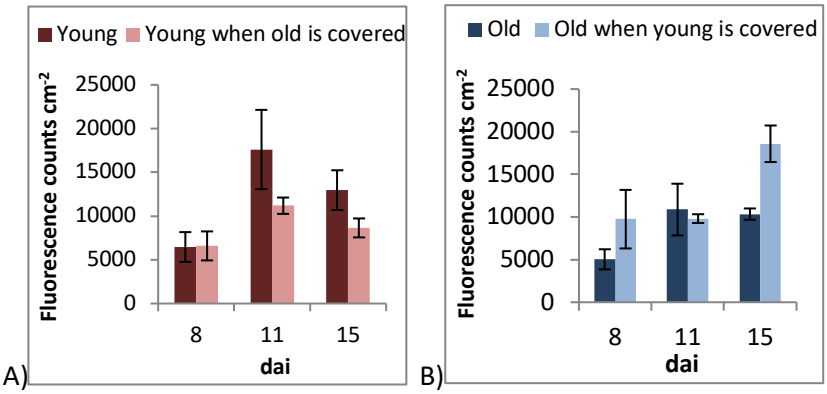

Figure 2.10. Growth of *PST*-79 in normal light conditions with selective leaf shading. Younger or older leaves were infected with *PST*-79, and the alternate leaves (see Figure 2.8 B, C, for schema) covered (or left uncovered) with aluminium foil. A, growth of *Pst* in younger leaves. B, growth of *Pst* in older leaves. Dark colour bars represent fungal chitin in uncovered plants; red for younger and blue for older leaves. Light colours bars indicate chitin when leaves were covered. Error bars represent standard error of four replicates. Asterisk represents significant differences compared to normal conditions using a t-test and a p-value lower than 0.05.

In an alternative approach, I removed the uninfected leaves from the plant, rather than shading them as before (Figure 2.8). The hypothesis underlying this experiment is that removing younger leaves reduces the sink demand, while removing older leaves removes a nutrient source. I measured fungal growth using the chitin technique at 4, 8, 9, 11, and 15 dai. The results of this experiment revealed that when older leaves were infected, fungal growth peaked at 11 dai with a small jump from 8 to 9 dai (Figure 2.11 A). When younger leaves were removed from these plants, the general effect was a significant reduction in growth with respect to uncut, with the first measurable increase occurring at 11 dai. I did not record the data for 15 dai because the leaves were wilted. Comparison between the data for uncut and cut plants revealed a significant difference in fungal growth at 11 dai. In younger leaves, fungal growth increased from four to 11 dai, with a marked increase from 8 to 9 dai. There was no increase after 11 dai (Figure 2.11).

When older leaves were removed, fungal growth increased gradually from four to 15 dai but with a very different pattern from the intact plants (Figure 2.11 A). There was no jump in growth between 8 and 9 dai, and growth increased gradually until 15 dai. The effect of this was marked differences in chitin between uncut and cut plants at 9 and 11 dai. In both experiments, leaf excision lead to lower fungal growth than when plants were left intact, but these differences were more marked in younger leaves (Figure 2.11).

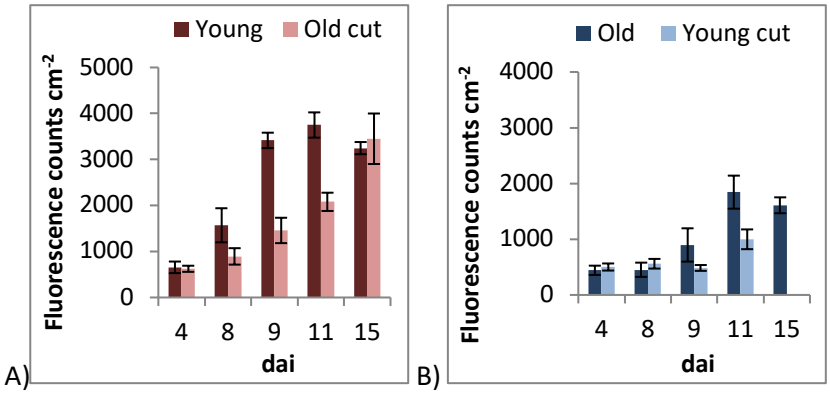

Figure 2.11. Growth of *PST*-79 under normal conditions and after selective leaf removal. Younger or older leaves were infected with *PST*-79, and the alternate leaves (see Figure 2.8 D, E, for schema) were removed or left intact. A, growth of *Pst* in younger leaves. B, growth of *Pst* in older leaves. Dark colour bars represent fungal chitin under normal growth conditions; red for younger and blue for older leaves. Light colours bars indicate chitin when leaves were removed. Error bars represent standard error of four replicates. Asterisk represents significant differences compared to normal conditions using a t-test and a p-value lower than 0.05.

In summary, it seems that older leaves could be a source of nutrients for younger leaves because fungal growth was lower when they were covered or cut (Figure 2.10, Figure 2.10). The fungal growth data are consistent with standard sink-source relationships. Covering younger leaves increased fungal growth in older leaves at 15 dai, suggesting removal of a sink. This did not occur when younger leaves were cut; infected older leaves had less growth and died at 15 dai. A possible confounding factor is that wounding the plant by cutting leaves could trigger stress responses or senescence signals that decrease fungal growth. This may detract from the data presented in Figure 2.11.

I have shown that experiments designed to manipulate photosynthate distributions affect fungal growth. Variables that contribute to photosynthate levels in the infected leaf include environmental and developmental conditions such as light intensity and leaf age. In plants, photosynthate flux is regulated by the concentrations of sucrose and hexoses in each tissue. The hexose: sucrose ratio defines if the tissue exports or imports nutrients. For example, high levels of hexoses stimulate sucrose import, while high levels of sucrose stimulate export to other tissues. To test the effect of sugars on fungal biomass accumulation, I devised a detached leaf experiment. I infected the youngest fully expanded leaf from young stage cv. Morocco plants (ie, the 6th leaf as depicted in Figure 2.8) with *PST*-79, excised the leaf at 4 dai, and transferred it to a 15 mL polypropylene tube containing ¼ Hoagland's solution, which contains nitrogen but no carbon component. The media was either supplemented with sucrose or not supplemented. The light regime for detached leaves was the same as for intact plants, but in a cabinet with vertical lights. I measured leaf chitin content at 4 and 10 days after excision (8 and 14 dai respectively), as these are informative time points as defined in Figure 2.7. The idea of the

detached experiments is to mimic the situation when the infected tissue is a sink importing sugars from distal organs/tissues. This experimental system allowed me to control the import of sugar compounds from exogenous sources. On average, under control conditions (unsupplemented solution) fungal growth increased as observed in previous experiments (Figure 2.12) and *Pst* sporulated at 14 dai (data not shown). This is a novel experiment showing that fungal growth is not affected in detached leaves and can be used to test different leaf conditions. I then tested different concentrations of sucrose (1.5 mM (5% w/v) and 60 mM (20% w/v) for their effects on fungal growth. Fungal growth was enhanced by sucrose addition relative to the unsupplemented control at both 8 and 14 dai (Figure 2.12). The clearest increase was with 5% sucrose at both time points. While the 20% treatment also increased fungal growth, it did so less than the 5% treatment. This may be in part because the excess of sucrose (20%) caused osmotic stress in the leaf, observed here as chlorosis. However, the fungal growth could still be measured, and where pustules developed the surrounding tissue remained green (data not shown). This may suggest that the infection helped to reduce the excess of sucrose, or that the fungus keeps the tissue alive through some alternate mechanism.

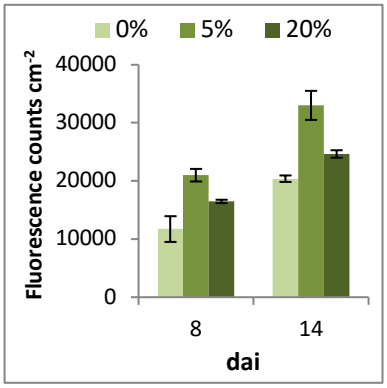

Figure 2.12. Growth of *PST*-79 on detached wheat leaves grown in liquid media, with or without added sucrose. The youngest fully expanded leaf of young stage cv. Morocco plants was infected with *Pst* after the appearance of the 7th leaf. I detached the infected leaves at 4 dai and transferred them to ¼x Hoagland's solution. Sucrose was added to the media as indicated. Leaf chitin content was recorded at 8 and 14 dai. Error bars represent the standard error of three replicates. Asterisk represents significant differences compared to 0% using a t-test and a p-value lower than 0.05.

To examine the effect of other carbohydrates on fungal growth, I tested the effect of exogenous sugars (fructose, glucose, sucrose) and the glucose derivative two-deoxy-D-glucose (2-DG) on *PST*-79 growth. The 2-DG acts as a competitive inhibitor of glycolysis after it has been phosphorylated by hexokinases. This depletes ATP from the cell and increases stress responses, making 2-DG-P toxic. This molecule should affect both plant and fungal metabolism. I examined the effects of adding 2.2 mM fructose, 2.2 mM glucose, 2.2 mM sucrose, or 2.2 mM 2-DG on fungal growth, using my detached leaf assay. Under control conditions (unsupplemented

solution) fungal growth was similar at 8 and 14 dai (Figure 2.13). This contradicts the results of Figure 2.12 where fungal growth increased, the difference might be associated with the plant growth conditions or the activity of the inoculum. The data were not highly variable as represented by the error bars. Detached leaves at 8 dai growing in Hoagland solution complemented with fructose, glucose or sucrose had less fungal growth compared to the control. Interestingly, growth was similar between control and when the media was supplemented with 2-DG (Figure 2.13). Less fungal growth at 8 dai in media supplemented with sucrose, glucose or fructose is difficult to explain, but the differences in concentrations (1.5 mM vs 2.2 mM in Figures 2.12 and 2.13 respectively) should be noted. In contrast, leaves in media supplemented with fructose, glucose or sucrose had more fungal growth at 14 dai than unsupplemented leaves. The 2-DG treatment did not show increased fungal growth at 14 dai. Overall the results suggest that endogenous plant sugars were sufficient to support the initial infection, but after eight dai exogenous sugars (fructose, glucose and sucrose) supplement fungal growth. There was no apparent fungal preference between the sugars. The glucose analogue, 2-DG, could not substitute for exogenous carbon, shown as similar growth to the unsupplemented solution. The results have two possible explanations; 2-DG does not have an effect on plant and fungal growth, or the fungus can survive on only those nutrients present at the time of infection.

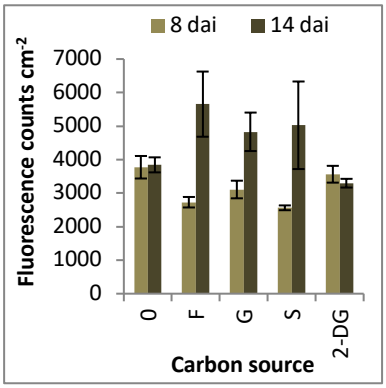

Figure 2.13. Growth of *PST*-79 on detached leaves in liquid media with or without exogenously supplied sugars. The experimental conditions were identical to Figure 2.12. 0, no carbohydrates; F, fructose; G, glucose; S, sucrose; 2-DG, 2-deoxyglucose. All sugars were added at 2 mM. Error bars represent standard error of four replicates. The experiment was repeated independently two times. Letter *a* represents significant differences compared to the control and letter *b* compared to fructose and sucrose; both using a t-test and a p-value lower than 0.05.

2.3.3 The growth profile of *PST*-79

Based on the results presented in this Chapter, it seems the studied variables have a major effect on *PST*-79 sporulation. There were no significant changes before 8 dai, therefore it is possible that nutrient availability is not limiting to fungal growth at these time points. After 8 dai, nutrients are limiting, consequently under low nutrient conditions the fungus grows less. A complementary experiment could be to examine pustule growth under different plant growth

conditions, such as low/high light regimes or with nutrient supplements. This might reveal if the changes at 14 dai are related to the accumulation of hyphae, or are due to the demands of spore production.

It seems that the increased fungal growth leading to sporulation requires more nutrients than can be sourced from the local infected tissue, requiring import from distal sources. This statement is based on certain conditions that I evaluated that affected nutrient availability, such as deprivation of light or forced changes in sink-source relationships. To test if sporulation relies on external sources of carbon, I devised a detached leaf experiment where I used the youngest fully expanded leaf (6^{th} leaf) from young stage cv. Morocco plants with the 7^{th} leaf emergent. I defined a leaf area (7 cm^2) for infection, and painted the whole leaf or one half of the leaf with *Pst* urediniospores to infect them (see Figure 2.14 A for schematic). After four dai I excised the defined leaf area and placed it in a vessel containing ¼x Hoagland's solution without added carbohydrates. This arrangement means that nutrients for fungal growth must be obtained from the host tissue. I grew the detached leaves under normal conditions (see section 2.2.1). The detached leaves remained green during the entirety of the experiment and sporulation occurred at 14 dai, even in the submerged part of the leaf. I harvested infected areas with a four cm^2 cork borer to standardise the area sampled (Figure 2.14 A), taking three leaf disks per infected leaf. I estimated fungal growth using the chitin detection technique as in previous experiments. I found that fungal growth increased over time in whole and half-infected leaves, and was similar in both types of leaves (Figure 2.14 B). These results suggest that healthy area close to the infection did not have an effect on fungal growth and rejects my hypothesis that proximal non-infected tissue is a source of nutrients. I repeated the same experiment but supplemented the media with different carbon sources; fructose, glucose or sucrose, each at 2.2 mM) (data not shown). Fungal growth was similar between the unsupplemented solution and each of the sugar solutions at 8 dai. Only the fructose treatment showed a difference at 14 dai, where the whole infected leaf had more fungal growth than the half-infected leaf. This is similar to the previous results (Fig 2.14) where healthy proximal tissue did not have increase fungal growth. The purpose of these experiments was to evaluate if healthy areas can provide nutrients to infected areas in a leaf. However, it seems that at the single leaf scale there is no clear role for proximal areas as a source of nutrients for infected areas.

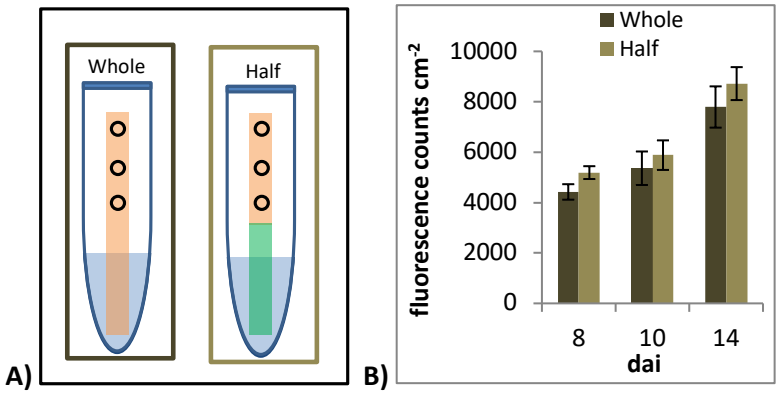

Figure 2.14 Growth of *PST*-79 in detached leaves. A, cartoon indicating the infection schema; the infected part of the leaf is represented in orange, and the uninfected area in green. The black circles represent the samples taken with a cork borer for chitin measurements. B, bar graph showing increase in chitin content per unit leaf area at different time points after infection (dai). Error bars represent the standard error of 5 replicates.

2.3.4 Effect of plant development on *PST*-79 biomass in resistant wheat lines

The experiments described above in this Chapter were performed on the susceptible wheat cv. Morocco and are based on the hypothesis that modification in photosynthate fluxes across the plant affects fungal growth. My results based on forced changes to host sink-source relationships (light intensity, detached leaves) support this idea. Sink and source tissues change during plant development because younger and older tissues have different nutrient requirements. The major sink in older wheat plants is the developing head containing the grains. In plants of this age, the major photosynthate sources are the youngest leaves called the flag and flag-1 leaves (Figure 1.9) (White and Edwards, 2008). In wheat, there is a type of genetic resistance against fungal biotrophs which is higher in plants with a flag leaf (adult plant resistance (APR)). This suggests a role for plant development in resistance, which given the nature of the flag leaf might be related to its metabolic status. In this section of Chapter Two I tried to determine if sink-source relationships could contribute to APR status. To test this, I used two resistant wheat lines, T_Yr18 and T_Yr46, which possess *APR* genes coding for an ABC transporter and hexose transporter respectively (Krattinger et al., 2009; Moore et al., 2015). As a control, I used the near-isogenic susceptible line cv. Thatcher (Section 2.2.1). As APR phenotypes, classically can be detected only in the field; the first experiment was to measure if the resistance phenotype could be detected in plants growing in artificial conditions (plant growth chamber). For this experiment, cv. Thatcher, T_Yr18 and T_Yr46 plants were grown in a chamber for two months until the flag leaf was fully expanded. The growth conditions were as described for cv. Morocco plants (Section 2.2.1). I painted the flag leaf of these plants with *PST*-79 urediniospores and kept them under the same growth conditions for 14 days. At the time of

infection, T_Yr18 had not yet developed the flag leaf, so instead I infected the last fully emerged leaf, knowing that it was not comparable. At 8 dai, infected cv. Thatcher had developed more chlorotic spots across the flag leaf than infected T_Yr46 (Figure 2.15). The infected T_Yr18 leaves had similar symptoms to infected cv. Thatcher flag leaves. None of the infected leaves produced spores (data not shown); however, the chlorotic spots were bigger and more abundant in cv. Thatcher and T_Yr18 than in T_Yr46. This phenotype could be attributed to growth chamber rather than field conditions. To correlate the phenotype with leaf chitin content, I tested fungal growth using the WGA-FITC assay. To ensure comparable time points to the previous experiments, I collected infected leaves at 8, 10 and 14 dai. Fungal growth in cv. Thatcher increased linearly over the three time points (Figure 2.16).

Due to technical errors, the T_Yr18 samples at 8 dai were lost, but despite this fungal growth increased from 10 to 14 dai. For T_Yr46, slight fungal growth was evident across the three time points but this was far less than for the Thatcher control. I did not observed sporulation in any of the infected leaves of Thatcher, T_Yr18 or T_Yr46. Comparing the three lines, more fungal growth was evident on the T_Yr18 line than on cv. Thatcher at 10 and 14 dai, and growth on these lines was far more than on the resistant T_Yr46 line at the same time points. There was already less growth of *PST*-79 on T_Yr46 than the parent line Thatcher at 8 dai. This is consistent with the symptoms of infection and the fact that APR is often higher in the flag leaf (Figure 2.16). As this first experiment was simply a proof of concept to show that *APR* phenotypes can also be detected in artificial growth conditions and the response is stronger in the presence of flag leaves, it was not repeated on T_Yr18 plants. This result showed that the *Yr46* resistance phenotype can be detected in artificial conditions, and that plant developmental stage is an important part of *APR* conferred by *Yr46*.

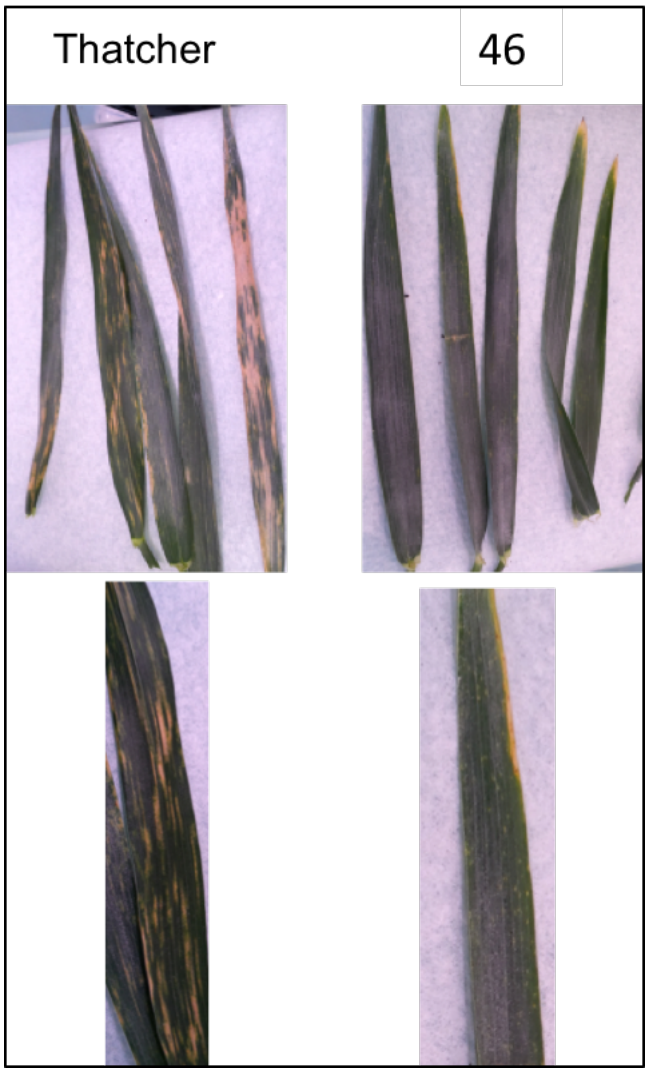

Figure 2.15. Photograph of infected flag leaves from Thatcher (left) and T_Yr46 (right) at 9 dai. Top panel, five representative flag leaves. Bottom panel, the zoom-in of one of the leaves of each genotype from the top panel.

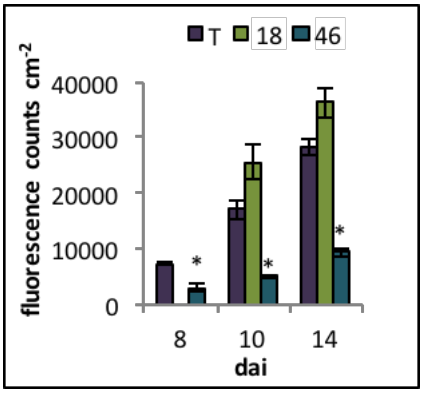

Figure 2.16. Growth of *PST*-79 on cv. Thatcher and its near-isogenic *APR* lines T_Yr46 and T_Yr18. T, Thatcher flag leaf; 34, T_Yr18 flag-1 leaf; 67, T_Yr46 flag leaf. Error bars represent the standard error of four replicates. Asterisk represents significant differences compared to cv. Thatcher, using a t-test and a p-value lower than 0.05.

I showed above (Section 2.3.2) that covering or excising leaves of young stage cv. Morocco influenced fungal growth. When older leaves were covered or removed, fungal growth decreased in younger leaves. To test if this also applies in adult plants, I devised an experiment in which adult T_Yr46 and cv. Thatcher lines were infected (on the flag leaf), while both the flag-1 and flag-2 leaves (older leaves) were blocked from light by aluminium foil or excised from the plant. I then measured fungal growth in the flag leaves at 8, 10 and 14 dai (Figure 2.17).

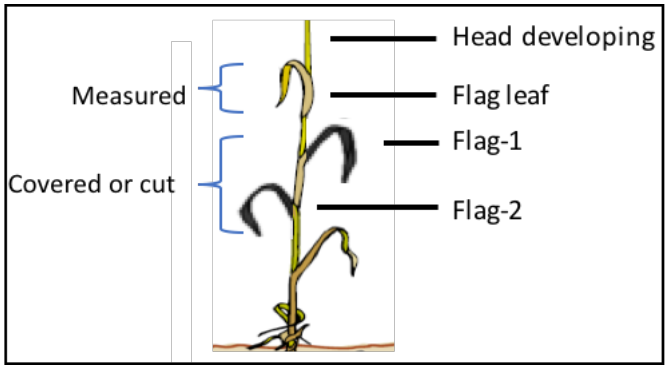

Figure 2.17. Scheme of *Pst* infections on adult cv. Thatcher and T_Yr46 flag leaves. The plants were infected when the flag leaf was fully expanded and the heads were developing but not yet emerged. The flag leaf was infected. In subsequent experiments, the flag-1 and flag-2 leaves were excised or shaded with aluminium foil.

PST-79 growth on cv. Thatcher increased strongly over time (Figure 2.18) as observed previously. Shading of both the flag-1 and flag-2 leaves with aluminium foil did not change the fungal growth profile significantly from unshaded plants (Figure 2.18 A). When flag-1 and flag-2 were removed from the plant, there was less fungal growth at 10 dai but more at 14 dai compared to unshaded control plants. Thus, fungal growth on cv. Thatcher was affected only by removing the older leaves, but not by shading. This result is similar to previous experiments in young stage cv. Morocco plants between 9 and 10 dai where fungal growth was also reduced when older leaves were removed (Figure 2.11 A, Figure 2.18 A). However fungal growth was not affected at 15 dai in cv. Morocco, whereas in cv. Thatcher it increased at 14 dai. The differences between cv. Morocco and Thatcher could be due to the different developmental stages of each plant used in my experiments; I studied younger cv. Morocco plants while the Thatcher experiments were on adult plants. An alternative hypothesis could be that these cultivars have different genetic backgrounds reflected in different physiological characteristics such as the number of stomata per unit leaf area or photosynthetic capacity.

A) 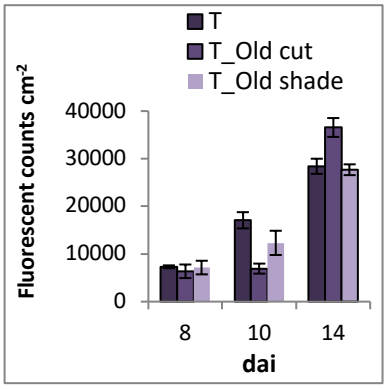

B) 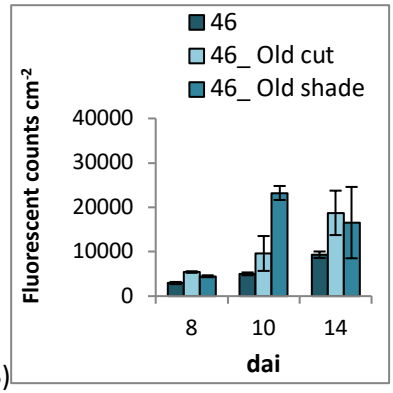

Figure 2.18 Growth of *PST*-79 on adult cv. Thatcher and T_Yr46 plants; effects of manipulation of older leaves. A, B Growth on cv. Thatcher and T_Yr46 flag leaves. T and 67, control conditions. Old cut, with excised flag-1 and flag-2 leaves (see Fig. 2.15 for schema). Old shade; flag-1 and flag-2 leaves covered with aluminium foil. The experimental conditions are explained in Figure 2.17. The experiments were performed concurrently and repeated twice. Error bars represent the standard error of four replicates. Asterisk represents significant differences compared to the control, using a t-test and a p-value lower than 0.05.

For the T-Yr46 line containing *Yr46*, *PST*-79 growth increased slightly over time as observed previously (Figure 2.18 B). Interestingly, greater fungal growth was seen when the flag-1 and flag-2 leaves were excised or shaded. When older leaves were removed from these plants, fungal growth was higher at 10 and 14 dai. With flag-1 and flag-2 were covered, fungal growth increased relative to unshaded plants at 8 and 10 dai, but declined at 14 dai (Figure 2.18 B). The only statistically significant difference in this experiment compared to control plants was in flag leaves with shaded older leaves at 10 dai. Thus, manipulation of both flag-1 and flag-2 increased fungal growth in the T_Yr46 flag leaf, suggesting that this overcame the effect of the *Yr46* gene. Potential reasons for this are yet unknown, but could be related to differences in carbon nutrition in the shaded and cut-off plants. Altering older leaves may change the import/export signals for photosynthates. In the context of the current results, the flag leaf is the strongest source leaf in the plant, so perhaps shading or cutting older leaves stresses the plants, making other leaves become sink. Thus, in manipulated plants nutrient flow, there may be more carbon nutrients available to the fungus. It follows that possibly the role of Yr46 is to oppose this effect. As *Yr46* encodes a hexose transporter, it may decreased the sugar levels available to the pathogen (Dodds and Lagudah, 2016). Another possibility relates to changes in flag leaf photosynthesis, since the changes (covering or cutting) in older leaves would be expected to alter nutrient reallocation. Higher rates of photosynthesis would mean that more carbon and nitrogen are available both to the plant and the fungus. I discounted a potential negative effect of a putative wounded tissue response due to leaf excision, because fungal growth was higher when older leaves were cut (Figure 2.18).

The main role of metabolism in adult plants is to provide nutrients for grain filling. Thus, flag leaves have increased photosynthetic capacity and contribute the photosynthate flux towards the heads. APR is effective at this developmental stage, therefore if all sinks are removed, this could change the metabolic conditions of the flag leaf leading to changes in expression levels or activity of the Yr46 transporter, consequently compromising resistance. To test this hypothesis, I measured fungal growth in intact or detached flag leaves from cv. Thatcher and T_Yr46 plants. Both experiments were performed concurrently. For the detached leaf experiment, I infected flag leaves, excised them at 4 dai and placed them in ¼x Hoagland's solution without carbohydrates. I grew the detached leaves in the conditions described above (Section 2.2.1). As observed previously (Figure 2.16), intact cv. Thatcher flag leaves allowed more fungal growth and produced more chlorotic spots than those of T_Yr46 (Figure 2.19 A, B), consistent with the *APR* phenotype of *Yr46*. Conversely, detached flag leaves from both cv. Thatcher and T_Yr46 accumulated similar amounts of chitin (Figure 2.19 C). A further phenomenon that I observed in the detached leaves was the development of black dots (Figure 2.19 d). The black dots appeared at 14 dai (the time of collection) but I did not follow their development further because I did not have sufficient samples to continue the experiment. The dots seemed to be a host response rather than an alternate *Pst* spore phase such as development of black teliospores, because they were flat translucent dots rather than black opaque dots on the leaf surface. Overall, my results show that APR was observable in both intact and detached leaves of T_Yr46. Chitin fluorescence counts detected using WGA-FITC were always below 15,000 and did not increase between 8 and 14 dai for T_Yr46. On the other hand, detached flag leaves of cv. Thatcher and T_Yr46 accumulated less fungal chitin than intact flag leaves. The lack of transcriptomic and metabolomic data from detached leaves limits the interpretation of the results, because it is not possible to associate resistance with changes in *Yr46* expression or changes in sugar levels.

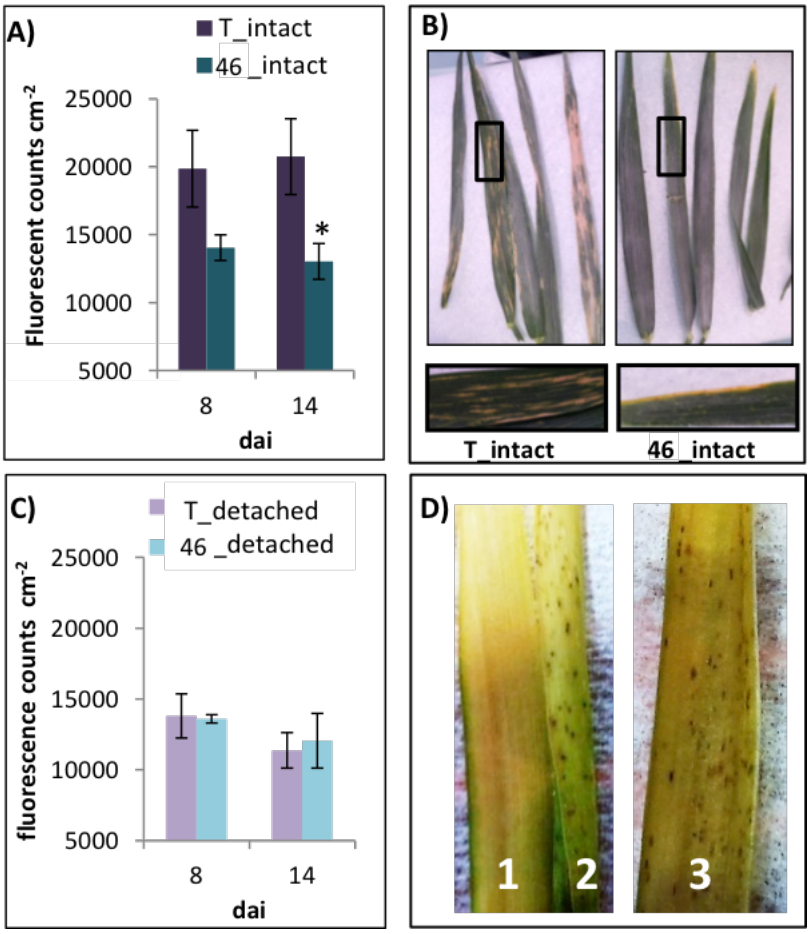

Figure 2.19. Growth of *PST*-79 on intact or detached flag leaves. A) Fungal growth on intact flag leaves from cv. Thatcher (T_intact) and T_Yr46 (67_intact). Chitin was measured by WGA-FITC assays at 8 and 14 dai. B) Flag leaves from cv. Thatcher and T_Yr46 infected with *PST*-79 at 14 dai showing chlorosis in both lines before chitin quantification. The top panel shows the characteristic phenotype in all samples collected. The black box, represented in the bottom panel, is a close up of the top panel. C) Fungal growth on detached flag leaves of cv. Thatcher (T_detached) and T_Yr46 (67_detached). D) Detached flag leaves from non-infected plants (1), from T_detached (2) and 67_detached (3). Leaves from cv. Thatcher (2) and T_Yr46 (3) had black spots across the infected area with a similar distribution in all collected samples. Error bars represent the standard error of 6 replicates. Asterisk represents significant differences compared to the susceptible line using a t-test and a p-value lower than 0.05.

A possible explanation for the results in (Figure 2.18, Figure 2.19) is that detachment of the leaves changed the type or concentration of leaf nutrients that in turn affected fungal growth. To evaluate the effect of exogenous carbon sources on fungal growth in APR plants, I measured chitin in detached infected T_Yr46, T_Yr18 and cv. Thatcher flag leaves in media with or without added glucose or sucrose. I used detached T_Yr18 flag leaves as a control for APR. For this experiment, I infected flag leaves of T_Yr46, T_Yr18 and cv. Thatcher with *PST*-79 urediniospores. I excised the leaves at 4 dai and placed them in ¼ Hoagland's solution without carbohydrates, or with 2.2 mM glucose or 2.2 mM sucrose. I grew the detached leaves in the same conditions described above (Section 2.2.1) and collected samples at 8 and 14 dai. After measuring fungal chitin, I found that fungal growth in the absence of added carbon was lower

in cv. Thatcher at 8 dai compared to T_Yr46 and T_Yr18 plants, but the values for all genotypes were similar by 14 dai (Figure 2.20). In glucose media, the fungal growth on all genotypes was similar at 8 dai, while at 14 dai cv. Thatcher leaves contained more chitin than T_Yr46 but these levels were similar to those in T_Yr18 leaves (Figure 2.20). When sucrose was added to the media, fungal growth was similar in all genotypes at 8 dai. Interestingly, more chitin accumulated in T_Yr18 leaves at the 14 dai time point compared to Thatcher and T_Yr46 (Figure 2.20). In summary, more fungus grew on detached flag leaves from cv. Thatcher at 14 dai in the presence of glucose, whereas T_Yr18 leaves grew more fungus in the presence of sucrose. Detached leaves from T_Yr18 and T_Yr46 were too variable in sucrose media, where T_Yr18 had more chitin content (Figure 2.20).

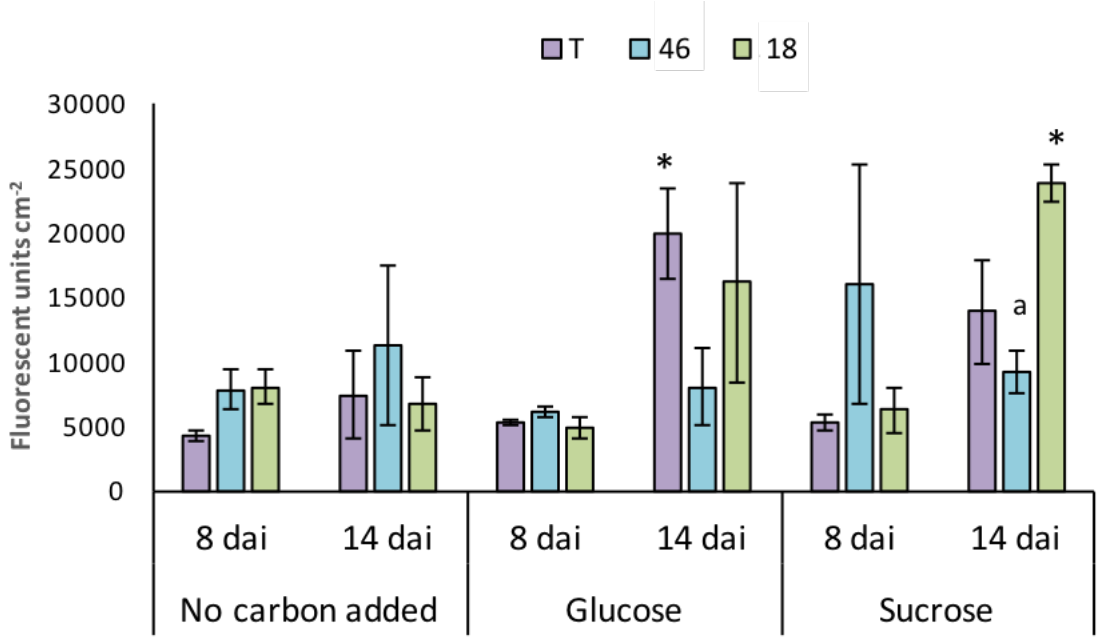

Figure 2.20 Growth of *PST*-79 on detached flag leaves of cv. Thatcher (T), T_Yr46 (67) and T_Yr18 (34) in media without added carbon source or supplemented with 2.2 mM glucose or 2.2 mM sucrose. Error bars represent standard error of four replicates. The experiment was repeated independently two times. Asterisk represents significant differences compared to media without carbon source, while *a* is compared to T_Yr18 at 14 dai, both using a t-test and a p-value lower than 0.05.

The stronger response of cv. Thatcher detached leaves to glucose over sucrose suggests that higher levels of glucose in the apoplast could be taken up directly by the infectious hyphae, or that higher glucose levels change the activity of sugar transporters in cv. Thatcher leaves favouring higher transport towards the infected cells. Detached leaves from T_Yr46 seem to support consistent fungal growth under all the three treatments, with fluorescence counts below 15,000. This suggests that the Yr46 function was not affected by adding exogenous carbon. In contrast, my data suggest that resistance conferred by the *Yr18* gene was overcome by addition of sucrose, but addition of glucose had a variable effect on fungal growth. One explanation could be that *Yr18*, which encodes an ABC transporter, transports sucrose into

infected cells where the fungus will take it up directly and after break sucrose down into hexoses. Overall the data need to be extended by comparisons between sugar levels in whole infected tissue versus the apoplast. The response to infection might be associated with accumulation of nutrients in the cytoplasm where the fungus can take them up, or potentially the transporters change the flux or direction of nutrients, restricting their access to the fungus by accumulating them

In summary, *PST*-79 extracts nutrients gradually from the plant during the asexual infection cycle to provide sufficient energy for its massive spore production. Here I altered plant nutrient status and studied the effects on fungal growth. Under growth conditions that were designed to reduce plant nutrients, fungal growth decreased mainly after 8 dai. This suggests that the fungus does not have high nutrient requirements in the early part of its cycle, but requires large amounts for sporulation. In a crop context, this means that high levels of fertilizer may allow the fungus to produce high numbers of spores due to the abundance of nutrients. A strategy to reduce infection could be to change the way fertilizers are applied in the field, or to design plants that accumulate different carbon containing molecules that the fungus cannot access to but can still be accumulated and used as energy molecules for the plant.

For APR, it seems that Yr46 prevents the flag leaf from acting as sink, reducing the cytoplasmic nutrients available to the fungus. Possibly the nutrients accumulate instead in the apoplast, or are transported to other tissues. However, to fully understand the mechanism(s) of APR resistance, new experimental approaches are required, considering for example accumulation of nutrients in plant compartments.

CHAPTER 3
Alterations in photosynthesis and metabolite pathways during *Pst* infections of wheat

3.1 Introduction

From Chapter Two, it is clear the fungus extracts enormous quantities of plant nutrients to the extent that the infected tissue changes in physiological status from source to sink. Several questions arise from this, such as: Does the fungus manipulate plant metabolism pathways directly? How are plant metabolic pathways affected? Which are the main plant nutrients that the fungus extracts? Is there a systemic response, at the level of primary nutrition, to the infection? In this Chapter, I evaluate the effects of *PST*-79 infection on primary plant metabolism with a particular focus on photosynthesis and its products.

Plants produce carbon nutrients by photosynthesis. This occurs in the chloroplast though two interconnected pathways; harvesting of light energy (photon capture) and carbon fixation. Photon capture occurs in the thylakoid membrane where photosystems II and I absorb photons though chlorophyll pigments. This process releases electrons that are transported via carriers along an energy gradient to produce nicotinamide adenine dinucleotide phosphate (NADPH) and ATP (adenosine triphosphate), key molecules for carbon fixation (Section 1.3.2.1 in Chapter 1). Photon capture is a plant performance indicator; healthy plants and younger leaves use light energy more efficiently. Under biotic and abiotic stresses such as pathogen infection or

wounding, photon capture is one of the first pathways to be affected (Berger et al., 2007). In stress conditions plants reduce chlorophyll and synthesis of thylakoid membrane proteins, consequently decreasing ATP and NAPDH production.

Photon capture efficiency can be measured via chlorophyll fluorescence dynamics. This is based on the principle that photons absorbed by plants may have one of three destinations; they can be re-emitted as chlorophyll fluorescence, used in photosynthesis (photochemical quenching), or can be dissipated as heat (non-photochemical quenching) (Maxwell, 2002). These three processes compete for photonic energy. For example, a decrease in chlorophyll fluorescence (quenching) means an increase in photochemical or non-photochemical quenching (Figure 3.1). Photochemical quenching (PQ) consists of a series of reactions that starts when chlorophyll pigments absorb photons and ends with the production of ATP, NADPH and oxygen (Fig 1.12; Chapter 1). When PQ is not possible due to saturation of the system (excess of photons), alterations in thylakoid membranes, photosystem damage, or pH changes in the chloroplast lumen, the excited chlorophyll returns to the ground state releasing the energy as heat; this is a measurable effect known as non-photochemical quenching (NPQ) and is a protection mechanism against excess light. The third possibility is the release of photons as fluorescence, which represents 1-5% of the light absorbed by chlorophyll (Quilliam et al., 2006).

For chlorophyll fluorescence dynamics, leaves or plants are placed in a chamber under a specialized camera which images chlorophyll fluorescence under normal and high light conditions (Figure 3.1). High light is used to saturate the photon capture pathway. As a consequence, the plant is unable to use the energy for photosynthesis which can only be re-emitted as fluorescence or dissipated as heat. I used the differences observed in chlorophyll fluorescence, under high and normal light stimuli, to calculate the potential and actual efficiency of photochemical quenching and NPQ during *PST*-79 infection in wheat (Table 3.1). Chlorophyll fluorescence dynamics represents the first part of this Chapter.

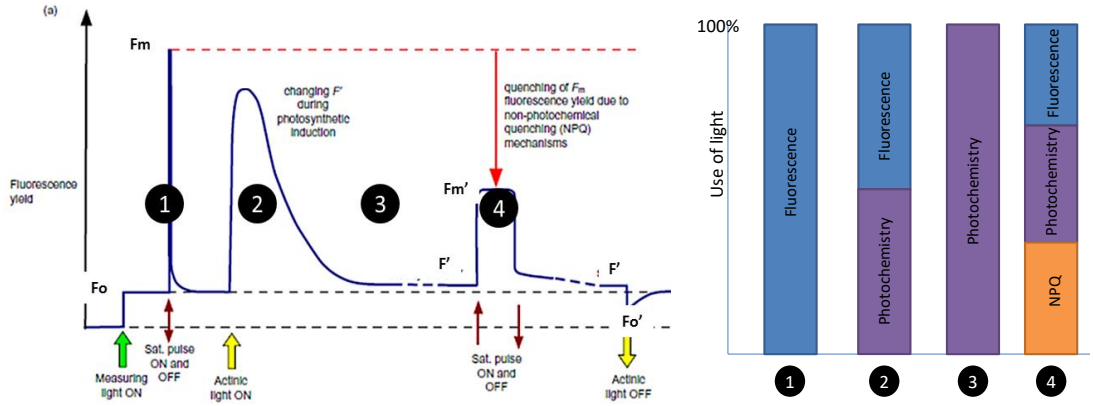

Figure 3.1. Chlorophyll fluorescence dynamics. The leaf is placed into a chamber where responses to normal and high light are measured as fluorescence. Inside the chamber there is a camera which captures and images fluorescence and controls the applied light intensity. The different light intensities and plant responses allow derivation of the three components of photonic energy dissipation; PQ, NPQ and fluorescence. Left panel shows the model of chlorophyll fluorescence dynamics of a leaf under different light conditions. Right panel shows the use of energy in healthy plants under the conditions in the left panel. The four phases are indicated by closed black circles (1-4). In Phase 1, the leaf is subjected to a brief saturating light pulse. All of this energy is released as fluorescence and the value, Fm, is the maximal fluorescence of the leaf. In Phase 2, actinic light (normal intensity light) is applied constantly, which leads to an initial burst of fluorescence that declines gradually as photonic energy is dispersed by photochemistry and fluorescence. By Phase 3, all incident energy is dissipated by photochemical quenching. In Phase 4, a saturating light stimulus is applied, with excess energy released by NPQ. The Fm' value is the maximum fluorescence when plants have been exposed to normal growth lighting. The fluorescence data acquired by the camera is transferred to a computer that calculates the efficiency of photon capture using the equations in Table 3.1. Fo, minimal fluorescence; F' maximum photochemical quenching; Fo', minimal fluorescence in darkness. Image from the left panel adapted from(Harbinson, 2013).

Table 3.1 Chlorophyll fluorescence dynamics equations.

Name	Equation	Explanation
Fv/Fm	F_o-F_m/F_m	Potential efficiency of PSII
NPQ	(F_m-F_m')/F_m'	Non-photochemical quenching
ΦPSII	F_m'-F'/F_m'	Proportion of absorbed photons that are used in photochemical quenching

The products of photon capture, ATP and NADPH, are required for carbon fixation. This is one of the most important metabolic processes in plants and occurs in the chloroplast stroma through the Calvin-Benson cycle (Chapter 1, Figure 1.12). In the cycle the enzyme Rubisco fixes CO_2 to produce a three-carbon molecule (triose), the starting point for the synthesis of larger carbohydrates. The cycle is controlled directly by the availability of ribulose 1,5-bisphosphate (RuBP), the catalytic activity of Rubisco, ATP and NADPH levels, and CO_2 concentrations. The

cycle is indirectly affected by light intensity, temperature, atmospheric pressure, pathogenic infections and the ease by which air passes through stomata (conductance).

One way to study the Calvin-Benson cycle is through the relationship between CO_2 fixation by Rubisco (also called assimilation (A) rates) and CO_2 concentrations (Ci) (Figure 3.2). This is plotted as a kinetic curve called the A/Ci curve. The A/Ci curve can be divided into three phases; Rubisco carboxylation activity (Vc), RuBP regeneration (J) and triose phosphate use (TPU) (Long and Bernacchi, 2003; Sharkey et al., 2007). The A/Ci curve helps to explain if Rubisco activity, RuBP availability, or triose levels are limiting factors in the cycle. The first phase of the A/Ci curve, Vc, helps to calculate the efficiency of Rubisco in fixing carbon (Figure 3.2) (von Caemmerer et al., 1994; Farquhar et al., 1980). The principle of the curve is based on the affinity of Rubisco for CO_2 and O_2. At low CO_2 concentrations, assimilation rates are limited by the interaction of Rubisco with O_2 while at higher CO_2 concentrations assimilation rates increase. The curve helps to calculate the Vmax constant (Vc) for Rubisco, based on Michaelis-Menten kinetics and the different CO_2 concentrations.

The second phase of the A/Ci curve, J, depends on RuBP regeneration. In theory, Rubisco activity should be linear with increasing CO_2 concentrations, however the activity is limited by substrate availability and the curve reaches a plateau at high CO_2 concentrations. This occurs when there is insufficient ATP and NADPH from photon capture to replenish RuBP. Therefore, Rubisco lacks its substrate, assimilation rates become constant, and excess CO_2 stays in the intercellular spaces. The third phase of the A/Ci curve, TPU, is where the cycle is limited by accumulation of triose-phosphate (triose-P). When triose-P cannot be used for sugar synthesis, triose-P levels rise, reducing the activity of the Calvin-Benson cycle and consequently the amount of CO_2 fixed. In the A/Ci curve, TPU is part of the A plateau at high CO_2 levels. I studied A/Ci curves in different light conditions, and I also measured leaf conductance to evaluate how the Calvin-Benson cycle is affected in wheat leaves infected with *Pst*. This represents the second part of this Chapter.

The main product of the Calvin-Benson cycle, triose-P, is used in the production of sucrose, fructans and starch. Starch is a carbon store, composed of long branched chains of glucose molecules and is deposited as insoluble granules in the chloroplast. Plants accumulate starch during the day when there are more sugars available than needed, and utilize it at night. In contrast to starch, sucrose and fructans are soluble sugars that accumulate in the vacuole or the cytoplasm during both day and night. The basic structure of fructans is a sucrose molecule with one or more fructose units. This type of carbohydrate is more abundant in the leaves and stems of cereals than starch (Valluru and Van den Ende, 2008; Van den Ende, 2013). Sucrose, fructans and starch indicate the metabolic status of the plant. For example, starch accumulation is

affected by starvation and senescence. Starch synthesis increases during starvation and is consumed faster at night; as a consequence plant growth slows down. During senescence, starch is degraded, mobilising carbon to younger tissues. Levels of starch, fructans and sucrose change during plant development and in respond to biotic and abiotic stresses. Source tissue produces sucrose and fructans that are exported to sink tissue, like seeds and roots. Sink tissues use hexoses in metabolic processes or accumulate glucose as starch. Under stress conditions, hexose levels increase as signals to trigger defence responses, for example to synthesize protective polysaccharides (Luna et al., 2010). Plant pathogens modify plant metabolism by increasing hexoses available for uptake by changing the metabolic status of the infected tissue to sink, stimulating the import of nutrients from source tissues (Doehlemann et al., 2008; Horst et al., 2008, 2010). In general sugars are signals that regulate photosynthesis, determine the metabolic stage of plants and are substrates for pathogens. In the last part of this Chapter, I measured levels of sugars and other primary metabolites, the activity of invertases, enzymes that breakdown sucrose, and the expression of genes related to metabolism. These data will help to answer the questions raised in Chapter 2 of how *PST*-79 infection affects wheat metabolism.

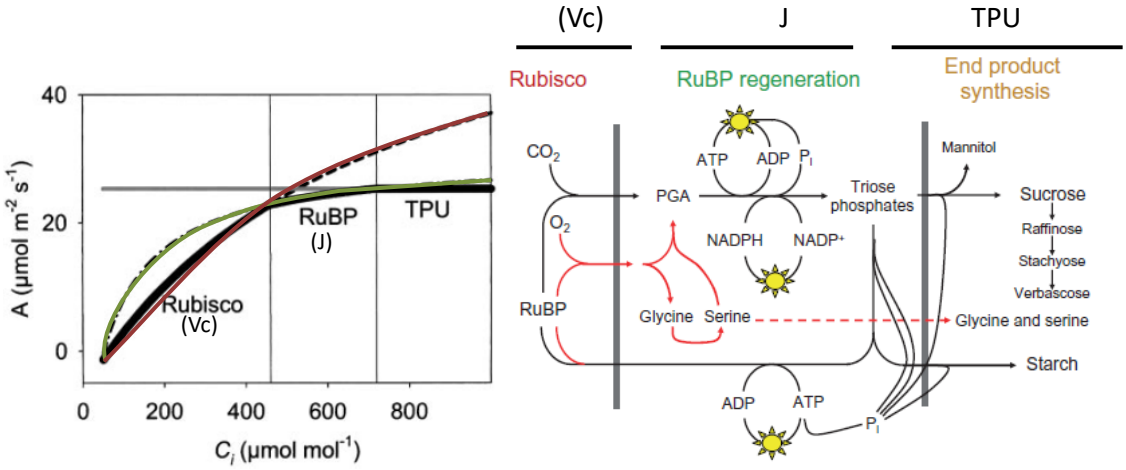

Figure 3.2. A/Ci curve model and limiting factors. The leaf is placed in a small chamber that measures the residual CO_2 that the plant does not absorb, and water vapour. The left panel is the theoretical A/Ci curve which reports the relationship between carbon fixation (A) and CO_2 concentration. The red curve is the theoretical activity of Rubisco with no limiting factors. The green curve indicates the activity of Rubisco when RuBP and triose-P are limiting; at the asymptote of the curve the fixation rates become constant. The black A/Ci curve is the combination of the red and green curves. At low CO_2 concentrations, the activity of Rubisco is almost linear. This corresponds to the first phase of the curve or the Rubisco carboxylation activity (Vc). At high CO_2 concentrations, the curve reaches a plateau, this comprises the second and third phases of the curve, limited by RuBP and triose-P (TPU) respectively. See text for details. The right panel depicts the metabolic processes underlying A/Ci curves. In the first phase of the A/Ci curve, the activity of Rubisco depends on CO_2 and O_2 concentrations. The second phase, J, is limited by the efficiency of the cycle in replenishing RuBP, which relies on the levels of ATP, NADPH and inorganic phosphorus (Pi). It is also dependent on 3-phosphoglycerate (PGA) levels, another component of the cycle that is replenished from glycine and serine. The third phase, TPU, relies on the triose-P levels in the chloroplast. Triose-P can be used to produce starch in the chloroplast or exported to the cytoplasm for sugar synthesis. If these processes are

reduced, triose-P accumulates and inhibits the cycle. Cartoons taken from Long and Bernacchi, 2003; Sharkey et al., 2007.

3.2 Materials and Methods

3.2.1 Biological materials

Most of the experiments are based on materials and methods from Section 2.2 of Chapter 2 unless otherwise stated. *Pst* infections were performed on young stage plants in which the 7th leaf had emerged but not expanded (approximately four-weeks old), and adult plants (flag leaf expanded). For study of the systemic responses to *Pst* infections, the flag and flag-1 leaves were evaluated. The flag leaf was completely infected (I_A) or mock inoculated (H_A) and compared to distal leaves that were not infected (I_B, H_B) (Figure 3.3).

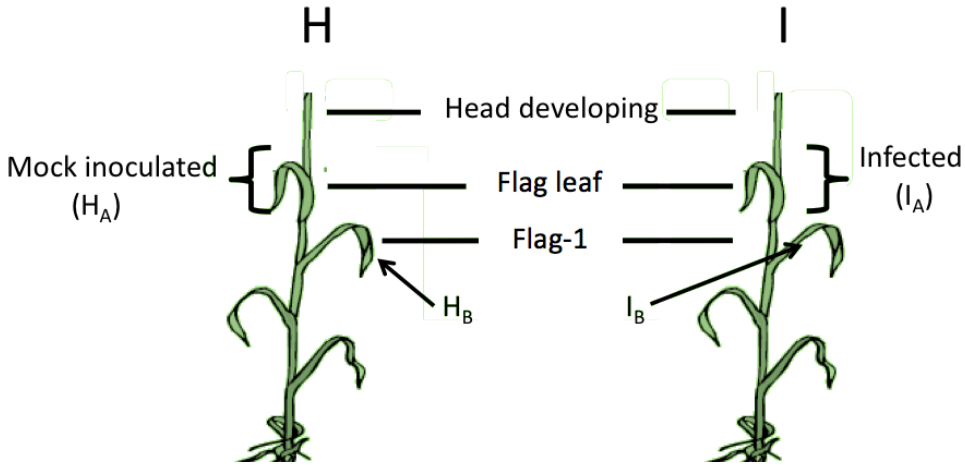

Figure 3.3. Scheme of *Pst* infections on wheat for the analysis of systemic responses. cv. Morocco plants were infected when the flag leaf was fully expanded and heads were developing but had not yet emerged. The flag leaf was mock (H_A) or *Pst* (I_A) inoculated. The flag-1 leaf was not infected (H_B; I_B). The flag and flag-1 leaves were harvested for analysis.

3.2.2 Photosynthesis pathway measurements - photon capture

3.2.2.1 Chlorophyll fluorescence dynamics measurements

To measure photon capture efficiency, healthy and infected young stage plants were used. Non-detached leaves were placed in an imaging fluorometer, FluorCam FC800-C (Photon Systems Instruments, Czech Republic) and kept in darkness for 30 min before measurements were taken. This oxidizes plastoquinone (Q_A) so that it can accept electrons. The plants were then exposed to actinic light (200 µE) and minimal fluorescence (F_o) was measured over five seconds. Subsequently, a brighter light burst (2200 µE) called the saturating pulse was applied for 600-800 ms. Maximum fluorescence (F_m) was measured for 200 ms during the saturating pulse. Twenty seconds after the saturating pulse was turned off, the actinic light was turned on and fluorescence was again measured (F'). After the fluorescence valued returned to baseline,

another saturating pulse (Fm') was applied. This cycle was repeated five times every 20 s. Fluorescence data were analysed using the software Fluorcam 7 (Photon Systems Instruments, Ltd. Czech Republic) using the equations of Table 3.1. Chlorophyll fluorescence dynamics are explained in Figure 3.1.

3.2.2.2. Chlorophyll quantification

Infected and healthy leaf disks from younger plants were harvested at various time points as described for each experiment. The leaf disks were stored in 2 mL tubes at -80°C before analysis. For chlorophyll extraction, samples were ground in 500 µL methanol using the Tissue-lyser (Qiagen) with one 5 mm metal bead for one min at 50 Hz. The samples were centrifuged at 2700 *g* for 5 min at 4°C. From each supernatant 100 µL was transferred to a single well of a 96-well transparent plastic plate (655101 Greiner Bio-One) and absorbance was measured at 663 nm, 645 nm and 750 nm. Chlorophyll calculations were based on (Porra et al., 1989) using the following equations:

$$\textbf{Chlorophyll a}\ (\mathrm{g}\cdot\mathrm{m}^{-2}) = \left(\frac{(18.22\cdot \mathrm{A}_{663}) - (9.55\cdot \mathrm{A}_{645})}{\mathrm{cm}^2}\right)/100$$

$$\textbf{Chlorophyll b}\ (\mathrm{g}\cdot\mathrm{m}^{-2}) = \left(\frac{(30.66\cdot \mathrm{A}_{645}) - (13.58\cdot \mathrm{A}_{663})}{\mathrm{cm}^2}\right)/100$$

$$\textbf{Total chlorophyll}\ (\mathrm{g}\cdot\mathrm{m}^{-2}) = \left(\frac{(24.12\cdot \mathrm{A}_{645}) + (2.71\cdot \mathrm{A}_{663})}{\mathrm{cm}^2}\right)/100$$

3.2.3 Photosynthesis pathway measurements - carbon fixation

3.2.3.1 Measurement of carbon fixation in leaves

I used a portable photosynthesis system (LI-COR® LI-6400XT) to measure assimilation rates. This instrument measures CO_2 and water exchange in leaves. The system uses fixed concentrations of CO_2 and H_2O (reference values) and measures their levels after the flow passes through the leaf (sample values). The differences between the reference and sample values reveals how much CO_2 the plant has removed for photosynthesis (assimilation rates) and how much water the plant is releasing through transpiration.

Young and adult stage cv. Morocco plants were used for experiments. Healthy and infected leaves were measured using four to 6 biological replicates. All plants were kept for 30 min in the laboratory prior to measurements for adaptation to new light and CO_2 conditions. For A/Ci curve

determination, incipient light was set to 1000 µE, the CO_2 reference concentration to 400 µmol mol^{-1}, air flow to 400 µmol s^{-1}, and the temperature to 20°C. Before measurements were taken, each leaf was left for 20 min in the LI-COR® chamber at 400 µmol CO_2 mol^{-1} for stomatal acclimation to the new environmental conditions. Increasing CO_2 concentrations from 50 to 2000 µmol mol^{-1} CO_2 were used to plot assimilation rates on the curve. When changing CO_2 concentrations, leaves were left for 30 to 90 s in the new CO_2 environment for stomatal acclimation. Carboxylation activity, triose phosphate use and respiration values were calculated using the (Sharkey et al., 2007) model as modified by Dr. Florian A. Busch (Australian National University; personal communication), where fixed conductance values were included.

3.2.4 Quantitative real time PCR

3.2.4.1 Extraction of mRNA and synthesis of cDNA

The plant material used for quantitative real time polymerase chain reaction (qRT-PCR) corresponded to experiments from distal and proximal experiments (Figure 3.3). A small area of leaf tissue, maximum 100 mg, was collected and frozen immediately in liquid nitrogen. Three biological replicates were collected at 4, 8, and 14 dai. Samples were ground in 2 mL Eppendorf tubes in liquid nitrogen using a TissueLyser (Qiagen). To extract RNA, one mL of TRIzol (Qiagen) was added to each frozen powder sample, vortexed for 30 s and incubated for 10-15 min in a fume hood. Next, 200 µL chloroform was added to each sample, inverted manually three times and incubated for 5 min in the fume hood. The tubes were centrifuged at 14,000 *g* for 15 min at 4°C. The aqueous phase was collected, mixed with 500 µL isopropanol and incubated for 10 min on the bench to precipitate nucleic acids. Samples were centrifuged at 14,000 *g* for 10 min at 4°C to pellet the nucleic acids. The pellet was washed in 1 mL 70% ethanol and centrifuged at 7, 500 *g* for 5 min at 4°C. The supernatant was discarded and pellets were air dried before suspension in 85 µL RNAase-free water. The solution was treated with 10 U DNaseI (NEB) and 10X DNase buffer at 37°C for 10 min to degrade contaminating DNA. To clean the RNA from degraded DNA, the sample volume was adjusted to 100 µL with RNase-free water and purified using the Spectrum™ Plant Total RNA kit (Sigma-Aldrich) following the manufacturer's protocol omitting the lysate filtration step. RNA was recovered in 50 µL RNase-free water directly from the spin column membrane. The integrity of the RNA was checked on an agarose gel. The concentration of the RNA was quantified by spectrophotometry using a NanoDrop™ apparatus. The concentration of the RNA was adjusted to 200 ng/µL with water. To synthesise cDNA, a High-Capacity cDNA Reverse Transcription Kit (Applied Biosystems) was used following the manufacturer's protocol. Random hexamers were used as primers on 2 ng of RNA template. The cDNA was diluted ten times to a final volume of 200 µL in MilliQ water before use.

3.2.4.2 Design of PCR primers to amplify wheat genes

Fourteen wheat genes were selected for expression analysis as representatives of the carbon and nitrogen metabolic pathways studied in this Thesis (Table 3.2). Primers were designed using the software Primer-BLAST (NCBI) leaving most parameters as default except that the genera *Puccinia* and *Triticum* were included in the BLAST to make sure the hits were only against the plant and not the fungus. Other changes were that the maximum length of the PCR product was set to 150 bp and the primer melting temperature to 63°C (Table 3.2). Because the reference wheat genome is cv. Chinese Spring ((The International Wheat Genome Sequencing Consortium, 2014)), the designed primers were checked for SNPs and their position with reference to the 3' of the transcript, using the Integrative Genomics Viewer (IGV, V2.3) and RNA-seq data from *Pst*-infected cv. Morocco (Jackson et al., unpublished data).

3.2.4.3 Quantitative real time PCR experiments

The quantitative PCR (qPCR) reactions were performed on the cDNAs generated in Section 3.2.4.3. Three biological and three technical replicates were used per gene. Before analysis of samples, primer quality was calculated using different dilutions of cDNA. Primer quality means that they cannot form dimers, they amplify in less than 40 cycles, and that amplicons increase exponentially in each cycle. The commercial qPCR mixture Fast SYBR® Green Master Mix was used for all amplifications and contains SYBR® Green, AmpliTaq Gold® Fast DNA polymerase, dNTPs with dUTP/dTTP, and optimized buffer (Applied Biosystems®). The protocol was adjusted for final volumes of 10 µL (Table 3.3). Amplifications were performed on a ViiA™ 7 Real-Time PCR instrument (Applied Biosystems) and analysed using the software QuantStudio™ V1.2 (Applied Biosystems®). The comparative C_T ($\Delta\Delta C_T$) method was used to calculate relative gene expression. This method is based on a double normalization of the target gene expression. The first normalizes against the endogenous control, in this case the 18S rRNA gene. This value is then normalized against a reference sample, which in this thesis is uninfected tissue.

Table 3.2. List of selected wheat genes and the primer sequence for qPCR s. The annotations are based on the Plant Genome and Systems Biology (http://pgsb.helmholtz-muenchen.de/plant/search.jsp).

Gene	Annotation (Function)	Wheat gene	Primers
Ta_18Sr	18S ribosomal RNA (Housekeeping gene)	Traes_5BL_1A355FBC5	F: AGGAGTTCCAGCACATCCTTC R: CCCTCTTGTTCATGTCGATGT
Ta_Rubisco	RuBisCO (Photosynthesis)	Traes_2BS_E68F1B47C	F: AGCAAGGTTGGCTTTGTCTT R: TTAACCTCCTCCACCTCGTT
Ta_AGP	ADP-glucose pyrophosphorylase (Starch pathway)	Traes_5AL_AE2EF1F20	F: ACTGACATGGAAAGAGGCGA R: CCTCGGCATTAGCAATGGTC
Ta_GPM	Glucose phosphomutase, putative (Sucrose pathway)	Traes_7AL_F70DA9639	F: TGGCGGTGGATCTATTTGAGA R: CTGTACTTCGCTGGTGTCAAC
Ta_BFF	Beta-fructofuranosidase (Cell-wall invertase)	Traes_2AL_E80BC759C	F: TACGTGTTCAACAACGGCAC R: GTCGGGGAGCACGTTCA
Ta_TPT	Triose-phosphate transporter domain (Calvin cycle)	Traes_5DL_0BFACD476	F: TTCTGCAGTCTTCTGGTCTGA R: ACCGAATGGGTAACTGGTGA
Ta_AS	Asparagine synthetase 3 (Nitrogen pathway)	Traes_5BL_7E69810D5	F: AGGTCATTCCTTCAGTGCCA R: ATGATGAGTCAAGGCCACCA
Ta_NASE	Nitrilase (Nitrogen pathway)	Traes_6AL_60AFB444B	F: GCCACTTTTGAGGACAGCA R: GGGAGCGCAGTATATCTCAATAC
Ta_FK1	Fructokinase-1 (Glycolysis)	Traes_3DL_CBD8FCDB3	F: GGATTTACGTGGAACTGTCC R: TGCAATGCCGATGGATCTTG
Ta_SPX	SPX domain-containing membrane protein (Phosphorus transport)	Traes_2DL_0DD946101	F: CGGAACACTTCGCTAAGGC R: CTTCTGAACCTAGAAGCAGAGGT
Ta_SFT	sucrose:fructan 6-fructosyltransferase (Fructan pathway)	Traes_7DS_E373FDD65	F: GAGGAGATTGAGACCCTCCG R: GGTGACGTCGCTAAGTTCAG
Ta_F6H	Fructan 6-exohydrolase (Fructan pathway)	Traes_2BL_16B7CE123	F: AATGGGAGCAGACTCGTGAA R: TGCACGACGTTTACTGAAGC
Ta_PSBP	PsbP (Photosystem II)	Traes_4AS_3D64BC0EF	F: GACCTAGGCCCAATGGATGA R: AGCGTACACTTCGGTTACCA

Table 3.3. Reaction mixtures for qRT-PCR

	Volumes per reaction
2x Fast SYBR® Green Master Mix	5 uL
Primer mix (forward and reverse)	200 nM
cDNA (from 2.10.3.1	2 uL
Total	To 10 uL

3.2.5 Measurements of photosynthesis products

3.2.5.1 Leaf dry weight and water content measurements

Young stage wheat plants were sprayed with spore/talcum mixture or talc for infection as described (Section 2.2.2 from Chapter 2), and leaves were harvested at different time points post infection. Each leaf was weighed and its area was measured using the LI-3100C Area Meter (LI-COR®). Leaves were covered in tissue paper and kept in an oven at 65°C for two days to dry. Individual leaves were weighed again to obtain their dry weight. To standardise the data, leaf weight was divided by leaf area. Water content was calculated as the difference between fresh and dry weights.

3.2.5.2 Extraction and quantification of starch in wheat tissue

Extraction and quantification of starch was based on (Smith and Zeeman, 2006). Leaf samples were freeze dried and ground into powder using a TissueLyser (Qiagen) with 5 mm metal beads at 45 cycles per second for two min. The powder was measured and one mL of 80% ethanol (fresh) was added for glucose extraction. The mixture was incubated at 70°C for three min. Samples were centrifuged at 3000 *g* for five min. This process was repeated three times or until the plant material turned white. To expose starch branches for enzymatic digestion and to remove glycogen, the white pellet was resuspended in 500 µL of MilliQ water and boiled for 20 min. Samples were centrifuged as before and the pellet was resuspended in 500 µL MilliQ water. This mixture was divided equally into two new tubes. The first fraction (Fraction 1) was mixed with 250 µL sodium acetate (0.2 M, pH 4.8) to quantify the remaining glucose after ethanol and water washes. The second fraction (Fraction 2) was used to quantify starch. This fraction was mixed with 250 µL sodium acetate pH (0.2 M, pH 4.8), 6 U α-amyloglucosidase (A1602, SIGMA) and 1.6 U α-amylase (A6380, SIGMA). All tubes were incubated at 37°C for 4 h with constant shaking in an orbital shaker at 200 rpm. The samples were centrifuged at 12000 *g* for five min and the supernatant was used for glucose assays.

To measure glucose levels, 185 µL starch assay buffer (Table 3.4) and 10 µL from each fraction were added to each well in a 96-well plastic plate. The absorbance was measured at 340 nm for 7 min (A'_1) to detect NADH. To each well, 4U of glucose-6-phosphate dehydrogenase (G6PDH; G5760 SIGMA) and 9 U hexokinase (HXK; H4502 SIGMA) were added to covert glucose to 6-phosphogluconate (6PG) and A_{340} was measured for 16 min (A'_2). Glucose absorbance was quantified (A'_2-A'_1) for both fractions. After this, the free glucose within Fraction 1 (not related to starch digestion) was subtracted from the total glucose in Fraction 2. From this difference, glucose concentrations were calculated using a linear regression from a glucose standard curve based on 0.05 mM, 0.2 mM, 0.4 mM, 0.6 mM, 0.8 mM and 1 mM standards. Glucose concentrations were normalized to dry weight and multiplied by 162, the mass of anhydroglucose, to convert values to µg starch.

Table 3.4. Starch assay buffer

Reagents	**Final Concentration**
2-[4-(2-hydroxyethyl)piperazin-1-yl]ethanesulfonic acid (HEPES, pH 7.5)	100 mM
$MgCl_2$	4 mM
NAD	1 mM
adenosine triphosphate (ATP)	0.5 mM
Sample	10 µL
MilliQ water	Up to 200 µL/well

3.2.5.3 Measurement of primary metabolites during infection

3.2.5.3.1 Extraction of apoplastic fluids from wheat leaves

Apoplastic fluids (AP) were extracted from four-week old and adult stage plants at different time points post infection. For four-week old plants, the youngest fully expanded leaf was sampled using five biological replicates. For adult stage plants, only flag leaves were studied, and AP was extracted from 7 to 12 flag leaves per time point. Leaves were peeled from the stem without cutting to avoid wounding. The AP extraction was performed at room temperature to avoid the changes in sugar concentrations that occur in cold temperatures (Olien and Clark, 1995). To extract AP, leaves were first weighed and then vacuum-infiltrated with a solution of 0.2 M sorbitol for enzymatic sugar quantification, or with 0.084 mg/mL nor-leucine for gas chromatography quantification. During extraction, the vacuum chamber was shaken to prevent bubble formation that might damage the tissue (and allow sugar leakage) during pressure release. Pressure was released from the vacuum two to three times to fully wet the leaves. Dark

infiltrated leaves were blotted dry, re-weighed and placed in the chamber of a 10 mL disposable syringe that in turn was placed in a 1.5 mL disposable tube. This apparatus was placed within a 50 mL Falcon tube for centrifugation (Figure 3.4). To reduce cytoplasmic contamination, leaves were centrifuged at 500 *g* for 5 min at 4°C. The liquid extracted from the leaves that collected in the 1.5 mL tube represents the AP.

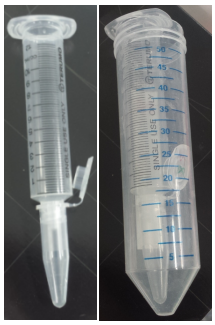

Figure 3.4. Apoplastic fluid extraction apparatus

3.2.5.3.2 Estimation of cytoplasmic contamination of apoplastic fluids

Cytoplasmic contamination of AP was detected by the activity of the cytoplasmic enzyme malate dehydrogenase (MDH). To measure MDH activity, an assay buffer was prepared as depicted in Table 3.5. Two µL of AP sample and 196 µL of MDH assay buffer were added to a well within a 96-well plate. The absorbance was measured (A1) at 340 nm for 5 min in a plate reader (Infinite® M1000 PRO, TECAN), after which 2 µL of 17 mM oxaloacetic acid (OAA) was added and A_{340} measured (A2) for 6 min or until absorbance stabilised. The following equation was used to calculate the percentage contamination:

$$\%contamination = ((A2_{sample} - A1_{sample}) \times 100)/((A2_{reference} - A1_{reference})$$

To establish the 100% percentage contamination level, healthy and infected leaves were ground separately with 0.2 M sorbitol. MDH activity was measured in each extract.

Table 3.5. MDH assay buffer

Reagents	**Final concentration**
OAA	0.17 mM
NADH	0.094 mM
Tris-HCl pH 7.5	0.1 M
sample	2 uL
MilliQ water	To 200 uL

3.2.5.3.3 Extraction of whole tissue polar metabolites

Maximum sugar accumulation occurs one hour before the night cycle. At this time of the cycle, the last expanded leaves from healthy and infected four-old week plants and the flag leaf from adult plants were harvested and frozen immediately in liquid nitrogen. Samples were freeze-dried for two days to avoid sugar degradation by enzymes and pulverised using a TissueLyser (Qiagen®) with 5 mm metal beads for 2 min at 45 cycles per second. The resulting leaf powder was weighed before sampling for sugars and starch measurements.

3.2.5.3.4 Gas chromatography–mass spectrometry analysis of polar components

The brown pellet from Section 3.2.5.3 was employed for gas chromatography–mass spectrometry analysis (GCMS) based on procedures from Chapter 2, Section 2.2.4.

3.2.5.3.5 Quantification of plant nutrients by enzymatic assays

Quantification of fructose, sucrose and glucose levels in extracts of polar components

The brown pellet from Section 3.2.5.3 was resuspended in 20-30 µL of water and 10 µL was used for sugar quantification. The remainder was used for nitrogen quantification (Section 3.2.5.5.2). Fructose, glucose and sucrose were quantified in the same extract based on the method of (Scholes et al., 1994). This process is based on the reduction of NAD to NADH. NADH absorbance at 340 nm was measured to quantify each sugar based on a standard curve. The first step in the sugar quantification by enzymatic assay was to measure the initial concentration of NADH in the extracts (first absorbance measurement at 340nm, A_1). The next step was to quantified glucose. The enzymes hexokinase (HXK) and glucose-6-phosphate dehydrogenase G6PDH were added to the extract to produce 6-phosphogluconate (6PG) from glucose and release NADH. After the HXK and G6PDH reaction the absorbance was measured again at 340nm (Second absorbance, A_2). The proportion of glucose and NADH is one to one, therefore the production of NADH can be directly correlated with the amount of glucose. The amount of glucose is the difference between the A_2 and A_1. When no further changes in absorbance could be detected (i.e. when glucose was exhausted), phosphoglucose isomerase (PGI) was added to quantify fructose by converting fructose to glucose. This glucose was then converted to 6PG resulting in reduction of NAD. The difference between this A_{340} (A_3) and the previous value for A_2 represent the levels of fructose in the sample. Finally, to measure sucrose, invertase (INV) was added to break sucrose down into glucose and fructose, which again can be measured as an increase in NADH absorbance (fructose is converted to glucose as in the previous step). The sucrose level can be

derived from the difference between the final A_{340} (A_4) and A_3. Since sucrose is one molecule of glucose and one of fructose, more NADH is generated during this step.

To perform the assays, 10 µL of each sample and 135 µL of sugar enzymatic assay buffer (Table 3.7) were added to each well. All enzyme solutions and the sugar assay buffer were prepared freshly (Table 3.6, Table 3.7). The volume of each enzyme was 5 µL per well, with the concentrations indicated in Table 3.7. Measurements were performed at 25°C in a 96-well plate using a plate reader (Infinite® M1000 PRO, TECAN). The absorbance was measured at 340 nm for 7 min (A1). A mixture of G6PDH and HXK were added to each well. The plate was shaken orbitally in the plate reader for one min at 200 rpm. The A_{340} was measured every minute for 16 min or until the absorbance was stable. The stable absorbance value was recorded as A2. PGI was added to each well and the plate was shaken as previously. The A_{340} was recorded over 16 min and the last stable point was recorded as A3. Finally, INV was added to each well and the same procedure followed. After 16 min, the last stable A_{340} was recorded as A4.

A standard curve was prepared to relate the absorbance values to sugar concentrations using comparable conditions to the experimental samples. The standards for the curve were mixtures of fructose, glucose and sucrose to mimic the situation in which all sugars are present in the same solution. The concentrations of each sugar within the standards were 0.05 mM, 0.1 mM, 0.2 mM, 0.6 mM, 0.8 mM, and 1.0 mM. The linear regression from the standards was used to calculate sugar concentrations for each sample. The values obtained for the experimental samples were normalized by dividing by the sample dry weight.

For apoplastic sugars, the concentration was normalized to the volume of extraction and the percentage of cytoplasmic contamination, following the equation:

$$
\begin{aligned}
&apoplastic\ sugar \\
&\quad = (sugar\ concentration \\
&\quad - (sugar\ concentrations \times cytoplasmic\ contamination) \\
&\quad \times infiltrated\ solution
\end{aligned}
$$

Table 3.6. Enzymes for sugar quantification.

Enzymes	**Initial solution**	**Units per sample**
HXK (H5000, SIGMA)	1.8 U HXK / µL	9
G6PDH (G8529, SIGMA)	0.8 U G6PDH / µL	4
PGI (P5381, SIGMA)	0.4 U/µL	2
INV (I4504, SIGMA)	17 U/µL	85

Table 3.7. Sugar enzymatic assay buffer.

Reagents	Final concentration (mM)
HEPES (pH 7.5)	100
$MgCl_2$	5
Dithiothreitol (DTT)	1
bovine serum albumin (BSA)	0.02 w/v
NAD	2
ATP	1
sample	10µL/well
Enzymes	5 µL of each enzyme/well
MilliQ water	To a final volume of 200 µL

Quantification of asparagine, ammonium and glutamine in wheat leaves

The resuspended brown pellets from Section 3.2.5.3 were also used to measure the levels of the nitrogenous compounds asparagine, ammonia, and glutamine, using the ASNAM kit from Megazyme©. From the extract 10 µL was used in each assay following the manufacturer's protocol for a microplate reader. Standards for ammonia, glutamine and asparagine were prepared separately, based on the Megazyme© protocol.

Extraction and measurements of invertase activities from wheat leaves

The method was modified from Krishnan et al., (1985). Four mm^2 leaf disks from healthy and infected plants were collected at different time points after infection and snap frozen in liquid nitrogen. Each sample was ground in a TissueLyser (Qiagen) at 45 sec^{-1} in 150 µL of invertase extraction buffer (Table 3.8) for one min. Samples were centrifuged 12,000 *g* at 4 °C for 10 min. Each supernatant was transferred to a new tube and kept on ice. The pellets were washed in 100 µL of invertase extraction buffer and centrifuged at 12,000 *g* for 20 min at 4°C. Each supernatant containing soluble invertases was mixed with the previous one. The pellet containing insoluble invertases was resuspended in 100 µL of invertase extraction buffer and 100 µL of 2 M NaCl. The resuspended pellets were incubated overnight at 4°C and then centrifuged at 12,000 *g* for 20 min at 4 °C.

Table 3.8. Invertase extraction buffer

Reagents	Final concentration
100 mM sodium phosphate (pH 6.5): 17.6 mL of 1 M Na_2HPO_4 32.4 mL of 1 M $NaH_2PO_4 \cdot H_2O$ 450 mL of MilliQ water	20 mM
Ethylenediaminetetraacetic acid (EDTA)	1 mM
Dithiothreitol (DTT)	1 mM
Protease inhibitor cocktail (Thermo)	1 minitablet/10 mL water
Glycerol	(10% v/v)

Table 3.9. List of buffers to measure the three invertase isoenzymes

Type of invertase	Buffer	pH
Cell-wall invertases	200 mM sodium acetate buffer	4.5
Vacuolar invertases	200 mM sodium acetate buffer	5.5
Neutral invertases	200 mM sodium phosphate buffer	7.2

For invertase activity assays, sucrose (a disaccharide) and raffinose (a trisaccharide) were used as substrates. Invertases hydrolyse sucrose into the monosaccharides glucose and fructose, and raffinose into glucose, sucrose and galactose. These sugars were then quantified using a colorimetric assay. For the assay the aromatic acid hydrazide 4-Hydroxybenzhydrazide (PAHBAH; H9882 SIGMA) reacts with the reduced carbohydrates in a hot alkaline solution to give a yellow colour which can be measured at 405 nm.

Raffinose and sucrose solutions were prepared at 200 mM in sodium acetate or sodium phosphate buffers (Table 3.9) at the appropriate pH for the different invertase isoforms (Table 3.9). To increase sugar solubility in the buffers they were incubated at 60°C for five min. Invertase extracts were mixed in Eppendorf tubes at 1:1 volumes with each substrate in the different buffers (Reaction Mixture) to measure the three invertases separately. The solutions were incubated at 37°C for 1 h with shaking on a small orbital shaker. Hexoses released by invertase activity were quantified by colorimetric assays. To detect hexoses, 25 µL of Reaction Mixture was mixed with 225 µL of 4 mg/mL PAHBAH solution (prepared fresh in 0.5 M sodium hydroxide) and incubated at 70°C for five min. At the same time, a glucose standard curve was prepared from a stock solution of 0.38 M glucose (Table 3.10). Each glucose standard (Table

3.10) was mixed with PAHBAH solution in the same volumes as for the experimental treatments and incubated in the same way. After the PAHBAH reaction, 100 µL of each mixture was transferred to a well of a 96-well plastic plate and the absorbance measured at 405 nm. The linear regression of the glucose standard curve was used to calculate µmoles of glucose which was used in the following equation:

$$U/ml\ enzyme = \frac{umoles\ of\ glucose}{5\ \mathrm{min} \times vol\ of\ enzyme \times 2}$$

Table 3.10. Glucose standards for invertase assays.

Tube	1 M glucose solution (µL)	MilliQ water (µL)	Final concentration (mg/mL)
1	1.25	95	0.35
2	2.5	90	0.7
3	5	80	1.4
4	7	70	2.1
5	10	60	2.8
6	12.5	12.5	3.5
7 (blank)		100	

3.3 Results and discussion

Photosynthesis pathway measurements - photon capture

3.3.1.1 Chlorophyll fluorescence dynamics in plants infected with *PST*-79

To understand the photon capture efficiency during infection, I measured and compared chlorophyll fluorescence dynamics in healthy and *Pst*-infected wheat plants. I infected whole young stage cv. Morocco plants when the 7th leaf emerged. I recorded data from the 6th and 5th leaves to find out if leaves of different ages respond differently to infection. The 6th leaf corresponds to the youngest fully expanded leaf while the 5th leaf is older. I recorded data at 2, 8 and 10 dai. I did not record data at 14 dai because the abundant fungal spores fluoresce, which might have interfered with the measurements. The same leaves were used throughout the experiment since the technique is not destructive.

To measure light reactions, I calculated the potential efficiency of PSII (Fv/Fm), the actual efficiency of PSII (ϕPSII), and non-photochemical quenching (NPQ) during the infection experiment (Table 3.1; Figure 3.5). The Fv/Fm values from both the 5th and 6th leaves decreased

over time but with different values in healthy and infected leaves (Figure 3.5A, B). Infected leaves had similar Fv/Fm values as healthy leaves at 2 dai, then at 8 dai were higher and at 10 dai were lower. The Fv/Fm profiles were similar for the 6th and 5th infected leaves, showing that the values are independent of leaf age and correlate inversely with fungal biomass profiles. The Fv/Fm value decline suggests that fungal infection changes the capacity of photosystem II to use light (Maxwell, 2002). The reasons for the higher values in infected leaves at 8 dai are not clear, but perhaps could be related to nutrient usage during the infection, which may enhance photosynthesis for nutrient replacement. For example at lower hexoses levels photosynthesis is induced (Nie et al., 1995). At 10 dai, the leaf tissue is disrupted by the emergence of pustules, therefore photosynthesis may decrease as a response to stress signals or mechanical damage. In relation to the age of the leaves (5th and 6th) it seems 5th leaves have less photosynthesis capacity than the 6th leaves. The 5th leaves are older and possibly they start senescence processes, one of them is reduction in carbon fixation capacity. This transition might explain why 6th are more affected by infection at 10 dai than 5th leaves.

The ϕPSII values (the actual efficiency of photosystem II) of healthy 5th leaves decreased markedly from 2 to 8 dai but remained stable at 10 dai (Figure 3.5C). The infected 5th leaves had lower values than healthy leaves at 2 dai, but were marginally higher at 8 and 10 dai. There two possible explanations to the decline from two to 8 dai, one is that ϕPSII is sensitive to changes in development and wheat plants have a transition from 2 to 8 days. Second explanation is that the sampling conditions were inappropriate for this parameter. The ϕPSII values for 6th leaves followed the same pattern as older leaves, decreasing at 8 dai and stabilising at 10 dai (Figure 3.5D). The ϕPSII values in response to *Pst* infection were independent of leaf age and showed that plants sense fungal infection at 2 dai, in contrast to Fv/Fm values which did not show an effect. In general, at 2 dai the potential PSII efficiency (Fv/Fm) is similar between healthy and infected plants but the actual photosynthesis (ϕPSII) is lower in infected plants. At 8 dai, it seems that photosystem II from infected plants was potentially more efficient but its real performance was similar to healthy plants. The major effect here seems to be developmental, and the actual performance was not lowered further by the fungal infection. At 10 dai the PSII efficiency in infected leaves compared to healthy leaves was lower, but the actual operating efficiency of ϕPSII was similar (Figure 3.5 A-D). These values suggest that the photosynthesis machinery was affected by the infection, but also that healthy plants performed poorly at 10 dai. The most common parameters used to evaluate PSII efficiency are Fv/Fm and ϕPSII values. Here I found that the values for these metrics were not highly correlated between healthy and *Pst* infected leaves. The Fv/Fm ratio showed significant differences at 8 and 10 dai, while ϕPSII values were

only different at 2 dai. It seems that the Fv/Fm values showed the immediate plant respond to the infection, whereas ϕPSII showed how they respond to accumulative stress.

The NPQ values (how the plant distributes the light energy) of uninfected 5th leaves showed a flat profile that declined at 10 dai. Compared to healthy leaves, the values of infected 5th leaf increased at 8 dai and decreased at 10 dai (Figure 3.5 E). The values for infected and uninfected leaves were similar at 2 and 10 dai, but much higher at 8 dai in infected leaves. The higher values at 8 dai are associated with a higher electron flow. The NPQ values for the 6th leaf followed a slightly different pattern from older leaves. The 6th healthy leaf NPQ values were stable across the time points and always higher than infected younger leaves (Figure 3.5 F). Infected 6th leaves showed a small peak at 8 dai and declined markedly at 10 dai. The higher NPQ peak at 8 dai in the infected 5th leaf might be explained as a protective mechanism against stress. These plants had high potential PSII activity for photosynthesis, observed as high Fv/Fm values at 8 dai, however the light energy was released as NPQ. The reason for the change from PQ to NPQ could be a response to changes in pH, since fungal infections increase the pH of the plant apoplast (Felle et al., 2004). A decrease of protons in the thylakoid due to changes in the electron transport chain stimulates the conversion of violaxanthin, a PSII pigment, to zeaxanthin and/or antheraxanthin. These changes stop the transport of electrons to the reaction centre of PSII and the energy is released as heat or NPQ (Govindjee, 2002).

The Fv/Fm, ϕPSII and NPQ values reported in the literature for rust fungal infections differ between them. The bean rust pathogen *Uromyces appendiculatus* increases NPQ in leaves, *Puccinia coronata var. avenae* decreases NPQ, and *P. triticina* does not affect NPQ (Kuckenberg et al., 2009; Peterson and Aylor, 1995; Scholes and Rolfe, 1996). In wheat leaves infected with *P. coronata var. avenae* and *U. appendiculatus*, ϕPSII values dimished only when symptoms appeared, while for leaves infected with *P. triticina* the values decreased at the beginning of infection (Kuckenberg et al., 2009; Peterson and Aylor, 1995; Rolfe and Scholes, 2010). The results diversity is associated with experimental conditions like host, sampling conditions, age of the plants. In conclusion, chlorophyll fluorescence dynamics should be measured for each rust fungus since leaves apparently do not respond in the same way during different infections. Wheat leaves infected with *PST*-79 showed reduced capacities of PSII and NPQ, and only NPQ values were affected by age.

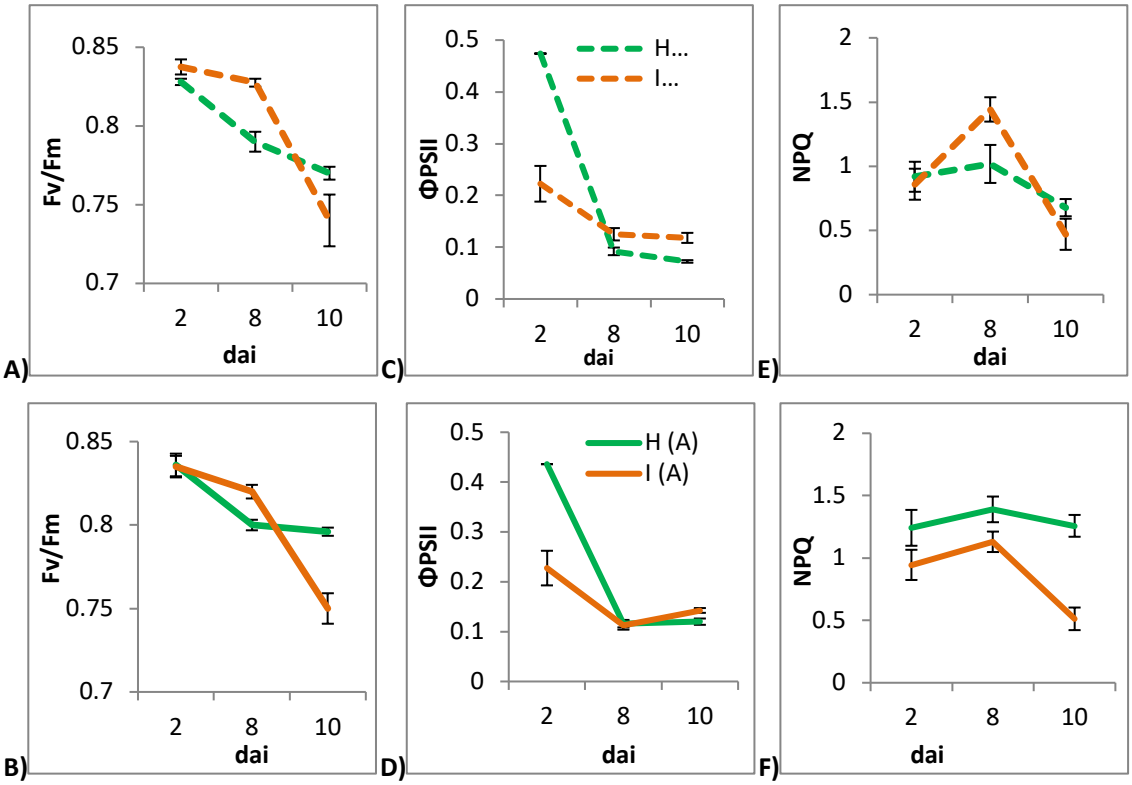

Figure 3.5. Parameters of chlorophyll fluorescence dynamics in old and young wheat leaves from healthy and infected plants. cv. Morocco plants were infected with *PST*-79 or mock-inoculated when the 7th leaf appeared. Green represents mock inoculated plants, orange represents plants infected with *PST*-79. Fv/Fm and PSII are the potential and actual efficiency of PSII respectively; while NPQ shows how plants cope with excess of light. The upper panel (dashed lines) are values from the 5th leaf (A, C and E), and the lower panel (solid lines) are values from the 6th leaf (B, D and F). Error bars represent standard error of 5 replicates. Asterisk represents significant differences compared to healthy leaves using a t-test and a p-value less than 0.05.

3.3.1.2 The chlorophyll content of healthy and *Pst*-infected plants

Photon capture efficiency depends not only on how plants use light energy in PQ or NPQ but also on the levels of chlorophyll pigments. Chlorophyll absorbs light energy, so lower chlorophyll levels mean that less energy is available for photochemistry. I measured chlorophyll levels in healthy and infected wheat plants to evaluate the effect of *Pst* infection. For these experiments, I infected or mock inoculated the fully expanded flag leaf of adult stage plants, and collected leaf disks to normalize chlorophyll levels to area. I measured chlorophyll a and chlorophyll b as the major pigments present in the photosystems. I measured chlorophyll levels at three rather than two dai because infection requires darkness for two days; therefore I allowed the plants to adapt to lighted conditions again before taking samples. Chlorophyll a was stable across the three time points in healthy flag leaves (Figure 3.6A). In infected flag leaves, chlorophyll a was stable at three and 8 dai and decreased markedly at 14 dai to about half the previous levels. Chlorophyll b levels were similar in healthy and infected leaves and were stable across the three time points (Figure 3.6B). Chlorophyll a is more abundant than chlorophyll b and this was also seen here. In

summary, chlorophyll a but not b decreased during *Pst* sporulation. The damage in tissue by infection could explain the decrease in chlorophyll, however chlorophyll b is not decreasing. One explanation is the tissue damage due to pustule eruption damaging leaf tissues. I obtained very similar results for young stage plants (data not shown), therefore the responses seem to be independent of the developmental stage of the plant.

To evaluate if chlorophyll levels respond systemically to *Pst* infection I measured chlorophyll levels in the flag-1 leaf. These experiments and nomenclature are based on Figure 3.3. I used the same plants described in the previous experiment and collected leaf disks from uninfected flag-1 leaves. The results revealed that chlorophyll a and b levels from the flag-1 leaves were similar between healthy and infected plants (Figure 3.6 C, D). For chlorophyll a, there was a marked decrease from 8 to 14 dai, whereas chlorophyll b increased significantly after 8 dai. In conclusion, changes in chlorophyll levels are not a systemic response to *Pst* infection.

The values for chlorophyll fluorescence dynamics and chlorophyll levels that I measured had similar profiles changing mainly at the sporulation phase, however they cannot be compared directly because the time points differed between the experiments. Fv/Fm values might also relate to the quality of proteins involved in electron transport during PQ rather than pigment contents. To investigate this, I evaluated the levels of two proteins involved in photon capture. These were subunit D1 from photosystem II and cytochrome f (Pb6f) (Figure 1.11, Chapter 1). The D1 protein binds and reduces chlorophyll a and is involved in water splitting. D1 has a high turnover because it is damaged by oxidation. The Pb6f protein is an electron carrier that transfers electron from photosystem II to photosystem I. For these experiments, I used healthy and *Pst*-infected flag leaves in adult plants, and evaluated the levels of proteins by western blot. I performed the experiments three times, changing the amounts of protein loaded and the antibody dilutions, but despite these measures the blots always showed non-specific cross-reacting bands (data not shown). Explanations for these results could include degradation of the target protein or the primary antibody cross-reacting with larger protein complexes; both of the phenomena have being reported for D1 (Agrisera antibodies, Sweden). Therefore, I could not obtain information about the levels of these proteins during infection.

As a general observation, infected plants at 8 dai had higher Fv/Fm levels but similar levels of chlorophyll compared to healthy leaves, while at 10 to 14 dai they had lower Fv/Fm levels and lower chlorophyll a content. The levels of Fv/Fm are associated with the efficiency of photosystem II in electron transfer, but also its capacity to capture photons via chlorophyll pigments. Based on these results and the NPQ values it seems that photosystem II from infected

plants is more efficient in photochemistry at 8 dai while the decrease at 10 dai is explained by lower levels of chlorophyll. In conclusion, to evaluate photon capture efficiency during *Pst* infection, chlorophyll fluorescence dynamics are informative at early stages of infection while chlorophyll levels are only informative during sporulation. An alternative approach could be to quantify chlorophyll in areas of uniform leaf infection to remove this aspect of variability from the measurements.

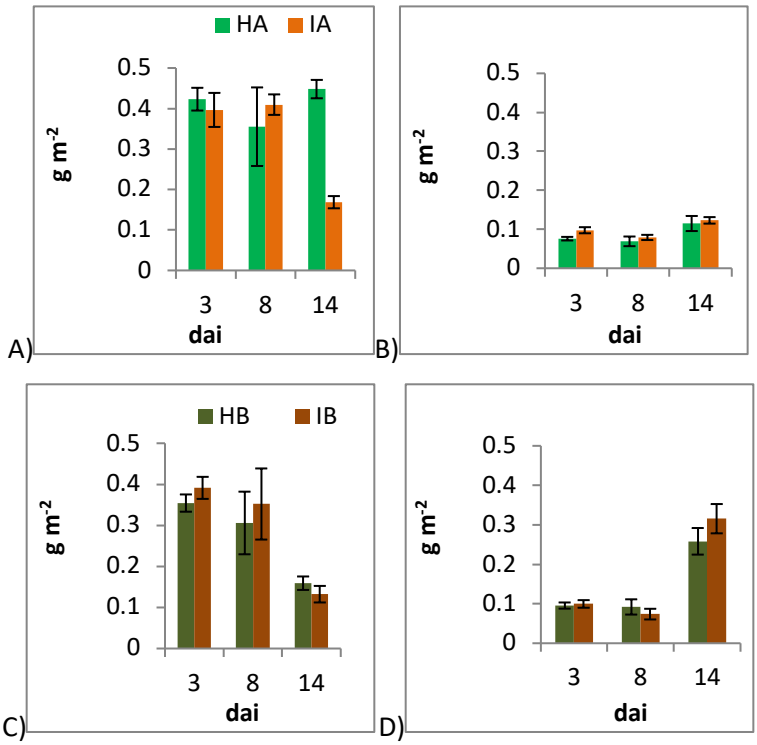

Figure 3.6. Chlorophyll a and b levels in flag and flag-1 leaves from adult plants. Infection and nomenclature are based on Figure 3.3, where only the flag leaf of adult plants was infected or mock inoculated. Chlorophyll a (A) and b (B) levels in healthy and infected flag leaves. Chlorophyll a (C) and b (D) levels in flag-1 leaves. Bars represent the average of 5 biological replicates. Error bars represent the standard error of 5 replicates. Asterisk represents significant differences compared to healthy leaves using a t-test and a p-value lower than 0.05.

3.3.2 Carbon fixation in *Pst*-infected leaves

In the previous section I showed that photon capture efficiency was affected by *Pst* infection. At the beginning of the infection, the actual photosynthesis efficiency (ΦPSII) decreased and chlorophyll levels halved at the end of the experiment. These changes might also affect carbon fixation because it is fundamentally connected to photon capture. In this section I evaluated carbon fixation during infection by measuring the Calvin-Benson cycle activity and expression of metabolis-associated genes.

I measured the Calvin-Benson cycle activity via A/Ci curves. From these curves, I obtained the values for Rubisco carboxylation activity (Vc), triose phosphate use (TPU) and respiration rates during the day (Rd). I did not measure RuBP regeneration (J) values since reliable values can only be obtained through correlations with electron transport rate, which I did not calculate. I performed these experiments on young stage wheat plants. I mock-inoculated or infected the 6th and the 5th leaves with *PST*-79 to represent a younger and an older leaf, respectively. I did the measurements at midday when stomata were fully adapted to the day light cycle.

The Vc values (Rubisco carboxylation activity) for the uninfected 5th leaf decreased modestly at 8 dai (Figure 3.7). The overall profile was fairly flat. For infected leaves the values were similar for the first two time points but decreased significantly 15 dai, indicative of lower carbon fixation due to fungal infection (Figure 3.7A). The 6th leaf had higher Vc values compared to the 5th leaf; this corresponds with the literature where younger leaves are reported to be more active photosynthetically (White and Edwards, 2008) Healthy 6th leaves showed increased Vc values at 8 dai from two dai, but decreased slightly at 15 dai. Similar to what was observed for the 5th leaf, Vc values for the infected 6th leaf was similar at 2 and 8 dai but declined strongly at 15 dai (Figure 3.7B). In summary, Rubisco carboxylation activity was not affected during the first period of infection but decreased to about half by the time *Pst* was sporulating. This also correlates with chlorophyll dynamics.

The values for TPU (Triose phosphate use) were very variable in all experiments, as can be seen by the size of the error bars (Figure 3.7 B, D). Because of this, there were no differences between healthy and infected leaves when the 6th leaf was infected. Although the results were also variable, TPU values were lower for infected 5th leaves compared to the healthy controls at 2 and 8 dai, and significantly lower at 15 dai. This suggests that carbon fixation in 5th leaf is limited in infected leaves by accumulation of triose in the chloroplast and less available phosphorus. The TPU decrease in infected 5th leaves at 15 dai could be related to an increase in phosphorylated sugars in the cytoplasm or the uptake of phosphorus by the fungus, as both trigger signals to reduce triose export to the cytoplasm.

I calculated respiration rates (Rd) using A/Ci curves. Respiration rates relate to the CO_2 produced by plant and fungal mitochondria during the day due via the Krebs cycle. Respiration rates increase during development as the plant requires more nutrients for growth, and under stress conditions. In healthy leaves, respiration rates were constant and similar between the leaf ages. For infected older leaves, respiration increased markedly at both 8 and 15 dai until it was about 2.5 times that of healthy leaves, while for younger infected leaves it was similar to healthy at 2

and 8 dai but increased at 15 dai also to about 2.5 times the healthy control. These results show that respiration rates increased with the accumulation of fungal biomass. This could be a plant stress response, but the high Rd levels could also be due to fungal respiration which is impossible to separate from host respiration in these experiments. To evaluate if fungal respiration could have an effect on the data, I measured assimilation rates with the lowest possible CO_2 level (50ppm). At lower levels of CO_2, it will be easier to see the effect of external sources of CO_2 on fungal respiration. I found that assimilation rates were similar between healthy and infected leaves. Two ideas raised from the experiment, one that 50ppm is still a high concentration to see an effect; and second that fungal respiration is lower than plant respiration.

In summary, the A/Ci curves suggest that infected tissue became a strong sink at 15 dai, because Rubisco activity decreased and respiration increased. These are indicators that photosynthesis is reduced. My results also show that leaves of different ages respond differently to *Pst* infection. To extend these experiments to adult plants, I measured assimilation rates in healthy and infected flag leaves after *Pst* infection. For these experiments, I mock-inoculated or *Pst*-infected fully expanded flag leaves. I used ambient CO_2 levels (400 ppm) and high CO_2 concentrations (1000 ppm) to reduce the effect of stomatal opening during measurements. I measured data at 8 and 15 dai only since there were no differences in the data at 2 dai in the previous experiments with the same leaves. At ambient CO_2 levels, assimilation rates were stable in healthy flag leaves at 8 and 15 dai, while for infected flag leaves the rates decreased at 15 dai (Figure 3.8A). Interestingly, assimilation rates were similar at 15 dai for infected plants at both CO_2 concentrations, however the rates as proportions of those in healthy plants differed. Healthy plants had 4 and 8 times higher assimilation rates than infected leaves at ambient and high CO_2 respectively. This suggests that the Rubisco in infected plants was saturated by small amounts of CO_2, and that the decrease in assimilation in old infected leaves was not due to CO_2 availability but to some other limiting factor. The fungal growth was not measured in the different CO_2 conditions but there were no visual differences in the disease development.

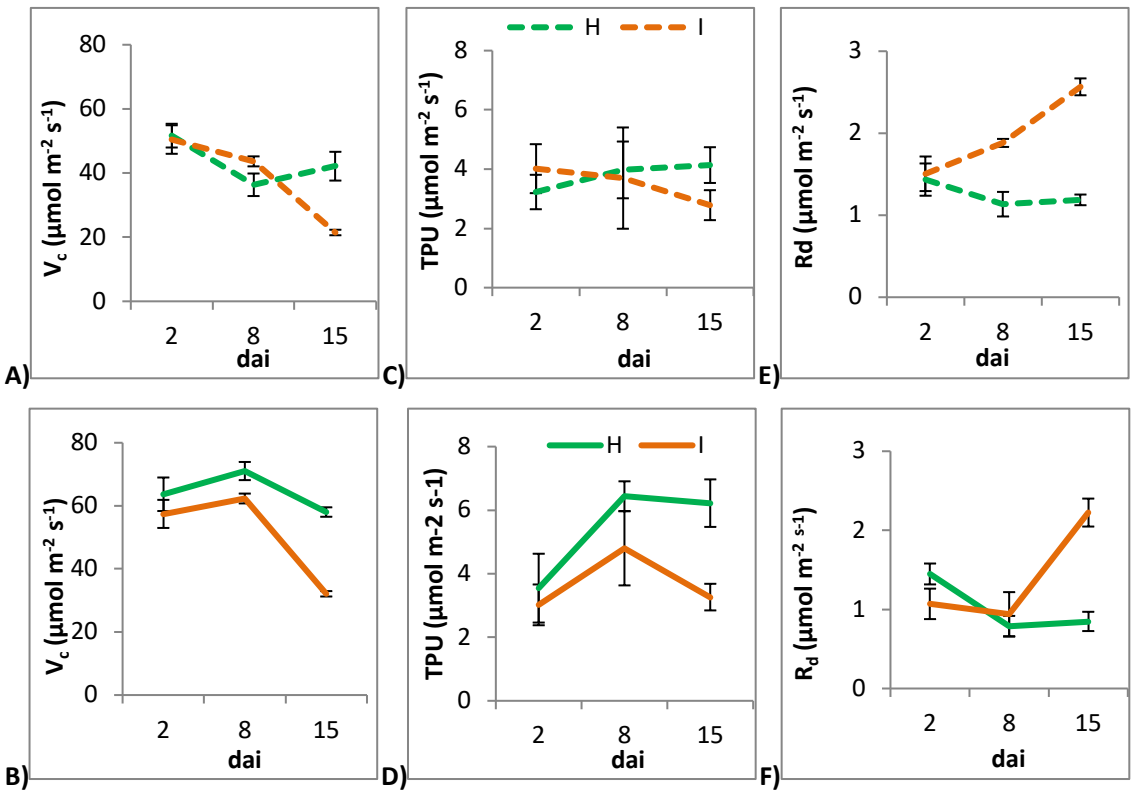

Figure 3.7. Parameters of A/Ci curves in 5th and 6th leaves from healthy and infected wheat plants. cv. Morocco plants were mock- (H) or *Pst*-infected (I) after the 7th leaf appeared. Upper panel (dashed lines) are values from the 5th leaf (A, C and E), lower panel (solid lines) are from the 6th leaf (B, D and F). Error bars represent the standard error of 6 replicates. Asterisk represents significant differences compared to healthy leaves using a t-test and a p-value less than 0.05.

To evaluate if carbon fixation responds systemically to *Pst* infection, I measured assimilation rates in the flag-1 leaf. These experiments and nomenclature are based on Figure 3.3. I used the same plants from the previous experiment and measured assimilation rates in flag-1 leaves, which were not infected. The assimilation rates in flag-1 leaves were similar between healthy and infected plants at both time points and CO_2 concentrations (Figure 3.8C, D). Thus, assimilation rates decreased in infected leaves during *Pst* sporulation but did not decline in uninfected leaves. Also, assimilation rates were similar between flag and flag-1 leaves, in contrast to 5th and the 6th leaves that had different Vc rates (Figure 3.7A, B).

My results are similar to other reports describing biotrophic fungal infections of cereals. The respiration rates of wheat leaves increased during *P. triticina* infection (Carretero et al., 2011). During *Blumeria graminis* f. sp. *hordei* infections of barley, CO_2 assimilation rates decreased (Swarbrick et al., 2006). Similar results were found in wheat infected with *P. triticina, Pgt* or *Pst* (Chen et al., 2015b; Livne, 1964; Owera et al., 1981). This shows that in infected plants, respiration rates increased and photosynthetic capacity decreased. In general, the plants

changed their metabolism from sugar synthesis to catabolism. The products of the reactions might be used for defences or for glycolysis (energy production); however, the sugars might be simply taken up by the fungus.

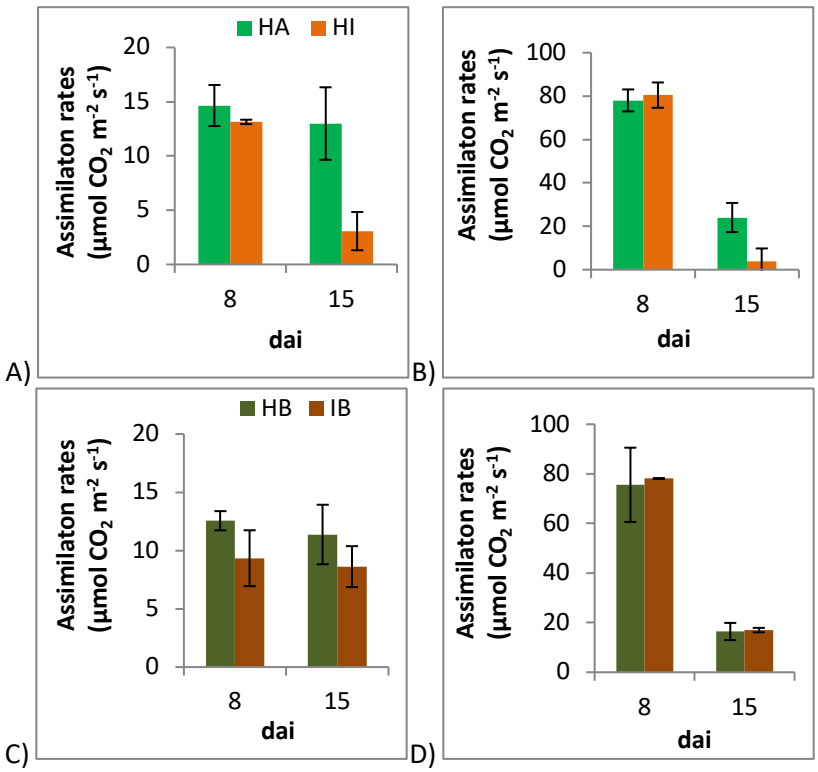

Figure 3.8. Assimilation rates of wheat flag leaves mock inoculated or infected with *PST*-79, and of the uninfected flag-1 leaf. Assimilation rates of healthy and infected flag leaves at 400 ppm (A) and 1000 ppm (B). Assimilation rates of flag-1 leaves at 400 ppm (C) and 1000 ppm (D). Bars represent the average of 5 biological replicates. Error bars represent the standard error of 5 replicates. Asterisk represents significant differences compared to healthy leaves using a t-test and a p-value lower than 0.05.

My results suggest that the Calvin-Benson cycle activity is low at 8 and 14 dai after *Pst* infection (Figure 3.7, Figure 3.8). I tested if these data were correlated with changes in the expression of the Rubisco small subunit gene (*Rbs*) and the triose-phosphate/phosphate translocator gene (*TPT*). Plants decrease the expression of the *Rbs* gene as a stress response, probably to reduce their photosynthetic capacity and shift to catabolism (Bilgin et al., 2010). The TPT regulates the movement of carbon as triose-P from the chloroplast to the cytoplasm to start the synthesis of sugars (Section 1.3.3, Chapter 1). Changes in the translocation rates increase triose concentrations in the chloroplast and as a consequence the Calvin-Benson cycle will decrease the carbon fixation rates due to substrate inhibition. For these experiments, I measured the transcript levels of *Rbs* and *TPT* in healthy and infected flag leaves. I followed the infection diagram from Figure 3.3 and the gene expression comparison showed in Figure 3.9. I used the comparative C_T ($\Delta\Delta C_T$) method for the analysis, using the expression levels of *18S* RNA and the expression values of infected leaves for normalization. In this analysis, the relative expression of

Rbs was very variable at 4 and 8 dai, but at 14 dai the levels were below one, which means that *Rbs* expression decreased in infected leaves by about half (Figure 3.10A). I observed the opposite results for *TPT* gene expression, where it increased over time, particularly at 14 dai (Figure 3.11A). The TPT is present only in the chloroplast, importing phosphate to the chloroplast and exporting triose-P to the cytoplasm. My results suggest that more triose-P could be exported to the cytoplasm to cope with the sugar demands in the cytoplasm due to the infection. Moreover, the reduced levels of *Rbs* at the end of the infection correlate with the lower carbon fixation rates observed in the previous experiments.

To determine if there are systemic responses and changes in development due to *Pst* infection, I measured and analysed gene expression levels as shown in Figure 3.9. For systemic responses, I compared the transcript levels of *Rbs* and *TPT* in flag-1 leaves that were not infected (HB vs IB). For changes in plant metabolism, I compared the expression levels between the flag and flag-1 leaves from the same plant. These comparisons should indicate the metabolic conditions within healthy plants (HA vs HB) and how this is altered during infections (IA vs IB). For systemic responses (IB vs HB), the *Rbs* relative expression had a large peak at 8 dai but declined at 14 dai (Figure 3.10B). This suggests that Rubisco small subunit expression was higher in the flag-1 leaf of infected flag leaves compared to that of healthy plants. Possibly infection of the flag leaf induces *Rbs* expression in flag-1 to compensate for diminished nutrient export by the infected flag leaf. Conversely, *TPT* values were close to one at all three time points, which suggests that *TPT* expression did not respond to the infection (Figure 3.11B). The results showed that the expression of *Rbs* but not *TPT* had a systemic response.

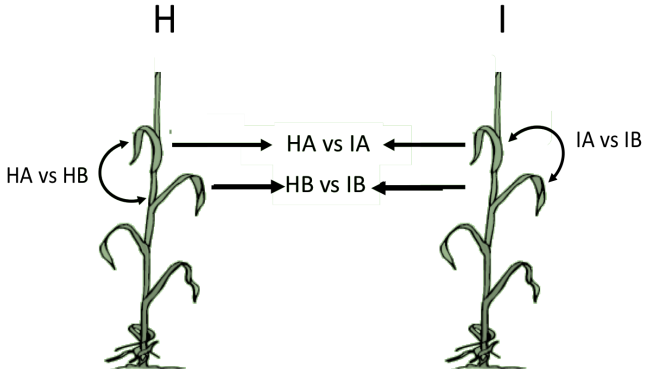

Figure 3.9. Diagram to illustrate gene expression comparisons. The comparisons were between healthy and infected flag leaves, between flag-1 leaves of the same plants, and between flag and flag-1 leaves within the one plant. Only the flag leaf was infected (IA) or mock inoculated (IB).

Healthy adult plants expressed *Rbs* and *TPT* differentially in the flag and flag-1 leaves. The flag leaves may have higher levels of expressed *Rbs* but lower levels of *TPT* compared to the flag-1 leaf (Figure 3.10 C; Figure 3.11 C). These results represent control conditions within healthy plants, which I then compared to infected plants. For *Rbs* expression, infected plants had the

opposite pattern to healthy plants; the expression decreased over time and was always below two (Figure 3.10 D). In contrast, the relative expression of *TPT* was similar in healthy and infected plants, decreasing over time to below one (Figure 3.11 D). In summary, only *Rbs* expression changed within the plant during infection. This suggests that the flag-1 leaf may compensate the nutrient requirements of the flag leaf by increasing the available Rubisco. Importantly, it is a clear indication of a systemic response to *Pst* infection.

Overall, *Rbs* and *TPT* were expressed differentially in healthy and infected plants, and within plants. Infected flag leaves had reduced *Rbs* expression compared to healthy flag and to the flag-1 leaves. This suggests that the plant's metabolism is affected when the flag leaf is infected. On the other hand, *TPT* expression increased in infected leaves compared to healthy flag leaves, but was unchanged relative to flag-1. This potentially means that *TPT* expression changes similarly throughout the plant even when only one of the leaves is infected.

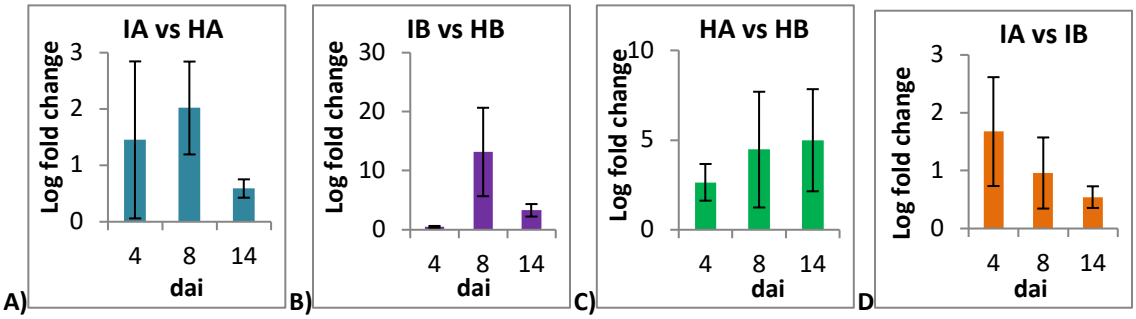

Figure 3.10. Expression of the Rubisco small subunit gene (*Rbs*) in healthy and *Pst*-infected adult wheat plants. The scheme of infections and comparisons are shown in Figure 3.3. A) Relative expression in infected flag leaves (IA) compared to healthy flag leaves (HA). B) Relative expression in uninfected flag-1 leaves from infected leaves (IB) and from healthy flag leaves (HB). C) Relative expression in healthy flag leaves compared to flag-1 leaves. D) Relative expression in infected flag leaves compared to flag-1 leaves on the same plant. Bars represent the average of three independent experiments, each comprising three biological replicates. Error bars represent the standard error of 9 samples.

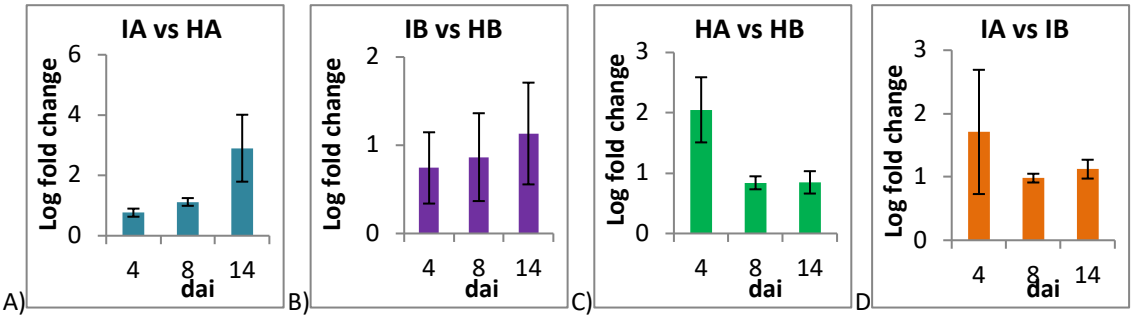

Figure 3.11. Expression of the triose-phosphate/phosphate translocator gene (*TPT*) in healthy and *Pst*-infected adult wheat plants. The scheme of infections and comparisons are shown in Figure 3.3. A) Relative expression in infected flag leaves (IA) compared to healthy flag leaves (HA). B) Relative expression in flag-1 leaves of infected plants (IB) compared to flag-1 leaves of healthy plants (HB) (only flag leaves were infected in these experiments). C) Relative expression in healthy flag leaves compared to Flag-1 leaves. D) Relative expression in infected flag leaves compared to flag-1 leaves on the same plant. Bars represent the average of three independent experiments, one comprising three biological replicates. Error bars represent the standard error of 9 samples.

3.3.3 Accumulation of photosynthates during infections

3.3.3.1 Dry weight of infected and healthy wheat plants

Based on the photon capture and carbon fixation data presented here, it seems that photosynthesis is affected negatively by *Pst* infection, and as a consequence the synthesis of photosynthates decrease. Nutrient levels regulate growth, which is proportional to dry biomass. Therefore, I measured the dry weight of healthy and infected leaves in younger plants to evaluate the effect of *Pst* infection on plant growth. For these experiments, I infected whole cv. Morocco plants as the 7th leaf emerged (Figure 3.12 A). I harvested the 6th, 5th and 4th leaves at 2, 8, and 14 dai for dry weight comparisons. The dry weights of healthy and infected leaves were similar at 2 and 8 dai, therefore I show data only from 8 dai (Figure 3.12 B). In healthy plants, the leaf dry weight was slightly higher in the 6th leaf compared to the 4th leaf while infected plants had similar values for the three leaves evaluated. At 14 dai the dry weight of healthy leaves decreased with the age of each leaf, such that the 6th leaves which were the youngest had the highest dry weight (Figure 3.12 C). This is potentially explained by remobilisation of nutrients from older to younger leaves or because the younger leaves are more active in carbon fixation. I also measured leaf dry weights in cv. Morocco adult plants, but only in healthy and *Pst*-infected flag leaves. The dry weights of the infected 4th and 5th leaves were greater than the corresponding healthy leaves. This possibly represents increased fungal biomass since the fungus sporulated at 14 dai. The carbon necessary to build that fungal biomass was fixed by the plant. This means that infected leaves produce or import more carbon, which is then taken up by the fungus.

Water content is an indicator of nutrient relocation. Water flow is required for cell growth and for nutrient import or export by osmotic pressure (Taiz and Zeiger, 2010). Therefore, I measured the water content of the same leaves used above for the fresh (data not shown) and dry weights experiments. The water contents of healthy and infected leaves were similar at 2 and 14 dai, but were higher in infected leaves at 8 dai (Figure 3.12 D, E). This may be the result of high osmotic pressure due to an increase in nutrient import triggered by the fungal sink. In summary, the results showed that the water content of infected leaves is higher at 8 dai while dry weight is higher at 14 dai, both by comparison to healthy plants. These data suggest that *Pst* infection alters carbon synthesis and distribution in plants and within single leaves. To test these ideas, I measured the dry weight of the leaf areas surrounding the infection where the fungus was not present, and secondly I measured the dry weight of heads. If there is greater carbon demand in infected tissue, the healthy tissue surrounding the infected area should have less dry weight since nutrients are allocated to the infected areas. However, I did not observe differences in dry weight between healthy and infected tissue areas at 8 and 14 dai (data not shown). Possibly the infection effect should be evaluated in the entire plant or in organs more sensitive to carbon fluxes. To evaluate this hypothesis, I collected heads from healthy and infected adult plants at 15 dai. For this experiment, I infected only the flag leaf. The heads from infected flag leaves were similar in length but were only half of the dry weight of healthy plants (Figure 3.13). This suggests that the fungus consumed nutrients that would normally have been used for grain-filling, and reflects the systemic effects of the infection. Moreover it shows the importance of the flag leaf in grain filling and how sensitive heads are to nutrient reallocation.

In conclusion, my results showed that leaf dry weight was higher in infected tissue and reduced in the heads. Dry weight reflects how much carbon is allocated to organs or tissues across plants. Therefore, infected tissue, including fungal tissue, accumulates more carbon. Since *Pst* is a heterotroph, its carbon must come from the plant. The nutrient reallocation caused by the infection is reflected in less nutrients to the heads and shifting the infected tissue to sink.

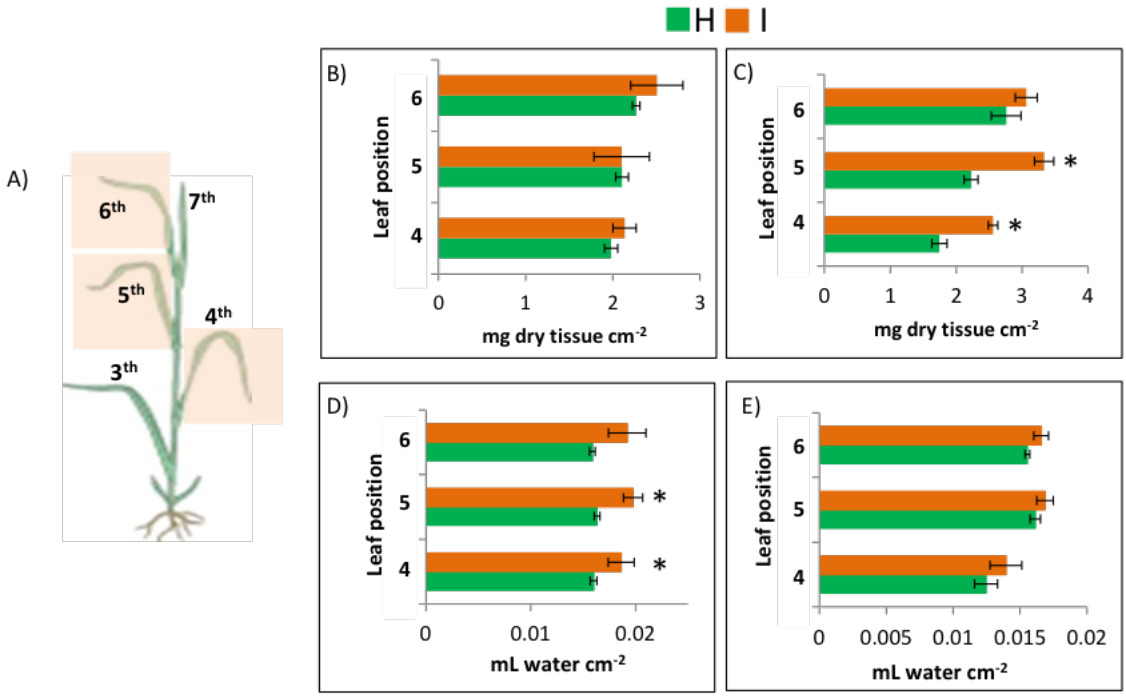

Figure 3.12 Dry weight and water content of healthy and infected wheat leaves. A) Four-week old plants were infected (I) or mock inoculated (H). The numbers represent the leaf positions. B, D) Dry weight and water content at 8 dai. C, E) Dry weight and water content at 14 dai. Error bars represent standard error of five replicates. Asterisk represents significant differences compared to healthy leaves using a t-test and a p-value lower than 0.05.

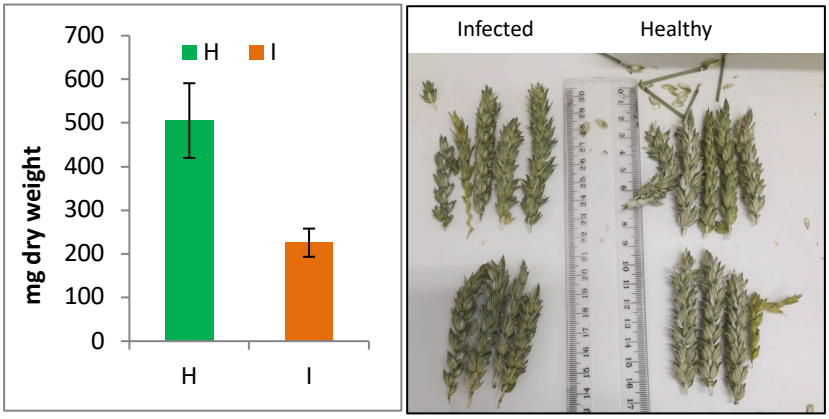

Figure 3.13. Dry weight of wheat heads from healthy and infected adult plants. Plants were infected or mock-inoculated only on the flag leaves. Left panel represents the average head weight of 6 plants. The heads were collected at 15 dai. Error bars represent the standard error. Asterisk represents significant differences compared to healthy leaves using a t-test and a p-value lower than 0.05. Right panel shows the collected heads from the left panel.

3.3.3.2 Starch and fructans metabolism in healthy and infected plants

In the previous section I showed that *Pst* induces carbon accumulation in infected tissue. Plants have various carbon stores (reviewed here in Section 1.3.3 of Chapter 1) that could contribute fungal biomass. I measured starch, one transitory storage compound, to investigate its contribution to dry weight changes in infected plants. I quantified starch levels in the aerial parts

of younger and adult cv. Morocco plants infected with *PST*-79. For younger plants, I infected all leaves and stems while for adult plants I infected only the flag and flag-1 leaves. I collected tissue one hour before the start of the night cycle (where starch accumulation should be maximal) unless otherwise indicated. I collected data at 2, 8 and 14 dai and compared them to those of healthy plants sampled similarly. The levels of starch in the healthy aerial parts of young stage plants increased over time, as expected for carbon accumulation during plant growth (Figure 3.14). The levels of starch in infected aerial parts were similar to healthy plants at 2 and 8 dai. The starch levels were very similar at 8 and 14 dai and were about one quarter of the healthy plant values. Based on these results, the reduction in starch during *Pst* sporulation could be associated with fungal starch consumption (indirectly), or alternatively the plant failed to accumulate starch during the infection. The aerial parts are a combination of stem and leaves which represent different pools of starch that might be mobilised differentially. To evaluate if *Pst* infection had the same effect on leaves and stems I measured starch in these tissues separately. The starch levels in stems were similar in healthy and infected plants at 2, 8 and 14 dai (data not shown). Therefore, the next step was to measure starch in leaves. I performed the starch measurements at 8 and 14 dai since I did not observe differences at 2 dai in previous experiments. For this study, I infected leaf areas only for a more uniform infection and took into account diurnal starch dynamics. I collected three samples for each time point; one before commencement of the dark period (8 am), one during the dark period (2 pm), and one before commencement of the light period (8 pm). The results at 8 dai for healthy and infected leaves showed that starch accumulated during the day and decreased at night; however infected leaves contained more starch throughout the measurement period (Figure 3.15 A). The results showed a faster rate of starch accumulation and decline in infected than healthy leaves. These results contradict the data from Figure 3.14 where starch decreased, possibly because the infection method changed (in the last experiment the infection was delimited to leaf areas). For the 14 dai data, the differences between healthy and infected leaves were greater than at 8 dai. Infected plants accumulated more starch than healthy plants, and starch levels were more stable in healthy plants at the beginning of the curve (Figure 3.15 B).

A possible explanation for the results at 14 dai is that in stress conditions, hexoses increase and high levels of glucose induce starch accumulation (Streb and Zeeman, 2012). In summary, infected plants accumulated less starch, but infected leaf areas had more starch than healthy plants. These results suggest that starch accumulation in infected plants is limited to locally infected areas or is mobilized and broken down to provide hexoses in infected tissue.

These first experiments were performed in young stage plants. To investigate starch accumulation in adult plants, I measured starch in healthy and *PST*-79-infected flag leaves. For these experiments, I collected infected leaf areas at 4, 8 and 14 dai. The starch levels in healthy flag leaves decreased over time, while it increased markedly in infected flag leaves (Figure 3.16 A). At 14 dai the starch levels in infected leaves were at least three times higher than in healthy leaves. The results provide one explanation for the decrease in dry weight for heads. The infected leaves accumulated carbon as starch, which would decrease the mobilization of carbon to heads.

If *Pst* infection decreases plant carbon export, this could affect the levels of starch in distal leaves. To test this, I measured the starch levels in the uninfected flag-1 leaf from the same plants of the previous experiment. In uninfected plants, starch levels were variable at 4 and 14 dai with a decrease at 8 dai (Figure 3.16 B). For infected plants, starch levels in flag-1 leaves were similar at 4 and 8 dai, and decreased at 14 dai. The levels of starch in infected plants were higher in flag-1 than flag leaves only at 8 dai. The variability in flag-1 leaves was higher than for flag leaves, however it seems from these results that starch accumulation might be affected in distal leaves during infection. Various possible explanations for these results could be that starch, in another carbohydrate form, is transported to the infected leaves, or high levels of glucose is accumulated as starch.

Finally, I measured expression of the ADP-glucose pyrophosphorylase (*AGPase)* gene in infected plants to see if it correlated with starch accumulation patterns. AGPase is the most important enzyme to initiate starch synthesis. I measured the transcript levels of this gene in healthy and infected flag leaves using qRT-PCR, and calculated its relative expression as explained in Section 3.3.2 and Figure 3.9. Infected and healthy flag leaves seemed to have similar levels of *AGPase* transcript levels since the relative expression values were between one and two with high variability (Figure 3.17 A). Similarly, no significant differences in expression levels were visible between infected flag leaves and proximal healthy flag-1 leaves (Figure 3.17 B). I next compared *AGPase* expression levels within plants to assess if its expression changes in different leaves. Within healthy plants, relative expression in the flag leaf compared to the flag-1 leaf was stable at 4 and 8 dai and slightly decreased at 14 dai, with values close to 1.3 (Figure 3.17 C). For infected plants, the comparison between infected flag leaf and uninfected flag-1 showed a stable relative expression due to the large error bars (Figure 3.17 D). In conclusion, starch accumulation did not correlate with *AGPase* expression. A future experiment could be to measure the expression of amylase genes and amylase enzymatic activity in infected and healthy

leaves since the changes of starch metabolism could be related to degradation of starch rather than changes in the synthesis.

In summary, plant growth can be measured as functions of dry weight and starch accumulation. In *Arabidopsis,* water and carbon levels contribute to leaf expansion (Pantin et al., 2011). In wheat, the differences in water content, dry weight and starch content between infected and healthy tissue suggest that the infection shifts the tissue to sink metabolism drawing nutrients from distal areas, but the influx of sugars are taken up not only by the fungus but also accumulate as starch. Diverse plant pathogen interactions modify starch levels differentially in their hosts. Starch levels decreased at 8 dai in wheat plants infected with *P. graminis* f.sp *tritici*, whereas some oomycete infections increased starch levels (Gamm et al., 2011; Heisterüber et al., 1994; Lemoine et al., 2013).

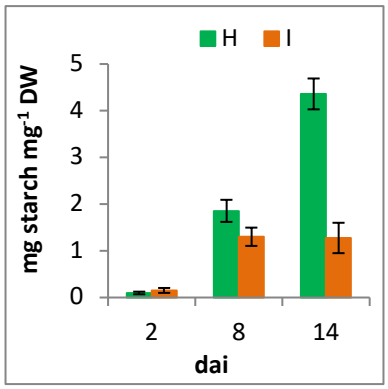

Figure 3.14. Starch levels in the aerial parts of healthy and infected wheat. Young stage cv. Morocco plants were infected with *PST*-79 when the 7th leaf appeared. Error bars represent the average of 5 biological replicates. Asterisk represents significant differences compared to healthy leaves using a t-test and a p-value lower than 0.05.

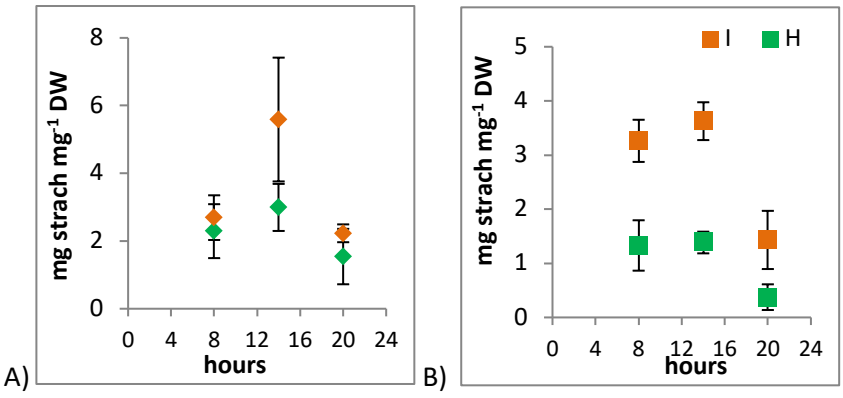

Figure 3.15. Starch levels in healthy and *Pst*-infected wheat leaves at different points during the light cycle. Samples were collected from cv. Morocco plants at 8 (A) and 14 (B) days after infection. There were three collection time points in a 16/8h light/night cycle. Error bars represent the standard error of 5 replicates. Asterisk represents significant differences compared to healthy leaves using a t-test and a p-value lower than 0.05.

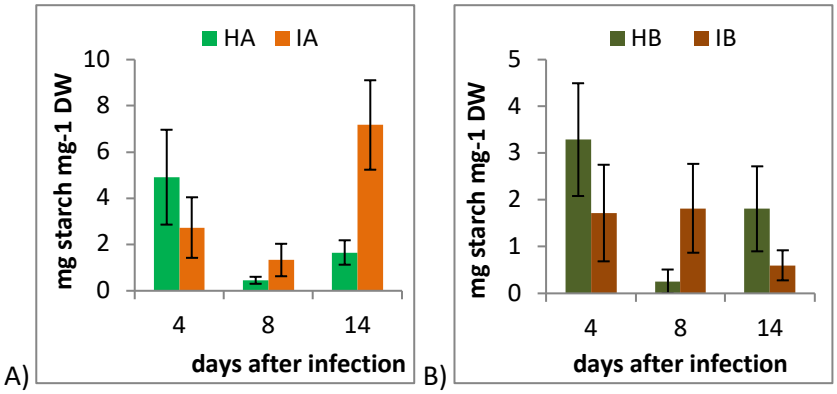

Figure 3.16. Starch levels in healthy and infected flag leaves, and non-infected flag-1 leaves from healthy and infected plants. Starch accumulation in flag leaves (A) and flag-1 leaves (B) from adult cv. Morocco plants one hour before the night period. Error bars represent the average of 5 biological replicates. Asterisk represents significant differences compared to healthy leaves using a t-test and a p-value lower than 0.05.

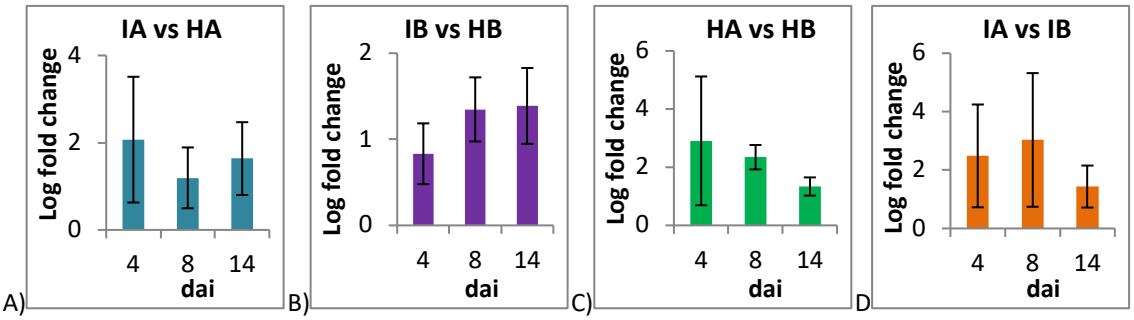

Figure 3.17. Expression of the *ADP-glucose pyrophosphorylase* gene in adult wheat plants. The scheme of infections and leaf comparisons are described in Figure 3.3. A) Relative gene expression in infected flag leaves (IA) compared to healthy flag leaves (HA). B) Relative gene expression in uninfected flag-1 leaves from infected plants (IB), compared to flag-1 leaves from healthy plants (HB). C) Relative gene expression in healthy flag leaves compared to flag-1 leaves of the same plant. D) Relative gene expression in infected flag leaves compared to flag-1 leaves of the same plant. Bars represent the average of three independent experiments each with three biological replicates. Error bars represent the standard error of 9 samples.

Fructans are another form of storage carbohydrate in cereals. In contrast to starch which is consumed only at night, plants accumulate and consume fructans during the 24 h growth cycle and transport them throughout the plant. Kestose is the smallest fructan, composed of one unit of sucrose and another of fructose. I measured kestose levels and the expression levels of two genes involved in its metabolism, to complement the dry weight and starch content measurements above. For these experiments, I mock-inoculated or infected the flag leaves of adult plants and collected leaf samples for analysis at 4, 8 and 14 dai. I quantified kestose levels by GCMS from these samples. I found that the values were similar in healthy and infected plants (data not shown). The next step was to evaluate the expression of kestose metabolism genes. I measured the relative expression of the *fructan-6-hexohydrolase* (*F6H*) and *sucrose:fructan 6-fructosyltransferase* (*SFT*) genes. The enzymes encoded by these genes are involved in kestose degradation and synthesis respectively. *F6H* expression was higher in infected than healthy flag

leaves at 4 and 8 dai but declined to zero at 14 dai, while the expression of *SFT* was negligible at 4 dai, but increased to about 3-fold at 8 and 14 dai (Figure 3.18 A; Figure 3.19 A). These patterns are essentially opposed and suggest that fructan degradation is reduced and its synthesis increased over the course of infection despite the fact that there were no clear differences in kestose levels. The apparent changes in fructan metabolism reported by gene transcription might be a response to an excess of hexoses due to the infection because plant hexose levels are increased under stress (Figure 3.21)(Xue et al., 2008) . The expression of these genes was also evaluated in flag-1 leaves. I found that *F6H* gene expression changed from under expression at 4 and 8 dai to overexpression (~5-fold) at 14 dai in flag-1 leaves of infected versus uninfected plants (Figure 3.18 B). This suggests that *F6H* expression responded systemically to the infection, enhancing degradation of kestose, and is consistent with carbon demand from the infected tissue. The *SFT* expression values in flag-1 leaves of uninfected plants (HB) were too variable to allow strong conclusions about a possible systemic response to *Pst* infection (Figure 3.19 B, C). In healthy plants, the expression levels of both *F6H* and *SFT* decreased in flag relative to flag-1 leaves markedly from 4 dai but were always higher in flag leaves (Figure 3.18 C; Figure 3.19 C). In infected plants, *F6H* expression in flag leaves decreased with respect to flag-1 leaves abruptly at 14 dai (Figure 3.18D). In contrast to healthy leaves, *SFT* expression in infected plants peaked at 8 dai but at 4 and 14 dai the values were close to one (Figure 3.19 D). Overall, my results suggest that *Pst* infection shifts fructan metabolism from degradation to synthesis, while the systemic response is to increase the breakdown of fructans.

In summary, I evaluated the dynamics of two sugar storage compounds, kestose and starch, during *Pst* infection by measuring their accumulation and changes in the expression of genes required for their synthesis or degradation. Starch accumulated in infected leaves but this observation was not supported by gene expression studies. For fructans, there were no differences in kestose abundance but gene expression suggested that kestose synthesis was induced in infected leaves. Another explanation for the lack of observed changes in kestose accumulation could be that the infected plants synthesise more fructans which are taken up by the fungus, hence the values are similar to those of healthy plants. Based on my results, *Pst* is apparently inducing accumulation of sugars in infected areas and stimulating degradation of storage compounds in distal tissue.

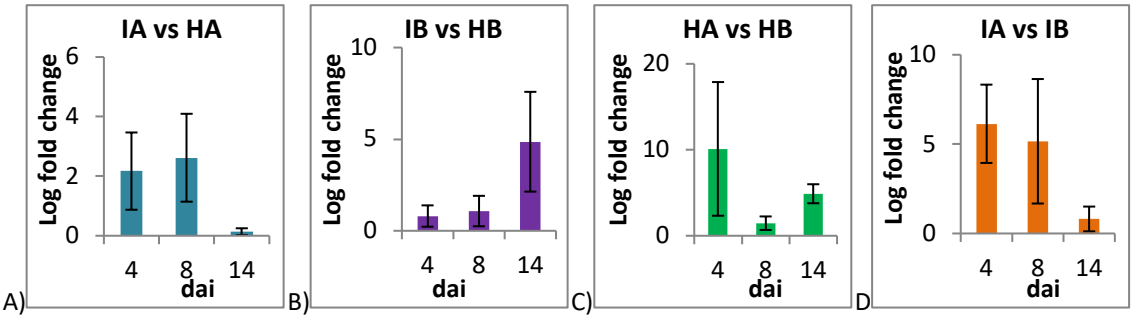

Figure 3.18. Relative expression of the *fructan-6-hexohydrolase* (*F6H)* gene in infected and healthy adult wheat plants. The scheme of infections and leaf comparisons are shown in Figure 3.3. A) Relative gene expression in infected flag leaves (IA) compared to healthy flag leaves (HA). B) Relative gene expression in healthy flag-1 leaves of infected plants (IB) compared to flag-1 leaves from healthy plants (HB). C) Relative gene expression in healthy flag leaves compared to healthy flag-1 leaves of the same plant. D) Relative expression in infected flag leaves compared to flag-1 leaves of the same plant. Bars represent the average of three independent experiments, each with three biological replicates. Error bars represent the standard error of 9 samples.

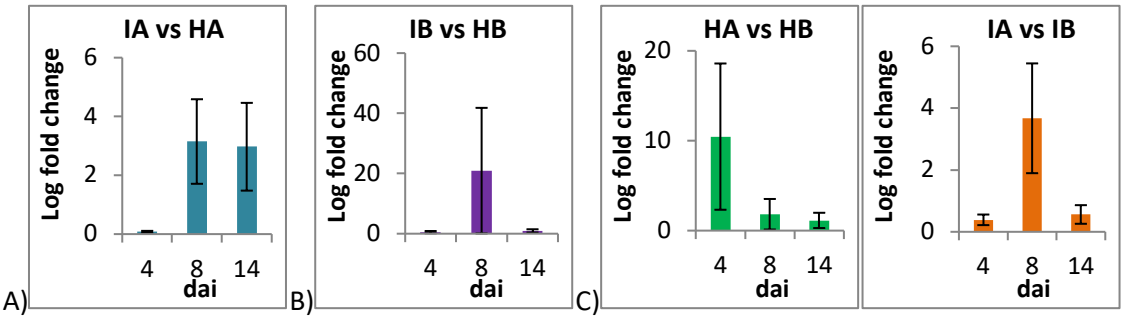

Figure 3.19 Relative expression of the *sucrose:fructan 6-fructosyltransferase* gene (*SFT)* in adult wheat plants. The scheme of infections and comparisons are in Figure 3.3. A) Relative expression in infected flag leaves (IA) compared to healthy flag leaves (HA). B) Relative expression in flag-1 leaves from infected plants (IB) compared to flag-1 leaves from uninfected plants (HB). C) Relative expression in healthy flag leaves compared to flag-1 leaves of the same plant. D) Relative expression in infected flag leaves compared to flag-1 leaves of the same plant. Bars represent the average of three independent experiments each with three biological replicates. Error bars represent the standard error of 9 samples.

3.3.4 Accumulation of primary metabolites during *Pst* infection

3.3.4.1 Hexose and sucrose metabolism during infection

Storage carbohydrate metabolism increased in wheat leaves during *Pst* infection. The synthesis of starch and fructans depends on glucose, fructose and sucrose levels. I evaluated if *Pst* infection changes the levels of these sugars in whole tissue and in the apoplast, since the fungus occupies the intercellular spaces. For apoplast extraction, I applied vacuum pressure to extract the apoplastic fluids. For these experiments, I infected or mock-inoculated both young stage and adult plants with *PST*-79 spores. I collected samples at 2 (young stage) or four (adult plants), 8 and 14 dai and performed a methanolic extraction of polar components to extract sugars.

For young stage plants, I measured the levels of glucose, fructose and sucrose by GCMS and compared them in healthy and infected leaves. I did not observe clear differences between samples for sucrose and fructose levels (data not shown); therefore I calculated the hexose to sucrose ratio for whole tissue and for the apoplast fraction (Figure 3.20). The ratio compares hexoses and sucrose in the plant to indicate the metabolic stage of the plant, either being a sucrose-producing source or a sink with increased levels of hexoses. The hexose:sucrose ratio in healthy leaves decreased linearly over time, which corresponds to the transition of young leaves from source to sink (Baud et al., 2002). The ratio for infected plants was lower than healthy leaves at 2 dai and slightly higher at 14 dai (Figure 3.20 A). These results are for whole tissue, and suggest that the plants were already responding to the infection by 2 dai. I propose two explanations for these results; firstly that the fungus secreted proteins that reduced the levels of hexoses since 2 dai, or that the plant changed its sugar metabolism, decreasing fungal access to plant hexoses. Conversely, the higher ratio in infected tissue at 14 dai suggests a shift to sink tissue. These results correlate with my previous results where sink tissue characteristics such as increased respiration rates and lower *Rubisco* expression levels occurred at 14 dai.

I also evaluated hexose:sucrose ratios in the apoplast. I could not calculate the values at 2 dai and 8 dai because the levels of sucrose were undetectable (Figure 3.20 B). There were major differences at 8 dai in the hexose:sucrose ratios in the apoplast of healthy and infected leaves, but the values for healthy and infected tissue were identical at 14 dai. As sucrose levels were zero, possibly the infection induced massive export of sucrose reducing sucrose levels. Alternatively, as a stress response, the plants are breaking down all stored sucrose. In general, the results from young stage plants suggest that *Pst* induced a shift to sink metabolism from 8 dai.

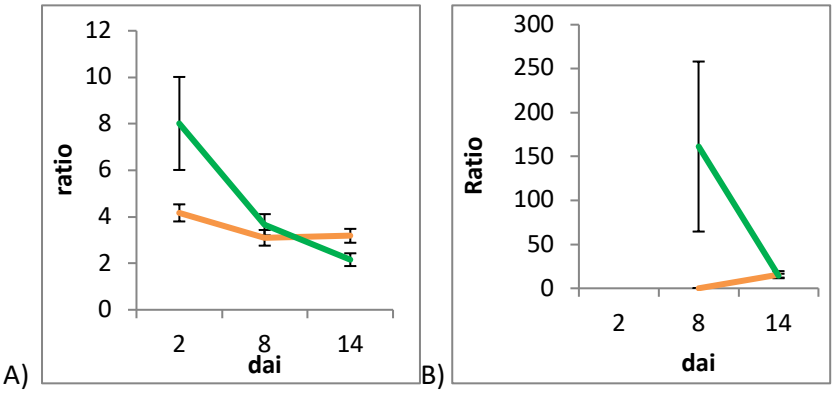

Figure 3.20. Hexose:sucrose ratios in whole leaves of young stage plants based on GCMS data. Ratios in whole tissue (A) and in the leaf apoplast (B) of plants infected when the 7th leaf appeared. Green colour represents healthy tissue while orange represents infected tissue. Error bars represent the standard error of 5 samples.

To complement the data from young stage plants I measured the levels of glucose, fructose and sucrose in adult plants. For these experiments, I used enzymatic quantification of sugars (Section 3.2.5.3.5.1). I evaluated these levels in whole flag leaves, the apoplastic fractions of flag leaves, and whole flag-1 leaves. The levels of glucose in healthy flag and flag-1 leaves increased over time, while the apoplast levels were stable (Figure 3.21). In infected plants, glucose levels changed; for whole flag leaves the glucose levels decreased gradually over time, but at 4 dai the levels were higher. For the apoplast, there are no values for four dai because these samples failed due to high levels of cytoplasmic contamination. There was more glucose in the apoplast of infected flag leaves than healthy flag leaves at 14 dai. Finally, for flag-1, glucose levels were higher in infected than healthy plants at 4 dai, but were similar at 8 and 14 dai. In summary, glucose levels change from the beginning of infection, accumulate more in the apoplast at 14 dai and respond systemically at the early stages of infection.

The levels of fructose were similar at 4 and 14 dai in healthy flag leaves but decreased at 8 dai. In the apoplast fraction of heathy flag leaves, the levels were stable, similar to glucose levels. Likewise, fructose levels in flag-1 leaves of uninfected plants increased over the course of the experiment (Figure 3.21). For infected flag leaves, the levels in whole tissue were similar or declined slightly over time, but were notably higher than in healthy flag leaves at 8 dai. Fructose levels in the apoplast fractions of infected flag leaves increased over time and were much higher at 14 dai compared to those of uninfected flag leaves. For flag-1 leaves of infected plants, the levels of fructose were higher than healthy flag-1 leaves at 4 dai, but decreased over time and were much lower at 14 dai. In summary, fructose levels and profiles were very similar to glucose for flag leaves, flag apoplast, and flag-1 leaves.

The levels of sucrose in the three experimental samples (whole flag, flag apoplast, and whole flag-1) were highly variable. This makes it difficult to draw conclusions about how the levels changed during the infection. However, the levels were similar within each sample type whether infected or not, but different between sample types. Sucrose was almost undetectable in the apoplast of flag leaves. The flag-1 leaf of infected plants had lower sucrose levels at 4 dai than did those from healthy plants. In general, sucrose levels were too variable to understand their role during infection, however it seems that sucrose might respond systemically to *Pst* infection. For other biotrophic fungal interactions, sucrose levels are not affected in *V. faba* infected with *U. fabae,* while *B. graminis* induces sucrose synthesis in barley (Molitor et al., 2011; Voegele et al., 2005).

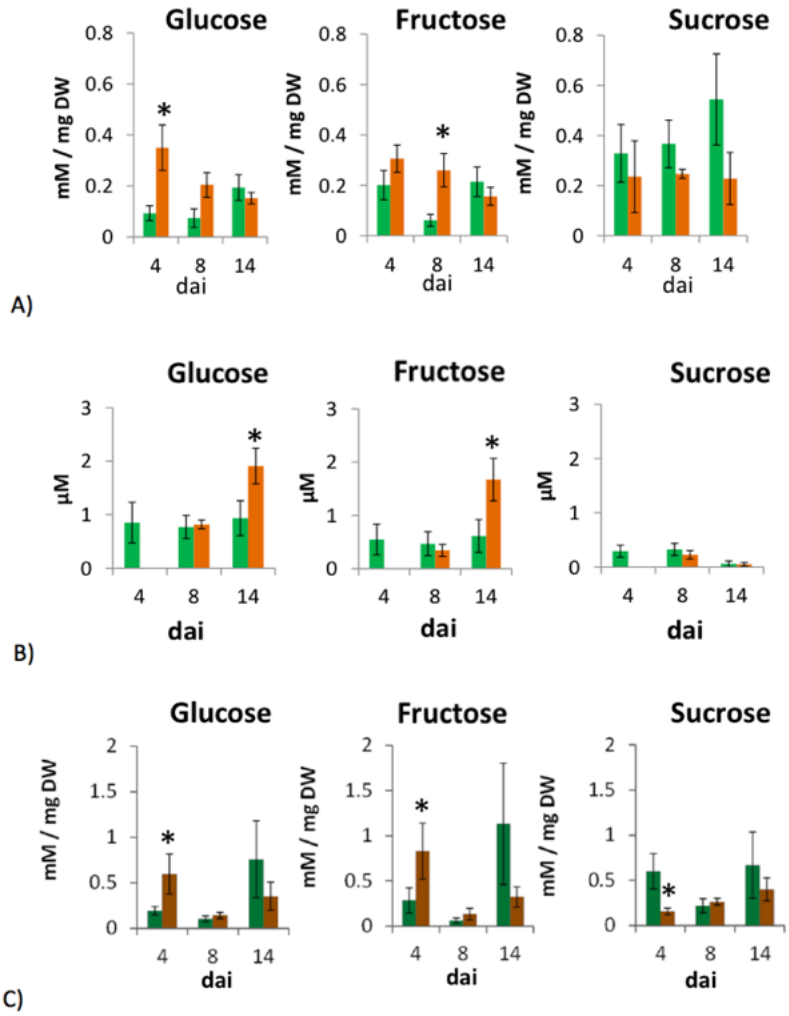

Figure 3.21. Abundance of glucose, fructose and sucrose in adult plants. The flag leaf from adult plants was infected with *PST*-79 or mock-inoculated, and sugars were extracted from whole flag leaves (A), flag leaf apoplast fractions (B) and flag-1 leaves (C). Green colour represents uninfected tissue while orange represents infected tissue. Bars represent the average of four biological replicates. Asterisks represent significant differences compared to healthy leaves using a t-test and a p-value lower than 0.05.

I calculated hexose:sucrose ratios using the data represented in Figure 3.21. Healthy flag leaves had similar values while apoplast values decrease across the infection period, suggesting these leaves undergo metabolic changes mainly at the apoplastic level (Figure 3.22). In contrast, infected flag leaves had higher ratios across the infection with four times the healthy leaf ratio at 4 dai (Figure 3.21 A). In the apoplast fractions, the ratios were consistent with the results for individual sugars (Figure 3.21) because the ratio was higher only at 14 dai where the hexose:sucrose ratio was ~20 times higher in infected than healthy flag leaves. This major difference could be related to the fact that very low sucrose values will increase the ratio dramatically. Another possibility is suggested by the function of flag leaf as a major producer of photosynthate for grain filling; hence hexoses might accumulate in the apoplast instead of being exported (Figure 3.21 B; Figure 3.22 B).

The hexose:sucrose ratio for flag-1 from healthy flag leaves increased over time, suggesting the leaf consume hexoses rather than produces them (Figure 3.22 C). This might be explained by continuous sucrose production by the flag leaf while the other leaves reduce their photosynthetic capacity as they age. The flag-1 leaves from infected plants had the opposite profile to healthy flag-1 leaves. It seems that the infected plants responded systemically to the infection by increasing hexose levels, and then instead of consuming sucrose at 14 dai they produced it.

In general, the ratios showed that young stage plants responded slower to *Pst* infection than did adult stage plants. In whole tissue, the hexose:sucrose ratio of infected adult plant was always higher than healthy plants, while infected young stage plants only showed this effect at 14 dai. The apoplast response can be associated with the age of the tissue. For young stage the respond was at 8 dai while for adult plant was at 14 dai. Possibly the differences in plant age reflect the different hexose and sucrose contents of healthy young and adult stage plants; hexoses were higher in younger plants while sucrose was detectable in adult plants. In conclusion, hexose to sucrose ratios help to understand the metabolic status (sink or source) of infected tissues, however most studies in other pathosystems report only the absolute values (Doehlemann et al., 2008; Heisterüber et al., 1994). Glucose, fructose and sucrose respond differentially during infection and respond systemically to *Pst* infection.

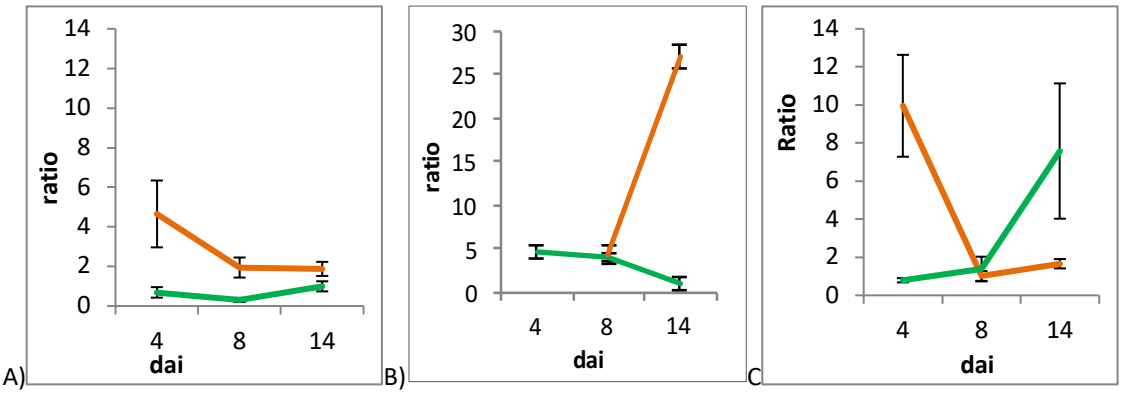

Figure 3.22. Hexose to sucrose ratios in adult plants. The ratios were calculated using the values of Figure 3.21 for whole flag leaves (A), flag leaf apoplastic fractions (B) and flag-1 leaves (C). Green colour represents healthy tissue while orange represents infected tissue. Values represent the average of four biological replicates.

The synthesis, degradation and compartmentalization of sucrose and hexoses is regulated by kinases (Granot et al., 2013). Among these kinases, I evaluated the transcript levels of fructokinase 1 (FK1) and wheat protein kinase 4 (WPK4) during *Pst* infection to examine their relationships to hexose:sucrose ratios. The enzyme FK1 is part of the glycolysis pathway and irreversibly phosphorylates fructose for pyruvate synthesis. The expression of the *FK1* gene

shows the direction of carbon metabolism in the plant, indicating if the plant is breaking down glucose for respiration or synthesizing glucose. The kinase WPK4 belongs to the SNF1-related protein kinases that respond to light stimuli and glucose deprivation (Ikeda et al., 2000). The expression levels of *FK1* and *WPK4* will indicate how carbon metabolism is affected during *Pst* infection. For these experiments, I evaluated the expression levels in healthy and infected flag leaves, and the flag-1 leaf from the same plants. I used the infection and comparison scheme from Figure 3.9.

Expression of *FK1* increased in infected flag leaves relative to healthy flag leaves over time with maximal expression of about 4-fold at 14 dai (Figure 3.23 A). In contrast, *FK1* expression in the flag-1 leaf of infected plants decreased from about 2 times that of healthy flag-1 leaves to have similar expression or closed to one. This suggests an early respond to the infection that disappear along the infection (Figure 3.23 B). In healthy plants the *FK1* transcript levels were similar between flag and flag-1 leaves, while in infected plants the expression levels increased in flag leaves at 8 and 14 dai (Figure 3.23 C, D). In summary, the contrasting expression data from flag and flag-1 leaves suggest that the infected tissue becomes sink and one of the most active pathways is glycolysis, while the flag-1 response is to become or maintain source metabolism, in which hexoses are used for sucrose synthesis rather than glycolysis. These results correlated with the hexose:sucrose ratios that showed higher values in infected flag leaves and an decrease in flag-1 leaves (Figure 3.22).

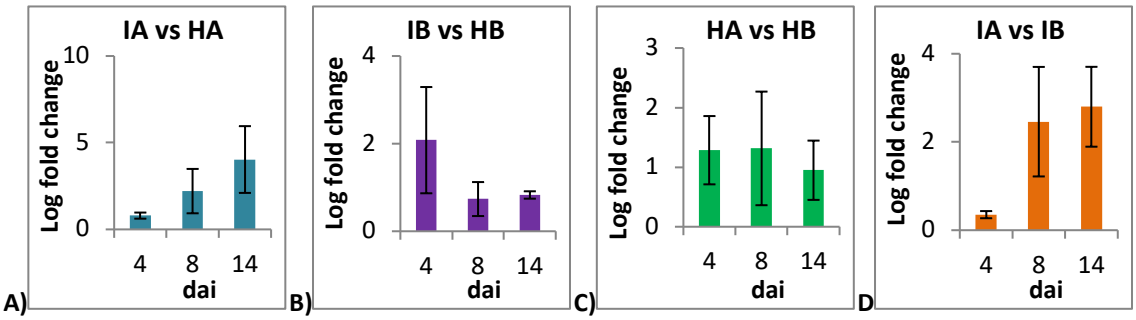

Figure 3.23. Relative expression of the *fructokinase-1* (*FK1)* gene in adult wheat plants infected with *Pst*. The scheme of infections and leaf comparisons are in Figure 3.3. A) Relative expression in infected flag leaves (IA) compared to healthy flag leaves (HA). B) Relative expression in flag-1 leaves from infected plants (IB) compared to flag-1 leaves from healthy flag leaves (HB). C) Relative expression in healthy flag leaves compared to flag-1 leaves of the same plant. D) Relative expression in infected flag leaves compared to flag-1 leaves of the same plant. Bars represent the average of three independent experiments each with three biological replicates. Error bars represent the standard error of 9 samples.

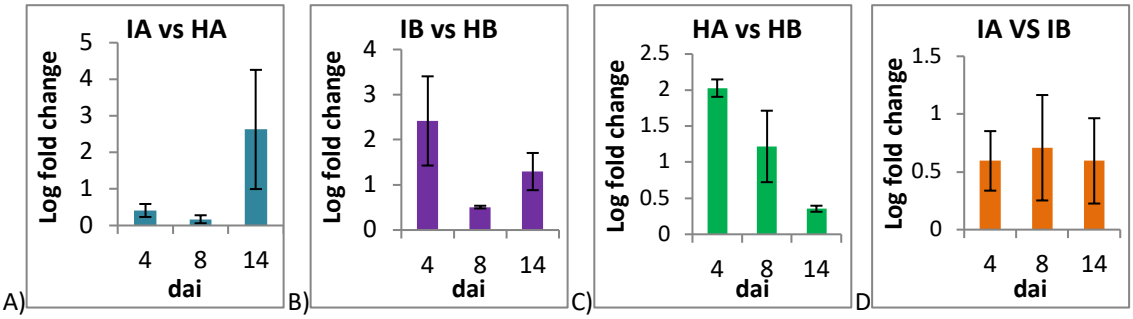

Figure 3.24. Relative expression of the *wheat protein kinase 4* (*WPK4*) gene in adult wheat plants. The scheme of infections and leaf comparisons are in Figure 3.3. A) Relative expression in infected flag leaves (IA) compared to healthy flag leaves (HA). B) Relative expression in flag-1 leaves from infected plants (IB) compared to flag-1 leaves from healthy flag leaves (HB). C) Relative expression in healthy flag leaves compared to flag-1 leaves of the same plant. D) Relative expression in infected flag leaves compared to flag-1 leaves of the same plant. Bars represent the average of three independent experiments each with three biological replicates. Error bars represent the standard error of 9 samples.

WPK4 was underexpressed in infected flag leaves at 4 and 8 dai relative to healthy flag leaves, and increased ~2-fold at 14 dai (Figure 3.24). In infected leaves, the WPK4 expression at 14 dai was almost 5 times relative to healthy plants (Figure 3.24 A). In flag-1 leaves of infected plants, *WPK4* expression was about 2 times that of the healthy flag-1 leaf at 4 dai, then decreased at 8 dai before recovering to rough equivalence at 14 dai (Figure 3.24 B). In healthy plants, *WPK4* expression decreased linearly over time in flag vs flag-1 leaves, while the relative expression in flag vs flag-1 leaves of infected plants was stable and below one (Figure 3.24 C, D). It seems that *WPK4* expression in infected plants responded systemically at 4 dai and locally at 14 dai compared to healthy plants. Based on these results, *WPK4* expression might reflect glucose deprivation only at the late stages of infection, and as a response the levels of hexoses in the host may increase (Figure 3.22 A). I observed a similar pattern for flag-1 leaves at 4 dai which suggests a rapid and early response to *Pst* infection (Figure 3.22 C, Figure 3.24 B).

3.3.4.2 Dynamics of selected amino acids during *Pst* infection

Carbon and nitrogen metabolism are interconnected. Plants use amino acids differently based on the availability of carbon (Calenge et al., 2006). Increasing the carbon supply induces nitrogen uptake, while nitrogen deficiencies cause leaf yellowing and reduce growth capacity. Nitrogenous components can work as carbon sinks to maintain carbon fixation and keep low concentration of free carbon. Based on this, I evaluated the levels of asparagine, glutamine, aspartate and glutamate in whole leaves and apoplastic fluids from healthy and infected young stage plants. These four amino acids respond to changes in carbon levels due to their high carbon to nitrogen ratios (Joy, 1988). They are also involved in nitrate assimilation and in the synthesis of other amino acids. For these experiments, I used the same extracts of Section

3.3.4.1 for sugar quantification and measured the four amino acids using GCMS. In whole tissue the levels of asparagine, glutamine and glutamate from healthy and infected leaves decreased over time, but was elevated in apoplastic fluids at 2 dai (Figure 3.25 A, B). In whole leaves, glutamate levels were similar between healthy and infected plants at all three time points, while for apoplastic fluids the levels were higher in infected tissue only at 14 dai. Asparagine and glutamine abundance at 14 dai were much higher in infected leaves than healthy leaves for whole tissue, while there were no significant differences in the apoplast fractions at this time point. For both asparagine and glutamine the levels at 2 dai were much higher in the apoplast fractions of infected tissue than healthy leaves. For aspartate, although the data were quite variable (high standard errors) in whole tissue, the levels in healthy leaves decreased at 14 dai while for infected leaves, the levels increased from two to 8 dai. The effect of this was to give quite dissimilar profiles between healthy and infected tissue. In contrast, the levels were significantly higher at 14 dai in infected than healthy tissue for the apoplastic fractions. In summary, infected whole tissue had more asparagine and glutamine at 14 dai while infected apoplastic fluids had more aspartate and glutamate. These results suggest different roles or destinations for these amino acids in the symplast and apoplast. One possible model is that the plant preferentially accumulates aspartate and glutamate in the apoplast and the increase observed in whole tissue reflects fungal metabolism. The apoplast values are mainly of plant origin while the whole tissue values include both plant and fungal biomass. Alternatively, the higher levels of aspartate and glutamate at 14 dai in the apoplast could be due to leakage from the infection or because of the sampling method. However, the extraction method includes a control for leakage and the values for cytoplasmic contamination were low (data not shown).

The increase in amino acids at 14 dai correlated with other studies where susceptible plants infected with necrotrophic or biotrophic fungi accumulated higher levels of amino acids (Horst et al., 2010a; Solomon and Oliver, 2001; Solomon et al., 2003). In maize infected with *U. maydis,* nitrogenic compounds are remobilized to infected areas and the levels of amino acids are higher than those of healthy leaves (Horst et al., 2010a). The grains from *Pgt*-infected wheat had lower levels of nitrogen as a consequence of changing nitrogen levels (Park et al., 1988). Finally, tomato leaves infected with *Cladosporium fulvum* had increased levels of glutamate, glutamine, asparagine, aspartate, probably due to the action of host proteases in response to the infection (Solomon and Oliver, 2001).

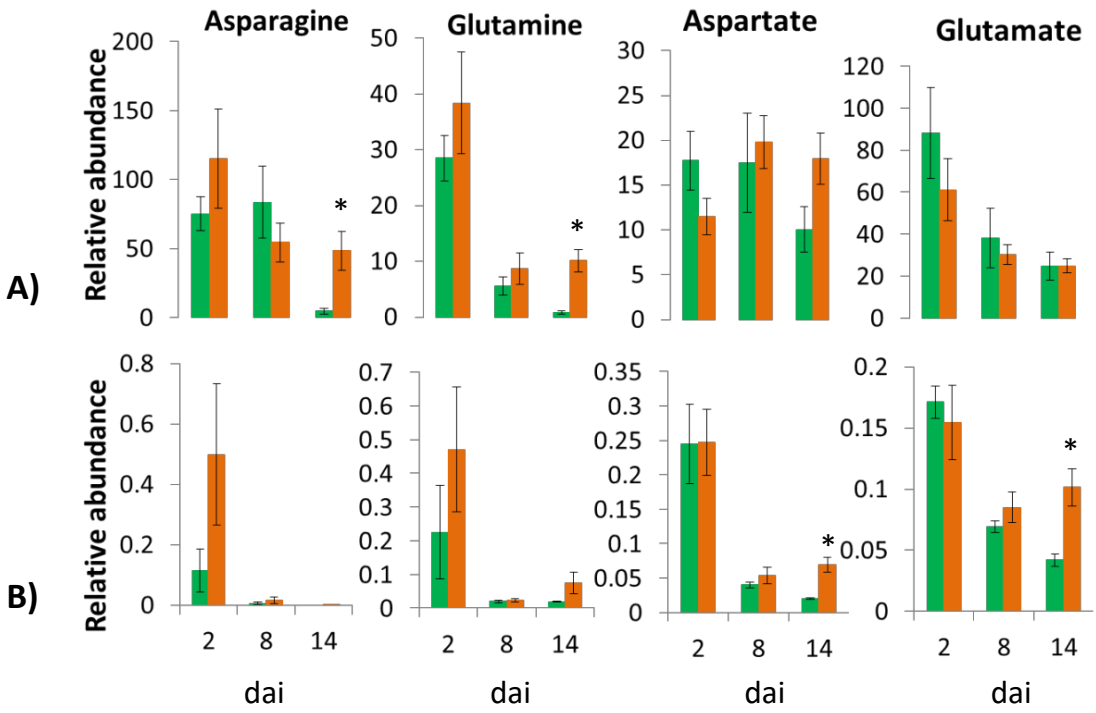

Figure 3.25. Relative abundance of amino acids in leaf extracts of young stage healthy and *Pst*-infected plants. Bars represent the relative abundance of whole tissue (A) and apoplastic fluids (B). Green colour represents healthy tissue while orange represents infected tissue. Error bars represent four biological replicates. Asterisk represents significant differences compared to healthy leaves using a t-test and a p-value lower than 0.05.

To complement the data from younger plants, I measured the levels of asparagine, glutamine and ammonia by enzymatic assays in the flag and flag-1 leaves of adult stage plants. I changed the quantification method because it is less time consuming than GCMS and provides absolute values for each amino acid. The enzymatic assay is based on the activity of glutamate dehydrogenase, which uses ammonium to reduce NADPH. I quantified the oxidized and reduced forms of NADPH by absorbance since NADPH but not NADP absorbs at 450 nm. I included ammonia (NH_4) in the analysis because it is fixed into glutamine and asparagine as part of the nitrogen assimilation pathway. For these experiments, I mock-inoculated or *Pst*-infected flag leaves and collected samples at 4, 8 and 14 dai. The NH_4 values for flag and flag-1 leaves were always variable; therefore I could not make reliable measurements for this metabolite during infection (data not shown). I did not detect glutamine using the enzymatic assay, probably because the values in my samples were below 0.005 g/L based on the detection limits indicated by the manufacturer (Megazyme). Asparagine levels were generally stable in healthy flag leaves with slightly higher values at 8 and 14 dai. In infected flag leaves, levels were similar to healthy leaves at 4 and 8 dai, but increased massively at 14 dai (Figure 3.26 A) where they were about 13 times higher in infected than in healthy leaves. In flag-1 leaves from heathy plants the amount of asparagine increased over time but was stable in flag-1 leaves from infected plants. The variability (indicated in the graphs as error bars) in flag-1 leaves does not allow me to determine

if asparagine has a role in the systemic response to *Pst* infection (Figure 3.26 B). In summary, infected leaves from young and adult stage plants had at least 10 times higher asparagine levels than healthy leaves at 14 dai. The higher levels of amino acids seen mainly at 14 dai suggests that sporulation is the most demanding stage of infection where the fungus might be accumulating more nitrogen. This hypothesis is consistent with *PST*-79 transcriptomic data, where genes coding for aspartate aminotransferase and asparaginase are up-regulated in germinated spores compared to haustoria (Garnica et al., 2013) and also with my data from Chapter 2 where aspartate and asparagine were higher in spores than in germinated spores (Figure 2.4).

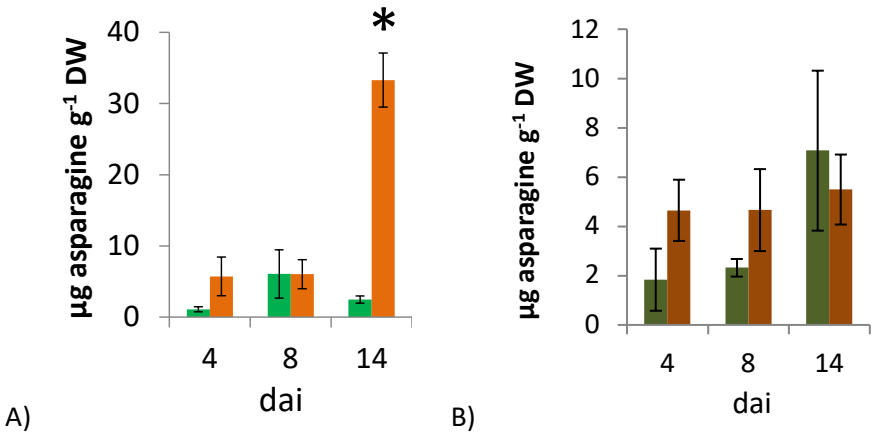

Figure 3.26. Concentration of asparagine in flag and flag-1 leaves of adult plants. A, B) Asparagine concentrations in infected and healthy flag leaves (A) and in distal leaves (B). Green colour represents healthy tissue while orange represents infected tissue. Bars represent the levels of asparagine in three independent experiments, each with five biological replicates. Asterisk represents significant differences compared to healthy leaves using a t-test and a p-value lower than 0.05.

I tested whether the concentration of asparagine was correlated with changes in the expression of the asparagine synthetase (*ASN*) gene, which generates asparagine from aspartate. The primers that I designed to amplify the wheat *ASN* gene did not amplify fungal genes based on the Primer-BLAST tool from the NCBI webpage (https://www.ncbi.nlm.nih.gov/tools/primer-blast/). For these expression experiments, I used the infection and sampling scheme from Figure 3.9. I used the same cDNA material from the previous qPCR performed in this Chapter (section 3.2.4). Then I calculated the expression of *ASN* and normalized it to the expression of the 18S rRNA housekeeping gene, and then compared it to values from different leaves to determine the relative expression. The relative expression of *ASN* in infected flag leaves was always higher than healthy leaves, by 13 times at 4 dai, 3 times at 8 dai and 500 times at 14 dai (Figure 3.27 A). For flag-1 leaves from infected plants the expression was always above that in healthy plants, and varied from 12 times at 4 dai to >5 time at 14 dai (Figure 3.27 B). These results showed that

Pst infection induced the expression of *ASN* both locally and in distal tissue. The *ASN* expression levels at 14 dai correlated with higher levels of asparagine at the end of infection (Figure 3.25 A, Figure 3.26 A) but not with the stable levels of asparagine in flag-1 leaves. Possibly, asparagine synthesis is active but it is remobilized to the infected leaf. The *ASN* expression levels in healthy plants decreased over time, while in infected plants the expression was close to two at 4 and 8 dai but increased to 50 times that in flag-1 leaves at 14 dai (Figure 3.27 C, D). The values for healthy plants suggest that *ASN* expression increased over time in flag-1 leaves which correlates with the rise of asparagine levels in that tissue (Figure 3.26 B).

In summary, asparagine metabolism respond to *Pst* infection independently of plant age. The asparagine levels increased mainly at 14 dai where the fungus has a higher demand of nutrients for sporulation. Based on the high expression of *ASN* also at 14 dai I propose a model where asparagine levels increase to compensate for the nitrogen demand from the infected tissue. The incoming asparagine is then taken up by fungal transporters to maintain the sink. I showed in Chapter 2 that the spores contained high asparagine levels compared to germinated spores, which might explain why the levels of asparagine were higher in whole tissue but not in the apoplast. It is important not to exclude that the fungus is also synthesizing asparagine, as showed by Garnica et al., (2013). Overall asparagine rather than glutamine has proposed to be the main precursor for amino acid synthesis, which could partially explain the higher levels of asparagine over glutamine (Snoeijers et al., 2000). Asparagine is a key nutrient for fungal growth as it has been shown that nitrogen fertilizers promote fungal disease development on plants, and pathogenic fungi upregulate their genes for nitrogen acquisition during plant infection (Hahn et al., 1997; Horst et al., 2010a; Solomon et al., 2003).

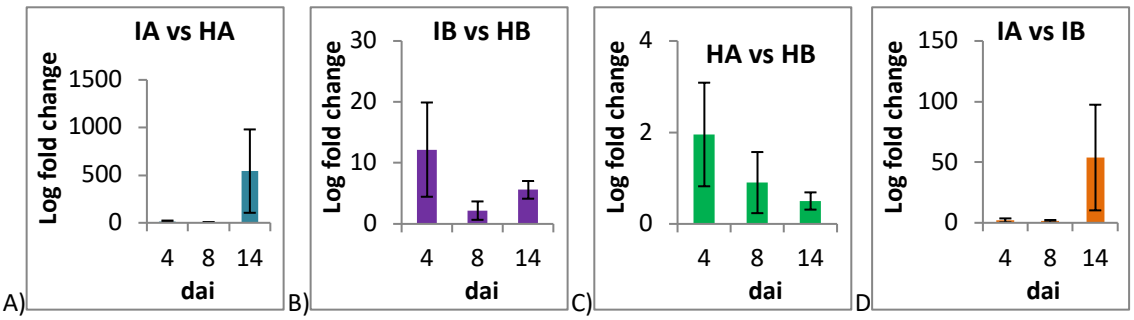

Figure 3.27. Relative expression of the *asparagine synthetase* (*ASN*) gene in adult wheat plants. The scheme of infections and comparisons are in Figure 3.3. A) Relative expression in infected flag leaves (IA) compared to healthy flag leaves (HA). B) Relative expression in flag-1 leaves from infected plants (IB) compared to flag-1 leaves from healthy plants (HB). C) Relative expression in healthy flag leaves compared to flag-1 leaves of the same plant. D) Relative expression in infected flag leaves compared to flag-1 leaves of the same plant. Bars represent the average of three independent experiments, each with three biological replicates. Error bars represent the standard error of 9 samples.

3.3.4.3 Polyol dynamics during *Pst* infection of wheat

While I could detect clear changes in carbon and nitrogen metabolites during *Pst* infection, because these studies were on whole tissue I am unable to tell if the nutrients were derived from the pathogen or the host. Polyols on the other side are sugar alcohols present in fungi as carbon storage molecules but are rare in cereals (Lemoine et al., 2013). Polyols are storage carbohydrates and osmoprotectants. Fungi accumulate them in response to hyperosmotic stress and to quench reactive oxygen species (ROS) (Clancy and Coffey, 1980; Meena et al., 2015; Reisener et al., 1962; Voegele et al., 2005). I quantified four polyols (mannitol, sorbitol, ribitol and arabitol) in *Pst*-infected and healthy tissue, in both whole tissue and apoplast fractions. These four polyols are present in several pathogenic fungi (Clancy and Coffey, 1980; Meena et al., 2015; Reisener et al., 1962; Voegele et al., 2005).

Arabitol and ribitol are five carbon polyols, synthesised from arabinose and ribose, respectively. Mannitol and sorbitol are six carbon polyols synthesised from reduced fructose and glucose. I used the extracts from Section 3.3.4.1 for to detect these compounds. I detected the polyols by GCMS comparing them with known standards. As expected the relative values of the four polyols were low in healthy whole leaves and apoplastic fluids; conversely they increased slightly at 8 and 14 dai with a relative abundance close to 0.5 in whole leaves (Figure 3.28; Figure 3.29). In infected plants, levels of all four polyols were close to zero or to the healthy plant values at 2 and 8 dai, but increased dramatically to be at least three or four times higher than healthy plants at 14 dai (Figure 3.28). Nevertheless, the lower levels of polyols could be also associated with low fungal biomass per leaf that makes harder to detect. Of the four, mannitol and sorbitol levels were much higher than those of arabitol and ribitol. The massive increase at 14 dai is probably related to fungal sporulation (Figure 2.6, Chapter 2). In summary, my results from this Chapter and from Chapter 2 correspond with other reports where polyols are present in tissue infected with biotrophic fungi including *Pgt*, *M. lini* and *U. appendiculatus* (Daly et al., 1967; Jackson and Frear, 1967; Reisener et al., 1962). Polyols are abundant in the spores of these fungi which explains why the levels are higher at 14 dai (when *Pst* is sporulating). From the proposed roles for polyols, *Pst* possibly uses them as carbon storage compounds and osmoprotectants since they are highly abundant at the end of infection rather than at the beginning.

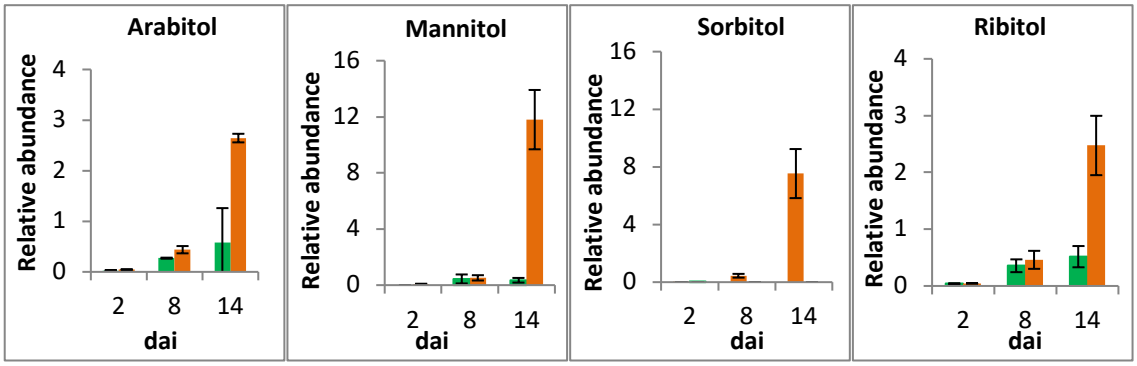

Figure 3.28. Relative abundance of polyols in leaves from young stage healthy and *Pst*-infected wheat plants. The peak areas for each polyol obtained by GCMS were normalized to the total area of all polar metabolites to obtain the relative abundance. Green colour represents healthy tissue while orange represents infected tissue. Bars represent the average of four biological replicates. Asterisk represents significant differences compared to healthy leaves using a t-test and a p-value lower than 0.05.

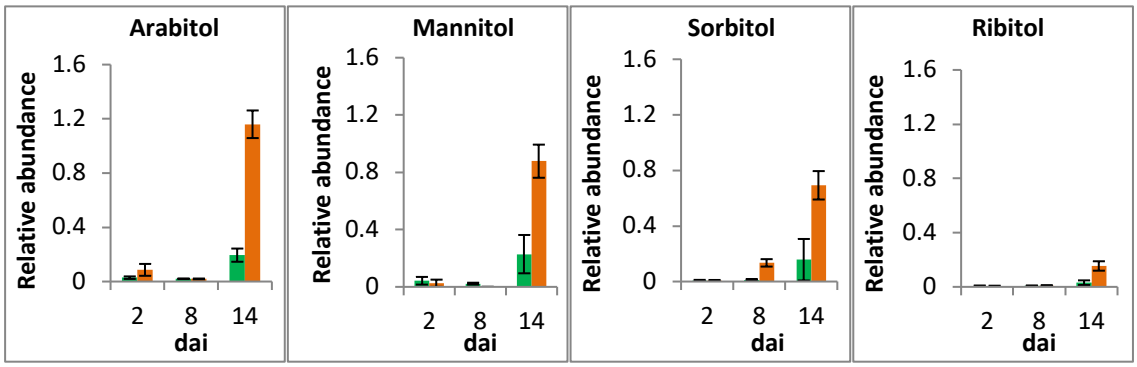

Figure 3.29. Relative abundance of polyols in apoplastic fluids from young stage healthy and *Pst*-infected wheat plants. The peak areas for each polyol obtained by GCMS were normalized to the total area of all polar metabolites to obtain the relative abundance. Green colour represents healthy tissue while orange represents infected tissue. Bars represent the average of four biological replicates. Asterisk represents significant differences compared to healthy leaves using a t-test and a p-value lower than 0.05.

3.3.4.4 The activity of invertase isoenzymes during *Pst* infection

Hexose and sucrose metabolism is regulated by invertases (β-fructofuranosidases) (Roitsch and González, 2004). These enzymes catalyse the hydrolysis of sucrose by cleaving the alpha-1,4-glycosidic bond, releasing glucose and fructose. Plants have three types of invertase isoenzymes, vacuolar, cytoplasmic and cell-wall invertases, that work at different pHs and are present in different subcellular compartments (Roitsch and González, 2004). Invertases increase the levels of hexoses in the plant, which are used not only for metabolic processes but make sugars accessible for uptake by fungal hexose transporters.

To understand the role of invertases during infection I measured their enzymatic activity by colorimetric assays. With this method, I quantified the released hexoses by light absorbance at

405 nm. For this experiment, I collected leaf disks from the flag leaves of healthy and infected adult plants at 4, 8 and 14 dai and extracted proteins from each sample. I divided each protein extract into 6 to evaluate the activity of the three isoenzymes on sucrose or raffinose substrates (Table 3.9). I used sucrose because is the major mobile sugar in plants, is present in all plant cell compartments and its concentrations correlate with sink-source relationships. Raffinose is derived from sucrose (composed of sucrose and galactose), is a storage water-soluble sugar in plants and is related to phloem loading (Lemoine et al., 2013).

The activity of vacuolar invertases (V-INV) was stable across the three time points in healthy and infected flag leaves for both sucrose and raffinose substrates (Figure 3.30). The activity of V-INV between healthy and infected flag leaves was significantly different only at 14 dai for sucrose where the infected flag leaves had slightly less activity (Figure 3.30 A). The activity of cytoplasmic invertases (C-INV) decreased in healthy flag leaves from four to 8 dai on the sucrose substrate (Figure 3.30 A). On the same substrate, the infected flag leaves had slightly more C-INV activity than healthy leaves. The activity of cytoplasmic invertases on raffinose was stable and similar between healthy and infected plants (Figure 3.30 B). Finally, the activity of cell-wall invertases (CW-INV) with sucrose was stable and similar in healthy and infected flag leaves (Figure 3.30 A). On raffinose, CW-INV decreased from four to 8 dai in healthy plants but at the other time point the values were similar and for infected plants the values were similar across the time points (Figure 3.30 B). Overall only V-INV changed at 14 dai with sucrose as substrate. My results contradict several reports where CW-INV activity increased as a response to pathogens infection (Proels and Hückelhoven, 2014; Sutton et al., 2007; Tauzin and Giardina, 2014) and a report where wheat C-INV increased during *Pst* infection (Liu et al., 2015a). There are three possible explanations for my results. Firstly, there could have been a technical problem where the sampling or extraction procedures stressed healthy plants, and that is why I could not observe differences between healthy and infected leaves. Another possibility is that I overestimated the physiological activity of invertases because invertase inhibitors were lost during the protein extraction. Invertases are regulated post-translationally by proteinaceous inhibitors that are pH-sensitive (Bonfig et al., 2010a). Alternatively, the extracted CW-INV could have more affinity to other substrate, like other polysaccharides rather than sucrose or raffinose.

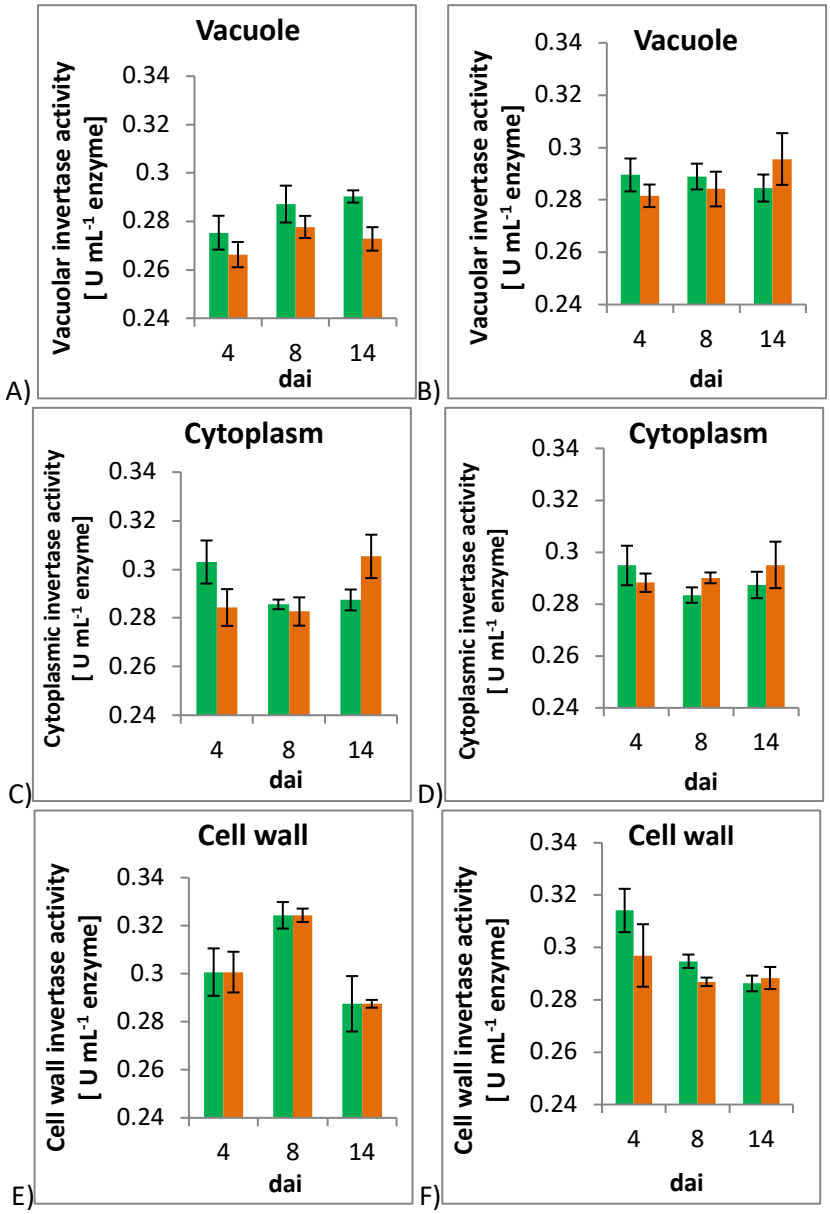

Figure 3.30. Activity of invertases in flag leaf extracts from adult wheat plants. Invertase activity on sucrose (A, C, E) and raffinose (B,D,F) substrates, under different pH regimes to separate the invertase activities present in the vacuole (A,B), cytoplasm (C, D) and cell wall (E, F). Green colour represents healthy tissue and orange represents infected tissue. Bars represent the average activity of four biological replicates. Asterisk represents significant differences compared to healthy leaves using a t-test and a p-value lower than 0.05.

To investigate if invertase activities change systemically in response to *Pst* infection, I repeated the colorimetric assay on flag-1 leaf extracts from healthy and infected plants. The V-INV activity on sucrose and raffinose was similar (Figure 3.31). For flag-1 leaves from healthy plants the activity was stable over time, whereas for flag-1 leaves from infected plants the activity was similar at 4 and 14 dai but slightly decreased at 8 dai. The C-INV activity in flag-1 leaves from healthy plants was stable over time on both sucrose and raffinose substrates (Figure 3.31). The flag-1 leaves from infected plants had more C-INV activity on both substrates at 4 dai and less activity at 8 dai, both compared to flag-1 from healthy plants. Lastly, the activity of CW-INV in flag-1 leaves from healthy plants was variable on sucrose and stable on raffinose (Figure 3.31).

For flag-1 leaves from infected plants the activity was lower on sucrose at 8 dai. In general, invertases responded systemically and differentially at each time point; however it must be pointed out that the differences were very small (close +0.002). The first response was detected in C-INV activity, and then by V-INV, and then CW-INV. These results correlate with high hexose levels at the beginning of infection in distal leaves (Figure 3.21). Overall the results from the invertase activity assay did not show significant differences that could be compared with my results from carbon metabolism studies. Possibly, as mentioned above, the sampling and extraction methods could affect or induce the activity of invertases in heathy tissue, masking the difference between conditions.

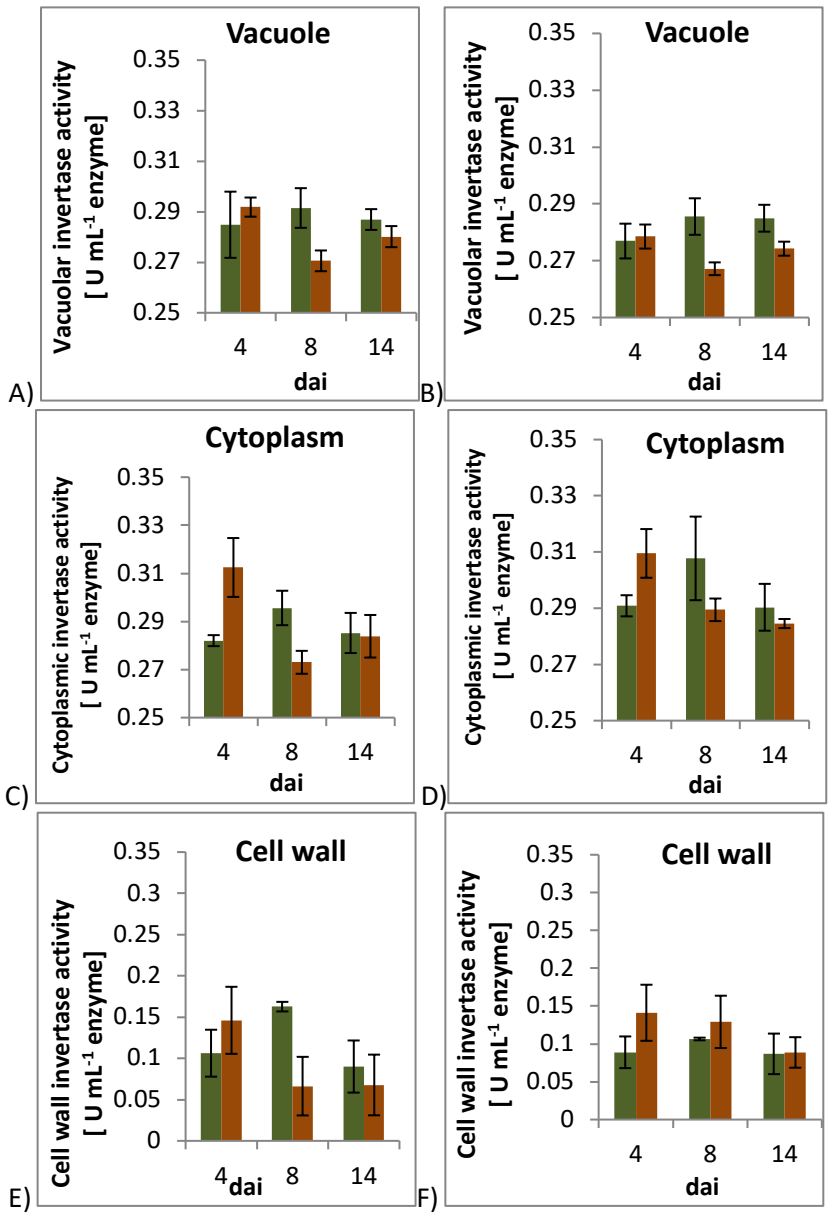

Figure 3.31. Activity of invertases in flag-1 leaf extracts from adult wheat plants. Invertase activity on sucrose (A, C, E) and raffinose (B,D,F) substrates, under different pH regimes to separate the invertase activities present in the vacuole (A,B), cytoplasm (C, D) and cell wall (E, F). Dark green colour represents healthy tissue and dark orange represents infected tissue. Bars represent the average activity of four biological replicates. Asterisk represents significant differences compared to healthy leaves using a t-test and a p-value lower than 0.05.

I complemented the invertase activity results with measurements of the expression levels of a *CW-INV* gene. This gene was upregulated in wheat seedlings infected with *Pst* (data from Dr. Diana Garnica, Australian National University). I evaluated its expression in healthy and infected flag leaves, and in uninfected flag-1 leaves from healthy and infected adult plants. I used the infection and comparison scheme from Figure 3.9 and the same cDNA from previous expression assays described in this Chapter. I employed the comparative C_T ($\Delta\Delta C_T$) method for the analysis, using the expression levels of the *18S rRNA* gene and the expression values of infected leaves for normalization. The relative expression of *CW-INV* in infected flag leaves was above three at 4 dai, decreased at 8 dai and increased strongly at 14 dai to about 11 times (Figure 3.32 A). The *CW-INV* expression in flag-1 leaves was variable but was generally higher in leaves of infected plants than healthy plants at all three time points, with a slight reduction at 8 dai and values above three at 4 and 14 dai (Figure 3.32 B). *CW-INV* expression correlated with the shift from source to sink tissue in flag leaves demonstrated with my previous results. However, these results do not correlate with CW-INV enzymatic activity assays presented in Figure 3.31. This might be explained by the fact that for activity assays I analyzed all CW-INV enzymes present in the protein extracts, whereas for expression I analyzed only one *CW-INV* gene of several such genes. In healthy plants, relative *CW-INV* expression levels decreased over time, while the opposite occurred in infected plants (Figure 3.32 C, D). These results suggest that the metabolism of infected flag leaves changes during infection to compensate for the demands of the new sink comprised by infected flag leaves.

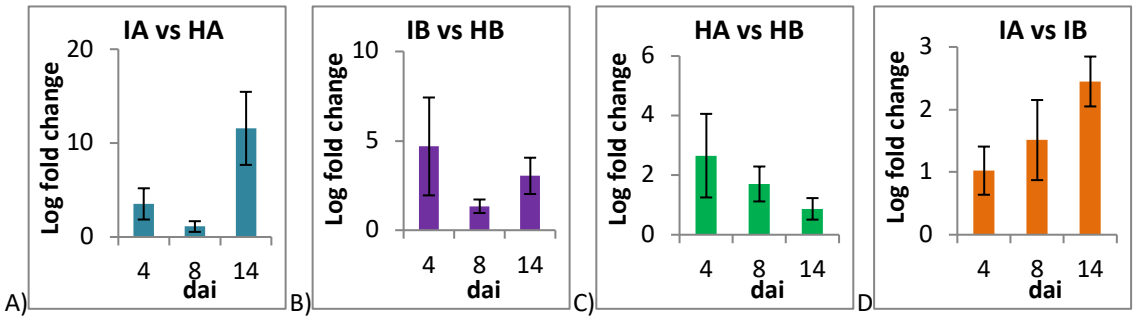

Figure 3.32 Relative expression of a cell-wall invertase gene (*CW-INV*) in adult wheat plants. The scheme of infections and comparisons are in Figure 3.3. A) Relative expression in infected flag leaves (IA) compared to healthy flag leaves (HA). B) Relative expression in flag-1 leaves from infected plants (IB) compared to flag-1 leaves from healthy plants (HB). C) Relative expression of healthy flag leaves compared to flag-1 leaves of the same plant. D) Relative expression of infected flag leaves compared to flag-1 leaves of the same plant. Bars represent the average of three independent experiments, each with three biological replicates. Error bars represent the standard error of 9 samples.

In this chapter I evaluated the metabolism of *Pst* infected wheat leaves from young and adult stage plants to address one of the central questions of my research; how the fungal infection affects plant metabolism. This question arises from the fact that the fungus is completely

dependent on plant nutrients for its development. To answer this, I evaluated photosynthesis pathways and their products in infected and distal non-infected leaves, since the infection may cause a systemic response. For photosynthesis pathways, I measured chlorophyll fluorescence dynamics and chlorophyll content as the source of energy for carbon fixation. For carbon fixation, I measured the capacity of the plant to use CO_2, respiration rates, and the expression of genes encoding Rubisco and the triose phosphate transporter involved in the mobilization of fixed carbon. Once fixed, carbon can be stored, reallocated or used. Based on this I measured starch and fructans as the storage carbohydrates, sucrose as the main mobile molecule in the plant, and hexoses as the sugars used in anabolic and catabolic processes. I complemented the data by measuring the activity and gene expression of carbon metabolism regulators such as hexokinases and invertases. Ultimately, carbon metabolism is associated with nitrogen metabolism, therefore I measure the levels of asparagine as the main amino acid used for nitrogen assimilation. The study of primary metabolism can help to furnish an explanation of how the host is able to stay alive during infection, and how it provides nutrients to the *Pst*.

I evaluated the infection in both young and adult stage plants since host development changes the utilisation of nutrients and as a consequence their allocation within the plant (Taiz and Zeiger, 2010). For example, in young stage plants the major sink tissue are roots and younger leaves, while for adult plants the developing heads are the major sink. In my experiments, I found that adult plants gave me a greater ability to detect systemic events due to the clear metabolic differences between flag and flag-1 leaves. My results contradict two published studies relating plant age to susceptibility to rust fungi. First, soybean susceptibility to *Phakopsora pachyrhizi* was related to plant age but not leaf position on the plant (Bonde et al., 2012). In contrast, I found differences between flag and flag-1 leaves. It is important to point out that cereals and legumes have different growth strategies which could explain these results. Legumes compared to cereals, can flower several times during a growth season, uptake nitrogen more efficiently and growing stems is from the auxiliary buds. The second study was in maize where developmental mutants that remain juvenile were more susceptible to *Puccinia sorghi* than normal adult plants (Abedon and Tracy, 1996). The maize mutants remain young because they increase biomass continuously by axillary branches, consequently starch accumulates more and flowering stops. This validates my results in susceptible young and adult plants, where starch and hexoses accumulates more. Overall, adult stage plants provide a more reliable way to evaluate infection since the flag leaf can be easily identified for infection; this will standardise the experiments by using the same type of leaf at the same developmental stage in independent experiments.

Based on the results presented in this Chapter, I conclude that infected tissue starts a transition to sink metabolism between two (or four) and 8 dai, and by 14 dai becomes a strong sink. The transition is based on changes in some but not all evaluated parameters at the first time point, which means that in some experiments infected plants still behaved as healthy plants early in infection. In both young and adult stage plants, early responses (at 2 or four dai) included the reduction in photosystem II capacity, an increase in the synthesis of asparagine, and an increase in the hexose:sucrose ratio. On the other hand, chlorophyll content, carbon fixation, starch content, dry weight, polyols levels and invertase activities were similar between healthy and infected plants. The fact that responses could be measured so early in the infection were somewhat surprising. It is possible that these changes are mediated by sensitive detection systems (for example PRRs) that respond to the penetration and growth of the fungus. However, these alterations are probably do not affecting the carbon transfer to the fungus since fungal growth was not affected (Figure 2.6, Chapter 2). Additionally, the fungus may be manipulating the plant to reduce adverse growth conditions, but more studies are required to validate this hypothesis. My results showed a delayed response to the infection, with more changes in gene expression but a delay respond in metabolites. In other hosts infected with biotrophic fungi reported changes from 12 h to four days after infection (Doehlemann et al., 2008; Ishiga et al., 2015; Voegele et al., 2005). The discrepancies between my results and the other studies could be associated with the plant developmental stages, the methodology used, the growth conditions and the variables measured. It is possible that results from host infected by biotrophic fungi are not directly comparable. The shift to strong sink status occurs mainly with sporulation, based on the ±2-fold change of most parameters. For example, chlorophyll levels, *Rbs* levels, head dry weights and carbon fixation decreased by more than half, while respiration, leaf dry weight, *FK1* and *AS* expression were doubled in infected leaves. The high dry weight at 14 dai correlates with greater fungal biomass as the fungus is producing millions of spores (Figure 2.6, Chapter 2). The localized increase in demand for carbon compounds decreases the nutrients available to other tissue and this was reflected as lower head weight. This shows, on a small scale, how stripe rust reduces wheat yield. I proposed that infected leaves are not able to produce sufficient nutrients to sustain the fungal biomass so require external sources to support the demands of *Pst*. Interestingly, I showed that chlorophyll content is reduced in susceptible host plants, perhaps as a way to shut down the carbon fixation (and promote sink formation), whereas chlorophyll increases in *Medicago truncatula* which is a non-host for *Phakopsora pachyrhizi* possibly to maintain carbon fixation at the site of infection (Ishiga et al., 2015). Besides decreasing the nutrients availability to other sink tissues including heads, it seems that flag-1 leaves may transition from sink to source metabolism at 14 dai when the flag leaves were infected with *Pst*, instead of remaining as sink. In addition, the sink marker genes *FK1* and *CW-*

INV expression decreased over time in flag-1 leaves. This might be associated with sugar transport from distal leaves to the site of infection. To my knowledge, systemic responses reported to plant pathogens are mainly related to defence signals, like increases in salicylic acid (Zheng et al., 2015) or priming plants to gain resistance by other organisms such as mycorrhizae (Molitor et al., 2011). I have found only one report, on maize infected with *U. maydis,* where the authors showed how nitrogen compounds from other organs in the plant are reallocated to infected tissues (Horst et al., 2010a).

Many of my results showed high variation, represented as large standard error values, which might be explained by the biology of the infection. As shown in Chapter 1 (Figure 1.6) *Pst* infections are seldom uniform, therefore the collected material is a mixture of healthy and infected cells. Consequently, the metabolic and transcriptomic changes due to the infection can be masked by the contributions from healthy tissue. To reduce the variation, different approaches should be taken in future experiments. One way to improve the data could be to increase the number of technical samples to enrich the sampled material with more infected cells. Another approach could be to evaluate the metabolomics and transcriptomics in specific cells or organelles, since the cells are not uniform and sugar and enzymes are compartmentalized, this new approach could give new information about the dynamics of the infection (Tiessen and Padilla-Chacon, 2013).

Sugars are not only products of photosynthesis but are also signals that indicate the metabolic status of each tissue. Sugars regulate senescence and starvation which are plant processes that require nutrient mobilization (Calenge et al., 2006; Morkunas et al., 2012; Scialdone and Howard, 2015). Reductions in sucrose levels, or increases in the demand of hexoses, such as occurs in infected tissue, could trigger starvation responses. Therefore, I evaluated if these processes could be part of the plant response to infection by measuring starch content at night, which represents stored plant carbon. Infected plants were not starving because starch levels did not decrease at night, in both young and adult stage plants (Figure 3.15, Figure 3.16B). Plants have energy resources when they are not fixing carbon. Plants may be starved for elements other than carbon, for example phosphorus is a key element in the transport of triose from the chloroplast and the regulation of starch synthesis, (Hacquard et al., 2016). Another metabolic process associated with nutrient remobilization, during stress and developmental changes, is senescence. I evaluated the expression levels of two senescence-associated genes (*SAG2, SAG12*) (data not shown) but the values were similar between healthy and infected tissue. Possibly more senescence markers are required to conclude how normal nutrient remobilization is regulated during infection.

Molecular plant-pathogen interaction studies typically focus on host recognition processes leading to the induction of immunity, and how pathogen avoids or suppresses it. I propose that plant development should also be part of these studies, since plant immunity interconnects with metabolism. For example higher levels of fructose in tomato reduces susceptibility to the necrotrophic fungus *Botrytis cinerea* (Lecompte et al., 2017). Also, expression of the SWEET sugar transporters is induced by plant pathogenic bacteria to allow infection (Verdier et al., 2012). From the host side, sugar transporters in *Arabidopsi*s are required for defence responses against bacteria and also in wheat for *Pst* resistance (Moore et al., 2015; Yamada et al., 2016). Here I showed how the comparison between healthy and infected plants provides information about the infection but also how it can be complemented with studies of plant development and metabolism within plants. For example, older and younger leaves do not respond identically, like comparison between four-old week plants and adult plants. In this chapter I showed how some steps in metabolic pathways changed at the transcript and metabolic level during infection, to make infected tissue a sink. The metabolic steps were chosen based on previous reports for biotrophic fungi or because they are key steps in photosynthesis. In the next chapter, I evaluated the whole wheat transcriptome to complement the result from previous chapters and have the bigger picture of wheat-*Pst* interaction.

CHAPTER 4
Changes in the wheat transcriptome during *Pst* infection

4.1 Introduction

Puccinia striiformis f. sp *tritici* infection shifts infected wheat tissue to sink, altering local and distal leaf metabolism (Chapter 3). The changes in infected leaves include increased carbon and nitrogen components, and increased transcript levels of genes that encode enzymes and transporters that affect plant nutrient flow. To extend the results from previous chapters to the whole wheat metabolism, I studied changes in the wheat transcriptome during *Pst* infection.

Bread wheat (*Triticum aestivum*) presents several challenges for DNA sequencing technologies due to its large genome size and high proportion of repetitive regions. The wheat genome is 17 gigabase pairs (Gbp) and is one of the larger plant genomes compared to rice (0.45 Gbp), maize (2.5 Gbp) and *Arabidopsis thaliana* (0.13 Gbp). Repetitive sequences comprised about 85% of the wheat genome, which hampers genome assembly and mapping. Despite these limitations, a publicly accessible draft wheat genome sequence from cv. Chinese Spring is available, which was generated by The Earlham Institute, Norwich, UK (http://www.earlham.ac.uk/sequencing-

wheat-genome#Toolsanddata-2). The genome is 75% assembled and 98,974 genes have been annotated.

The bread wheat genome is hexaploid with seven pairs of chromosomes derived from three ancestral diploid progenitors (2n=14). The individual lineages contributed three subgenomes represented by the letters A, B and D (Figure 4.1). Wheat phylogeny models suggest that the genome (AABBDD) came from two main hybridizations events ((Marcussen et al., 2014). First, the ancestors for the subgenomes A and B hybridized around 0.8 million years ago (Mya). The second event was between the tetraploid AABB and the ancestor for subgenome DD around 0.4 Mya. The consequence of these hybridizations was the triplication of most wheat genes. The three gene copies reside at the equivalent locus in each subgenome and are called homeologues. The higher gene copy number creates problems for breeding and genomics analyses. For example, during gene expression analysis is difficult to differentiate which of the homeologues are expressed and if the number of copies correlates with protein abundance. Moreover, repetitive fragments are problematic as they cannot be assembled properly and decrease genome contiguity (The International Wheat Genome Sequencing Consortium, 2014).

Despite the difficult nature of the wheat genome, several studies on wheat transcriptomics have been published (Dobon et al., 2016; Erayman et al., 2015; Fox et al., 2014; Jia et al., 2013; Liu et al., 2015b). One current widely used technique for wheat transcriptomic analysis is RNA-sequencing (RNA-seq). The most common RNA-seq technology platform is lllumina which generates short DNA sequence reads of 150-300 bp. This platform uses high-throughput cDNA sequencing to detect changes in gene expression by quantifying the number of reads that map to each gene copy or homeologue (Wang et al., 2009). RNA-seq has been used to characterize wheat transcriptome responses under biotic and abiotic stresses (Dobon et al., 2016; Erayman et al., 2015; Fox et al., 2014; Jia et al., 2013; Liu et al., 2015b). Most the studies related to biotic stresses, however, focus on wheat defence responses. Therefore, the main purpose of this Chapter was to understand from a metabolic point of view how the wheat transcriptome responds to *PST*-79 infection. These data complement the results from Chapters 2 and 3.

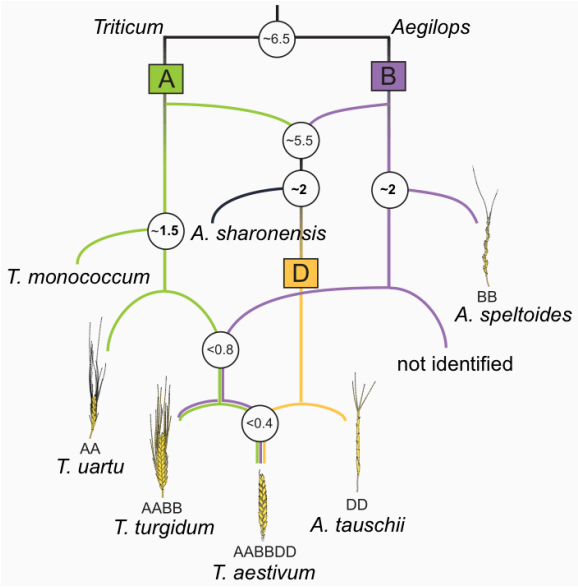

Figure 4.1.Phylogeny of bread wheat (*T. aestivum*). The circles indicate elapsed time in million years ago (Mya). The coloured lines represent the hybridization history of the three subgenomes. Subgenomes A (*Triticum*) and B (*Aegilops*) gave rise to the cereal species *T. monococcum* and *A. speltoides*, respectively. The subgenome donors appeared around 6.5 Mya; while the cereals appeared close to 2 Mya. The diploid *T. uartu* hybridized 0.8 Mya with the predecessor of *A. speltoides* to give rise to *T. turgidum* (AABB). This tetraploid then hybridized 0.4 Mya with the diploid *A. tauschii* (DD) to give origin to the hexaploid, bread wheat (AABBDD). Diagram taken from (Marcussen et al., 2014).

4.2 Materials and Methods

4.2.1 Wheat gene expression analysis using RNA-seq data from the Illumina platform

I studied the changes in the wheat transcriptome during *PST*-79 infection using the bioinformatics pipeline outlined in Figure 4.2. Dr. Diana Garnica (The Australian National University; unpublished data) generated the biological materials and raw sequence reads that I used for my study. Young stage (Z13) wheat plants from cv. Morocco were infected with *PST*-79 and harvested two hours after inoculation (0 dai), six and nine days after inoculation (dai). The RNA was extracted from three biological replicates at each time point using an RNAeasy kit (Qiagen). Library preparation and sequencing were done at the Ramaciotti Centre for Genomics (University of New South Wales, Australia) with Illumina technology and 100 bp paired-end libraries. The resulting datasets contained between 11-19 million paired reads.

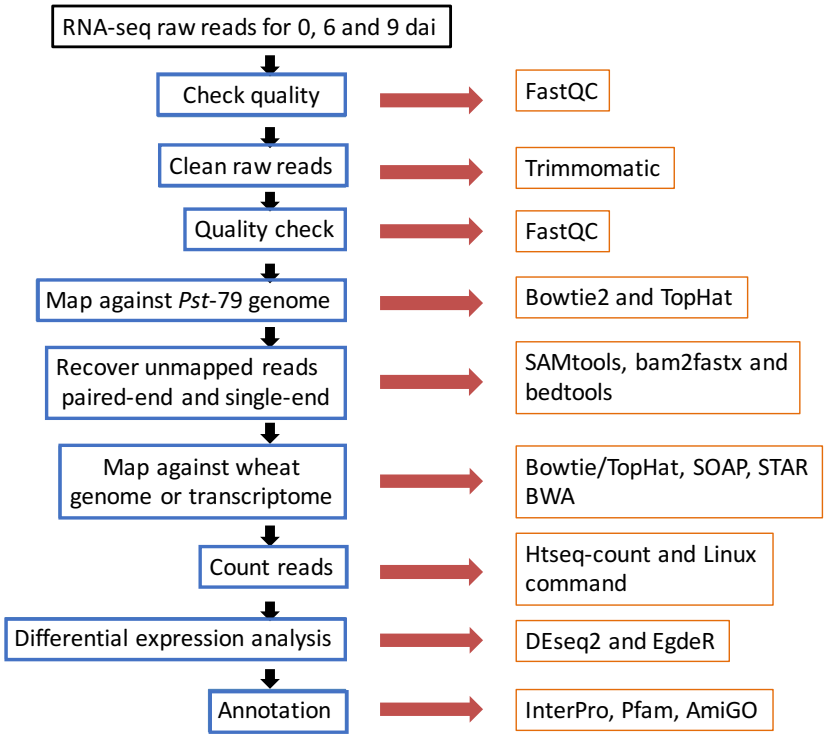

Figure 4.2. Pipeline for wheat gene expression analysis during *Pst* infection. The black box represents the starting material (raw sequence reads). Blue boxes represent the bioinformatics procedures and orange boxes represent the programs used for each task.

The raw RNA-seq reads generated by Illumina sequencing were checked for quality with FastQC (http://www.bioinformatics.babraham.ac.uk/projects/fastqc/). The reads were cleaned from adaptors and poor quality sequences using the program Trimmomatic (Bolger et al., 2014). After trimming, read quality was checked again using FastQC. The cleaned sequences were mapped against the *PST*-79 genome (Jackson et. al. unpublished data) using the program TopHat (Trapnell et al., 2009). The unmapped reads, which are mainly plant sequences, were recovered using SAMtools (Li et al., 2009). The recovered sequences were converted to Fastq files using the bamtofastq command from the software bedtools (http://bedtools.readthedocs.io/en/latest/). The sequences were separated into paired-end and single-end reads using the SAMtools command. The recovered reads were mapped against the wheat transcriptome (MIPS v2.2 from July 18, 2014) using the Burrows-Wheeler Alignment tool (BWA) (Li and Durbin, 2009). MIPS is now Plant Genome and Systems Biology (PGSB, http://pgsb.helmholtz-muenchen.de/plant/index.jsp). The wheat transcriptome has approximately 193,667 transcripts and splice variants. The variants were defined with RNA-seq dataset from different wheat organelles. The annotation is derived from databases from wheat cDNA and grasses protein sequences (The International Wheat Genome Sequencing Consortium, 2014).

Reads that mapped to the wheat transcriptome were extracted with SAMtools. The paired-end reads that mapped to the wheat genome were counted using the program HTseq-counts. The single-end reads were counted using Linux commands (Table 4.1) because HTseq-counts does not accept singletons. Reads were annotated with a generic feature format (GFF) file for the wheat genome generated by Dr. Megan McDonald (The Australian National University). Differential expression analysis was done in RStudio (v. 3.2.0) with DESeq2 and EdgeR (Love et al., 2014; Robinson et al., 2010). These two R programs uses the read counts to calculate the relative abundance for each gene which can be associated to expression levels. In EdgeR, the low counts command was modified by Dr. Sylvain Foret (The Australian National University), to normalize the data thru multiplication of the gene counts by million and divided by the number of samples, in this case 9. Then, the normalized data was filtered, to only keep genes present in all samples. The script is:

```
minCounts <- c(1, 5, 10, 50,1000000)
minSamples <- c(1:9)
genesDetected <- matrix(0,
                    nrow=length(minCounts),
                    ncol=length(minSamples),
                    dimnames=list(minCounts, minSamples))
genesDetected
colnames(genesDetected) <- minSamples
rownames(genesDetected) <- minCounts
i <- 1
for (minCount in minCounts)
{ j <- 1
  for (minSample in minSamples)
{  genesDetected[i, j] <- rowSums(ykeep$counts >= minCount) >= minSample j <- j + 1 }
  i <- i + 1}
genesDetected
```

The up and down-regulated wheat genes were annotated with Ensembl-BioMart (http://plants.ensembl.org/biomart/martview/590fff7adc62af974935260c534bc344), InterPro classification, Pfam databases and the PGSB webpage (http://pgsb.helmholtz-muenchen.de/plant/search.jsp).

Table 4.1.Commands for RNA-seq analysis of wheat transcriptomics during *Pst* infection.

Program	Command	Explanation
Trimmomatic	fasta:2:30:10 SLIDINGWINDOW:10:24 MINLEN:85	Keep sequences with a minimum length of 85 bp and a Phred quality score above 24
SAMtools	For R2 reads: samtools view -bf 128 For R1 reads: samtools view -bf 64 For single end reads: samtools view –bF	Command to extract from the unmapped file, the first segment of the template (64), the last segment of the template (128) and single reads (-bF)
BWA	For single-end reads: Bwa mem –C For paired-end: Bwa mem –Cp	-C is an option to transfer read meta information to the SAM output. -p assume both pair-end read are in the same file
SAMtools	For pair-end reads: samtools view –f 0x02 –b For single-end reads: samtools view –F 0x04 –b	Command to extract properly aligned sequences Command to extract single end reads that were mapped
HTseq-counts	python -m HTSeq.scripts.count -f bam -m union -s no -t transcript -i gene_id -a 0	Command for counting reads based on the GFF file
Linux	Cut –f 3 <file> > outfile | sort -n | uniq –c > <out file>	Linux command to count single-end reads

4.3 Results and discussion

4.3.1 Processing of raw RNA-seq data from *Pst*-infected wheat

The wheat transcriptome analysis was based on RNA-seq data generated by Dr. Diana Garnica (The Australian National University), who infected young stage wheat plants with *PST*-79 and harvested mRNA for RNA-seq at 0, 6 and 9 dai, here labelled as IT0, IT6 and IT9 respectively. These time points do not correspond to the previous chapters data points, since these data was generated by someone else. The first step in the pipeline (Figure 4.2) was to clean the raw sequence reads of adaptors and primers. Using the same software, I removed reads with low quality scores, based on the chromatogram that was used to call the nucleotide bases. For IT0 and IT6 samples I recovered the reads as 80% paired-end and three to seven percent as single-end reads (Table 4.2).

For IT9, more than 80% of paired-end reads were recovered from one of the three biological IT9 replicates, IT9_3, and 66-68% were recovered from the IT9_1 and IT9_2 replicates respectively paired-end. The lower values for these replicates was compensated by a higher number of single-end reads. In general, more than 90% of the reads were recovered in all samples after cleaning (Section 4.2.1). Of these, 66-86% were recovered as paired-end reads and the rest as

single-end reads (Table 4.2). The single-end reads means that only one of the sequences that constitutes the paired-end read was kept, named forward or reverse. Most of the single-end reads were forward reads, suggesting a possible sequencing bias. With the cleaned reads, I proceeded to the next step.

Table 4.2. Illumina RNA-seq data from *Pst*-infected wheat leaves at zero (IT0), 6 (IT6) and 9 (IT9) days after infection. The values are the reads before (input read pairs) and after trimming (surviving) with trimmomatic software. Surviving reads are divided into paired-end reads (PE, both surviving) and single-end reads (SE, forward and reverse). Forward and reverse reads represent the forward and reverse complement (reverse) sequences of a broken paired-end read where only one of them survived. Reads are represented as million (M) reads. There are three biological replicates for each sample, indicated by the numbers 1-3.

Sample	Input Read Pairs (M)	Both Surviving (PE) (%)	Forward Only Surviving (%)	Reverse Only Surviving (%)
IT0_1	13.6	84.09	6.91	3.97
IT0_2	15.6	83.64	7.05	4.06
IT0_3	17.2	83.81	7.09	4.01
IT6_1	18.9	84.54	6.75	3.83
IT6_2	19.9	84.59	6.65	3.89
IT6_3	18.2	84.18	6.81	3.98
IT9_1	116.6	68.55	14.75	5.68
IT9_2	73.2	66.91	15.64	5.63
IT9_3	16.1	86.95	5.47	3.63

The next step in the pipeline was to remove the reads with homology to *PST*-79. For this step, I mapped the recovered reads from Table 4.2 to a *PST*-79 draft genome generated by Dr. Diana Garnica and Mr Will Jackson (unpublished, The Australian National University). As expected, the percentage of reads that mapped to *PST*-79 was almost zero in the three biological replicates of IT0 (Table 4.3). On average, about 3 million reads mapped to the *PST*-79 genome in the IT6 replicates. In the IT9 data, all three biological replicates contained very large numbers of reads that mapped to the *PST*-79 genome, but these samples were quite variable (17-66 million reads). The variation within these samples may be associated with an uneven infection, suggesting that the tissue samples for IT9_3 and IT9_2 accumulated less fungal biomass than IT9_1. Alternatively, poor quality reads in these replicates did not align to the *Pst* genome. Overall, the number of mapped reads corresponded to the expected increase in fungal biomass at these time points.

Table 4.3. Numbers and percentages of reads that mapped to the *PST*-79 draft genome and wheat transcriptome. The clean reads (total reads) from Table 4.2 were aligned to the *PST*-79 draft genome. The reads that did not mapped to the *Pst* genome (selected reads) were separated in paired-end and single-end reads. Both read sets were mapped separately to the wheat transcriptome. Reads are represented as million (M) reads. For each sample, there are three biological replicates indicated by the numbers 1-3.

Samples	Clean reads mapped against *PST-79*		Selected reads mapped to the wheat			
			Paired-end reads		Single-end reads	
	Total reads	Mapped reads	New input reads	Mapped reads	New input reads	Mapped reads
	(M)	(%)	(M)	(%)	(M)	(%)
IT0_1	24.48	0.01	22.91	92.75	1.49	89.84
IT0_2	27.93	0.01	26.18	88.19	1.74	90.48
IT0_3	30.67	0.02	28.76	83.33	1.9	84.99
IT6_1	33.88	11.87	19.15	46.04	1.81	87.91
IT6_2	35.81	8.4	28.46	85.08	1.84	87.08
IT6_3	32.61	11.58	27.05	86.08	1.79	87.47
IT9_1	183.7	35.99	101.05	76.48	16.53	78.23
IT9_2	113.5	24.79	73.24	79.46	12.15	82.85
IT9_3	29.42	56.7	12.04	66.94	0.7	68.24

The reads that did not map to the *PST*-79 genome should have been derived from wheat mRNAs. I extracted the file containing unmapped sequences from the data presented in Table 4.3 and separated them into single-end and paired-end reads using the software SAMtools, bam2fastx and bedtools, as this step is required by the aligning software. I tried to map the RNA-seq reads to the wheat genome using the STAR (Dobin et al., 2013), SOAP (Li et al., 2008) and TopHat software. However, I did not have access to the requisite computer platform that could support the mapping of genomes larger than 4 Gb. As an alternative, I mapped the single-end and paired-end reads separately onto the wheat transcriptome which is smaller than 1 Gb. For mapping the reads, I used the software Burrows-Wheeler Aligner (BWA). I performed the alignment with the paired-end and single-end reads separately as the software does not run all files at the same time. For IT0 replicates, more than 80% of the paired-end and single-end reads mapped to the wheat genome with low variability between the biological replicates (Table 4.3). More than 80% of the paired-end reads from IT6_2 and IT6_3 mapped to the wheat transcriptome, while for IT6_1 this figure was only 46%. In contrast, 87% of the single-end reads from all IT6 replicates mapped to the wheat transcriptome. Finally, the percentage of paired-end and single-end reads that mapped to the wheat transcriptome in the IT9 datasets was very variable. The replicates IT9_1 and IT9_2 contained very large numbers of reads, but only 76-78% of paired-end reads and 64-75% of single-end reads mapped to the wheat transcriptome. On the other hand, only 67% paired-end reads and 68% of single-end reads of IT9_3 mapped to wheat genes. This implies

that the unmapped reads from the results presented in Table 4.3 were not wheat reads, or that the wheat transcriptome is incomplete.

I used the paired-end and single-end reads that mapped to the wheat transcriptome from Table 4.6 to count the number of reads that mapped to each wheat gene, which provides a measure of gene expression. When I did this analysis, I was unable to separate the homeologues of each gene because the alignment tool BWA is unable to recognize them. Consequently, the reads were dispersed between homeologues and alternative gene transcripts. I concatenated the counts for single-end and paired-end reads results and created a table containing all the read counts that I used for differential gene expression analysis, using the R programming environment. I did this analysis using the R package DESeq. However, the variance between biological replicates was very high (data not shown) so I changed to the R Package EdgeR, which is more flexible to change the normalization parameters, thus reducing variability between samples. I plotted the biological coefficient variance (BCV) which is the relative standard deviation divided by the mean. This reduces the variation due to the sample size and measures de dispersion of gene expression in each RNA sample. The BCV plot indicated that the biological replicate IT9_2 is different from the other two IT9 samples (Figure 4.3). To remove the source of this variability, I used the script provided by Dr. Sylvain Floret (see section 4.2.1).

The filter removed 5-10% of the reads and maintained a minimum of 61365 reads for each gene in the 9 samples. This is possibly removing homeologues as the software (BWA) does not differentiate them. I plotted the filtered data with BCV (Figure 4.4). The new figure (Figure 4.4) showed biological replicates closer than Figure 4.3, the distance between samples was reduce and the figure also showed that BCV is very sensitive to low abundant genes. The biological replicates for IT0 clustered together as in Figure 4.3. The filtering reduced the variation between the replicates for the IT6 and IT9 samples, as replicates clustered closer than in Figure 4.3 and the scale of the graph is reduced (Figure 4.4). I then proceeded to the next step in the pipeline as the normalized and filtered data were less variable than before.

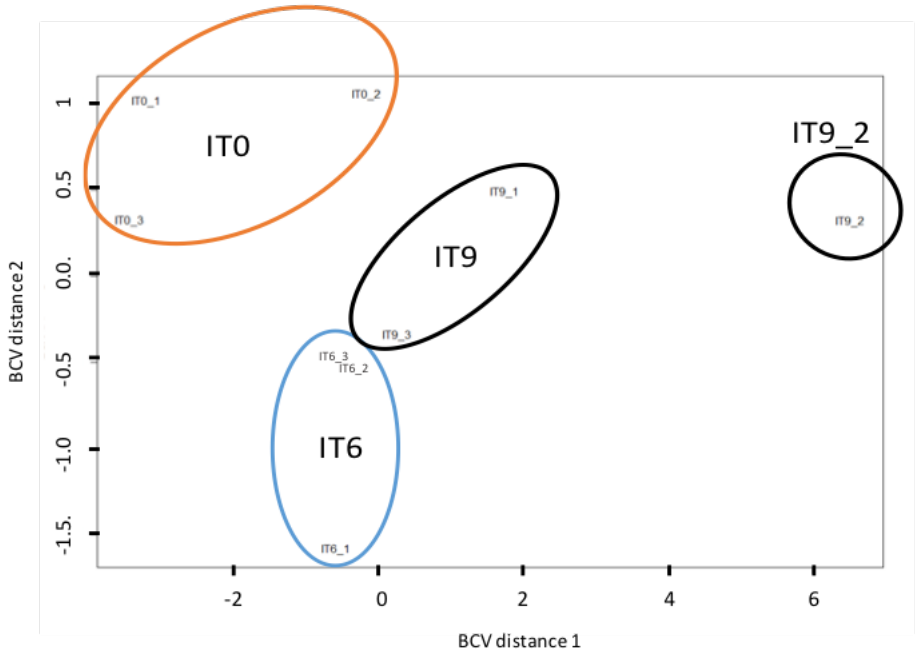

Figure 4.3. Biological coefficient of variation plot for all biological replicates of IT0, IT6 and IT9. The variation was calculated with the counts for all genes in each sample. The dispersion is explained by two vectors.

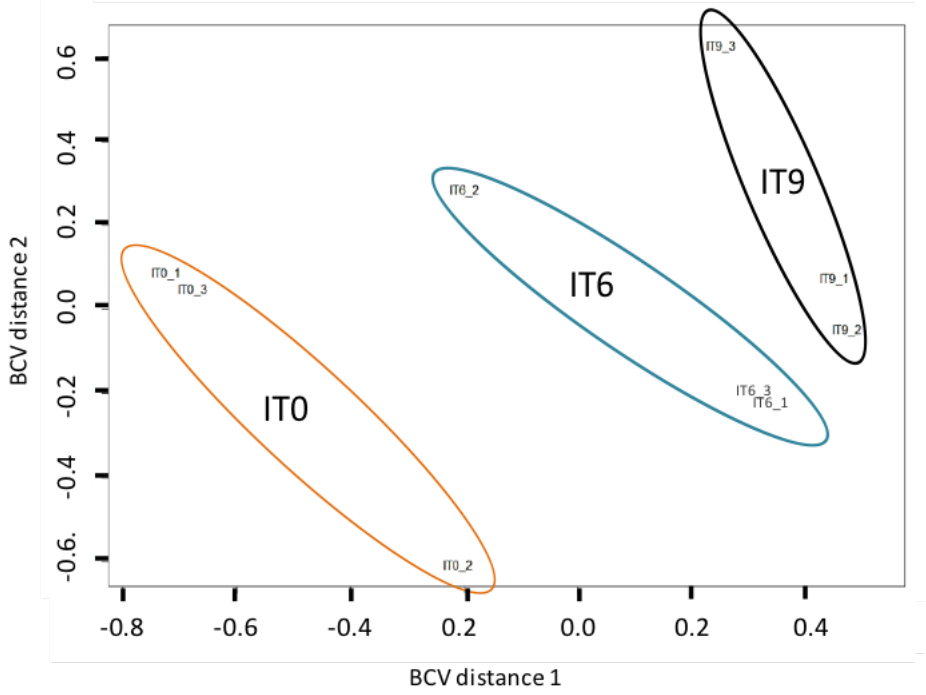

Figure 4.4. Biological coefficient of variation plot of samples after count per million normalization and filtering genes with low numbers of counts.

4.3.2 Differential expression of wheat genes during *Pst* infection

For differential gene expression analysis, I used the EdgeR package. This compares two samples and takes biological replicates into account for statistical analysis. The samples are nominated as reference and treated. The reference sample represented the initial condition of the analysis.

In this study that is IT0 since this is the steady state of the plant before fungal infection. The treated sample denotes the condition evaluated, in this case *Pst*-infected leaves (IT6 and IT9). To assign significance to the data, I used three statistics thresholds provided by EdgeR. These are the p-value, the fold-change and the false discovery rate (FDR). The p-value informs us if the mean expression is different between the reference and treated samples. Genes with a p-value above 0.05 were discarded from the analysis. The fold-change is the logarithm base two of the treated sample compared to the reference sample. Genes with values between the interval minus two and two were discarded from the analysis. The FDR controls the proportion of results that are false positives. The FDR is an adjusted p-value to controlled the samples that could be false positives. I kept genes with values lower than 0.05. I used IT0 as the reference sample and I compared it to IT6, and to IT9. After these comparisons, I kept genes with the p-value, FDR, fold-change values defined above. I retained 281 up-regulated genes and 178 down-regulated genes for the comparisons IT0-IT6 and the same number of genes for IT0-IT9 comparison. I analysed the gene ontologies (GO) of this gene set using the EnsemblPlants platform and the software BioMart (http://plants.ensembl.org/biomart/martview/10d02b64ef8ed8aa1c209e9d1747ef55). In the forthcoming sections I discuss some of the differentially expressed genes based on relevant results from previous Chapters and I show the changes in genes underlying relevant wheat metabolic pathways during infection.

4.3.2.1 Gene expression changes at 6 and 9 dai

The most common gene ontology (GO) categories in the differentially expressed genes for 6 and 9 dai samples compared separately to 0 dai were catalytic activity, hydrolase activity, responses to biotic and oxidative stress, cellulose synthase activities, transferase activity, carbohydrate metabolism and transmembrane transport (Figure 4.5). These categories were similar in the 6 and 9 dai time points, with differences only for hydrolase activity. For both time points, 15% of up-regulated genes correspond to transmembrane transport and 11% to catalytic activity. The only category with up-regulated genes was cellulose synthase. From down-regulated genes, 6.5% were related to defence responses and this was the only category with down-regulated genes. The differences between time points for hydrolase category was associated with more down-regulated genes for IT6. While IT6 has 6.5% down-regulated genes and 4.5 % up-regulated genes for this category; IT9 has 4.5% for both down and up-regulated genes. The small differences in gene expression might be associated with specific hydrolases involved in defence responses or there are hydrolases also affected during normal plant metabolism.

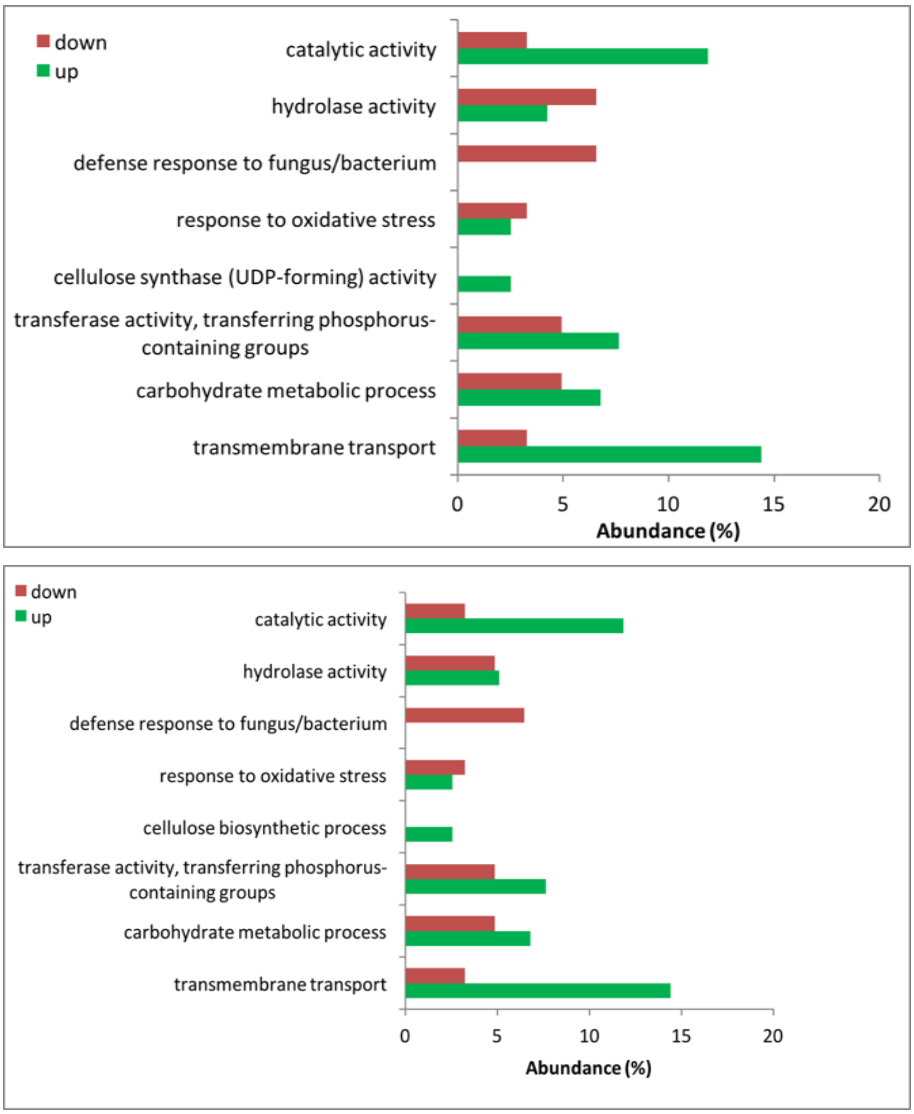

Figure 4.5 Gene ontology (GO) classifications of differentially expressed genes 6 dai (upper panel) and 9 dai (lower panel) with respect to 0 dai (IT6). The up-regulated (green) and down-regulated genes (red) were associated with GO classifications, here showing the most common categories. For the analysis 100 genes were used. The 3 replicates are combine as one therefore there are no error bars.

To better understand the specific function of genes involved in the GO study, I analysed four of the 8 GO classifications in detail (hydrolase activity, carbohydrate metabolism, transport and defence responses). I chose these four categories because I want to know how the plant respond to *Pst* infection; as nutrient metabolism and defence responses. For plant metabolism, I focus in carbon metabolism, from fixation (carbohydrate metabolism), transport to different tissues and catabolism (hydrolases). I also included the classification nitrogen metabolism, because these pathways are related to pathogen demand as well as plant metabolism, as I showed in Chapter 3. From these five classifications, I chose genes at 6 and 9 dai with fold changes higher than 3 and lower than -3.

The hydrolases activity category was represented mainly by glycosyl hydrolases (GHs). These enzymes are involved in cell-wall remodelling and catabolism of carbohydrates by breaking the glycosidic bonds through hydrolysis. Compared to necrotrophic interaction, biotrophic fungi genome has few group of genes coding for glycosyl hydrolases, to avoid cell damage and keep longer interaction with a living host (Duplessis et al., 2011). Cell-wall damage will trigger defence responses which biotrophic fungi try to avoid (Vallarino and Osorio, 2012). From the differentially expressed genes at 6 dai, there were only four down-regulated genes in the GH families 18, 19 and 36 (Table 4.4). I did not find member of these families in the list of up-regulated genes. The substrate for GH18 and GH19 enzymes is chitin while for enzymes of the GH16 family it is raffinose. The three genes I identified from the GH18 and GH19 families are possibly supressed by fungal effectors to avoid fungal cell wall damage and allow growth (Duplessis et al., 2011). The gene from GH36 family might be related to changes in sink metabolism, since this enzyme is involved in pathway of unloading sucrose and hexoses to the phloem (Peters et al., 2010).

At 9 dai, the families 19, 36, 45, 17 and 32 were down-regulated and GH1 and GH16 were up-regulated. I could not find GH18 in the 9 dai expressed genes. For the upregulated genes, the gene from GH1 encodes an extracellular enzyme that releases glucose, from the cell-wall, as β-D-glucose (www.cazy.org). The gene from GH16 encodes an apoplastic enzyme involved in cell-expansion by breaking cellulose microfibrils links. These two up-regulated GHs might be associated with cell-wall modifications as a response to fungal infection, or contribute to plant growth and are not responding to the infection. The downregulated GH32 gene encodes an exohydrolase involved in breakdown of fructans which are common storage carbohydrates in cereals. The repression of this gene suggests that fructans are not mobilised during infection. Compared to my results from Chapter 3, I could not detect changes in fructan levels but a gene coding for *fructan-6-hexohydrolase* was also downregulated at 14 dai. The low expression of the GH45 gene, coding for a wound-induced protein, might be associated with a fungal strategy to avoid immune responses. Since the fungus can infect and sporulate in this wheat variety, the repression of genes might be associated with a successful infection instead of a plant defence strategy. In general, it seems that a successful infection requires the repression of glycosyl hydrolases from different GH families. The higher number of repressed families at 9 dai compared to 6 dai could be associated with fungal changes just before sporulation, since this stage of fungal development demands more plant nutrients, as shown in Chapter 2.

Table 4.4. List of differentially wheat expressed genes with their glycosyl hydrolase classifications. The differentially expressed genes have p-values and FDR-values lower than 0.05, they are from 6 and 9 dai compared to 0 dai. The purple shade represents the down-regulated genes and the green represents up-regulated genes. The annotations and family classification are based on the PGSB (http://pgsb.helmholtz-muenchen.de/plant/plantsdb.jsp) and uniprot (www.uniprot.org/) webpages.

Glycosyl hydrolases				
Time point	**Wheat gene**	**Fold change**	**Annotation**	**Family**
6 dai	Traes_7AS_CA7E36BC0	-3.45	Seed imbibition 2	36
	Traes_1BL_83AA7C022	- 2.29	Endochitinase A2	19
	Traes_1AL_7402A5761	- 2.18	Chitinase 2	18
	Traes_5BL_568AADCD2	-3.12	Chitinase family protein	19
9 dai	Traes_7AL_8C4A9BEBF	3.12	Xyloglucan endotransglucosylase	16
	Traes_5BL_58CAE6F7B	2.67	Beta glucosidase 11	1
	Traes_2AL_E80BC759C	-2.22	Fructan 6-exohydrolase	32
	Traes_2AL_1FDA0035F	-2.34	Stachyose synthase	36
	Traes_5BL_568AADCD2	-2.40	Chitinase family protein	19
	Traes_3B_FBE2447AA2	-2.82	Glucan endo-1,3-beta-glucosidase	17
	Traes_7AS_CA7E36BC0	-1.76	Seed imbibition 2	36
	Traes_2BL_5FF85C7F2	-2.45	Wound-induced protein	45

The GO classifications carbohydrate metabolism, transport and nitrogen metabolism contained the same differentially expressed genes at 6 and 9 dai. The results for both times points are presented in Table 4.6, Table 4.7 and Table 4.8. In the carbohydrate metabolism category, genes encoding a phosphofructokinase B (PfkB) and two lectin domains were up-regulated with a fold-change higher than three (Table 4.5). The enzyme PfkB catalyses the irreversible step from fructose-6-phosphate to fructose-1,6-biphosphate in glycolysis (Gilkerson et al., 2012). Upregulation of *PfkB* suggests that host metabolism is directed to pyruvate (energy) production, rather than to synthesis of carbohydrates. The other two up-regulated genes encode lectin receptor protein kinases. These proteins have two extracellular lectin domains paired with an intracellular protein kinase domain. The lectin domain binds to carbohydrates and probably transmits this signal through the kinase domain (Schallus et al., 2008). These receptors are involved in microbial perception and plant development (Lannoo et al., 2014). One of the receptors identified here has an extracellular malectin domain which is associated with cell expansion and sensing cell wall integrity (Cheung and Wu, 2011; Haruta et al., 2014). They have been also reported to contribute to or suppress resistant responses against oomycetes and fungi

(Bouwmeester et al., 2014; Hok et al., 2011; Kessler et al., 2010). The symbiosis receptor kinase (SymRK) has a malectin domain involved in root symbioses with rhizobia bacteria and mycorrhizal fungi and membrane assembly (Holsters, 2008). Another receptor like kinase involve in development and defence responses is FERONIA (FER). This receptor is involved in pollen tube reception and in susceptibility to powdery mildew (Kessler et al., 2010). In Arabidopsis *fer* mutants the pollen keeps growing instead of releasing the sperm and the incidence of powdery mildew entrance was lower compared to wild type plants. Based on these studies, the up-regulation of genes coding for lectin receptors may be associated with wheat perception of fungal infection. The fungus needs to penetrate the cell wall to form haustoria, which represents a modification to the plant cell wall that may be detected by the host. However, the up-regulation of these genes was clearly not sufficient to activate defence response. Therefore, another possibility is that they are susceptibility genes required for infection. This could be similar to FER phenotype and the susceptibility gene *Mildew resistance locus o (MLO)*. MLO are membrane proteins involved in pollen tube reception and root morphogenesis. They are also required for powdery mildew susceptibility in barley and it has a similar function in dicots, like grapes (Kessler et al., 2010; Pessina et al., 2016).

From carbohydrate metabolism GO classification there were four down-regulated genes. Two of these genes encode copies of the Rubisco small subunit, one encodes a fatty acyl-coenzyme A reductase 1 (*FAR1*) and the other an exostosin-2 (Table 4.5). The down-regulation of the genes encoding Rubisco small subunit was expected as repression of photosynthesis and its associated genes is a typical plant response to biotic and abiotic stresses (Bilgin et al., 2010; Doehlemann et al., 2008; Parry et al., 2002; Sun et al., 2014). The other down-regulated gene, *FAR1*, encodes an enzyme involved in suberin deposition, a waxy substance present in the cell wall. In Arabidopsis, FAR1 accumulates during abiotic stress and wounding (Domergue et al., 2010). Finally, the exostosin-2 gene encodes a xyloglucan galactosyltransferase involved in cellulose synthesis (Madson et al., 2003). These two last genes are involved in deposition of material into cell walls, which is also a defence mechanism during fungal invasion. When the fungus penetrates the cell-wall the plant increases the synthesis of callose, a β-glucan polymer, to avoid further colonization (Voigt, 2014). The suppression of these two genes could be mediated by the fungus to allow haustoria formation. In general, genes associated with carbohydrate metabolism is consistent with my results from Chapter 3 where infected tissue has a sink metabolism.

Table 4.5. List of differentially wheat expressed genes under the carbohydrate metabolism classification. The differentially expressed genes have p-values and FDR-values lower than 0.05, they are from 6 and 9 dai compared to 0 dai. The purple shade represents the down-regulated genes and the green represents up-regulated genes. The annotations and family classification are based on the PGSB (http://pgsb.helmholtz-muenchen.de/plant/plantsdb.jsp) and uniprot (www.uniprot.org/) webpages.

Time point	Wheat gene	Fold change	Annotation
6 and 9 dai	Traes_3DL_CBD8FCDB3	2.76	Carbohydrate kinase (PfkB)
	Traes_2BL_1629018E8	2.42	Malectin/receptor-like protein kinase family protein
	Traes_3AS_1D618944D	2.04	Legume lectin domain, receptor kinase 2
	Traes_2DS_FA532168A	-2.03	RuBisCO small subunit domain
	Traes_2BS_E68F1B47C	-2.3	RuBisCO small subunit domain
	Traes_5DL_5597A11EC	-4.2	Fatty acyl-coenzyme A reductase 1
	Traes_4DS_6FA01281C	-2.2	Exostosin-2

The transport GO classification showed seven differentially expressed genes at 6 and 9 dai compared to 0 dai (Table 4.7). Six genes were up-regulated and encode sugar, oligopeptide and ion transporters. Two of the ion transporters are specific for zinc (Zn^{+2}) and potassium (K+). The zinc transporter belongs to the major facilitator superfamily (MFS) and the potassium transporter to the voltage-gated ion superfamily. In Arabidopsis, a zinc-induced facilitator-like 1 (ZIFL1) transporter is associated with auxin, drought and defence responses by inducing stomatal closure, and can also transport potassium (Remy et al., 2013). Considering the upregulation of a K+ transporter, infected plants require higher amounts of potassium. Potassium is involved in sucrose synthesis, triose-phosphate export and phosphorylation of hexoses for glycolysis (Börnke and Sonnewald, 2011). Possibly, K+ transporter expression increases potassium levels for nutrient synthesis during fungal infection (Wang et al., 2013).

Of the up-regulated transporter genes, two encode a SWEET sugar transporter and a facilitated glucose transporter member 12 (GLUT12). The SWEET transporters reside in the plasma membrane and tonoplasm (Chen, 2014). They can transport hexoses or sucrose and have been associated with development and immunity. In development, SWEET transporters are required for phloem loading and seed filling (Chen, 2013; Le Hir et al., 2015; Sosso et al., 2015). In pathogenesis, bacteria induce the expression of rice *SWEETs* to increase the available sugars in the apoplast where they reside (Chen et al., 2010). SWEETs are also induced during infection by the necrotrophic fungus *Botrytis cinerea* in tomato stems, and in *Medicago* roots by the oomycete *Pythium* spp. (Asai and Kobayashi, 2016; Chen et al., 2015a). In the compatible wheat-*Pst* pathosystem, it seems that *SWEET15* may act as a susceptibility gene since the infection is successful. The other upregulated gene, *GLUT12*, has mainly been described in mammals but it

seems it can locate to the tonoplasm or plant plasma membranes (Pedrazzini et al., 2013). Possibly GLUT12, as SWEET15, are up-regulated during a compatible interaction to provide nutrients to the pathogen. Alternatively, its upregulation is a stress response without benefit to the pathogen. Finally, the other two up-regulated genes belong to the oligopeptide transporter family (OPT). They are yellow stripe like 7 (YSL7) and proton-dependent oligopeptide transporter (POT). YSL7 and POT are plasma membrane proteins. In Arabidopsis, YSL7 is involved in pollen and seed development (Curie et al., 2009). YSL transports iron in the form metal-non-proteinogenic amino acid nicotianamine. The POT is involved in the uptake of small peptides, but some are annotated as nitrate permeases(Paulsen and Skurray, 1994; Tsay et al., 2007). Thus, it is difficult to assign a role for this gene in the wheat-*Pst* interaction. The *YSL7* and *POT* genes have not been related to defence responses, however possibly the infection is altering the nutrient transport to seeds since the infected tissue is shifting to sink status. Lastly, the only down-regulated gene in the transport classification encodes an ATP-binding cassette (ABC) transporter G family member 33. The alternative designation is pleiotropic drug resistance protein 5 (PDR5). PDR transporters reside in the plasma membrane and respond to abiotic and biotic stresses (Crouzet et al., 2006). The expression of *PDR5* in Arabidopsis is induced by abscisic acid (ABA) and it seems to extrude fungal toxins (Van Den Brûle et al., 2002). If PDR transporters are involved in the expulsion of cytotoxic compounds, perhaps down-regulation seen here is mediated by the fungus to prevent defence responses. In general, regulation of transport genes in infected wheat seems to be associated with the fungal requirements, where more sugars and ions are required for growth.

Table 4.6 List of differentially wheat expressed genes in the transport classification. The differentially expressed genes have p-values and FDR-values lower than 0.05, they are from 6 and 9 dai compared to 0 dai. The purple shade represents the down-regulated genes and the green represents up-regulated genes. The annotations and family classification are based on the PGSB (http://pgsb.helmholtz-muenchen.de/plant/plantsdb.jsp) and uniprot (www.uniprot.org/) webpages.

Time point	Wheat gene	Fold change	Annotation
6 and 9 dai	Traes_4BS_1DCF82CB7	2.2	Zinc induced facilitator-like 1
	Traes_7DS_4DEABD294	2.94	SWEET sugar transporter, plants
	Traes_7DL_460D33AEA	2.76	Proton-dependent oligopeptide transporter.
	Traes_2AL_CC6133527	2.00	Oligopeptide transporter. YELLOW STRIPE like 7
	Traes_5BL_F43BDBCB9	2.14	Potassium transporter family protein
	Traes_4BS_6E9FDF39C	2.73	Facilitated glucose transporter member 12-like
	Traes_4AL_603B6DC64	-3.70	ABC transporter G family member 33

The GO classification nitrogen metabolism, contained 6 genes with significant fold-changes at 6 and 9 dai. Four of the six genes were up-regulated, and the other two were down-regulated

(Table 4.8) All up-regulated genes were related to glutamate, asparagine and aspartate biosynthesis. The down-regulated genes were associated with lysine and glutamine metabolism. The up-regulated genes encode a glutamate decarboxylase (GAD), a gamma-glutamyl phosphate reductase (γ-GPR), an asparagine synthase (ASN) and acetylornithine aminotransferase 2 (AA2). The GAD enzyme is involved in the decarboxylation of glutamate to GABA. GABA accumulates in plants in response to stresses and is also involved in priming the plants to enhance resistance to abiotic stresses (Baum et al., 1993; Vijayakumari et al., 2016). γ-GPR resides in chloroplasts and is involved in accumulation cell-wall proline-rich proteins (Stein et al., 2011). The ASN enzyme produces asparagine from aspartate. Finally, AA2 produces glutamate from 2-oxoglutarate and is involved in arginine synthesis (Frémont et al., 2013). In Arabidopsis, *AA2* overexpression increases *Pseudomonas syringae* growth and represses salicylic acid accumulation (Lee et al., 2008). Overall the up-regulated genes suggest that the infection induces amino acid synthesis. This may be because the fungus is taking large amounts of nitrogen from plant cells, which must be replaced. In Chapter 3, I showed that asparagine levels were at least double in infected leaves compared to healthy leaves. I also showed by qPCR that *ASN* expression was highly upregulated in infected tissue compared to healthy leaves. These results are consistent with a need for the plants to increase amino acid synthesis during infection. Finally, the down-regulated genes encode a lysine-specific demethylase 3B, which reduces the methylation levels of histone H3 and in Arabidopsis is associated with the flowering locus (FLC) (Jiang et al., 2007). The other gene encodes a glutamine--fructose-6-phosphate aminotransferase (GFPT) involved in glutamine and glutamate metabolism (McKnight et al., 1992). GFPT is associated with D-glucosamine biosynthesis. The enzyme can produce glucosamine and glutamate from glutamine, and vice versa. For the down-regulated genes, I cannot suggest their roles during infection since they have broad functions and catalyse reversible reactions.

Table 4.7. List of differentially expressed wheat genes under the nitrogen metabolism classification. The differentially expressed genes have p-values and FDR-values lower than 0.05, they are from 6 and 9 dai compared to 0 dai. The purple shade represents the down-regulated genes and the green represents up-regulated genes. The annotations and family classification are based on the PGSB (http://pgsb.helmholtz-muenchen.de/plant/plantsdb.jsp) and uniprot (www.uniprot.org/) webpages.

Time point	Wheat gene	Fold change	Annotation
6 and 9 dai	Traes_4DL_F8CEC5A40	2.9	Glutamate decarboxylase
	Traes_3DL_3E215D878	2.63	Gamma-glutamyl phosphate reductase
	Traes_5BL_7E69810D5	2.72	Asparagine synthase 3
	Traes_1BL_C6ACA137C	3.75	Acetylornithine aminotransferase
	Traes_5BL_E0966FFC5	-3.47	Lysine-specific demethylase 3B
	Traes_3B_C750AAC9D	-2.10	Glutamine--fructose-6-phosphate aminotransferase

The final GO classification that I analysed was defence responses. There were 7 differentially expressed genes at 6 dai with fold-changes higher than three (Table 4.8). At 9 dai, the same genes were present with three further up-regulated identified genes. From the up-regulated genes at 6 and 9 dai, two of the four genes encode phenylalanine ammonia-lyase 2 (PAL). This enzyme is part of the phenyl propanoid pathway and produces secondary metabolites, some of which are involved in defence responses and plant growth (Dixon and Paiva, 1995). PAL is associated with lignin deposition in plant growth, a component of secondary plant cell wall (Barros et al., 2016). Knockdown of *PAL* expression in the model grass *Brachypodium distachyon* reduces root growth, enhances susceptibility to fungal pathogens and increases carbohydrate availability (Cass et al., 2015). Another upregulated gene at 6 and 9 dai was *catalase 2* (*CAT2*). In Arabidopsis, CAT2 localized in glyoxysomes, peroxisomes and mitochondria (Mhamdi et al., 2010). It protects cell by reducing hydrogen peroxide to oxygen and water. CAT2 regulates oxidative stress signals, and nitrogen and phosphate starvation (Kandlbinder et al., 2004; Vandenabeele et al., 2004). The role of CAT2 in the wheat-*Pst* interaction could be to reduce stress or antimicrobial compounds triggered by the fungus. In this case, *CAT2* may be acting as a susceptibility gene. I found upregulation of another *PAL* gene and a further *CAT2* gene at 9 dai. However it seems that these genes might be homeologues of the *PAL* and *CAT2* genes - mentioned above. They reside on the same chromosome but from different sub-genomes. For example, the *PAL* genes reside on chromosome two, but one is on the long arm of the 2A while the 9 dai gene is on the long arm of 2B. Similarly, for *CAT2*, both genes are on chromosome 6 but one is on the short arm of 2A while the 9 dai gene is on chromosome two genome D short arm.

Lastly, a coiled-coil - nucleotide binding site - leucine-rich repeat protein (CC-NBS-LRR) was up-regulated both at 6 and 9 dai. Based on BLAST homologies, this is similar to the resistance protein leaf rust-1 (*Lr1*) that recognises *P. triticina* (Cloutier et al., 2007). This gene recognizes the *P. triticina* avirulence gene *Avr1*. The reported location for *Lr1* is on chromosome 5D. Despite this, I found that the gene identified in this study was located on chromosome 6D. Possibly this discrepancy is due to a chromosomal rearrangement, as the published *Lr1* is from another cultivar or the gene had a duplication (Cloutier et al., 2007; Krattinger and Keller, 2016).

The 9 dai dataset possessed one gene that was absent in the 6 dai dataset, encoding a polyphenol oxidase E (PPO). PPO enzyme is present in the chloroplast and catalyses the oxidation of phenol to quinones. They are associated with biotic and abiotic responses but the biological functions are uncertain (Boeckx et al., 2015). From the defence category, there were three down-regulated genes at 6 and 9 dai (Table 4.8). They encode m*etacaspase 1 (MC1), peroxidase* and *jasmonate-induced protein* (*JIP*). The MC1 is a proteinase, involved in oxidative stress related to hypersensitive responses (HR) and a positive regulator of cell death (Coll et al., 2010). Peroxidases remove hydrogen peroxide from chloroplasts and the cytosol. They are involved in defence responses and cell wall modification (Francoz et al., 2015). Finally, JIP has an extracellular Jacalin-like lectin domain and is induced by the hormone jasmonic acid (JA). Arabidopsis with low JA content are male sterile and decrease defence responses (Turner et al., 2002). JA also accumulates during wounding or osmotic stress. Based on JA roles, JIP may be down-regulated to avoid defence responses during infection however the observed response could be associated with a crosstalk with SA (Jeyaprakash et al., 2002; Turner et al., 2002). In summary, the down-regulated genes are directly associated with oxidative environments and triggering cell death. The mechanisms through which biotrophic fungi keep the plant alive are not well understood, but the down-regulation of these genes suggests manipulation by *Pst* to modify toxic environments.

In general, defence GO classifications for the differentially expressed genes in the 6 and 9 dai datasets suggests that the plant perceives the fungus. However, because the wheat cv. Morocco is susceptible, *Pst* must be able to overcome resultant defences (Table 4.8). Interestingly, oxidative responses seemed to be regulated differentially since the *CAT2* gene was up-regulated whereas a plant peroxidase was down-regulated. Peroxidases are the main peroxide regulators in chloroplasts, probably because they have low affinity for H_2O_2 compared to catalases (Mhamdi et al., 2010). One hypothesis that arises from these observations, is whether *Pst* secretes proteins to target specific organelle responses. However, most studies focus of how the fungus uptakes nutrients.

Table 4.8 List of differentially expressed wheat genes in the defence response classification. The differentially expressed genes have p-values and FDR-values lower than 0.05, they are from 6 and 9 dai compared to 0 dai. The purple shade represents the down-regulated genes and the green represents up-regulated genes. The annotations and family classification are based on the PGSB (http://pgsb.helmholtz-muenchen.de/plant/plantsdb.jsp) and uniprot (www.uniprot.org/) webpages.

Time point	Wheat gene	Fold change	Annotation
6 dai and 9 dai	Traes_2BS_88CF42F2E	2.63	Phenylalanine ammonia-lyase 2
	Traes_6DL_F504536D5	2.76	CC-NBS-LRR (Leaf rust 1, Lr1)
	Traes_6AS_7FB8 F9A66	2.42	Catalase 2
	Traes_2AL_9D78F85E2	2.6	Phenylalanine ammonia-lyase 2
	Traes_4DL_78052B65C	-2.15	Metacaspase 1
	Traes_1DS_578ADDF80	-3.08	Peroxidase
	Traes_7DS_26341EE29	-3.58	Jasmonate-induced protein, putative
Only 9 dai	Traes_6DS_3522B8EF6	2.63	Catalase 2
	Traes_6DS_DBB150A6A	2.92	Polyphenol oxidase E
	Traes_2BL_5A50FDA1A	2.41	phenylalanine ammonia-lyase 2

Overall, differential gene expression in the five GO classifications (glycosyl hydrolases, carbohydrate and nitrogen metabolism, transport, and defence responses) correlated with previous results reported in Chapters 2 and 3, where *Pst* infected leaves changed to sink metabolism from source. Some characteristics of sink tissue are reduced expression of Rubisco, and increase flux of nutrients related to glycolysis like hexokinases and sugar transporters and with amino acid synthesis. The 6 dai time point was not measured in the previous Chapters, however it was clear that the wheat transcriptome responded to the infection at this stage of the infection. The gene expression responses were more sensitive than the changes in physiological and metabolic variables evaluated at 8 dai, even though the fungal biomass is low at 6 dai (Figure 2.6, Chapter 2). Based on the gene expression data presented in this Chapter, I propose that *Pst* has active and passive strategies to complete its life cycle. One active strategy is to block defence responses such as hydrolases and defence-related responses. These were differentially repressed between 6 and 9 dai with respect to 0 dai. Another active strategy is the direct nutrient uptake by secretion of invertases and expression of hexose transporters. This has been reported before for biotrophic fungi (Voegele, 2006). The passive strategy is by stressing the plant to induce sink metabolism transition. This was observed with the induction of genes coding for transporters, nutrient anabolism and the repression of photosynthesis–related genes. Alternatively, fungal transporters are more efficient in nutrient uptake than the plant transporters.

The 6 and 9 dai datasets seem to be very similar based on their individual comparisons to 0 dai. To compare the 6 and 9 dai datasets directly, I changed the reference sample from the IT0 to the IT6 sample. By normalizing the IT9 against the IT6 data, I identified the changes between 6 and 9 dai that were not evident when the samples were normalized individually to IT0. From this comparison, I found 93 differentially expressed genes. Some of the most common GO classifications that these genes fell into included starch biosynthesis, chitinase activity, responses to endoplasmic reticulum stress, defence responses to bacterium and oxidoreductase activity (Figure 4.6). The down-regulated genes coded for chitinases or were involved in starch biosynthesis. The differently expressed chitinase genes at 9 dai are reported in Table 4.4. There are two down-regulated genes at 9 dai, *subtilase* and *2-oxoglutarate Fe (II)-dependent dioxygenase*, that might be associated with defence responses as they are associated with senescence and formation of plant hormones, respectively (Farrow and Facchini, 2014; Figueiredo et al., 2014).

The down-regulated genes associated with starch biosynthesis encoded phosphoglucomutase, chlororespiratory reduction 7, glycerophosphoryl diester phosphodiesterase, and phosphoenolpyruvate carboxykinase (PEPCK) (Table 4.10). These four genes are annotated as part of starch synthesis however they are also involved in carbon fixation processes. The first three of these enzymes are related to carbon assimilation, synthesis and degradation of starch, chloroplast stability and stabilization of the NADH dehydrogenase-like complex (NDH) (Kamruzzaman Munshi et al., 2005; Periappuram et al., 2000). The NDH complex is located in the thylakoid membrane and is associated with electron cycling of photosystem I electrons (Peng et al., 2012). The NDH complex releases protons into the chloroplast lumen to establish and maintain the proton gradient force. PEPCK produces phosphoenolpyruvate (PEP) from oxaloacetate, a key step in the gluconeogenesis pathway. PEP can also be a substrate for starch synthesis (Penfield et al., 2012). In Chapter 3 I showed that starch accumulated in *Pst*-infected flag leaves areas (Figure 3.16). Based on the genes expression results and the metabolite quantification it seems carbon fixation does not affect starch accumulation or there are alternative pathways for accumulation.

The genes up-regulated from 6 to 9 dai are mainly associated with the GO categories responses to bacterium and endoplasmic reticulum stress. The genes from the bacterium responses classification were mentioned in Table 4.5 and Table 4.8. These genes were present at 6 and 9 dai but are more highly expressed at 9 dai. Another upregulated gene associated with defence responses encoded tryptophan synthase alpha chain which is involved in the synthesis of secondary metabolites (Ascencio-Ibáñez et al., 2008). This correlates with the induction of PAL

in 6 and 9 dai databases (Table 4.8). The other up-regulated gene codes for a protein from photosystem II (PSII). PSII can release electrons as superoxide anion radicals when the chloroplastic electron transport chain is damaged (Pospíšil, 2009). Overall, from 6 to 9 dai there was an increase in the expression of genes controlling catabolic responses. The few changes in gene expression between 6 and 9 dai may represent a fungal strategy to suppress defence responses before sporulation.

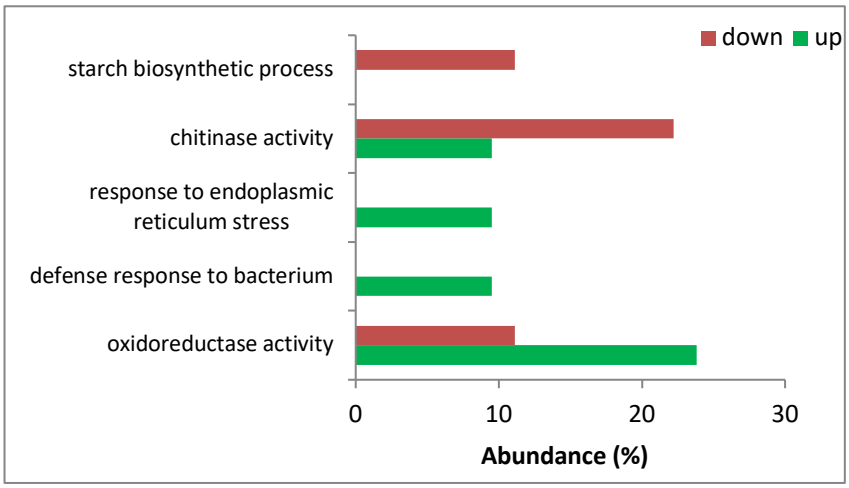

Figure 4.6. Gene ontology (GO) classifications of differentially expressed genes at 9 dai compared to 6 dai. For the analysis 100 genes were used. The up-regulated (green) and down-regulated genes (purple) were associated with the GO classifications shown here.

Table 4.9. List of differentially-expressed wheat genes in all GO classifications from 9 dai relative to 6 dai. The genes have p-values and FDR-values lower than 0.05. The purple shade represents the down-regulated genes and the green represents up-regulated genes. The annotations and family classification are based on the PGSB (http://pgsb.helmholtz-muenchen.de/plant/plantsdb.jsp) and uniprot (www.uniprot.org/) webpages.

Wheat gene	Fold change	Annotation
Traes_1DL_7657153A4	2.10	Tryptophan synthase alpha chain
Traes_6DL_0A92A2224	2.12	Photosystem II CP43 chlorophyll apoprotein
Traes_5DS_D131C3703	-2.45	Subtilase family protein
Traes_7AL_F70DA9639	-2.01	Phosphoglucomutase, putative
Traes_3B_6642D8694	-1.59	Chlororespiratory reduction 7
Traes_3B_6642D8694	-2.65	Glycerophosphoryl diester phosphodiesterase
Traes_7DS_D0996C347	-2.21	2-oxoglutarate Fe (II)-dependent dioxygenase superfamily protein
Traes_4BL_A33060036	-2.08	Phosphoenolpyruvate carboxykinase (PEPCK)

To obtain an overview of plant metabolism during *Pst* infection, I took all of the differentially expressed genes that were similarly expressed in the 6 and 9 dai datasets relative to 0 dai. I visualized the gene annotations using the software MapMan (version 10) using the wheat transcriptome annotation from MIPS v.2.2. The software uses 13 categories to differentiate the

genes. These are; amino acid metabolism, cell-wall, gluconeogenesis, glycolysis, lipid metabolism, major and minor carbohydrate (CHO) metabolism, nitrogen metabolism, tricarboxylic acid (TCA) pathway, nucleotide metabolism, oxidative pentose phosphate (OPP), secondary metabolism, redox and photosynthesis (Figure 4.7). Within the 13 categories, most of the downregulated genes were present in the photosynthesis category. This is divided into light reactions, Calvin-Benson cycle, photorespiration and tetrapyrrole (chlorophyll metabolism pathway). These four sub-categories contain mainly down-regulated genes. These results correspond with what I observed in Chapter 3, where the infected tissue shift metabolic status to become a sink that import nutrients, rather than producing them. The remaining 12 categories contain combinations of differentially expressed genes, which I explain in the next paragraphs.

The category carbon metabolism is divided into minor and major carbohydrates (CHO) sub-categories. The minor CHO metabolism sub-categories include trehalose, raffinose, sugar alcohol and callose metabolism. Raffinose is a storage carbohydrate composed of sucrose and galactose and is involved in phloem loading through polymer trapping. Raffinose metabolism contain some up and some down-regulated genes therefore there is not a clear role during infection (Figure 4.7). Trehalose metabolism, is represented by genes encoding mainly trehalose-6-phosphate phosphatase (TPP) and trehalose-6-phosphate synthase (TPS). The TPP dephosphorylates trehalose to make it available for degradation into glucose (Ponnu et al., 2011). TPS uses sucrose and UDP-glucose to produce trehalose-6-phosphate, which can be a signal for starch synthesis. The *TPP* genes identified here were upregulated by infection while the *TPS* genes were down-regulated. The differences between *TPS* and *TPP* gene expression suggest that trehalose could be another source of glucose during infection while trehalose-6-phoshate is not synthesized possibly due to lower levels of sucrose. The subcategories sugar kinases and sugar alcohols contained mostly repressed genes. Some of these genes codes for xylulose kinases and myo-inositol, respectively. Xylulose is associated with the production of sterols and is produced in the pentose phosphate pathway. The diverse roles for these genes makes difficult to correlated with a specific function during infection. Finally, callose metabolism contain only up-regulated genes. Callose is a plant polysaccharide that accumulates during wounding or under biotic stress (O'Connell and Panstruga, 2006). Possibly, as suggested previously, the plant can perceive *Pst* but this is insufficient to reduce the infection. For minor CHO metabolism only trehalose and callose gene expression showed clear roles during infection.

The major CHO category is divided into sucrose and starch metabolism subcategories. Genes associated with degradation had a clearer expression pattern compared to synthesis genes. In

degradation, genes for starch metabolism were mostly down-regulated while for sucrose they were mostly up-regulated. The genes involved in starch degradation are alpha and beta amylases, starch phosphorylase, phosphatases and starch transporters. The up-regulated genes in sucrose degradation encoded fructokinases and the three invertases isoenzymes. In sucrose degradation subcategory, the gene coding for sucrose synthase (Susy) was strongly down-regulated. Based on CHO metabolism schema (Figure 4.7). I suggest several scenarios. First scenario is that sucrose is directed to produce hexoses for glycolysis instead of being used for membrane synthesis, as *Susy* but not *invertases* are repressed. This could contradict the expression of genes for callose synthesis, but also suggests that there is an alternative callose synthesis path and possibly is specific to a pathogen attack respond. Second scenario is that infected leaves to stay as sink tissue, accumulates starch in the cells to keep a flow of nutrients towards infected leaves. An explanation for repression of starch degradation associated genes could be due to changes in phosphorus levels. As mentioned earlier in this chapter, phosphorus is a key element for starch metabolism and triose transport. If the fungus is using this element or Phosphorus is diverted to other pathways starch degradation could be repressed.

The cell wall category contains downregulated genes related to cell-wall proteins, pectins and cellulose synthesis. The upregulated genes encode hemicellulose synthesis, cell wall degradation and cell wall synthesis. The repression of cellulose synthesis correlates with the down-regulation of *Susy* in sucrose degradation subcategory. Interestingly, genes related to hemicellulose metabolism were up-regulated by infection but cellulose was repressed. Hemicellulose is a polysaccharide of mannose, glucose or xylose and it fortifies the cell-wall by interaction with cellulose (Malinovsky et al., 2014). Possibly hemicellulose synthesis gene expression is associated to reinforcement of the cell-wall as observed for callose. Alternatively, cellulose but not hemicellulose could be repressed as a stress response, like photosynthesis genes.

The lipids category is divided in phospholipids synthesis, general lipid synthesis and degradation. In the phospholipid synthesis subcategory, there were genes strongly induced encoded for triacylglycerol (TGA) biosynthesis which are also induced by abscisic acid. In the same subcategory, there were strong down-regulation of genes for steroids synthesis. Most of the genes in the synthesis and degradation subcategories were up-regulated, except for genes coding for lipid beta-oxidation reductase and triacylglycerol lipases that were strongly down-regulated. The results are potentially associated with rearrangements in the host cell membrane to allow haustoria formation. Alternatively, lipids are recruited by the fungi as source of energy due to their higher energy content. *Pst* could induce the synthesis of lipids as reported for other

biotrophic fungi (Jiang et al., 2017). Moreover, lipids are required by arbuscular mycorrhiza for colonization and by the oomycete *Golovinomyces cichoracerum* for higher spore production.

The oxidative pentose phosphate (OPP) pathway is parallel to glycolysis and generates pentoses (5-carbon sugars) (Taiz and Zeiger, 2010). The pathway is divided into irreversible oxidative and reversible reductive reactions. The oxidative reaction produces ribulose-5-phosphate and NADPH (R5P) from glucose-6-phosphate (G6P). NADPH can be used for fatty acid synthesis. R5P is the substrate for nucleotides, coenzymes, DNA and RNA synthesis. The reductive reaction generates xylulose, erythrose, fructose-6-phosphate (F6P) and glyceraldehyde-3-phosphate (G3P) from R5P. F6P and G3P can enter glycolysis pathway. In this study, the OPP oxidative reaction contained more up-regulated genes while the reductive reaction had mainly repressed genes (Figure 4.7). The reductive reaction is reversible therefore is difficult to conclude which direction of the reaction was more affected. On the other hand, the induction of genes related to the oxidative reaction raises several hypotheses. First, infected tissue has enough glucose that G6P can be used for R5P synthesis. Second, is that infected tissue requires more NADPH for lipids synthesis. Third, is that NADPH is used to reduce glutathione, this form can be used to neutralize reactive oxygen species in infected cells. The third hypothesis correlates with upregulated genes from the glutathione category (Figure 4.7).

The nucleotides metabolism category, contain mostly upregulated genes except for the salvage pathway that was down-regulated (Figure 4.7). The higher number of genes associated with nucleotide synthesis, correlated with the increase in the OPP oxidative phase, where more R5P is produced. In the salvage pathway, nucleotides are synthesized with intermediates from DNA and RNA degradation. This process occurs more efficiently than de novo synthesis (Moffatt and Ashihara, 2002). The repression of the genes associated with the salvage pathway suggest the plant is still able to produce nucleotides and does not require alternative pathways.

The gluconeogenesis pathway generates glucose from non-carbohydrate sources like lactate, glycerol and amino-acids. Most of the genes in this category were up-regulated (Figure 4.7). As I showed in Chapter 3, infected tissue had higher glucose levels compared to healthy leaves (Figure 3.21). Therefore, glucose not only might come from sucrose degradation but also from other carbon-containing sources, in this case through gluconeogenesis pathway. This could explain the increase expression of genes from the lipid pathway and fermentation to produce substrates for gluconeogenesis.

The amino acids category is divided in synthesis and degradation (Figure 4.7). In the subcategory synthesis, there are several up and down regulated genes related to the same amino acid, however genes related to aspartate were only repressed. In chapter 3, I found more levels of aspartate in infected leaves compared to healthy leaves (Figure 3.25). This suggests that the fungus, but not the plant, is accumulating aspartate during infection. In the amino acids degradation subcategory, most of the genes were up-regulated, except for serine, glycine and cysteine related genes that were only down-regulated. Degradation of amino acids suggest three scenarios. First, the infected tissue requires more carbon and the host degrades amino acids with high carbon. Second scenario, infected tissue cannot assimilate more nitrogen therefore uses the existing amino acids as source of nitrogen. Third scenario, the plant is stress and as a response it degrades more amino acids. The first and last scenario correlates with the upregulation of genes from the ammonia (NH_4) degradation subcategory. The genes in this subcategory encode subunits of the enzyme glutamate dehydrogenase. This enzyme converts glutamine to keto-glutarate. Keto-glutarate can be used in the TCA cycle. Glutamate dehydrogenase seems to be activated by stress and carbon deficiency, releasing carbon to supply the TCA (Robinson et al., 1991). In the degradation of amino acids subcategory, the repression of genes related to serine, glycine and cysteine can also be linked to the TCA cycle. Cysteine is produced from serine and serine accumulates during photorespiration, cytosolic glycolysis and in the Calvin cycle (Ros et al., 2014). Moreover, cysteine carbons are substrates for pyruvate synthesis (Hildebrandt et al., 2015). Based on the differential expression genes in amino acids category, it seems the infected tissue requires more carbon skeletons for respiration and is taking them from amino acids.

The TCA category is divided in carbonic anhydrases and organic transformation subcategories (Figure 4.7). The carbonic anhydrases have up and down-regulated genes, therefore is not possible to conclude their role during infection. The organic transformation subcategory had repressed genes associated with lipoamide dehydrogenase and up-regulated genes encoding succinate dehydrogenase and oxoglutarate dehydrogenase. Lipoamide dehydrogenase (LPD) is a subunit of mitochondria enzyme complexes, like α-ketoglutarate dehydrogenase and pyruvate dehydrogenase (Lutziger and Oliver, 2001). LPD is part of different mitochondrial metabolic processes therefore is difficult to assign a role during infection. The induced genes in the organic transformation subcategory are part of consecutive reactions in the TCA cycle. Oxoglutarate or keto-glutarate dehydrogenase oxidises keto-glutarate to Succinyl-Coenzyme A (SuCoA). The converted version of SuCoA, succinate, is oxidised by succinate dehydrogenase to produce fumarate. The expression of these two genes correlates with the increase in respiration rates observed in chapter 3 for infected leaves (Figure 3.7).

The genes associated with secondary metabolites are divided into 6 metabolic subcategories. They are terpenoids, flavonoids, waxes, phenylpropanoid and phenolics, sulphur-containing (S-misc) and biotin synthesis (misc). The first three subcategories had a mix of down and up-regulated genes which makes difficult to conclude about their role during infection. The phenylpropanoid subcategory had mainly upregulated genes related to lignin biosynthesis and the phenolics subcategory had mostly down-regulated genes encoding the enzyme laccase. Laccase is associated with cell wall integrity and possibly with lignin synthesis (Ranocha et al., 2002). The contradictive results from phenylpropanoid and phenolics subcategories in relation to lignin synthesis, suggest that the upregulated genes can be associated with production of secondary metabolites in response to stress (Vogt, 2010). Biotin subcategory contain only down-regulated genes. Biotin, vitamin B7, is a cofactor for different metabolic process. Therefore, is difficult to associate a role during infection. Finally, the sulfur-containing subcategory had genes related to glycosinolates synthesis and degradation. Glucosinolates contain sulfur and nitrogen derived from glucose and amino acids. The most down-regulated gene in this category is a sulfotransferase from the jasmonic acid pathway. This relates to my previous hypothesis where I suggest that JA is supressed to avoid defence responses (Table 4.8). The most up-regulated genes encode cytochrome P450 (CYP). CYP is involve in several metabolic reactions, as biotin is difficult to suggest a role during infection. Alternatively, biotin and glucosinolates might be taken up by the fungus as a source of sulphur because biotrophic fungi lack genes related to assimilate it and rely on the host as a supply.

Overall, the Mapman graphical output provided an overview of the metabolism of *Pst*-infected wheat leaves. Although many of the alterations in gene expression can be rationalised by what is already known about plant-fungal interactions, in other cases it is not possible to distinguish whether the changed gene expression is a direct outcome of infection, or if it is changed in favour of the host or the pathogen. I suggest that this approach should be used only for whole metabolic pathways, as the expression of single genes can be better understood if they are in context with a pathway. A single gene will not let conclude about its role during infection, but if the whole pathway where that gene belongs is up-regulated that provides extra information to understand what is happening during infection.

The key pathways affected during infection are suggestive of a shift in host metabolism from source to sink metabolism. These include the degradation of bigger molecules like sucrose and peptides to hexoses and amino acids, and the reduction in carbon, nitrate and sulphate assimilation. Interestingly starch degradation genes were largely down-regulated implying high levels of starch in infected leaves. The repression of these genes could explain the higher levels

of starch that I measured in *Pst*-infected leaves areas compared to healthy areas (Figure 3.14, Chapter 3). As plants use transitory starch during the night when the levels of carbon are low (Scialdone and Howard, 2015), this implies that starch was never synthesized (due to fungal carbon demands), or that the fungus supresses this pathway to maintain the sink status. This hypothesis need to be tested measuring starch levels in healthy plants from the same metabolic age as the infected plants to discard the possibility that they are just developmental changes rather than responses to infection.

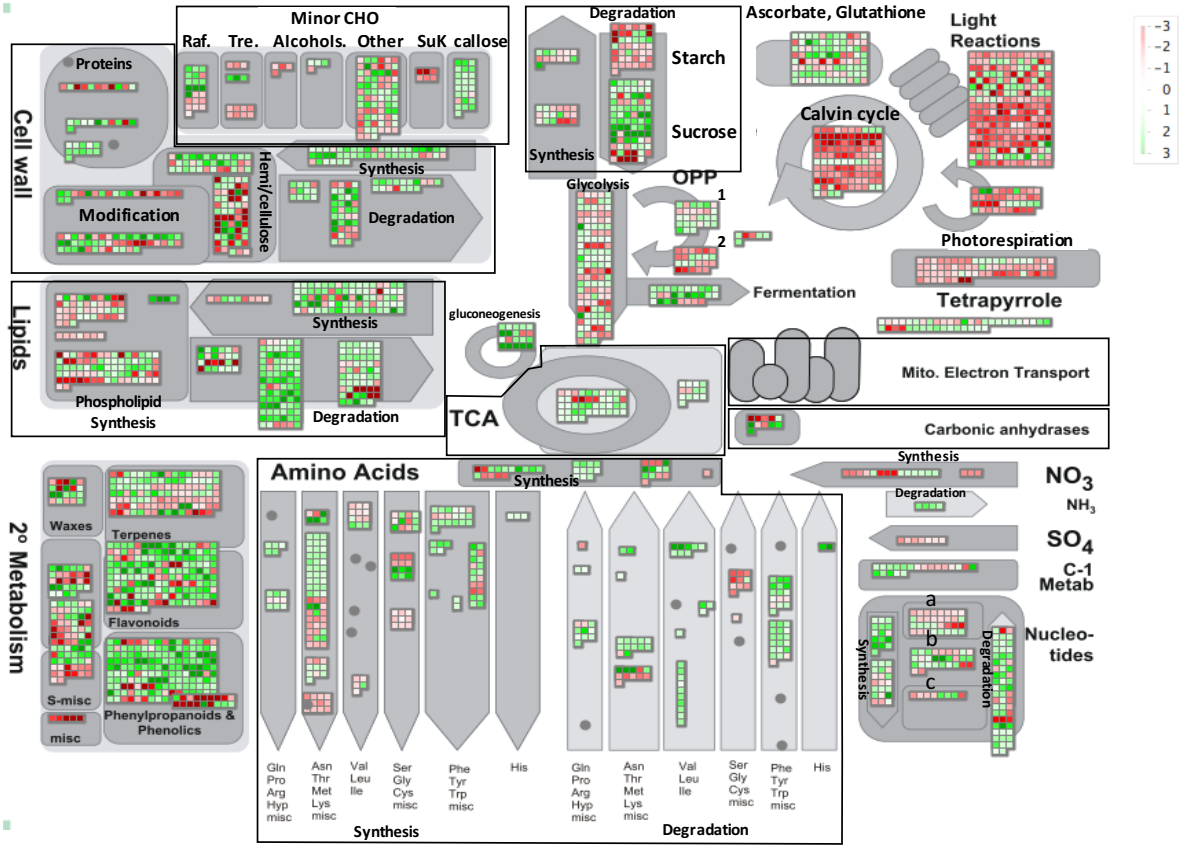

Figure 4.7. Metabolic overview of common differentially-expressed genes in the IT6 and IT9 datasets using MapMan. The categories are labelled and discussed in the text. The Minor carbohydrates (CHO) represent raffinose (Raf), trehalose (Tre), sugar alcohols (alcohols), other minor carbohydrate(other) and sugar kinases(SuK). In the oxidative pentose phosphate pathway (OPP) there are oxidative (1) and reductive (2) reactions. In the nucleotide metabolism, there are also phosphotransferase (a), salvage (b) and general synthesis (c) processes. The small squares in each metabolic category represents genes that are upregulated (green) or downregulated (red) compared to IT0. The expression levels are in log2 scale.)

The main purpose of this Chapter was to understand, from a metabolic point of view, how the wheat transcriptome responds to *Pst* infection during a compatible interaction. A minor limitation to this study was the mixture of host and fungal sequences in plant extracts due to the obligate nature of the infection. I could remove the fungal sequences in-silico by mapping the reads to the fungal genome and recovering the unmapped reads. This approach worked efficiently, leaving only the wheat sequence reads which provided to be sufficient for

transcriptomic studies. For a more precise study other software should be used that recognize homeologues and count them as a single gene. This will increase the fold change of a gene instead of dispersing the reads in different groups.

With the data collected at 0, 6 and 9 dai, it is possible to conclude that changes in the wheat transcriptome shifts are consistent with a shift to sink metabolism from source after 6 days of infection, and that the differentially expressed genes identified at 6 dai were similar at 9 dai. This is even though the fungal biomass is at least twice that at 9 dai than at 6 dai (Figure 2.6). In contrast to these results, fungal metabolism changed more markedly between 6 and 9 dai. At 6 dai the growth is asymptomatic while the 9 dai time point is one day before pustule eruption, where the fungus takes very large amounts of plant nutrients for spore production. This means that *Pst* must extract host nutrients more aggressively during sporulation, but the plant did not seem to sense damage or increase nutrients flow. This also suggests that the fungus can avoid defense responses that might affect pustule formation. However, to test this statement I would need transcriptomic data from tissue sampled after pustule eruption.

The expression data from this study was based on Dr. Diana Garnica study where she designs the experiment to analyze the pathogen transcriptomics. This data was useful to get an overview of the plant transcriptomics. For better understanding of the host, I would change the experimental design to include healthy tissue at 0, 6 and 9 dai as correct controls. The controls and infected plants should be grown in parallel to have the same developmental stage during sample collection. During plant development nutrient demands change, for example younger leaves will increase the export of nutrient while their grow to provide nutrients to newer leaves. The infection can also induce changes in cells with *Pst* to import more nutrients. In this scenario, the gene expression analysis could be wrong if the infected plants are not compared with plants with the same capacity to respond to nutrient flow. It will be more difficult to interpret if the changes are a developmental respond or from the infection. The changes by development could be remove if the infected plants are compared to healthy plants from the same age. For example, in these experiments the cell-wall rearrangements could be part of normal growth during development or adjustment to hyphae penetration. Likewise, bigger sugars like raffinose, could be just involved in phloem loading during development or could have a role during infection that has not been reported.

The major changes in the wheat transcriptome during infection involved genes encoding photosynthesis-associated pathways, amino acid metabolism, glycosyl hydrolases (GHs) and stress-associated responses. All photosynthesis-related pathways including light reactions, the

carbon fixation cycle and photorespiration were down-regulated. This implies that the infected tissue cannot satisfy all carbon nutrient requirements for the fungus and hence requires external sources of carbon, consistent with the change to sink metabolism during infection. Apparent sucrose degradation rather than synthesis reaffirms this metabolic shift. It seems that sucrose is a carbon currency that is distributed to different parts of the plant. Possibly sucrose is converted to hexoses during the infection. With lower levels of sucrose, starch metabolism is reduced as a signal to use the glucose in sucrose anabolism.

The shift to sink metabolism during the infection is also reflected by changes in nitrate, and amino acid metabolism. The expression of most of the genes related to glutamine and asparagine anabolism increased while nitrate fixation was reduced. If infected tissue cannot fix nitrogen, they rely on stored or external sources to keep the nutrient demands. Some stored sources of nitrogen could be chlorophyll and Rubisco. For example, the down-regulation of Rubisco suggest that that nitrogen that would normally be incorporated into this protein will be now available for other uses. External sources could be glutamine and asparagine, like sucrose, they are mobile molecules in the plant. These two amino acids are common substrates in pathways for amino acids synthesis therefore they are a source of nitrogen skeletons for other compounds.

Another class of differentially expressed genes encoded GHs. These enzymes were mainly suppressed during infection. Members of these enzymatic families not only degrade fungal chitin but regulate plant cell wall structure (Minic, 2008). The suppression of GH genes could be mediated by fungal effectors, as plants can trigger defence responses when they perceive changes in the cell wall structure (Malinovsky et al., 2014). Therefore, this observation could be associated with biotrophic fungal strategies to avoid triggering cell death. Biotrophic plant pathogenic fungi by comparison to necrotrophic fungi secrete lower numbers of cell-wall degrading enzymes (Duplessis et al., 2011; Presti et al., 2015), probably to avoid host defence responses.

Defence responses are usually the first point of interest when studying plant-pathogen interactions. I only saw differentially expressed genes in jasmonic acids but not in other plant hormones, like salicylic acid or abscisic acid (ABA). There is evidence that these two hormones could be part of defence or susceptibility responses. Accumulation of salicylic acid in perl millet conferred resistance to leaf rust (*Puccinia substriata*) (Crampton et al., 2009). ABA induce the expression of sugar transporters that confer susceptibility to oomycetes (Hayes et al., 2007). Here I showed that primary metabolism pathways complement these studies and could be use

as metabolic markers for early detection of infection. For example, kinases involved in irreversible metabolic steps that define the carbon flow, such as hexokinases, might provide markers of pathogenesis. Phosphorylation of hexoses by hexokinases directs them to glycolysis rather than synthesis of bigger molecules. This suggests that sugar phosphorylation is a key pathway for sink metabolism. Other informative enzymes include invertases and Susy. The invertases breakdown sucrose most likely to increase glycolysis substrates for fungal uptake or plant respiration, while Susy breakdowns sucrose for cell wall synthesis. Overall the wheat responses evident in the transcriptome seem to represent basal immunity that *Pst* is able to overcome. Nevertheless, the most common wheat responses to infection were related to reprograming plant metabolism to become sink tissue.

CHAPTER 5
General discussion

Both plants and their fungal pathogens require carbon and nitrogen nutrients for growth. Biotrophic rust fungi acquire all of the necessary nutrients from their hosts while keeping the plant alive and avoiding defence responses. At the end of the cycle the spores have stored sufficient energy to allow them to restart the cycle. On the other hand, cereals distribute nutrients according to the requirements of each organ, keeping a controlled nutrient flow (Schippers et al., 2015). In seedlings, nutrients are distributed to younger leaves and roots for growth, while in adult plants, seeds take priority, so most of the photosynthates produced during vegetative growth is used to fill the developing grains. In the context of plant immunity, adult wheat plants apparently possess resistance mechanisms against *Pst* that are not active in seedlings (Ellis et al., 2014). Seedling resistance, which also operates in adult plants, is usually controlled by NB-LRR proteins. In contrast, adult plant resistance (APR) is active only when the flag leaf develops, or when the plant reaches the adult stage (Denissen, 1993). The proteins underlying APR are not the common NB-LRR proteins associated with specific recognition but some of them are transmembrane transporter proteins (Fu et al., 2009; Krattinger et al., 2009; Moore et al., 2015). APR has been proposed to trigger non-canonical defence response(s) where possibly changes in nutrient levels, developmental stages or transport of toxic metabolites may reduce fungal growth.

In recent times plant metabolism has been studied in context with immunity since some defence-related genes encode sugar transporters (Chen, 2014; Dodds and Lagudah, 2016; Hayes et al., 2007; Moore et al., 2015; Yamada et al., 2016). Possibly, the mechanism of these transporters is to reduce the movement of nutrients, such as sugars, indirectly starving the pathogen. Sugars are required not only for pathogen growth but also indicate the sink tissue demand in plants (Schippers et al., 2015). The mechanisms and pathways that underlie defense responses where sugars are involved are not well understood since most studies have focused on recognition by R proteins and on pathways related to oxidative responses (Dodds and Rathjen, 2010).

Perspective

In this thesis, I present an overview of wheat metabolism during the interaction with *PST*-79. I combined the use of plant physiology and molecular biology techniques to understand how *Pst* infection alters wheat metabolism and development. It is known that biotrophic fungi take sugars from the host, consequently decreasing the photosynthesis-related metabolism of infected tissue (Doehlemann et al., 2008; Voegele and Mendgen, 2003). Some indicators of this metabolic transition include an increase in nutrient import from other tissues (Horst et al., 2010a), a reduction in seed size because the major sink is now the infected tissue rather than the heads (Gao et al., 2014), increases in hexoses in the infected tissue (Doehlemann et al., 2008), and a reduction in photosynthesis (Doehlemann et al., 2008; Ishiga et al., 2015; Scholes and Rolfe, 1996). From the pathogen side, upregulated genes in biotrophic fungi include sugar transporters and invertases that increase the pathogens' capacity to take up plant nutrients (Garnica et al., 2013; Voegele et al., 2001, 2006). Overall, the infected tissue represents a new sink that competes with other plant sink tissues for nutrients. For the *Pst*-wheat interaction, there are few reports on changes in wheat metabolism during infection (Dobon et al., 2016; Garnica et al., 2013; Liu et al., 2015a). As part of my PhD research, I tried to understand the requirements of each organism and how these are affected during the interaction. I postulated three initial hypotheses. The first is that *Pst* enhances carbon fixation during infection, to increase the amount of available nutrients. The second is that plant primary metabolites are lower at infection sites due to uptake by the fungus. The third is that *Pst* growth is affected by the developmental age of the leaves and the whole plant.

My results show that *Pst* did not enhance photosynthesis in infected leaves, and there was no reduction in the measured carbon and nitrogen compounds in infected tissues (Chapter 3). All of the photosynthesis-related parameters that I measured decreased by at least half in infected leaves compared to healthy leaves. Nutrient synthesis decreased in the infected tissue and hence the pathogen must have exploited the plant's storage compounds and distal tissues to provide them. Thus, I reject my first hypotheses. I am not able to conclude about my second hypothesis because the extraction protocols that I used cannot separate fungal from plant material. Therefore, I could not determine the origin of the nutrients. Related to my third hypothesis, I could not detect clear differences related to fungal growth and plant metabolism between young and adult stage plants, however systemic responses to infection were clearer in adult stage plants. However, I only saw systemic responses in adult plants because the infection protocol was different from that in young stage plants. For the latter, all leaves where infected

while for adult plants, only the flag leaf was infected. This affects the transfer of nutrients between infected and uninfected tissues.

To complement the host data, I studied the nutrient requirements of *PST*-79. I evaluated how fungal growth was affected when plant metabolism was manipulated by changing light conditions, wounding or cutting leaves, and when adding external sugars to the leaves. Based on my results, it seems that *PST*-79 can grow under low nutrient conditions but sporulation is affected if the host limitations are constant. I propose that *Pst* has two strategies during its asexual life cycle. The first is during the biotrophic phase. In this phase, *Pst* takes only small amount of nutrients to maintain a balance within the plant. This allows the fungus to grow without triggering defence responses. The second strategy is during the sporulation phase. The fungus takes up large amount of host nutrients for spore development, which triggers stress responses (Coleman et al., 2009; Granot et al., 2013). However, by this stage the fungus has already colonized large parts of the whole plant and is able to complete its life cycle. The fungal nutrient demand correlates with a strong transition to sink metabolism in the infected tissue.

Based on my results, infected tissue has reduced photosynthesis capacity but a greater accumulation of fungal biomass. This suggests that storage components and distal tissues are alternative sources of nutrients for *Pst*. To test this idea, I evaluated systemic responses (in uninfected leaves) in adult stage plants. I assayed the flag-1 leaf because it is immediately below the infected flag leaf and has different photosynthesis parameters compared to the flag leaf (Figure 1.9). When only the flag leaf was infected, I found increased sucrose levels in flag-1 leaves, and that genes associated with sink metabolism in these leaves were down-regulated. These responses contrast with those in the infected flag leaf of the same plant, and suggest that the infection stimulates nutrient mobilization from flag-1 to flag leaves (Bancal et al., 2012; Horst et al., 2010a). It follows that flag-1 leaves may transition from sink to source metabolism during sporulation, instead of remaining as sink. This result, so far as I know, has not been reported in any other studies. To my knowledge, the only clear example is maize infected with *U. maydis,* where nitrogen compounds from distal tissues are relocated to infected tissues or tumours (Horst et al., 2010a). Bearing in mind that flag leaves do not normally create a nutrient demand (rather the opposite), flag-1 leaves become new nutrient sources to compensate the demands of the infected flag leaves.

Nutrient reallocation in whole plants is partly regulated by sugar concentrations in the apoplast. More sucrose in the apoplast suggest that cells are exporting nutrients, while more hexoses means that it is importing nutrients as a sink tissue (Granot et al., 2013). I measured apoplastic

sugars in infected and healthy flag leaves and compared these to total sugar levels in whole flag leaves. I found that before fungal sporulation, infected but not healthy whole leaves tissues had high levels of hexoses. During sporulation, I found high levels of hexoses only in the apoplast of infected leaves. The changes in hexose levels in whole tissue versus the apoplast correlates with the two fungal strategies I proposed in a previous paragraph. It seems that during the first phase of the *Pst* life cycle, the fungus is able to survive with nutrients from infected cells, while during sporulation there is a strong signal from the apoplast to import more sugars. The common experimental approach during plant-pathogen studies is to evaluate whole tissue fractions, however in this work I showed that the study of the apoplastic fraction helps to understand the change to sink metabolism. I suggest that future studies should evaluate apoplast and symplast pathways separately to understand not only how the host responds to the infection, but also to locate the nutrient sources used by the fungus.

I restricted my research to wheat and studied only the *PST*-79 isolate, which was the first incursion in Australia in 1979. A more aggressive incursion of *Pst* was recorded in 2002, known colloquially as the WA (Western Australia) isolate (Wellings et al., 2003). Possibly, this strain is more aggressive because it has accumulated genetic mutations that have modified its metabolism (Schwessinger, 2017). This might be reflected in more efficient ways to alter host metabolism. Additionally, I evaluated wheat only, but future efforts could be expanded to other plant species to determine the common metabolic responses to biotrophic pathogens. This knowledge might be useful to understand, from a metabolic point of view, how non-host resistance works. For example, rice is resistant to rusts and powdery mildew (Ayliffe et al., 2011). It is possible that this resistance is associated with different nutrient contents or transporters.

In this work, I changed the *PST*-79 infection method to understand better how plant development affects *Pst* infection, and how plant nutrients are allocated during the infection. Dr. Diana Garnica, a previous PhD student in the Rathjen Laboratory at ANU, standardized the infection protocol on seedlings. Her method consisted of spraying spores on to whole young stage plants so that all aerial parts of the plant are infected. My work focussing more on host responses demanded a different mode of infection. I needed to delimit the infection to specific areas, to make the infection as uniform as possible, and to study single leaves at different metabolic stages. For example, the flag leaf (the last leaf before booting) of adult stage plants because it contributes to grain filling. Therefore, I changed the method to infect precise areas by painting leaves with spores. This method was useful to compare infected flag leaves with uninfected flag-1 leaves, or even different areas within the same infected leaf. I was able to

detect a role for distal leaves during infection using this approach, which would not have been possible with the previous method.

The biotrophic phase of *Pst*

I used three-time points during infection to approximate the key phases of the asexual cycle of the fungus. These were colonization (between 2 and 4 dai), biotrophic growth (at 8 dai) and sporulation (at 14 or 15 dai). I used two-time points for the colonization phase because some parameters are affected by the growing conditions of the plant. Therefore, I needed to acclimate the infected plants before taking measurements. For sporulation, I mainly used 14 dai, but when the experimental equipment was not available I measured at 15 dai. One of the major difficulties was in measuring differences between healthy and infected tissue at 8 dai due to variability between the biological replicates. The variation at 8 dai may be explained from different perspectives. One is from an experimental point of view, where the techniques were not sensitive enough to detect small changes in the leaves. For example, for the detection of invertase activities, if the proteinaceous inhibitor is not extracted with the invertases there will be an overestimation of their activity (Bonfig et al., 2010b). The limitations to the analysis are also related to the extraction procedure, in which information on sugar localization is lost because heathy and infected cells from a single infected leaf are ground together during extraction. An alternative approach for future studies will be to use labelled sugars to consider compartmentalization. I propose two approaches. One is to use mass spectrometry imaging. This technique is based on the molecular ion imaging technique of tissue imprinted onto a surface that can then be used in mass spectrometry (Dong et al., 2016). The resolution of the technique should be sufficient to be able to differentiate individual cells and maybe even organelles. Another approach could be to introduce labelled carbon into the plant. The labelling could be via carbon isotopes or a fluorescent tag. These could be later detected by microscopy. For fluorescently-labelled carbon molecules it will first be necessary to see if the plant can assimilate them (Bhunia et al., 2013; Hindie et al., 1992). The implementation of these techniques will resolve the localization of photosynthates, whether they are in the plant apoplast, vacuole, cytoplasm, or if they are mainly located in the fungal hyphae or haustoria.

To reduce the intrinsic variation of the infections, I compared sugar and gene expression levels on a proportional basis. I used two types of ratios; among leaves, and within the plant. Among leaves refers to the ratio between infected leaves over healthy leaves. Within the plant refers to the ratio between flag and flag-1 leaves. These ratios allowed me to detect metabolic transitions that would otherwise have been obscured by the sampling error and intrinsic plant

variability. Moreover, within the plant ratios helped me to differentiate normal metabolic transitions occurring in healthy plants from those changes caused by the infection. Therefore, I propose the use of ratios as a useful way to process the original raw values to evaluate plant nutrient transitions.

A model for Adult Plant Resistance

Following the idea that changes in host nutrient levels are a part of plant immune responses (Govind et al., 2016; Trouvelot et al., 2014), I studied adult plant resistance (APR) as a means of gaining insight to this phenomenon. APR is often higher in flag leaves and is the last leaf to develop before flowering. The flag leaf also has the highest photosynthetic capacity compared to older leaves. For these experiments, I used a resistant line that contains the *APR* gene *Yr46* which encodes a sugar transporter (Moore et al., 2015). *Yr46* increases resistance to both rusts and powdery mildew, which are distantly related biotrophic pathogens. As a control, I used the near-isogenic susceptible line cv. Thatcher. The Yr46 transporter is homologous to the Arabidopsis Sugar Transporter Protein 13 (STP13), which has been reported to play a role in immunity to the bacterium *Pseudomonas syringae* (Yamada et al., 2016). The homolog in grapevine, VvHXT5, has been reported to increase sugar accumulation in infected tissue, which benefits the growth of the pathogen *Erysiphe necator* (Hayes et al., 2010). Other sugar transporter genes such as *SWEETs* act as susceptibility genes, as bacterial pathogens can induce their expression to increase the transport of sucrose to the apoplast where the bacterium resides (Boch and Bonas, 2010). In general, the data suggest that creating new sinks stimulates susceptibility, while removing sinks increases resistance. This concept correlates with one of the roles of VvHXT5 which increases sink strength in plants susceptible to the oomycete powdery mildew (Hayes et al., 2010). Therefore, the role of Yr46 could be to maintain the flag leaf's metabolic status as source tissue by reducing the accumulation of glucose in infected cells. Yr46 is a H^+/hexose symporter (Moore et al., 2015). Based on this, I propose that Yr46 reduces the capacity of the flag leaves to import hexoses, keeping the tissue as source. This is similar to the hypothesis of Moore and collaborators (2015). *Pst* is still able to grow to some extent in *Yr46* plants, so some sugar must be available. Similarly to STP13, the capacity to transport sugars in *Yr46* plants might change during infection (Yamada et al., 2016). Possibly, Yr46 is still able to import glucose to the cell, but only at low levels that sustains the *Pst* biotrophic phase but not the production of spores.

I suggested that *Pst* infection induces nutrient reallocation towards infected leaves. This also occurs naturally in the plant, during senescence and sugar starvation. Senescence is the last

metabolic stage of plant tissues. Plants recycle carbon and nitrogen components by exporting them to other leaves (Avila-Ospina et al., 2014). Sugar starvation, on the other hand, is the lack of nutrients in the cell. This triggers the reduction in available carbohydrates by decreasing starch consumption at night (Morkunas et al., 2012; Sulpice et al., 2009). I assessed if senescence and sugar starvation signals are triggered during infection in susceptible plants as a response to changes in nutrient levels. I measured the gene expression levels of two senescence associated genes (*SAGs*), and determined the starch levels at night. I found that starch in both healthy and infected levels was completely consumed at night. The expression levels of *SAGs* were similar between healthy and infected plants. Based on these results, it seems that senescence and sugar starvation signals were not triggered during infection. Nevertheless, the experiments should be repeated in *Yr46* resistant lines as plants carrying the *APR* gene *Yr18* typically display senescence in leaf tips, which may prevent fungal growth or induce the mobilization of nutrients to other leaves (Häffner et al., 2015). Senescence signals triggered by pathogen recognition could be a strategy to control biotrophic pathogens because they need to keep the tissue alive to proliferate. Senescence may also influence the biotrophic growth phase of hemibiotrophic pathogens. Rice plants expressing *Yr18* exhibited partial resistance to the fungal pathogen *Magnaporthe oryzae* (Krattinger et al., 2016). Resistance genes and fungicides are widely used to control plant disease. However they can be easily overcome over time (Ellis et al., 2014). It would be interesting to evaluate in the long term how senescence counteracts biotrophic fungi and if it could influence colonization by necrotrophic pathogens. For example, could senescence responses open new niches for necrotrophic pathogens?

Plant hormones were not the focus of this thesis, however future studies should examine their roles during biotrophic interactions. Hormones can regulate carbon partitioning, and fungi can produce molecules similar to plant hormones to manipulate plant responses (Chanclud and Morel, 2016). The classic example is the hormone gibberellin, which is involved in stem elongation, seed germination, and flowering. In 1938, studying the foolish seedling rice disease, a Japanese group found that the fungal pathogen *Gibberella fujikuroi* (*Fusarium moniliforme*) secretes a substance to induce seedling elongation. This substance was identified and named gibberellin after the pathogen (De Bruyne et al., 2014). Another example is barley leaves infected with *Puccinia hordei,* which develop a green island phenotype around disease lesions due to an increase in chlorophyll content (Scholes and Farrar, 1987). One hypothesis for this phenotype is that *P. hordei* induces or secretes cytokinins to maintain carbon fixation (Scholes and Farrar, 1987; Stirk et al., 2006). As a consequence, there is a continuous supply of nutrients towards the infection. Two further hormones well-studied in plant pathogen interactions are salicylic acid (SA) and jasmonic acid (JA). SA and JA work antagonistically (Fan et al., 2009). They

regulate defense responses against biotrophic and necrotrophic pathogens, respectively. The levels of these hormones are affected by the hormone abscisic acid (ABA). It seems that ABA induces JA accumulation but suppresses SA-related responses (Carvalho et al., 2015). This correlates with the fact that ABA is associated with susceptibility to biotrophic fungal infections. For example, ABA is manipulated by the hemibiotrophic bacterial pathogen *Pseudomonas syringae* to reduce SA responses, allowing colonization (Fan et al., 2009; Großkinsky et al., 2014). ABA also seems to be necessary for colonization by arbuscular mycorrhizal fungi (Lievens et al., 2017). This could be related to its role in plant cell wall sensing (Hamann et al., 2009). Moreover, ABA induces the expression of the hexose transporter gene *VvHT5* in grapevine. This gene is upregulated specifically during grapevine powdery mildew infection in susceptible grapevine (Hayes et al., 2010). Possibly the induction of *VvHT5* during infection is mediated by ABA, increasing the flow of carbon towards the infection. The involvement of ABA, cytokinins, SA, and JA in biotrophic interactions raises several hypotheses that should be addressed in future studies. The first is that biotrophic fungi mimic or take advantage of abiotic stress responses to increase and maintain the flow of nutrients towards the site of infection, changing the tissue metabolism to sink. For example, ABA is also associated with tolerance to drought by closing stomata, and this reduces photosynthesis rates (Fan et al., 2009). ABA might benefit *Pst* infection before colonization, as the germinated spores need to penetrate the cell wall through stomata. In the cytoplasm, ABA signals interact with SNF1-related kinase 2 (SnRK2) a serine/threonine kinase (Miyakawa et al., 2013). SnRK2 responds to abiotic stresses and regulates several metabolic processes, such as growth regulation and stress tolerance. It will be interesting to evaluate if SnRK2 affects sugar levels during *Pst* infection. Alternatively, a second hypothesis is that primary plant responses are associated with cell wall perception events such as wounding as the fungus attempts to penetrate the cell wall. The fungus selectively avoids host oxidative responses but allows the accumulation of hexoses (Mittler and Blumwald, 2015). This idea still needs to be evaluated in the laboratory, as presumably fungus produces polyols to quench ROS (Voegele et al., 2005). In general hormones may interconnect pathways to coordinate responses to development, abiotic and biotic stresses.

In my thesis, I suggested that plant immunity and development should be studied together, and that systemic responses provide additional information to understand the infection. I suggest including markers such as specific enzymes that act unidirectionally in key metabolic pathways. These could indicate if carbon and/or nitrogen components are used in anabolism or catabolism pathways. This will reveal what the pathway is doing during biotrophic interactions, and possibly which are the major resources used by the plant and pathogen. The canonical thinking in the field of plant immunity is that recognition of pathogen molecules trigger defence responses,

similar to the well-mapped pathways in animals. Here I propose that plants might recognize what the pathogens are doing. The main goal of pathogens is to take nutrients from the plant. For this, they alter plant metabolism, a tightly regulated group of pathways, directly or indirectly. Therefore, the plant may recognise, possibly indirectly, imbalances or alterations of these pathways, triggering stress responses. This type of resistance could be a stable strategy to reduce fungal infection, as the pathogen would have to change its infection strategy to successfully colonize the plant

REFERENCES

Abedon, B.G., and Tracy, W.F. (1996). Corngrass 1 of maize (*Zea mays* L.) delays development of adult plant resistance to common rust (*Puccinia sorghi Schw.*) and european corn borer (*Ostrinia nubilalis Hubner*). J. Hered. *87*, 219–223.

Ali, S., Gladieux, P., Leconte, M., Gautier, A., Justesen, A.F., Hovmøller, M.S., Enjalbert, J., and de Vallavieille-Pope, C. (2014). Origin, migration routes and worldwide population genetic structure of the wheat yellow rust pathogen *Puccinia striiformis* f.sp. *tritici*. PLoS Pathog 10, e1003903.

Allen, P.J. (1965). Metabolic aspects of spore germination in fungi. Annu. Rev. Phytopathol. *3*, 313–342.

Anderson, J.M. (1986). Photoregulation of the composition, function, and structure of thylakoid membranes. Annu. Rev. Plant Physiol. *37*, 93–136.

Antico, C.J., Colon, C., Banks, T., and Ramonell, K.M. (2012). Insights into the role of jasmonic acid-mediated defenses against necrotrophic and biotrophic fungal pathogens. Front. Biol. *7*, 48–56.

Asai, Y., and Kobayashi, Y. (2016). Increased expression of the tomato SISWEET15 gene during grey mold infection and the possible involvement of the sugar efflux to apoplasm in the disease susceptibility. J. Plant Pathol. Microbiol. *07*.

Ascencio-Ibáñez, J.T., Sozzani, R., Lee, T.-J., Chu, T.-M., Wolfinger, R.D., Cella, R., and Hanley-Bowdoin, L. (2008). Global analysis of Arabidopsis gene expression uncovers a complex array of changes impacting pathogen response and cell cycle during geminivirus infection. Plant Physiol. *148*, 436–454.

Avila-Ospina, L., Moison, M., Yoshimoto, K., and Masclaux-Daubresse, C. (2014). Autophagy, plant senescence, and nutrient recycling. J. Exp. Bot. *65*, 3799–3811.

Ayliffe, M., Devilla, R., Mago, R., White, R., Talbot, M., Pryor, A., and Leung, H. (2011). Nonhost resistance of rice to rust pathogens. Mol Plant Microbe Interact *24*, 1143–1155.

Ayliffe, M., Periyannan, S.K., Feechan, A., Dry, I., Schumann, U., Wang, M.-B., Pryor, A., and Lagudah, E. (2013). A simple method for comparing fungal biomass in infected plant tissues. Mol. Plant. Microbe Interact. *26*, 658–667.

Bancal, M.-O., Hansart, A., Sache, I., and Bancal, P. (2012). Modelling fungal sink competitiveness with grains for assimilates in wheat infected by a biotrophic pathogen. Ann. Bot. *110*, 113–123.

Barros, J., Serrani-Yarce, J.C., Chen, F., Baxter, D., Venables, B.J., and Dixon, R.A. (2016). Role of bifunctional ammonia-lyase in grass cell wall biosynthesis. Nat. Plants *2*, 16050.

Baud, S., Boutin, J.-P., Miquel, M., Lepiniec, L., and Rochat, C. (2002). An integrated overview of seed development in *Arabidopsis thaliana* ecotype WS. Plant Physiol. Biochem. *40*, 151–160.

Baum, G., Chen, Y., Arazi, T., Takatsuji, H., and Fromm, H. (1993). A plant glutamate decarboxylase containing a calmodulin binding domain. Cloning, sequence, and functional analysis. J. Biol. Chem. *268*, 19610–19617.

Beddow, J.M., Pardey, P.G., Chai, Y., Hurley, T.M., Kriticos, D.J., Braun, H.-J., Park, R.F., Cuddy, W.S., and Yonow, T. (2015). Research investment implications of shifts in the global geography of wheat stripe rust. Nat. Plants 15132.

Berger, S., Benediktyová, Z., Matouš, K., Bonfig, K., Mueller, M.J., Nedbal, L., and Roitsch, T. (2007). Visualization of dynamics of plant–pathogen interaction by novel combination of chlorophyll fluorescence imaging and statistical analysis: differential effects of virulent and avirulent strains of *P. syringae* and of oxylipins on *A. thaliana*. J Exp Bot *58*, 797–806.

Bernoux, M., Ellis, J.G., and Dodds, P.N. (2011). New insights in plant immunity signaling activation. Curr Opin Plant Biol *14*, 512–518.

Bethenod, O., Le Corre, M., Huber, L., and Sache, I. (2005). Modelling the impact of brown rust on wheat crop photosynthesis after flowering. Agric. For. Meteorol. *131*, 41–53.

Bhunia, S.K., Saha, A., Maity, A.R., Ray, S.C., and Jana, N.R. (2013). Carbon nanoparticle-based fluorescent bioimaging Probes. Sci. Rep. *3*.

Bilgin, D.D., Zavala, J.A., Zhu, J., Clough, S.J., Ort, D.R., and DeLUCIA, E.H. (2010). Biotic stress globally downregulates photosynthesis genes. Plant Cell Environ. *33*, 1597–1613.

Boch, J., and Bonas, U. (2010). *Xanthomonas* AvrBs3 Family-Type III effectors: discovery and function. Annu Rev Phytopathol *48*.

Boeckx, T., Winters, A.L., Webb, K.J., and Kingston-Smith, A.H. (2015). Polyphenol oxidase in leaves: is there any significance to the chloroplastic localization? J. Exp. Bot. *66*, 3571–3579.

Bolger, A.M., Lohse, M., and Usadel, B. (2014). Trimmomatic: a flexible trimmer for Illumina sequence data. Bioinformatics *30*, 2114–2120.

Bonde, M.R., Nester, S.E., and Berner, D.K. (2012). Effects of soybean leaf and plant age on susceptibility to initiation of infection by *Phakopsora pachyrhizi*. Plant Health Prog.

Bonfig, K.B., Gabler, A., Simon, U.K., Luschin-Ebengreuth, N., Hatz, M., Berger, S., Muhammad, N., Zeier, J., Sinha, A.K., and Roitsch, T. (2010a). Post-translational derepression of invertase activity in source leaves via down-regulation of invertase inhibitor expression is part of the plant defense response. Mol. Plant *3*, 1037–1048.

Bonfig, K.B., Gabler, A., Simon, U.K., Luschin-Ebengreuth, N., Hatz, M., Berger, S., Muhammad, N., Zeier, J., Sinha, A.K., and Roitsch, T. (2010b). Post-translational derepression of invertase activity in source leaves via down-regulation of invertase inhibitor expression is part of the plant defense response. Mol. Plant *3*, 1037–1048.

Börnke, F., and Sonnewald, S. (2011). Biosynthesis and metabolism of starch and sugars. In Plant Metabolism and Biotechnology, H. Ashihara, A. Crozier, and A. Komamine, eds. (John Wiley & Sons, Ltd), pp. 1–25.

Both, M., Csukai, M., Stumpf, M.P.H., and Spanu, P.D. (2005). Gene expression profiles of *Blumeria graminis* indicate dynamic changes to primary metabolism during development of an obligate biotrophic Pathogen. Plant Cell *17*, 2107–2122.

Bouwmeester, K., Han, M., Blanco-Portales, R., Song, W., Weide, R., Guo, L.-Y., van der Vossen, E.A.G., and Govers, F. (2014). The Arabidopsis lectin receptor kinase LecRK-I.9 enhances resistance to *Phytophthora infestans* in Solanaceous plants. Plant Biotechnol. J. *12*, 10–16.

Braun, D.M., and Slewinski, T.L. (2009). Genetic Control of Carbon Partitioning in Grasses: Roles of Sucrose Transporters and Tie-dyed Loci in Phloem Loading. Plant Physiol. *149*, 71–81.

Bushnell W, R.A. (1984). The Cereal Rust (St. Paul, Minnesota: Academic Press, Inc).

Cabib, E., Shaw, J.A., Mol, P.C., Bowers, B., and Choi, W.-J. (1996). Chitin biosynthesis and morphogenetic processes. In biochemistry and molecular biology, P.D.R. Brambl, and P.D.G.A. Marzluf, eds. (Springer Berlin Heidelberg), pp. 243–267.

von Caemmerer, S., Evans, J., Hudson, G., and Andrews, T.J. (1994). The kinetics of ribulose-1,5-bisphosphate carboxylase/oxygenase in vivo inferred from measurements of photosynthesis in leaves of transgenic tobacco. Planta *195*, 88–97.

Calenge, F., Saliba-Colombani, V., Mahieu, S., Loudet, O., Daniel-Vedele, F., and Krapp, A. (2006). Natural variation for carbohydrate content in Arabidopsis. Interaction with complex traits dissected by quantitative genetics. Plant Physiol. *141*, 1630–1643.

Calonge, F.D. (1967). Chlorophyll and total nitrogen in barley rust infection. Trans. Br. Mycol. Soc. *50*, 397-IN2.

Cantu, D., Govindarajulu, M., Kozik, A., Wang, M., Chen, X., Kojima, K.K., Jurka, J., Michelmore, R.W., and Dubcovsky, J. (2011). Next generation sequencing provides rapid access to the genome of *Puccinia striiformis* f. sp. *tritici*, the causal Agent of wheat stripe rust. PLoS ONE *6*, e24230.

Cao, Y., Liang, Y., Tanaka, K., Nguyen, C.T., Jedrzejczak, R.P., Joachimiak, A., and Stacey, G. (2014). The kinase LYK5 is a major chitin receptor in Arabidopsis and forms a chitin-induced complex with related kinase CERK1. ELife *3*, e03766.

Carretero, R., Bancal, M.O., and Miralles, D.J. (2011). Effect of leaf rust (*Puccinia triticina*) on photosynthesis and related processes of leaves in wheat crops grown at two contrasting sites and with different nitrogen levels. Eur. J. Agron. *35*, 237–246.

Carvalho, L.C., Vidigal, P., and Amâncio, S. (2015). Oxidative stress homeostasis in grapevine (*Vitis vinifera* L.). Front. Environ. Sci. *3*.

de Carvalho, M.C. da C.G., Costa Nascimento, L., Darben, L.M., Polizel-Podanosqui, A.M., Lopes-Caitar, V.S., Qi, M., Rocha, C.S., Carazzolle, M.F., Kuwahara, M.K., Pereira, G.A.G., et al. (2016). Prediction of the in planta *Phakopsora pachyrhizi* secretome and potential effector families. Mol. Plant Pathol. *18*, 363–377.

Cass, C.L., Peraldi, A., Dowd, P.F., Mottiar, Y., Santoro, N., Karlen, S.D., Bukhman, Y.V., Foster, C.E., Thrower, N., Bruno, L.C., et al. (2015). Effects of Phenylalanine Ammonia Lyase (PAL) knockdown on cell wall composition, biomass digestibility, and biotic and abiotic stress responses in *Brachypodium*. J. Exp. Bot. *66*, 4317–4335.

Catanzariti, A.M., Dodds, P.N., Lawrence, G.J., Ayliffe, M.A., and Ellis, J.G. (2006). Haustorially expressed secreted proteins from flax rust are highly enriched for avirulence elicitors. Plant Cell *18*, 243–256.

Cesari, S., Moore, J., Chen, C., Webb, D., Periyannan, S., Mago, R., Bernoux, M., Lagudah, E.S., and Dodds, P.N. (2016). Cytosolic activation of cell death and stem rust resistance by cereal MLA-family CC–NLR proteins. Proc. Natl. Acad. Sci. 201605483.

Chanclud, E., and Morel, J.-B. (2016). Plant hormones: a fungal point of view. Mol. Plant Pathol. *17*, 1289–1297.

Chang, Q., Liu, J., Wang, Q., Han, L., Liu, J., Li, M., Huang, L., Yang, J., and Kang, Z. (2013). The effect of *Puccinia striiformis f. sp. tritici* on the levels of water-soluble carbohydrates and the photosynthetic rate in wheat leaves. Physiol. Mol. Plant Pathol. *84*, 131–137.

Chen, L.-Q. (2014). SWEET sugar transporters for phloem transport and pathogen nutrition. New Phytol. *201*, 1150–1155.

Chen, H.-Y., Huh, J.-H., Yu, Y.-C., Ho, L.-H., Chen, L.-Q., Tholl, D., Frommer, W.B., and Guo, W.-J. (2015a). The Arabidopsis vacuolar sugar transporter SWEET2 limits carbon sequestration from roots and restricts *Pythium* infection. Plant J. *83*, 1046–1058.

Chen, L.-Q., Hou, B.-H., Lalonde, S., Takanaga, H., Hartung, M.L., Qu, X.-Q., Guo, W.-J., Kim, J.-G., Underwood, W., Chaudhuri, B., et al. (2010). Sugar transporters for intercellular exchange and nutrition of pathogens. Nature *468*, 527–532.

Chen, W., Wellings, C., Chen, X., Kang, Z., and Liu, T. (2014). Wheat stripe (yellow) rust caused by *Puccinia striiformis f. sp. tritici*. Mol. Plant Pathol. *15*, 433–446.

Chen, Y.-E., Cui, J.-M., Su, Y.-Q., Yuan, S., Yuan, M., and Zhang, H.-Y. (2015b). Influence of stripe rust infection on the photosynthetic characteristics and antioxidant system of susceptible and resistant wheat cultivars at the adult plant stage. Plant Physiol. 779.

Cheung, A.Y., and Wu, H.-M. (2011). THESEUS 1, FERONIA and relatives: a family of cell wall-sensing receptor kinases? Curr. Opin. Plant Biol. *14*, 632–641.

Chini, A., Fonseca, S., Fernandez, G., Adie, B., Chico, J.M., Lorenzo, O., Garcia-Casado, G., Lopez-Vidriero, I., Lozano, F.M., Ponce, M.R., et al. (2007). The JAZ family of repressors is the missing link in jasmonate signalling. Nature *448*, 666–671.

Clancy, F.G., and Coffey, M.D. (1980). Patterns of translocation, changes in invertase activity, and polyol formation in susceptible and resistant flax infected with the rust fungus *Melampsora lini*. Physiol. Plant Pathol. *17*, 41–52.

Clark, J.S.C., and Spencer-Phillips, P.T.N. (1993). Accumulation of photoassimilate by Peronospora viciae (Berk.) Casp. and leaves of Pisum sativum L.: evidence for nutrient uptake via intercellular hyphae. New Phytol. 124, 107–119.

Cloutier, S., McCallum, B.D., Loutre, C., Banks, T.W., Wicker, T., Feuillet, C., Keller, B., and Jordan, M.C. (2007). Leaf rust resistance gene Lr1, isolated from bread wheat (*Triticum aestivum* L.) is a member of the large psr567 gene family. Plant Mol. Biol. *65*, 93–106.

Coffey, M.D., Palevitz, B.A., and Allen, P.J. (1972). The fine structure of two rust fungi, *Puccinia helianthi* and *Melampsora lini*. Can. J. Bot. *50*, 231–240.

Coleman, H.D., Yan, J., and Mansfield, S.D. (2009). Sucrose synthase affects carbon partitioning to increase cellulose production and altered cell wall ultrastructure. Proc. Natl. Acad. Sci. *106*, 13118–13123.

Coll, N.S., Vercammen, D., Smidler, A., Clover, C., Breusegem, F.V., Dangl, J.L., and Epple, P. (2010). Arabidopsis Type I metacaspases control cell death. Science *330*, 1393–1397.

Cook, D.E., Mesarich, C.H., and Thomma, B.P.H.J. (2015). Understanding plant immunity as a surveillance system to detect invasion. Annu. Rev. Phytopathol. *53*, 541–563.

Cooper, B., Neelam, A., Campbell, K.B., Lee, J., Liu, G., Garrett, W.M., Scheffler, B., and Tucker, M.L. (2007). Protein accumulation in the germinating *Uromyces appendiculatus* Uredospore. Mol. Plant. Microbe Interact. *20*, 857–866.

Cossins, E.A., and Chen, L. (1997). Folates and one-carbon metabolism in plants and fungi. Phytochemistry *45*, 437–452.

Crampton, B.G., Hein, I., and Berger, D.K. (2009). Salicylic acid confers resistance to a biotrophic rust pathogen, *Puccinia substriata*, in pearl millet (Pennisetum glaucum). Mol. Plant Pathol. *10*, 291–304.

Crouzet, J., Trombik, T., Fraysse, Å.S., and Boutry, M. (2006). Organization and function of the plant pleiotropic drug resistance ABC transporter family. FEBS Lett. *580*, 1123–1130.

Cuddy, W., Parl, R., Bariana, H., Singh, D., Roake, J., and Platz, G. (2016). Cereal rust report (Plant breeding institute, The university of Sydney).

Cunnac, S., Lindeberg, M., and Collmer, A. (2009). *Pseudomonas syringae* type III secretion system effectors: repertoires in search of functions. Curr Opin Microbiol *12*, 53–60.

Curie, C., Cassin, G., Couch, D., Divol, F., Higuchi, K., Le Jean, M., Misson, J., Schikora, A., Czernic, P., and Mari, S. (2009). Metal movement within the plant: contribution of nicotianamine and yellow stripe 1-like transporters. Ann. Bot. *103*, 1–11.

Dakouri, A., McCallum, B., Radovanovic, N., and Cloutier, S. (2013). Molecular and phenotypic characterization of seedling and adult plant leaf rust resistance in a world wheat collection. Mol. Breed. 1–15.

Daly, J.M., Knoche, H.W., and Wiese, M.V. (1967). Carbohydrate and lipid metabolism during germination of uredospores of *Puccinia graminis tritici.* Plant Physiol. *42*, 1633–1642.

De Bruyne, L., Höfte, M., and De Vleesschauwer, D. (2014). Connecting Growth and Defense: The emerging roles of brassinosteroids and gibberellins in plant innate immunity. Mol. Plant *7*, 943–959.

De Wit, P.J.G.M. de (2016). *Cladosporium fulvum* Effectors: weapons in the arms race with tomato. Annu. Rev. Phytopathol. *54*, 1–23.

Delledonne, M., Xia, Y., Dixon, R.A., and Lamb, C. (1998). Nitric oxide functions as a signal in plant disease resistance. Nature *394*, 585–588.

Denissen, C.J.M. (1993). Components of adult plant resistance to leaf rust in wheat. Euphytica *70*, 131–140.

Devadas, R., Simpfendorfer, S., Backhouse, D., and Lamb, D.W. Effect of stripe rust on the yield response of wheat to nitrogen. Crop J.

Dias, A.P.S., Li, X., Harmon, P.F., Harmon, C.L., and Yang, X.B. (2010). Effects of shade intensity and duration on asian soybean rust caused by *Phakopsora pachyrhizi*. Plant Dis. *95*, 485–489.

Dixon, R.A., and Paiva, N.L. (1995). Stress-induced phenylpropanoid metabolism. Plant Cell *7*, 1085–1097.

Dobon, A., Bunting, D.C.E., Cabrera-Quio, L.E., Uauy, C., and Saunders, D.G.O. (2016). The host-pathogen interaction between wheat and yellow rust induces temporally coordinated waves of gene expression. BMC Genomics *17*, 380.

Dodds, P.N., and Lagudah, E.S. (2016). Starving the enemy. Science *354*, 1377–1378.

Dodds, P.N., and Rathjen, J.P. (2010). Plant immunity: towards an integrated view of plant–pathogen interactions. Nat Rev Genet *11*, 539–548.

Dodds, P.N., Lawrence, G.J., Catanzariti, A.M., Ayliffe, M.A., and Ellis, J.G. (2004). The *Melampsora lini* AvrL 567 avirulence genes are expressed in haustoria and their products are recognized inside plant cells. Plant Cell *16*, 755–768.

Doehlemann, G., Wahl, R., Horst, R.J., Voll, L.M., Usadel, B., Poree, F., Stitt, M., Pons-Kuhnemann, J., Sonnewald, U., Kahmann, R., et al. (2008). Reprogramming a maize plant: transcriptional and metabolic changes induced by the fungal biotroph *Ustilago maydis*. Plant J *56*, 181–195.

Domergue, F., Vishwanath, S.J., Joubès, J., Ono, J., Lee, J.A., Bourdon, M., Alhattab, R., Lowe, C., Pascal, S., Lessire, R., et al. (2010). Three Arabidopsis fatty acyl-coenzyme A reductases, FAR1, FAR4, and FAR5, generate primary fatty alcohols associated with suberin deposition. Plant Physiol. *153*, 1539–1554.

Dong, Y., Li, B., Malitsky, S., Rogachev, I., Aharoni, A., Kaftan, F., Svatoš, A., and Franceschi, P. (2016). Sample preparation for Mass spectrometry imaging of plant tissues: A Review. Front. Plant Sci. *7*.

Doodson, J.K., Manners, J.G., and Myers, A. (1965). Some effects of yellow rust (*Puccinia striiformis)* on 14Carbon assimilation and translocation in wheat. J. Exp. Bot. *16*, 304–317.

Du Fall, L.A., and Solomon, P.S. (2013). The necrotrophic effector SnToxA induces the synthesis of a novel phytoalexin in wheat. New Phytol. *200*, 185–200.

Duplessis, S., Cuomo, C.A., Lin, Y.-C., Aerts, A., Tisserant, E., Veneault-Fourrey, C., Joly, D.L., Hacquard, S., Amselem, J., Cantarel, B.L., et al. (2011). Obligate biotrophy features unraveled by the genomic analysis of rust fungi. Proc. Natl. Acad. Sci.

Ehrlich, M.A., and Ehrlich, H.G. (1969). Uredospore development in *Puccinia graminis.* Can. J. Bot. *47*, 2061–2064.

Ellis, J.G., lagudah, E., Spielmeyer, W., and dodds, peter (2014). The past, present and future of breeding rust resistant wheat. Front. Plant Sci. *5*.

Elmore, J.M., Lin, Z.-J.D., and Coaker, G. (2011). Plant NB-LRR signaling: Upstreams and Downstreams. Curr. Opin. Plant Biol. *14*, 365–371.

Eom, J.-S., Chen, L.-Q., Sosso, D., Julius, B.T., Lin, I., Qu, X.-Q., Braun, D.M., and Frommer, W.B. (2015). SWEETs, transporters for intracellular and intercellular sugar translocation. Curr. Opin. Plant Biol. *25*, 53–62.

Erayman, M., Turktas, M., Akdogan, G., Gurkok, T., Inal, B., Ishakoglu, E., Ilhan, E., and Unver, T. (2015). Transcriptome analysis of wheat inoculated with *Fusarium graminearum.* Front. Plant Sci. *6*.

Fan, J., Hill, L., Crooks, C., Doerner, P., and Lamb, C. (2009). Abscisic acid has a key role in modulating diverse plant-pathogen interactions. Plant Physiol.

Farquhar, G.D., Caemmerer, S., and Berry, J.A. (1980). A biochemical model of photosynthetic CO2 assimilation in leaves of C3 species. Planta *149*, 78–90.

Farrow, S.C., and Facchini, P.J. (2014). Functional diversity of 2-oxoglutarate/Fe(II)-dependent dioxygenases in plant metabolism. Front. Plant Sci. *5*.

Felle, H.H., Herrmann, A., Hanstein, S., Hückelhoven, R., and Kogel, K.-H. (2004). Apoplastic pH signaling in barley leaves attacked by the powdery mildew fungus *Blumeria graminis f. sp. hordei*. Mol. Plant-Microbe Interact. MPMI *17*, 118–123.

Figueiredo, A., Monteiro, F., and Sebastiana, M. (2014). Subtilisin-like proteases in plant–pathogen recognition and immune priming: a perspective. Front. Plant Sci. *5*.

Flor, H.H. (1971). Current Status of the Gene-For-Gene Concept. Annu Rev Phytopathol *9*, 275–296.

Fox, S.E., Geniza, M., Hanumappa, M., Naithani, S., Sullivan, C., Preece, J., Tiwari, V.K., Elser, J., Leonard, J.M., Sage, A., et al. (2014). De-novo transcriptome assembly and analyses of gene expression during photomorphogenesis in diploid wheat *Triticum monococcum*. PLoS ONE *9*.

Francoz, E., Ranocha, P., Nguyen-Kim, H., Jamet, E., Burlat, V., and Dunand, C. (2015). Roles of cell wall peroxidases in plant development. Phytochemistry *112*, 15–21.

Frémont, N., Riefler, M., Stolz, A., and Schmülling, T. (2013). The Arabidopsis TUMOR PRONE5 Gene encodes an acetylornithine aminotransferase required for arginine biosynthesis and root meristem maintenance in blue light1[C][W][OA]. Plant Physiol. *161*, 1127–1140.

Fu, D., Uauy, C., Distelfeld, A., Blechl, A., Epstein, L., Chen, X., Sela, H., Fahima, T., and Dubcovsky, J. (2009). A kinase-START gene confers temperature-dependent resistance to wheat stripe rust. Science *323*, 1357–1360.

Gamm, M., Héloir, M.-C., Bligny, R., Vaillant-Gaveau, N., Trouvelot, S., Alcaraz, G., Frettinger, P., Clément, C., Pugin, A., Wendehenne, D., et al. (2011). Changes in carbohydrate metabolism in *Plasmopara viticola*infected grapevine leaves. Mol. Plant. Microbe Interact. *24*, 1061–1073.

Gao, H., Niu, J., Yang, X., He, D., and Wang, C. (2014). Impacts of powdery mildew on wheat grain sugar metabolism and starch accumulation in developing grains. Starch - Stärke *66*, 947–958.

Garnica, D.P., Upadhyaya, N.M., Dodds, P.N., and Rathjen, J.P. (2013). Strategies for wheat stripe rust pathogenicity identified by transcriptome sequencing. PLoS ONE *8*, e67150.

Garnica, D.P., Nemri, A., Upadhyaya, N.M., Rathjen, J.P., and Dodds, P.N. (2014). The ins and outs of rust haustoria. PLoS Pathog. *10*.

Gaufichon, L., Reisdorf-Cren, M., Rothstein, S.J., Chardon, F., and Suzuki, A. (2010). Biological functions of asparagine synthetase in plants. Plant Sci. *179*, 141–153.

Gilkerson, J., Perez-Ruiz, J.M., Chory, J., and Callis, J. (2012). The plastid-localized pfkB-type carbohydrate kinases FRUCTOKINASE-LIKE 1 and 2 are essential for growth and development of Arabidopsis thaliana. BMC Plant Biol. *12*, 102.

Gimenez-Ibanez, S., Ntoukakis, V., and Rathjen, J.P. (2009). The LysM receptor kinase CERK1 mediates bacterial perception in Arabidopsis. Plant Signal. Behav. *4*, 539–541.

Gou, J.-Y., Li, K., Wu, K., Wang, X., Lin, H., Cantu, D., Uauy, C., Dobon-Alonso, A., Midorikawa, T., Inoue, K., et al. (2015). Wheat stripe rust resistance protein WKS1 reduces the ability of the thylakoid-associated ascorbate peroxidase to detoxify reactive oxygen species. Plant Cell.

Govind, S.R., Jogaiah, S., Abdelrahman, M., Shetty, H.S., and Tran, L.-S.P. (2016). Exogenous trehalose treatment Enhances the activities of defense-related enzymes and triggers resistance against downy mildew disease of pearl millet. Front. Plant Sci. *7*.

Govindjee (2002). A Role for a light-harvesting antenna complex of photosystem II in photoprotection. Plant Cell Online *14*, 1663–1668.

Granot, D., David-Schwartz, R., and Kelly, G. (2013). Hexose kinases and their role in sugar-sensing and plant development. Front Plant Sci *4*, 44.

Griffey, C.A. (1993). Effectiveness of adult-plant pesistance in reducing grain yield loss to powdery mildew in winter Wheat. Plant Dis. *77*, 618.

Großkinsky, D.K., van der Graaff, E., and Roitsch, T. (2014). Abscisic acid–cytokinin antagonism modulates resistance against *Pseudomonas syringae* in tobacco. Phytopathology *104*, 1283–1288.

Guo, P., Cao, Y., Li, Z., and Zhao, B. (2004). Role of an endogenous nitric oxide burst in the resistance of wheat to stripe rust. Plant Cell Environ. *27*, 473–477.

Gururani, M.A., Venkatesh, J., Upadhyaya, C.P., Nookaraju, A., Pandey, S.K., and Park, S.W. (2012). Plant disease resistance genes: Current status and future directions. Physiol. Mol. Plant Pathol. *78*, 51–65.

Hacquard, S., Kracher, B., Hiruma, K., Münch, P.C., Garrido-Oter, R., Thon, M.R., Weimann, A., Damm, U., Dallery, J.-F., Hainaut, M., et al. (2016). Survival trade-offs in plant roots during colonization by closely related beneficial and pathogenic fungi. Nat. Commun. *7*, 11362.

Häffner, E., Konietzki, S., and Diederichsen, E. (2015). Keeping control: The role of senescence and development in plant pathogenesis and defense. Plants *4*, 449–488.

Hahn, M., and Mendgen, K. (1997). Characterization of In Planta—Induced rust genes isolated from a haustorium-sSpecific cDNA library. Mol. Plant. Microbe Interact. *10*, 427–437.

Hahn, M., Neef, U., Struck, C., Gottfert, M., and Mendgen, K. (1997). A putative amino acid transporter is specifically expressed in haustoria of the rust fungus *Uromyces fabae*. Mol Plant Microbe Interact *10*, 438–445.

Hamann, T., Bennett, M., Mansfield, J., and Somerville, C. (2009). Identification of cell-wall stress as a hexose-dependent and osmosensitive regulator of plant responses. Plant J. *57*, 1015–1026.

Harbinson, J. (2013). Improving the accuracy of chlorophyll fluorescence measurements. Plant Cell Env. *36*, 1751–1754.

Harder, D.E., and Chong, J. (1984). Structure and Physiology of haustoria. In Origins, Specificity, Structure and Physiology, (Academic Press), pp. 431–476.

Harder, D.E., and Chong, J. (1991). Rust haustoria. in electron microscopy of plant pathogens, (Springer Berlin Heidelberg), pp. 235–250.

Harder, D.E., and Mendgen, K. (1982). Filipin-sterol complexes in bean rust- and oat crown rust-fungal/plant interactions: Freeze-Etch Electron Microscopy. Protoplasma *112*, 46–54.

Haruta, M., Sabat, G., Stecker, K., Minkoff, B.B., and Sussman, M.R. (2014). A Peptide hormone and its receptor protein Kinase Regulate Plant Cell Expansion. Science *343*, 408–411.

Hayafune, M., Berisio, R., Marchetti, R., Silipo, A., Kayama, M., Desaki, Y., Arima, S., Squeglia, F., Ruggiero, A., Tokuyasu, K., et al. (2014). Chitin-induced activation of immune signaling by the rice receptor CEBiP relies on a unique sandwich-type dimerization. Proc. Natl. Acad. Sci. U. S. A. *111*, E404–E413.

Hayes, M.A., Davies, C., and Dry, I.B. (2007). Isolation, functional characterization, and expression analysis of grapevine (Vitis vinifera L.) hexose transporters: differential roles in sink and source tissues. J Exp Bot *58*, 1985–1997.

Hayes, M.A., Feechan, A., and Dry, I.B. (2010). Involvement of Abscisic Acid in the Coordinated Regulation of a Stress-Inducible Hexose Transporter (VvHT5) and a Cell Wall Invertase in Grapevine in Response to Biotrophic Fungal Infection[W]. Plant Physiol. *153*, 211–221.

Heisterüber, D., Schulte, P., and Moerschbacher, B.M. (1994). Soluble carbohydrates and invertase activity in stem rust-infected, resistant and susceptible near-isogenic wheat leaves. Physiol. Mol. Plant Pathol. *45*, 111–123.

Hemetsberger, C., Herrberger, C., Zechmann, B., Hillmer, M., and Doehlemann, G. (2012). The Ustilago maydis effector Pep1 suppresses plant Immunity by inhibition of host peroxidase activity. PLOS Pathog *8*, e1002684.

Herrera-Foessel, S.A., Singh, R.P., Lillemo, M., Huerta-Espino, J., Bhavani, S., Singh, S., Lan, C., Calvo-Salazar, V., and Lagudah, E.S. (2014). Lr67/Yr46 confers adult plant resistance to stem rust and powdery mildew in wheat. Theor. Appl. Genet.

Hildebrandt, T.M., Nunes Nesi, A., Araújo, W.L., and Braun, H.-P. (2015). Amino Acid Catabolism in Plants. Mol. Plant *8*, 1563–1579.

Hindie, E., Coulomb, B., and Galle, P. (1992). SIMS microscopy: a tool to measure the intracellular concentration of carbon 14-labelled molecules. Biol. Cell *74*, 89–92.

Hoagland, D., and Arnon, D. (1950). The water-culture method for growing plants without soil. Calif. Agric. Exp. Stn. Circ. *347*, 1–32.

Hodson, D.P. (2011). Shifting boundaries: challenges for rust monitoring. Euphytica *179*, 93–104.

Hok, S., Danchin, E.G.J., Allasia, V., Panabières, F., Attard, A., and Keller, H. (2011). An Arabidopsis (malectin-like) leucine-rich repeat receptor-like kinase contributes to downy mildew disease. Plant Cell Environ. *34*, 1944–1957.

Holsters, M. (2008). SYMRK, an enigmatic receptor guarding and guiding microbial endosymbioses with plant roots. Proc. Natl. Acad. Sci. U. S. A. *105*, 4537–4538.

Horst, R.J., Engelsdorf, T., Sonnewald, U., and Voll, L.M. (2008). Infection of maize leaves with Ustilago maydis prevents establishment of C4 photosynthesis. Compat. Host-Microbe Interact. Strateg. Perspect. *165*, 19–28.

Horst, R.J., Doehlemann, G., Wahl, R., Hofmann, J., Schmiedl, A., Kahmann, R., Kämper, J., Sonnewald, U., and Voll, L.M. (2010a). *Ustilago maydis* infection strongly alters organic nitrogen allocation in maize and stimulates productivity of systemic source leaves. Plant Physiol *152*, 293–308.

Horst, R.J., Doehlemann, G., Wahl, R., Hofmann, J., Schmiedl, A., Kahmann, R., Kämper, J., and Voll, L.M. (2010b). A model of Ustilago maydis leaf tumor metabolism. Plant Signal. Behav. *5*, 1446–1449.

Hovmøller, M.S., Sørensen, C.K., Walter, S., and Justesen, A.F. (2011). Diversity of Puccinia striiformis on Cereals and Grasses. Annu. Rev. Phytopathol. *49*, 197–217.

Hovmøller, M.S., Walter, S., Bayles, R.A., Hubbard, A., Flath, K., Sommerfeldt, N., Leconte, M., Czembor, P., Rodriguez-Algaba, J., Thach, T., et al. (2016). Replacement of the European wheat yellow rust population by new races from the centre of diversity in the near-Himalayan region. Plant Pathol. *65*, 402–411.

Ikeda, Y., Koizumi, N., Kusano, T., and Sano, H. (2000). Specific Binding of a 14-3-3 Protein to Autophosphorylated WPK4, an SNF1-related wheat protein kinase, and to wpk4-phosphorylated nitrate reductase. J. Biol. Chem. *275*, 31695–31700.

Ishiga, Y., Rao Uppalapati, S., Gill, U.S., Huhman, D., Tang, Y., and Mysore, K.S. (2015). Transcriptomic and metabolomic analyses identify a role for chlorophyll catabolism and phytoalexin during Medicago nonhost resistance against Asian soybean rust. Sci. Rep. *5*, 13061.

Islam, T., Croll, D., Gladieux, P., Soanes, D., Persoons, A., Bhattacharjee, P., Hossain, S., Gupta, D., Rahman, M.M., Mahboob, M.G., et al. (2016). Emergence of wheat blast in Bangladesh was caused by a south american lineage of *Magnaporthe oryzae*. BioRxiv 059832.

Jackson, L.L., and Frear, D.S. (1967). Lipids of Rust Fungi: I. Lipid Metabolism of Germinating Flax Rust Uredospores. Can. J. Biochem. *45*, 1309–1315.

Jeyaprakash, A.A., Geetha Rani, P., Banuprakash Reddy, G., Banumathi, S., Betzel, C., Sekar, K., Surolia, A., and Vijayan, M. (2002). Crystal Structure of the Jacalin–T-antigen Complex and a Comparative Study of Lectin–T-antigen Complexes. J. Mol. Biol. *321*, 637–645.

Jia, J., Zhao, S., Kong, X., Li, Y., Zhao, G., He, W., Appels, R., Pfeifer, M., Tao, Y., Zhang, X., et al. (2013). Aegilops tauschii draft genome sequence reveals a gene repertoire for wheat adaptation. Nature *496*, 91–95.

Jiang, D., Yang, W., He, Y., and Amasino, R.M. (2007). Arabidopsis relatives of the human lysine-specific Demethylase1 repress the expression of FWA and FLOWERING LOCUS C and thus promote the floral transition. Plant Cell *19*, 2975–2987.

Jiang, Y., Wang, W., Xie, Q., Liu, N., Liu, L., Wang, D., Zhang, X., Yang, C., Chen, X., Tang, D., et al. (2017). Plants transfer lipids to sustain colonization by mutualistic mycorrhizal and parasitic fungi. Science eaam9970.

Jin, Y., Szabo, L.J., and Carson, M. (2010). Century-old mystery of *Puccinia striiformis* life history solved with the identification of Berberis as an alternate host. Phytopathology *100*, 432–435.

Joy, K.W. (1988). Ammonia, glutamine, and asparagine: a carbon–nitrogen interface. Can. J. Bot. *66*, 2103–2109.

K. Mendgen, M. Hahn, and Deising, and H. (1996). morphogenesis and mechanisms of penetration by plant pathogenic Fungi. Annu. Rev. Phytopathol. *34*, 367–386.

Kamruzzaman Munshi, M., Kobayashi, Y., and Shikanai, T. (2005). Identification of a novel protein, CRR7, required for the stabilization of the chloroplast NAD(P)H dehydrogenase complex in Arabidopsis. Plant J. *44*, 1036–1044.

Kandlbinder, A., Finkemeier, I., Wormuth, D., Hanitzsch, M., and Dietz, K.-J. (2004). The antioxidant status of photosynthesizing leaves under nutrient deficiency: redox regulation, gene expression and antioxidant activity in Arabidopsis thaliana. Physiol. Plant. *120*, 63–73.

Kemen, E., Kemen, A.C., Rafiqi, M., Hempel, U., Mendgen, K., Hahn, M., and Voegele, R.T. (2005). Identification of a protein from rust fungi transferred from haustoria into infected plant cells. Mol Plant Microbe Interact *18*, 1130–1139.

Kemen, E., Kemen, A., Ehlers, A., Voegele, R., and Mendgen, K. (2013). A novel structural effector from rust fungi is capable of fibril formation. Plant J. *75*, 767–780.

Kessler, S.A., Shimosato-Asano, H., Keinath, N.F., Wuest, S.E., Ingram, G., Panstruga, R., and Grossniklaus, U. (2010). Conserved molecular components for pollen tube reception and fungal invasion. Science *330*, 968–971.

Knauf, G.M., Welter, K., Muller, M., and Mendgen, K. (1989). The haustorial host-parasite interface in rust-infected bean leaves after high-pressure freezing. Physiol. Mol. Plant Pathol. *34*, 519–530.

Kneale, J., and Farrar, J.F. (1985). The Localization and Frequency of Haustoria in Colonies of Brown Rust on Barley Leaves. New Phytol. *101*, 495–505.

Koh, S., André, A., Edwards, H., Ehrhardt, D., and Somerville, S. (2005). Arabidopsis thaliana subcellular responses to compatible Erysiphe cichoracearum infections. Plant J. *44*, 516–529.

Kolmer, J.A., Ordonez, M.E., and Groth, J.V. (2001). The Rust Fungi. In ELS, (John Wiley & Sons, Ltd), p.

Kovinich, N., Kayanja, G., Chanoca, A., Otegui, M.S., and Grotewold, E. (2015). Abiotic stresses induce different localizations of anthocyanins in Arabidopsis. Plant Signal. Behav. *10*.

Krattinger, S.G., and Keller, B. (2016). Molecular genetics and evolution of disease resistance in cereals. New Phytol. *212*, 320–332.

Krattinger, S.G., Lagudah, E.S., Spielmeyer, W., Singh, R.P., Huerta-Espino, J., McFadden, H., Bossolini, E., Selter, L.L., and Keller, B. (2009). A putative ABC transporter confers durable resistance to multiple fungal pathogens in wheat. Science *323*, 1360–1363.

Krattinger, S.G., Sucher, J., Selter, L.L., Chauhan, H., Zhou, B., Tang, M., Upadhyaya, N.M., Mieulet, D., Guiderdoni, E., Weidenbach, D., et al. (2016). The wheat durable, multipathogen resistance gene Lr34 confers partial blast resistance in rice. Plant Biotechnol. J. *14*, 1261–1268.

Krishnan, H.B., Blanchette, J.T., and Okita, T.W. (1985). Wheat Invertases: characterization of cell wall-bound and soluble forms. Plant Physiol. 78, 241–245.

Kuckenberg, J., Tartachnyk, I., and Noga, G. (2009). Temporal and spatial changes of chlorophyll fluorescence as a basis for early and precise detection of leaf rust and powdery mildew infections in wheat leaves. Precis. Agric. *10*, 34–44.

Lannoo, N., Damme, V., and M, E.J. (2014). Lectin domains at the frontiers of plant defense. Front. Plant Sci. *5*.

Lecompte, F., Nicot, P.C., Ripoll, J., Abro, M.A., Raimbault, A.K., Lopez-Lauri, F., and Bertin, N. (2017). Reduced susceptibility of tomato stem to the necrotrophic fungus Botrytis cinerea is associated with a specific adjustment of fructose content in the host sugar pool. Ann. Bot. *119*, 931–943.

Lee, M.W., Jelenska, J., and Greenberg, J.T. (2008). Arabidopsis proteins important for modulating defense responses to Pseudomonas syringae that secrete HopW1-1. Plant J. Cell Mol. Biol. *54*, 452–465.

Le Hir, R., Spinner, L., Klemens, P.A.W., Chakraborti, D., de Marco, F., Vilaine, F., Wolff, N., Lemoine, R., Porcheron, B., Géry, C., et al. (2015). Disruption of the sugar transporters AtSWEET11 and AtSWEET12 affects vascular development and freezing tolerance in Arabidopsis. Mol. Plant *8*, 1687–1690.

Lemoine, R., La Camera, S., Atanassova, R., Dedaldechamp, F., Allario, T., Pourtau, N., Bonnemain, J.L., Laloi, M., Coutos-Thevenot, P., Maurousset, L., et al. (2013). Source-to-sink transport of sugar and regulation by environmental factors. Front Plant Sci *4*, 272.

Li, H., and Durbin, R. (2009). Fast and accurate short read alignment with Burrows-Wheeler transform. Bioinforma. Oxf. Engl. *25*, 1754–1760.

Li, H., Handsaker, B., Wysoker, A., Fennell, T., Ruan, J., Homer, N., Marth, G., Abecasis, G., Durbin, R., and Subgroup, 1000 Genome Project Data Processing (2009). The Sequence Alignment/Map format and SAMtools. Bioinformatics *25*, 2078–2079.

Liang, J., Liu, X., Li, Y., Wan, Q., Ma, Z., and Luo, Y. (2015). Population Genetic Structure and the Migration of Puccinia striiformis f. sp. tritici between the Gansu and Sichuan Basin Populations of China. Phytopathology.

Lievens, L., Pollier, J., Goossens, A., Beyaert, R., and Staal, J. (2017). Abscisic Acid as Pathogen Effector and Immune Regulator. Front. Plant Sci. *8*.

Link, T.I., Lang, P., Scheffler, B.E., Duke, M.V., Graham, M.A., Cooper, B., Tucker, M.L., van de Mortel, M., Voegele, R.T., Mendgen, K., et al. (2014). The haustorial transcriptomes of Uromyces appendiculatus and Phakopsora pachyrhizi and their candidate effector families. Mol. Plant Pathol. *15*, 379–393.

Liu, J., Han, L., Huai, B., Zheng, P., Chang, Q., Guan, T., Li, D., Huang, L., and Kang, Z. (2015a). Down-regulation of a wheat alkaline/neutral invertase correlates with reduced host susceptibility to wheat stripe rust caused by Puccinia striiformis. J. Exp. Bot. erv428.

Liu, Z., Xin, M., Qin, J., Peng, H., Ni, Z., Yao, Y., and Sun, Q. (2015b). Temporal transcriptome profiling reveals expression partitioning of homeologous genes contributing to heat and drought acclimation in wheat (Triticum aestivum L.). BMC Plant Biol. *15*.

Livne, A. (1964). Photosynthesis in Healthy and Rust-Affected Plants. Plant Physiol *39*, 614–621.

Long, S.P., and Bernacchi, C.J. (2003). Gas exchange measurements, what can they tell us about the underlying limitations to photosynthesis? Procedures and sources of error. J Exp Bot *54*, 2393–2401.

Love, M.I., Huber, W., and Anders, S. (2014). Moderated estimation of fold change and dispersion for RNA-seq data with DESeq2. Genome Biol. *15*, 550.

Luna, E., Pastor, V., Robert, J., Flors, V., Mauch-Mani, B., and Ton, J. (2010). Callose Deposition: A Multifaceted Plant Defense Response. Mol. Plant. Microbe Interact. *24*, 183–193.

Lutziger, I., and Oliver, D.J. (2001). Characterization of Two cDNAs Encoding Mitochondrial Lipoamide Dehydrogenase from Arabidopsis. Plant Physiol. *127*, 615–623.

Maclean, D.J., and Scott, K.J. (1976). Identification of glucitol (sorbitol) and ribitol in a rust fungus, Puccinia graminis f. sp. tritici. J Gen Microbiol *97*, 83–89.

Madson, M., Dunand, C., Li, X., Verma, R., Vanzin, G.F., Caplan, J., Shoue, D.A., Carpita, N.C., and Reiter, W.-D. (2003). The MUR3 gene of arabidopsis encodes a xyloglucan galactosyltransferase that is evolutionarily related to animal exostosins. Plant Cell *15*, 1662–1670.

Malinovsky, F.G., Fangel, J.U., and Willats, W.G.T. (2014). The role of the cell wall in plant immunity. Front. Plant Sci. *5*.

Marcussen, T., Sandve, S.R., Heier, L., Spannagl, M., Pfeifer, M., The International Wheat Genome Sequencing Consortium, Jakobsen, K.S., Wulff, B.B.H., Steuernagel, B., Mayer, K.F.X., et al. (2014). Ancient hybridizations among the ancestral genomes of bread wheat. Science *345*, 1250092.

Maxwell (2002). Chlorophyll fluorescence—a practical guide.

Mayama, S., Bordin, A.P.A., Morikawa, T., Tanpo, H., and Kato, H. (1995). Association of avenalumin accumulation with co-segregation of victorin sensitivity and crown rust resistance in oat lines carrying the Pc-2 gene. Physiol. Mol. Plant Pathol. *46*, 263–274.

McKnight, G., Sl, M., Sl, M., Rr, T., S, M., Po, S., and Pj, O. (1992). Molecular cloning, cDNA sequence, and bacterial expression of human glutamine:fructose-6-phosphate amidotransferase. J. Biol. Chem. *267*, 25208–25212.

Meena, M., Upadhyay, R.S., Prasad, V., Zehra, A., and Gupta, V.K. (2015). Mannitol metabolism during pathogenic fungal–host interactions under stressed conditions. Plant Biot. Interact. 1019.

Mendgen, K., and Hahn, M. (2002). Plant infection and the establishment of fungal biotrophy. Trends Plant Sci. *7*, 352–356.

Mendgen, K., and Nass, P. (1988). The activity of powdery-mildew haustoria after feeding the host cells with different sugars, as measured with a potentiometric cyanine dye. Planta *174*, 283–288.

Mendgen, K., Struck, C., Voegele, R.T., and Hahn, M. (2000). Biotrophy and rust haustoria. Physiol. Mol. Plant Pathol. *56*, 141–145.

Mhamdi, A., Queval, G., Chaouch, S., Vanderauwera, S., Van Breusegem, F., and Noctor, G. (2010). Catalase function in plants: a focus on Arabidopsis mutants as stress-mimic models. J. Exp. Bot. *61*, 4197–4220.

Milus, E.A., Kristensen, K., and Hovmoller, M.S. (2009). Evidence for increased aggressiveness in a recent widespread strain of Puccinia striiformis f. sp. tritici causing stripe rust of wheat. PHYTOPATHOLOGY *99*, 89–94.

Minic, Z. (2008). Physiological roles of plant glycoside hydrolases. Planta *227*, 723–740.

Mitchell, D.T. (1979). Carbon dioxide exchange by infected first leaf tissues susceptible to wheat stem rust. Trans. Br. Mycol. Soc. *72*, 63–68.

Mittler, R., and Blumwald, E. (2015). The Roles of ROS and ABA in Systemic Acquired Acclimation[OPEN]. Plant Cell *27*, 64–70.

Miya, A., Albert, P., Shinya, T., Desaki, Y., Ichimura, K., Shirasu, K., Narusaka, Y., Kawakami, N., Kaku, H., and Shibuya, N. (2007). CERK1, a LysM receptor kinase, is essential for chitin elicitor signaling in Arabidopsis. Proc. Natl. Acad. Sci. *104*, 19613–19618.

Miyakawa, T., Fujita, Y., Yamaguchi-Shinozaki, K., and Tanokura, M. (2013). Structure and function of abscisic acid receptors. Trends Plant Sci. *18*, 259–266.

Moffatt, B.A., and Ashihara, H. (2002). Purine and pyrimidine nucleotide synthesis and metabolism. Arab. Book Am. Soc. Plant Biol. *1*.

Moldenhauer, J., Moerschbacher, B.M., and Van Der Westhuizen, A.J. (2006). Histological investigation of stripe rust (Puccinia striiformis f.sp. tritici) development in resistant and susceptible wheat cultivars. Plant Pathol. *55*, 469–474.

Molitor, A., Zajic, D., Voll, L.M., Pons-Kühnemann, J., Samans, B., Kogel, K.-H., and Waller, F. (2011). Barley leaf transcriptome and metabolite analysis reveals new aspects of compatibility and piriformospora indica–mediated systemic induced resistance to powdery mildew. Mol. Plant. Microbe Interact. *24*, 1427–1439.

Moore, J.W., Herrera-Foessel, S., Lan, C., Schnippenkoetter, W., Ayliffe, M., Huerta-Espino, J., Lillemo, M., Viccars, L., Milne, R., Periyannan, S., et al. (2015). A recently evolved hexose transporter variant confers resistance to multiple pathogens in wheat. Nat. Genet. *47*, 1494–1498.

Morkunas, I., Borek, S., Formela, M., and Ratajczak, L. (2012). Plant responses to sugar starvation. In carbohydrates - comprehensive studies on glycobiology and glycotechnology, C.-F. Chang, ed. (InTech), p.

Murray, D.C., and Walters, D.R. (1992). Increased photosynthesis and resistance to rust infection in upper, uninfected leaves of rusted broad bean (*Vicia faba L.*). New Phytol. *120*, 235–242.

Neumann, S., Paveley, N.D., Beed, F.D., and Sylvester-Bradley, R. (2004). Nitrogen per unit leaf area affects the upper asymptote of *Puccinia striiformis f.sp. tritici* epidemics in winter wheat. Plant Pathol. *53*, 725–732.

Nie, G., Hendrix, D.L., Webber, A.N., Kimball, B.A., and Long, S.P. (1995). Increased accumulation of carbohydrates and decreased photosynthetic gene transcript levels in wheat grown at an elevated CO2 concentration in the field. Plant Physiol. *108*, 975–983.

O'Connell, R.J., and Panstruga, R. (2006). Tete a tete inside a plant cell: establishing compatibility between plants and biotrophic fungi and oomycetes. New Phytol. *171*, 699–718.

Olien, C.R., and Clark, J.L. (1995). Freeze-induced changes in carbohydrates associated with hardiness of barley and rye. Crop Sci. *35*, 496.

Orczyk, W., Dmochowska-Boguta, M., Czembor, H.J., and Nadolska-Orczyk, A. (2010). Spatiotemporal patterns of oxidative burst and micronecrosis in resistance of wheat to brown rust infection. Plant Pathol. *59*, 567–575.

Owera, S.A.P., Farrar, J.F., and Whitbread, R. (1981). Growth and photosynthesis in barley infected with brown rust. Physiol. Plant Pathol. *18*, 79–90.

Pantin, F., Simonneau, T., Rolland, G., Dauzat, M., and Muller, B. (2011). Control of leaf expansion: A developmental switch from metabolics to hydraulics. Plant Physiol. *156*, 803–815.

Park, R., Rees, R., and Platz, G. (1988). Some effects of stripe rust infection in wheats with adult plant resistance. Aust. J. Agric. Res. *39*, 555–562.

Parry, M., Andraloj, J., Khan, S., Lea, P., and Keys, A. (2002). Rubisco activity: effects of drought stress. Ann. Bot. *89*, 833–839.

Patel, T.K., and Williamson, J.D. (2016). Mannitol in plants, fungi, and plant–fungal interactions. Trends Plant Sci. *0*.

Paul, N.D., and Ayres, P.G. (1986). The effects of nutrient deficiency and rust infection on the relationship between root dry weight and length in groundsel (*Senecio vulgaris L.*). Ann. Bot. *57*, 353–360.

Paulsen, I.T., and Skurray, R.A. (1994). The POT family of transport proteins. Trends Biochem. Sci. *19*, 404.

Pedrazzini, E., Komarova, N.Y., Rentsch, D., and Vitale, A. (2013). Traffic routes and signals for the tonoplast. Traffic *14*, 622–628.

Penfield, S., Clements, S., Bailey, K.J., Gilday, A.D., Leegood, R.C., Gray, J.E., and Graham, I.A. (2012). Expression and manipulation of phosphoenolpyruvate carboxykinase 1 identifies a role for malate metabolism in stomatal closure. Plant J. Cell Mol. Biol. *69*, 679–688.

Peng, L., Fukao, Y., Fujiwara, M., and Shikanai, T. (2012). Multistep assembly of chloroplast NADH dehydrogenase-like subcomplex A requires several nucleus-encoded proteins, including CRR41 and CRR42, in *Arabidopsis*. Plant Cell Online *24*, 202–214.

Periappuram, C., Steinhauer, L., Barton, D.L., Taylor, D.C., Chatson, B., and Zou, J. (2000). The Plastidic phosphoglucomutase from Arabidopsis. A reversible enzyme reaction with an important role in metabolic control. Plant Physiol. *122*, 1193–1200.

Pessina, S., Lenzi, L., Perazzolli, M., Campa, M., Costa, L.D., Urso, S., Valè, G., Salamini, F., Velasco, R., and Malnoy, M. (2016). Knockdown of MLO genes reduces susceptibility to powdery mildew in grapevine. Hortic. Res. *3*, 16016.

Peters, S., Egert, A., Stieger, B., and Keller, F. (2010). Functional identification of Arabidopsis ATSIP2 (At3g57520) as an alkaline α-galactosidase with a substrate specificity for raffinose and an apparent sink-specific expression pattern. Plant Cell Physiol. *51*, 1815–1819.

Peterson, R.B., and Aylor, D.E. (1995). Chlorophyll fluorescence induction in leaves of *Phaseolus vulgaris* infected with bean rust (*Uromyces appendiculatus*). Plant Physiol. *108*, 163–171.

Ponnu, J., Wahl, V., and Schmid, M. (2011). Trehalose-6-phosphate: connecting plant metabolism and development. Front Plant Sci *2*, 70.

Porra, R.J., Thompson, W.A., and Kriedemann, P.E. (1989). Determination of accurate extinction coefficients and simultaneous equations for assaying chlorophylls a and b extracted with four different solvents: verification of the concentration of chlorophyll standards by atomic absorption spectroscopy. Biochim. Biophys. Acta BBA - Bioenerg. *975*, 384–394.

Pospíšil, P. (2009). Production of reactive oxygen species by photosystem II. Biochim. Biophys. Acta BBA - Bioenerg. *1787*, 1151–1160.

Prats, E., Mur, L. a. J., Sanderson, R., and Carver, T.L.W. (2005). Nitric oxide contributes both to papilla-based resistance and the hypersensitive response in barley attacked by *Blumeria graminis f. sp. hordei*. Mol. Plant Pathol. *6*, 65–78.

Presti, L.L., Lanver, D., Schweizer, G., Tanaka, S., Liang, L., Tollot, M., Zuccaro, A., Reissmann, S., and Kahmann, R. (2015). Fungal effectors and plant susceptibility. Annu. Rev. Plant Biol. *66*, 513–545.

Pretorius, Z.A., Singh, R.P., Wagoire, W.W., and Payne, T.S. (2000). Detection of virulence to wheat stem rust resistance gene Sr31 in P*uccinia graminis. f. sp. tritici* in Uganda. Plant Dis. *84*, 203–203.

Proels, R.K., and Hückelhoven, R. (2014). Cell-wall invertases, key enzymes in the modulation of plant metabolism during defence responses. Mol. Plant Pathol. *15*, 858–864.

Quilliam, R.S., Swarbrick, P.J., Scholes, J.D., and Rolfe, S.A. (2006). Imaging photosynthesis in wounded leaves of *Arabidopsis thaliana*. J Exp Bot *57*, 55–69.

Rabe, F., Ajami-Rashidi, Z., Doehlemann, G., Kahmann, R., and Djamei, A. (2013). Degradation of the plant defence hormone salicylic acid by the biotrophic fungus *Ustilago maydis.* Mol. Microbiol. *89*, 179–188.

Ranocha, P., Chabannes, M., Chamayou, S., Danoun, S., Jauneau, A., Boudet, A.-M., and Goffner, D. (2002). Laccase down-regulation causes alterations in phenolic metabolism and cell wall structure in poplar. Plant Physiol. *129*, 145–155.

Rauscher, M., Ádám, A.L., Wirtz, S., Guggenheim, R., Mendgen, K., and Deising, H.B. (1999). PR-1 protein inhibits the differentiation of rust infection hyphae in leaves of acquired resistant broad bean. Plant J. *19*, 625–633.

Reisener, H.J., Goldschmid, H.R., Ledingham, G.A., and Perlin, A.S. (1962). Formation of trehalose and polyols by wheat stem rust (*Puccinia graminis tritici*) uredospores. Can. J. Biochem. Physiol. *40*, 1248–1251.

Remy, E., Cabrito, T.R., Baster, P., Batista, R.A., Teixeira, M.C., Friml, J., Sá-Correia, I., and Duque, P. (2013). A Major facilitator superfamily transporter plays a dual role in polar auxin transport and drought stress tolerance in *Arabidopsis*. Plant Cell *25*, 901–926.

Ridout, C.J., Skamnioti, P., Porritt, O., Sacristan, S., Jones, J.D., and Brown, J.K. (2006). Multiple avirulence paralogues in cereal powdery mildew fungi may contribute to parasite fitness and defeat of plant resistance. Plant Cell *18*, 2402–2414.

Rinaldo, A., Gilbert, B., Boni, R., Krattinger, S.G., Singh, D., Park, R.F., Lagudah, E., and Ayliffe, M. (2017). The Lr34 adult plant rust resistance gene provides seedling resistance in durum wheat without senescence. Plant Biotechnol. J. *15*, 894–905.

Robinson, M.D., McCarthy, D.J., and Smyth, G.K. (2010). edgeR: a Bioconductor package for differential expression analysis of digital gene expression data. Bioinformatics *26*, 139–140.

Robinson, S.A., Slade, A.P., Fox, G.G., Phillips, R., Ratcliffe, R.G., and Stewart, G.R. (1991). The Role of glutamate dehydrogenase in plant nitrogen metabolism. Plant Physiol. *95*, 509–516.

Rodriguez-Algaba, J., Walter, S., Sørensen, C.K., Hovmøller, M.S., and Justesen, A.F. (2014). Sexual structures and recombination of the wheat rust fungus *Puccinia striiformis* on *Berberis vulgaris*. Fungal Genet. Biol. *70*, 77–85.

Roitsch, T., and González, M.-C. (2004). Function and regulation of plant invertases: sweet sensations. Trends Plant Sci. *9*, 606–613.

Rolfe, S., and Scholes, J. (2010). Chlorophyll fluorescence imaging of plant–pathogen interactions. Protoplasma *247*, 163–175.

Rolland, F., Baena-Gonzalez, E., and Sheen, J. (2006). Sugar sensing and signaling in plants: conserved and novel mechanisms. Annu. Rev. Plant Biol. *57*, 675–709.

Ros, R., Muñoz-Bertomeu, J., and Krueger, S. (2014). Serine in plants: biosynthesis, metabolism, and functions. Trends Plant Sci. *19*, 564–569.

Rosenberg, M., Krištofiková, L., Proksa, B., and Magdolen, P. (1992). The formation of polyols and fatty acids during L-lactic acid fermentation by *Rhizopus arrhizus*. Biotechnol. Lett. *14*, 45–48.

Schallus, T., Jaeckh, C., Fehér, K., Palma, A.S., Liu, Y., Simpson, J.C., Mackeen, M., Stier, G., Gibson, T.J., Feizi, T., et al. (2008). Malectin: A novel carbohydrate-binding protein of the endoplasmic reticulum and a candidate player in the early steps of protein N-glycosylation. Mol. Biol. Cell *19*, 3404–3414.

Schippers, J.H.M., Schmidt, R., Wagstaff, C., and Jing, H.-C. (2015). Living to die and dying to live: The survival strategy behind leaf senescence. Plant Physiol. *169*, 914–930.

Scholes, J., and Rolfe, S. (1996). Photosynthesis in localised regions of oat leaves infected with crown rust (*Puccinia coronata*): quantitative imaging of chlorophyll fluorescence. Planta *199*, 573–582.

Scholes, J.D., and Farrar, J.F. (1987). Development of symptoms of brown rust of barley in relation to the distribution of fungal mycelium, starch accumulation and localized changes in the concentration of chlorophyll. New Phytol. *107*, 103–117.

Scholes, J.D., Lee, P.J., Horton, P., and Lewis, D.H. (1994). Invertase: Understanding changes in the photosynthetic and carbohydrate metabolism of barley leaves infected with powdery mildew. New Phytol. *126*, 213–222.

Schumann, G.L., and Leonard, K.J. (2000). Stem rust of wheat (black rust). Plant Health Instr.

Schwessinger, B. (2017). Fundamental wheat stripe rust research in the 21(st) century. New Phytol. *213*, 1625–1631.

Scialdone, A., and Howard, M. (2015). How plants manage food reserves at night: quantitative models and open questions. Plant Physiol. *6*, 204.

Shafiei, R., Hang, C.U.I., Kang, J.-G., and Loake, G.J. (2007). Identification of loci controlling non-host disease resistance in *Arabidopsis* against the leaf rust pathogen *Puccinia triticina*. Mol. Plant Pathol. *8*, 773–784.

Sharkey, T.D., Bernacchi, C.J., Farquhar, G.D., and Singsaas, E.L. (2007). Fitting photosynthetic carbon dioxide response curves for C3leaves. Plant Cell Env. *30*, 1035–1040.

Shiferaw, B., Smale, M., Braun, H.-J., Duveiller, E., Reynolds, M., and Muricho, G. (2013). Crops that feed the world 10. Past successes and future challenges to the role played by wheat in global food security. Food Secur. *5*, 291–317.

Shimizu, T., Nakano, T., Takamizawa, D., Desaki, Y., Ishii-Minami, N., Nishizawa, Y., Minami, E., Okada, K., Yamane, H., Kaku, H., et al. (2010). Two LysM receptor molecules, CEBiP and OsCERK1, cooperatively regulate chitin elicitor signaling in rice. Plant J *64*, 204–214.

Singh, R.P., Hodson, D.P., Huerta-Espino, J., Jin, Y., Bhavani, S., Njau, P., Herrera-Foessel, S., Singh, P.K., Singh, S., and Govindan, V. (2011). The emergence of Ug99 races of the stem rust fungus is a threat to world wheat production. Annu. Rev. Phytopathol. *49*, 465–481.

Smith, A.M., and Stitt, M. (2007). Coordination of carbon supply and plant growth. Plant Cell Environ. *30*, 1126–1149.

Smith, A.M., and Zeeman, S.C. (2006). Quantification of starch in plant tissues. Nat Protoc. *1*, 1342–1345.

Snoeijers, S.S., Pérez-García, A., Joosten, M.H.A.J., and Wit, P.J.G.M.D. (2000). The effect of nitrogen on disease development and gene expression in bacterial and fungal plant pathogens. Eur. J. Plant Pathol. *106*, 493–506.

Soanes, D.M., Chakrabarti, A., Paszkiewicz, K.H., Dawe, A.L., and Talbot, N.J. (2012). Genome-wide transcriptional profiling of appressorium development by the rice blast fungus *Magnaporthe oryzae.* PLOS Pathog. *8*, e1002514.

Solomon, P., and Oliver, R. (2001). The nitrogen content of the tomato leaf apoplast increases during infection by *Cladosporium fulvum*. Planta *213*, 241–249.

Solomon, P.S., Tan, K.-C., and Oliver, R.P. (2003). The nutrient supply of pathogenic fungi; a fertile field for study. Mol. Plant Pathol. *4*, 203–210.

Song, X., Rampitsch, C., Soltani, B., Mauthe, W., Linning, R., Banks, T., McCallum, B., and Bakkeren, G. (2011). Proteome analysis of wheat leaf rust fungus, *Puccinia triticina*, infection structures enriched for haustoria. Proteomics *11*, 944–963.

Sosso, D., Luo, D., Li, Q.-B., Sasse, J., Yang, J., Gendrot, G., Suzuki, M., Koch, K.E., McCarty, D.R., Chourey, P.S., et al. (2015). Seed filling in domesticated maize and rice depends on SWEET-mediated hexose transport. Nat. Genet. *47*, 1489–1493.

Spencer-Phillips, P.T.N., and Gay, J.L. (1980). Electron microscope autoradiography of 14C photosynthate distribution at the haustorium-host interface in powdery mildew of *Pisum sativum*. Protoplasma *103*, 131–154.

Spielmeyer, W., Mago, R., Wellings, C., and Ayliffe, M. (2013). Lr67 and Lr34 rust resistance genes have much in common – they confer broad spectrum resistance to multiple pathogens in wheat. BMC Plant Biol. *13*, 1–9.

Stein, H., Honig, A., Miller, G., Erster, O., Eilenberg, H., Csonka, L.N., Szabados, L., Koncz, C., and Zilberstein, A. (2011). Elevation of free proline and proline-rich protein levels by simultaneous manipulations of proline biosynthesis and degradation in plants. Plant Sci. *181*, 140–150.

Stirk, W.A., Thomson, S.V., and van Staden, J. (2006). Effect of rust-causing pathogen (*Puccinia thlaspeos*) on auxin-like and cytokinin-like activity in dyer's Woad (*Isatis tinctoria*). Weed Sci. *54*, 815–820.

Stitt, M., and Zeeman, S.C. (2012). Starch turnover: pathways, regulation and role in growth. Curr Opin Plant Biol *15*, 282–292.

Streb, S., and Zeeman, S.C. (2012). Starch Metabolism in *Arabidopsis*. Arab. Book Am. Soc. Plant Biol. *10*, e0160.

Struck, C., Hahn, M., and Mendgen, K. (1996). Plasma Membrane H+-ATPase activity in spores, germ tubes, and haustoria of the rust fungus *Uromyces viciae-fabae*. Fungal Genet. Biol. *20*, 30–35.

Sulpice, R., Pyl, E.-T., Ishihara, H., Trenkamp, S., Steinfath, M., Witucka-Wall, H., Gibon, Y., Usadel, B., Poree, F., Piques, M.C., et al. (2009). Starch as a major integrator in the regulation of plant growth. Proc. Natl. Acad. Sci. *106*, 10348–10353.

Sun, J., Sui, X., Hunag, H., Wang, S., Wei, Y., and Zhang, Z. (2014). Low light stress down-regulated rubisco gene expression and photosynthetic capacity during cucumber (*Cucumis sativus* L.) leaf development. J. Integr. Agric. *13*, 997–1007.

Sutton, P.N., Gilbert, M.J., Williams, L.E., and Hall, J.L. (2007). Powdery mildew infection of wheat leaves changes host solute transport and invertase activity. Physiol. Plant. *129*, 787–795.

Swarbrick, P.J., Schulze-Lefert, P., and Scholes, J.D. (2006). Metabolic consequences of susceptibility and resistance (race-specific and broad-spectrum) in barley leaves challenged with powdery mildew. Plant Cell Env. *29*, 1061–1076.

Taiz, L., and Zeiger, E. (2010). Plant physiology (Sunderland, MA: Sinauer Associates).

Tauzin, A.S., and Giardina, T. (2014). Sucrose and invertases, a part of the plant defense response to the biotic stresses. Plant Biot. Interact. *5*, 293.

Tetlow, I.J., and Farrar, J.F. (1993). Apoplastic sugar concentration and pH in barley leaves infected with brown rust. J Exp Bot *44*, 929–936.

The International Wheat Genome Sequencing Consortium (2014). A chromosome-based draft sequence of the hexaploid bread wheat (*Triticum aestivum*) genome. Science *345*, 1251788.

Tiessen, A., and Padilla-Chacon, D. (2013). Subcellular compartmentation of sugar signalling: Links among carbon cellular status, route of sucrolysis, sink-source allocation, and metabolic partitioning. Front. Plant Sci. *3*.

Tomitani, A., Knoll, A.H., Cavanaugh, C.M., and Ohno, T. (2006). The evolutionary diversification of cyanobacteria: Molecular–phylogenetic and paleontological perspectives. Proc. Natl. Acad. Sci. U. S. A. *103*, 5442–5447.

Trapnell, C., Pachter, L., and Salzberg, S.L. (2009). TopHat: discovering splice junctions with RNA-Seq. Bioinforma. Oxf. Engl. *25*, 1105–1111.

Trevanion, S. (2002). Regulation of sucrose and starch synthesis in wheat (*Triticum aestivum* L.) leaves: role of fructose 2,6-bisphosphate. Planta *215*, 653–665.

Trouvelot, S., Héloir, M.-C., Poinssot, B., Gauthier, A., Paris, F., Guillier, C., Combier, M., Trdá, L., Daire, X., and Adrian, M. (2014). Carbohydrates in plant immunity and plant protection: roles and potential application as foliar sprays. Front. Plant Sci. *5*.

Tsay, Y.-F., Chiu, C.-C., Tsai, C.-B., Ho, C.-H., and Hsu, P.-K. (2007). Nitrate transporters and peptide transporters. FEBS Lett. *581*, 2290–2300.

Turner, J.G., Ellis, C., and Devoto, A. (2002). The Jasmonate signal pathway. Plant Cell *14*, S153–S164.

Upadhyaya, N.M., Mago, R., Staskawicz, B.J., Ayliffe, M., Ellis, J., and Dodds, P. (2013). A bacterial type III secretion assay for delivery of fungal effector proteins into wheat. Mol. Plant. Microbe Interact. 131024073736001.

Vallarino, J.G., and Osorio, S. (2012). Signaling role of oligogalacturonides derived during cell wall degradation. Plant Signal. Behav. *7*, 1447–1449.

Vallavieille-Pope, C. de (INRA, Huber, L., Leconte, M., and Goyeau, H. (1995). Comparative effects of temperature and interrupted wet periods on germination, penetration, and infection of *Puccinia recondita* f.sp. *tritici* and *P. striiformis* on wheat seedlings. Phytopathol. USA.

Valluru, R., and Van den Ende, W. (2008). Plant fructans in stress environments: emerging concepts and future prospects. J Exp Bot *59*, 2905–2916.

Van Den Brûle, S., Müller, A., Fleming, A.J., and Smart, C.C. (2002). The ABC transporter SpTUR2 confers resistance to the antifungal diterpene sclareol. Plant J. *30*, 649–662.

Van den Ende, W. (2013). Multifunctional fructans and raffinose family oligosaccharides. Plant Physiol. *4*, 247.

Vandenabeele, S., Vanderauwera, S., Vuylsteke, M., Rombauts, S., Langebartels, C., Seidlitz, H.K., Zabeau, M., Van Montagu, M., Inzé, D., and Van Breusegem, F. (2004). Catalase deficiency drastically affects gene expression induced by high light in *Arabidopsis thaliana*. Plant J. *39*, 45–58.

Verdier, V., Triplett, L.R., Hummel, A.W., Corral, R., Cernadas, R.A., Schmidt, C.L., Bogdanove, A.J., and Leach, J.E. (2012). Transcription activator-like (TAL) effectors targeting OsSWEET genes enhance virulence on diverse rice (Oryza sativa) varieties when expressed individually in a TAL effector-deficient strain of *Xanthomonas oryzae*. New Phytol. *196*, 1197–1207.

Vijayakumari, K., Jisha, K.C., and Puthur, J.T. (2016). GABA/BABA priming: a means for enhancing abiotic stress tolerance potential of plants with less energy investments on defence cache. Acta Physiol. Plant. *38*, 230.

Voegele, R.T. (2006). *Uromyces fabae*: development, metabolism, and interactions with its host *Vicia faba*. FEMS Microbiol Lett *259*, 165–173.

Voegele, R.T., and Mendgen, K. (2003). Rust haustoria: nutrient uptake and beyond. New Phytol. *159*, 93–100.

Voegele, R.T., Struck, C., Hahn, M., and Mendgen, K. (2001). The role of haustoria in sugar supply during infection of broad bean by the rust fungus *Uromyces fabae*. Proc. Natl. Acad. Sci. *98*, 8133–8138.

Voegele, R.T., Hahn, M., Lohaus, G., Link, T., Heiser, I., and Mendgen, K. (2005). Possible roles for mannitol and mannitol dehydrogenase in the biotrophic plant pathogen *Uromyces fabae*. Plant Physiol *137*, 190–198.

Voegele, R.T., Wirsel, S., Möll, U., Lechner, M., and Mendgen, K. (2006). Cloning and characterization of a novel invertase from the obligate biotroph *Uromyces fabae* and analysis of expression patterns of host and pathogen invertases in the course of infection. Mol. Plant. Microbe Interact. *19*, 625–634.

Vogt, T. (2010). Phenylpropanoid Biosynthesis. Mol. Plant *3*, 2–20.

Voigt, C.A. (2014). Callose-mediated resistance to pathogenic intruders in plant defense-related papillae. Front. Plant Sci. *5*.

Walter, S., Ali, S., Kemen, E., Nazari, K., Bahri, B.A., Enjalbert, J., Hansen, J.G., Brown, J.K.M., Sicheritz-Pontén, T., Jones, J., et al. (2016). Molecular markers for tracking the origin and worldwide distribution of invasive strains of *Puccinia striiformis*. Ecol. Evol. *6*, 2790–2804.

Wang, M., Zheng, Q., Shen, Q., and Guo, S. (2013). The critical role of potassium in plant stress response. Int. J. Mol. Sci. *14*, 7370–7390.

Wang, Z., Gerstein, M., and Snyder, M. (2009). RNA-Seq: a revolutionary tool for transcriptomics. Nat. Rev. Genet. *10*, 57–63.

Wang, Z., Zhao, J., Chen, X., Peng, Y., Ji, J., Zhao, S., Lv, Y., Huang, L., and Kang, Z. (2015). Virulence variations of *Puccinia striiformis* f. sp. *tritici* isolates collected from *Berberis* spp. in China. Plant Dis. *100*, 131–138.

Wellings, C.R. (2007). Puccinia striiformis in Australia: a review of the incursion, evolution, and adaptation of stripe rust in the period 1979–2006. Aust. J. Agric. Res. *58*, 567–575.

Wellings, C.R., McIntosh, R.A., and Hussain, M. (1988). A new source of resistance to *Puccinia striiformis* f. sp. *tritici* in spring wheats (Triticum aestivum). Plant Breed. *100*, 88–96.

Wellings, C.R., Wright, D.G., Keiper, F., and Loughman, R. (2003). First detection of wheat stripe rust in Western Australia: evidence for a foreign incursion. Australas. Plant Pathol. *32*, 321–322.

White, J. and Edwards, J. (2008). Wheat Growth & Development. New South Wales Department of Primary Industries. ISBN 978 0 7347 1894 5

Xue, G.-P., McIntyre, C.L., Glassop, D., and Shorter, R. (2008). Use of expression analysis to dissect alterations in carbohydrate metabolism in wheat leaves during drought stress. Plant Mol. Biol. *67*, 197–214.

Yamada, K., Saijo, Y., Nakagami, H., and Takano, Y. (2016). Regulation of sugar transporter activity for antibacterial defense in Arabidopsis. Science 5692.

Yang, M., and Vousden, K.H. (2016). Serine and one-carbon metabolism in cancer. Nat. Rev. Cancer *16*, 650–662.

Zhao, J., Wang, L., Wang, Z., Chen, X., Zhang, H., Yao, J., Zhan, G., Chen, W., Huang, L., and Kang, Z. (2013). Identification of eighteen *Berberis* species as alternate hosts of *Puccinia striiformis* f. sp. *tritici* and virulence variation in the pathogen isolates from natural infection of *Barberry* plants in China. Phytopathol. 130320072657003.

Zhao, J., Zhuang, H., Zhan, G., Huang, L., and Kang, Z. (2015). Proteomic analysis of *Puccina striiformis* f. sp. *tritici* (Pst) during uredospore germination. Eur. J. Plant Pathol. 1–12.

Zhao, J., Wang, M., Chen, X., and Kang, Z. (2016). Role of alternate hosts in epidemiology and pathogen variation of cereal Rusts. Annu. Rev. Phytopathol. *54*, 207–228.

Zheng, X., Zhou, M., Yoo, H., Pruneda-Paz, J.L., Spivey, N.W., Kay, S.A., and Dong, X. (2015). Spatial and temporal regulation of biosynthesis of the plant immune signal salicylic acid. Proc. Natl. Acad. Sci. 201511182.